Journal of Analytical Methods in Chemistry

Quality Control of Natural Product Medicine and Nutrient Supplements

Guest Editors: Shuang-Qing Zhang, Feng Wei, Yu-Ming Fan, Feng Sun, Ying-Yong Zhao, and Shuhua Bai

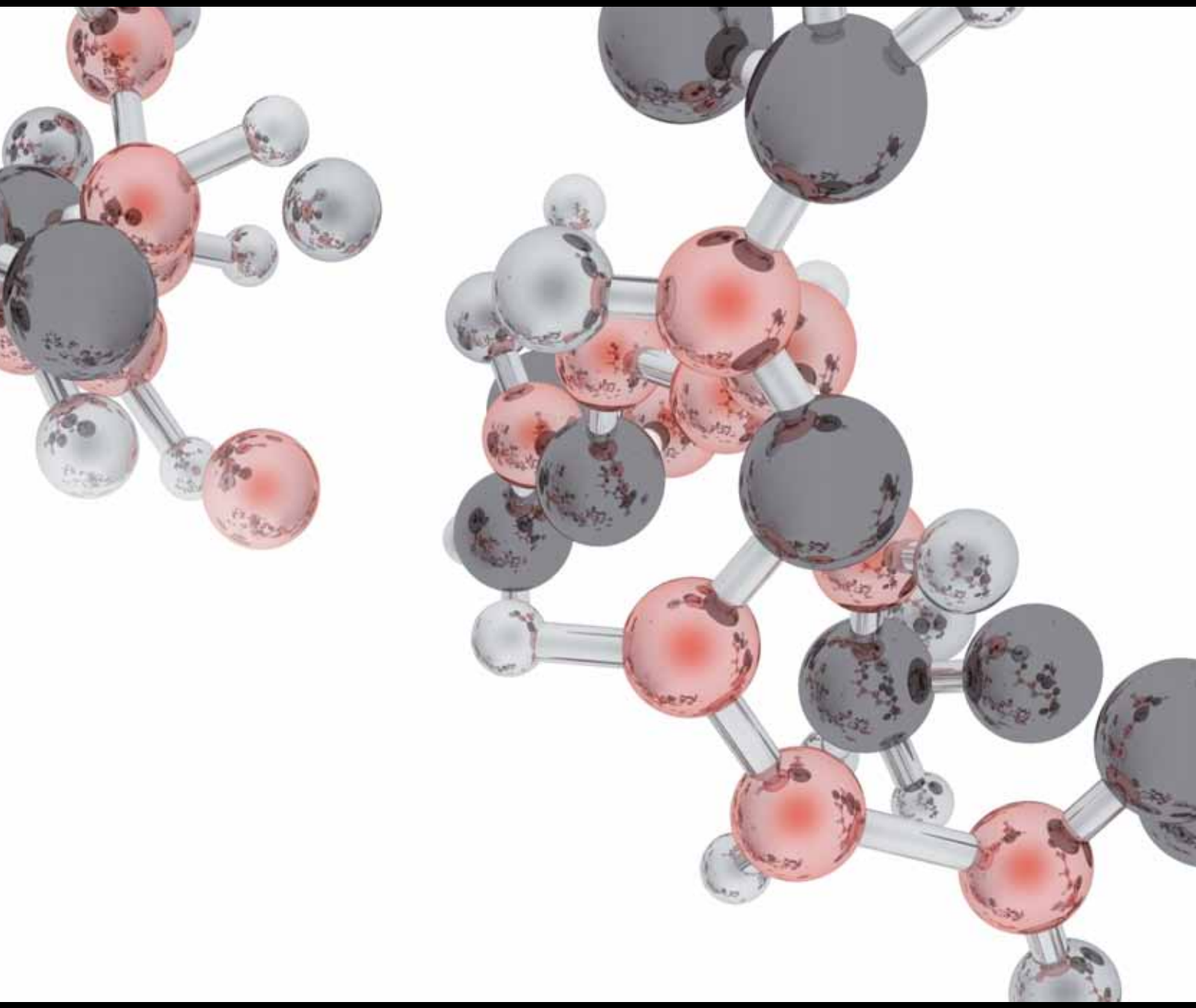

Quality Control of Natural Product Medicine and Nutrient Supplements

Journal of Analytical Methods in Chemistry

Quality Control of Natural Product Medicine and Nutrient Supplements

Guest Editors: Shuang-Qing Zhang, Feng Wei, Yu-Ming Fan, Feng Sun, Ying-Yong Zhao, and Shuhua Bai

Editorial Board

Contents

Hindawi Publishing Corporation
Journal of Analytical Methods in Chemistry
Volume 2013, Article ID 182573, 2 pages
http://dx.doi.org/10.1155/2013/182573

Editorial

Quality Control of Natural Product Medicine and Nutrient Supplements

Shuang-Qing Zhang,[1] Feng Wei,[2] Yu-Ming Fan,[3] Feng Sun,[4] Ying-Yong Zhao,[5] and Shuhua Bai[6]

[1] *Department of Nutrition and Metabolism, National Institute for Nutrition and Food Safety, China Center for Disease Control and Prevention, Beijing 100050, China*
[2] *Department of Traditional Chinese Medicine and Ethnic Medicine, National Institutes for Food and Drug Control, Beijing 100050, China*
[3] *National Institutes for Food and Drug Control, Beijing 100050, China*
[4] *Department of Obstetrics & Gynaecology, Yong Loo Lin School of Medicine, National University of Singapore, MD Block 11, CRC 03-09, 10 Medical Drive, Singapore 117597*
[5] *Key Laboratory of Resource Biology and Biotechnology in Western China of Ministry of Education, College of Life Sciences, Northwest University, No. 229 Taibai North Road, Xi'an, Shaanxi 710069, China*
[6] *Department of Basic Pharmaceutical Sciences, School of Pharmacy, Husson University, Bangor, ME 04401, USA*

Correspondence should be addressed to Ying-Yong Zhao; zyy@nwu.edu.cn

Received 8 July 2013; Accepted 8 July 2013

Natural product medicine (NPM) has been used to prevent and treat various human diseases in China, India, Japan, and other countries for centuries. Due to its long historical clinical uses and excellent therapeutic efficacy, NPM more and more attracts global attention, and many research institutes and pharmaceutical companies have been actively exploring NPM as a source for new drug discovery and development [1]. However, the characteristics of NPM are roles of multicomponents and multitargets due to its multiple components. If only few constituents are emphasized, the holistic characteristics of NPM will be ignored [2].

With the development of globalization and modernization of NPM, an important issue is the consistency and control ability of quality of NPM. Traditionally, identification of NPM is performed according to its morphological character, one or a few markers' thin-layer chromatography identification, and/or content determination [3, 4]. However, these methods do not provide a complete profile of the NPM, so it can't distinguish NPM with similar appearance and/or similar main chemical constitutions.

The characteristics of action of NPM are synergistic action of multicomponents and multitargets [5]. By a combination of multiple components, NPM may produce its beneficial effects by interacting with different cell signaling pathways and biological networks, achieving the same therapeutic efficacy of a normal isolated compound at much lower doses of isolated compounds [6]. Thus, a comprehensive method which could reflect the variation of most constituents in the NPM is necessary, especially the variation correlating with pharmacological and clinical efficacy. With the development of various modern technologies, advanced chemical, pharmacological, and biological technologies have facilitated an increasing number of researchers in the search for possible ways to explore the potential healthcare benefits of this multicomponents interaction system. In recent years, the analysis of NPM has begun to emphasize more on the integrative and holistic properties of NPM [7]. The chromatographic or spectroscopic fingerprint and multicomponents quantification have been used for the quality control of NPM in the past ten years. Based on some chromatographic or spectroscopic methods, the properties of absorption, distribution, metabolism, and excretion of NPM have been analyzed to screen the bioactive markers. In addition, the genomics and proteomics have been applied to

Table 1: The analytical techniques and methods of natural product medicine.

Analytical techniques	Chromatographic or spectroscopic methods
Thin-layer chromatography (TLC) techniques	High-performance TLC (HPTLC), microemulsion TLC (ME-TLC), and so forth
Gas chromatography (GC) techniques	GC-MS, two-dimensional GC (GC × GC), and so forth
High performance liquid chromatography (HPLC) techniques	HPLC-UV, HPLC-DAD, HPLC-ELSD, HPLC-FLD, HPLC-RID, HPLC-MS, HPLC-CEAD, HPLC-ESI/TOF-MS, UPLC-ESI/TOF-MS, and so forth
Capillary electrophoresis (CE) techniques	CE, capillary zone electrophoresis (CZE), micellar electrokinetic chromatography (MEKC), nonaqueous CE (NACE), capillary electrochromatography (CEC), and so forth
Infrared spectroscopy (IR) techniques	FT-IR, two-dimensional infrared (2D-IR), and so forth
Near-infrared spectroscopy (NIR) techniques	NIR, two-dimensional near-infrared (2D-NIR), and so forth
Nuclear magnetic resonance (NMR) techniques	Quantitative NMR (qNMR), diffusion-ordered spectroscopy (DOS) NMR, three-dimensional DOSY NMR, and so forth

the investigation of NPM. The different analytical techniques and methods of NPM are shown in Table 1.

In this special issue of quality control of NPM and nutrient supplements, 15 research papers have been published by the previously mentioned chromatographic or spectroscopic methods and contributed to quality control of NPM. These papers focused on the quantification analysis of multiple chemical components, bioactivity and their mechanism of actions of chemical components, and pharmacokinetics and tissue distribution studies.

Firstly, multicomponents determinations play a critical role in evaluating the quality of NPM and understanding the synergistic action of multicomponents and multitargets. Multicomponents quantitative methods of NPM were reported in this special issue. Among the analytical methods for NPM, HPLC with easy operation, high accuracy, and wide suitability is still the most popular method for the qualitative and quantitative analyses of NPM. For example, simultaneous quantification of limonin and six alkaloids in *Evodia rutaecarpa* has been completed by HPLC-DAD method. The results indicated that the quality control of *Evodia rutaecarpa* could be simplified to the measurement of four constituents and that limonin, 1-methyl-2-undecyl-4(1H)-quinolone, and dihydroevocarpine should also be served as the chemical markers together with evodiamine for the quality control of *Evodia rutaecarpa*.

Secondly, active components of NPM should be clarified by different methods in order to achieve better quality control of NPM and nutrient supplements. The bioactivities of pure compounds or crude extract form NPM have been evaluated by *in vitro* or *in vivo* experiments in this special issue.

Last but not least, with the development of pharmacy, more and more researchers focus their attention on pharmacokinetics in drug discovery. Pharmacokinetics including absorption, distribution, metabolism, and excretion is regarded as the foundation of new drug discovery. Pharmacokinetics encompasses a broad spectrum of experiment and connotation. Five articles devoted to pharmacokinetics and identification of metabolites from pure compounds or crude extract of NPM. The complexity of single herbs or compound preparations causes diverse pharmacokinetics, and these articles provide key information for researchers in the future studies.

All in all, the published research papers will contribute to the development, improvement, validation, and/or extension of application of analytical methodology in the natural medicine sciences and nutrition supplements. Quality control of NPM has to establish reasonable analytical methods for analyzing the active constituents in NPM in order to clarify their therapeutic basis and mechanism of action more clearly.

Shuang-Qing Zhang
Feng Wei
Yu-Ming Fan
Feng Sun
Ying-Yong Zhao
Shuhua Bai

References

[1] P. S. Xie and E. Wong, *Chinese Medicine-Modern Practice (Annals of Traditional Chinese Medicine)*, vol. 1, World Scientific Publishing, Singapore, 2005.

[2] E. H. Liu, L. Qi, K. Li, C. Chu, and P. Li, "Recent advances in quality control of traditional Chinese medicines," *Combinatorial Chemistry and High Throughput Screening*, vol. 13, no. 10, pp. 869–884, 2010.

[3] Y. Liang, P. Xie, and F. Chau, "Chromatographic fingerprinting and related chemometric techniques for quality control of traditional Chinese medicines," *Journal of Separation Science*, vol. 33, no. 3, pp. 410–421, 2010.

[4] L. Yin, B. Lu, Y. Qi et al., "Simultaneous determination of 11 active components in two well-known traditional Chinese medicines by HPLC coupled with diode array detection for quality control," *Journal of Pharmaceutical and Biomedical Analysis*, vol. 49, no. 4, pp. 1101–1108, 2009.

[5] Anonymous, *The Inner Canon of Emperor Huang*, Chinese Medical Ancient Books Publishing House, Beijing, China, 2003.

[6] L. Wang, G. Zhou, P. Liu et al., "Dissection of mechanisms of Chinese medicinal formula Realgar-Indigo naturalis as an effective treatment for promyelocytic leukemia," *Proceedings of the National Academy of Sciences of the United States of America*, vol. 105, no. 12, pp. 4826–4831, 2008.

[7] P. Li, L. W. Qi, E. H. Liu, J. Zhou, and X. D. Wen, "Analysis of Chinese herbal medicines with holistic approaches and integrated evaluation models," *Trends in Analytical Chemistry*, vol. 27, no. 1, pp. 66–77, 2008.

Hindawi Publishing Corporation
Journal of Analytical Methods in Chemistry
Volume 2013, Article ID 951319, 7 pages
http://dx.doi.org/10.1155/2013/951319

Research Article

Antitumor Molecular Mechanism of Chlorogenic Acid on Inducting Genes GSK-3β and APC and Inhibiting Gene β-Catenin

Ruoshi Xu,[1] Qiumei Kang,[2] Jie Ren,[2] Zukun Li,[2] and Xiaoping Xu[2]

[1] *West China School of Stomatology, Sichuan University, Chengdu, Sichuan 610041, China*
[2] *West China School of Pharmacy, Sichuan University, Chengdu, Sichuan 610041, China*

Correspondence should be addressed to Xiaoping Xu; 371748507@qq.com

Received 24 January 2013; Accepted 6 March 2013

Academic Editor: Yu-Ming Fan

Objective. Inhibiting gene β-catenin and inducting genes GSK-3β and APC, promoting the tumor cell apoptosis in Wnt pathway, by chlorogenic acid were discussed (CGA). *Method.* The different genes were scanned by the 4*44K mouse microarray chips. The effect of the three genes was confirmed by RT-PCR technique with CGA dosage of 5, 10, and 20 mg/kg. *Result.* The expression of GSK-3β and APC was upregulated in group of 20 mg/kg dosage ($P < 0.05$) and the expression of β-catenin was downregulated in the same dosage ($P < 0.05$). *Conclusion.* The results infer that the multimeric protein complex of β-catenin could be increased by CGA upregulated genes GSK-3β and APC, which could inhibit the free β-catenin into the nucleus to connect with TCF. So the transcriptional expression of the target genes will be cut to abnormal cell proliferation. It is probably one of the ways that can stop the tumor increase by CGA.

1. Introduction

Chlorogenic acid is the ester of caffeic acid and quinic acid in shikimate pathway, which is commonly found in some plants, such as honeysuckle, Cortex Eucommiae, Semen Coffea Arabica, and green tea. Chlorogenic acid has antibacterial, antiviral, clear free radicals, and antitumor effects [1]. In recent years, the effective anticancer activity and low toxicity of chlorogenic acid were constantly confirmed and draw the attention of the people [2–4]. Kurata et al. [5] showed that the inhibition of tumor cell proliferation effect of chlorogenic acid was enhanced with increasing dose; they speculated that this inhibition of tumor cell proliferation may be obtained by enhancing the activity of the DNA ladder and caspase-3 as well as increasing the expression of c-Jun. Gmnado and Feng et al. showed that the in vitro experiments show that the anticancer mechanism of CGA contains inhibition of cell growth, regulation of cell cycle, and induction of apoptosis pathways, such as (1) to reduce ROS expression to reduce cell growth/reproduction signal transduction pathway of NF-κB, AP-l, and MAPKs to reduce cancer cell viability, (2) to improve the activity of the NAD (P)H and GST, (3) to inhibit the expression of tetradecanoyl method wave alcohol acetate (TPA), in order to reduce the c-Jun NH2-terminal kinase, p38 kinase, and MAPK kinase-4 to prevent cancer transformation, and (4) to stimulate the expression of NF-E2-related factor and the activity of GST regulated by Nrf2 downstream cascade links antioxidant response element (ARE) to inhibit the growth of cancer cells [6, 7]. Chlorogenic acid is considered to be an effective cancer chemical repellant because of its significant inhibitory effect on colorectal cancer, liver cancer, and laryngeal [8]. In this paper, the biological gene chip technology was used to detect the variation of a whole set of gene sequences in breast tumor-bearing mice cells in the dynamic treatment cycle with CGA. The differential genes were screened by using genomics profiling, which was also the potential target gene associated with tumor disease according to the gene GO characteristic quality. Further verification testing must be designed, such as accurate quantitative PCR technology and

western blot technology, to verify the potential target point in the treatment of chlorogenic acid for tumors.

2. Instrument and Material

2.1. Tumor Lines and Animals. EMT-6 mice breast tumor lines were preserved by Key Laboratory of Transplant Engineering and Immunology, Ministry of Health, West China Hospital, Sichuan University. Female BALB/C mice, weighing 17~18 g, and originally purchased from Experimental Animal Center of Sichuan University, have been bred in the ordinary small animal housing of the same center where the feeding conditions comply with GB 14925-2001 with the ambient temperature of 19 ± 3°C and humidity of 55 ± 15%.

2.2. Instruments and Regents. CO_2 incubator (MCO-15AC, SANYO, JP), biological safety cabinets (NU-425, NUAIRE, USA), electronic balance (JY12001, Sartorius, USA), high-speed centrifuge (TGL-16G, Shanghai, China), PCR (ABI-9700, ABI, USA), hybridization oven (G2545A, Agilent, USA), scanner (G2565BA, Agilent, USA), spectrophotometer (ND1000, NanoDrop, Autoclave), Quantitative PCR instrument (Bio-Rad, USA), IQ2-cryogenic high-speed centrifuge, standard 96-well plate, Clean Bench, Sujing Group Aetna, ChemiDoc XRS + system medium (Gibco, China), Calf serum (Minhai, Lanzhou, China), 0.25% trypsin (Gibco, USA), double antibiotics (penicillin and streptomycin sulfate) (North China), Cy3 NHS ester (lot no. PA13105), GE healthcare, aaUTP Ambion (AM8436), Low RNA Input Linear Amplification Kit (lot no. 5184–3523), Gene Expression Hybridization Kit (lot no. 5188–5242), 5188–5327 Gene Expression Wash Buffer Kit (including wash buffers 1 and 2), Stabilization and Drying Solution (lot no. 5185–5979), Gasket slide (lot no. G2534-60003a), 4*44K mouse microarray, Hybridization CGAmber (lot no. G2534A), Agilent USA, RNeasy Mini kit (lot no. 74106), QIAGEN, USA. Trizol reagent, Invitrogen. DEPC, Oligo, 5x reaction buffer, Riblock Rnase Inhibitor, dNTP MIX, RevertAid M-MulV, 2*Taq Master Mix novoprotein, IQTM SYBR Green Supermix, Bio Rad. RevertAid First Strand cDNA Synthesis Kit, Fermentas, fluorescent imager DNA ladder, novoprotein, chlorogenic acid for injection (CGA, lot no. 061101, 30 mg), white powder for injection (content of 99.87%), offered by Sichuan Jiuzhang Biological Chemical Technology Development Co. Ltd. Docetaxel for injection (DX, lot no. 10112611, 20 mg), purchased from Jiangsu Hengrui Medicine Co. Ltd. IFNα-2b (20110908, 500 IU) purchased from Anhui Anke Biotechnology (Group) Co. Ltd. 0.9% saline (NS, lot no. A060418) (Kelun, Sichuan, China).

2.3. Preparation of Sample Solution. To use CGA solution, CGA freeze-dried powder was dissolved with sterile saline to make concentrations of CGA sample solution that were 1, 0.5, and 0.25 mg·mL^{-1}, respectively.

To use DX solution, 20 mg of DX injection powder was diluted with 1.5 mL of special solvent. To this, about 8.0 mL of saline was added to be stock solution of 2 mg·mL^{-1}. The stock solution was diluted to be sample solution with the concentration of 0.25 mg·mL^{-1} with saline before use.

To use IFNα-2b solution, IFNα-2b was diluted with 20 mL sterilized saline.

3. Methods

3.1. Preparation of Balb/c-EMT-6 Mice Model

3.1.1. Preparation and Subcultivation. The anabiotic EMT-6 breast tumor lines were implanted subcutaneously into the right forelimb of mice. The tumor-bearing mice were obtained until the tumor grew to 1 cm × 1 cm × 1 cm. Then took out the tumor, cleaned it with NS, weighed it, cut it into pieces, and placed it in a homogenizer. NS (about 1 : 4) was added to the homogenizer, and cell suspension was obtained after fast homogenate. 0.2 mL of the cell suspension was inoculated subcutaneously into the right forelimb of mice and was randomized.

3.1.2. Experiment Design. 30 female BABL/C mice were randomly divided into 6 groups ($n = 5$), including normal saline (negative) group, CGA high-dose group (20 mg·Kg^{-1}), CGA middle-dose group (10 mg·Kg^{-1}), CGA low-dose group (5 mg·Kg^{-1}), DX positive control group (5 mg·Kg^{-1}), and IFNα-2b positive control group (5 million U·Kg^{-1}).

After being inoculated for 24 hours, the NS group, CGA groups, and IFNα-2b positive control group were continuously subcutaneously administered for 12 days. The DX group was administered interday for 6 times. The tumors were taken after 24 hrs of the last administration, then weighed, cut into pieces, frozen in liquid nitrogen, and stored at −70°C after segmentation package.

3.2. Detection of the Level Changes of Cell Gene with Gene Chip

3.2.1. Total RNA Extraction. The lysis/binding buffer was added, 1 mL per 0.1 g tissue, for homogenate on ice to prevent RNA degradation. Adding homogenate additive (1/10) into the homogenate; the homogenate was vortexed, mixed, and kept on ice for 10 min. Then added phenol and chloroform mixture in the same volume as lysis, vortex them for 30 s, centrifuged them in 10,000 g for 5 minutes at room temperature. Added the absolute ethanol to the supernatant, then vortex and mixed them, made them going through the purification column repeatedly, centrifuged them at 10000 g for 15 seconds, discarded the supernatant. Added 350 μL Wash I, centrifuged them for 5 s to purify the column, then centrifuged at 10,000 g for 15 s, discarded filtrate. Added 10 μL DNase I and 70 μL buffer RDD to the film, placed them for 15 min, and then successively added 350 μL Wash 1 and 500 μL Wash 2, centrifuged them for 5 s, cleaned the purification columns two times. Each cleaning must be centrifugal at 10,000 g for 15 s and discard the filtrate. Added 100 μL 95°C preheated nuclease-free water to spin column and placed the spin column in a new collection tube after the second cleaning. The total RNA would be obtained after

Table 1: The Primer information of these four genes.

Gene symbol	Forward primer	Reverse primer
GSK-3β	ACC ATC CTT ATC CCT CCA	CAg Aag Cgg CgT TAT Tg
APC	CAC TgA gAA TAA ggC TgA C	TTC CgT AAT ATC CCA CC
β-Catenin	ggT gCT ATT CCA CgA CT	CCC TTC TAC TAT CTC CTC C
GAPDH	CAA GGT CAT CCA TGA CAA CTT TG	GTC CAC CAC CCT GTT GCT GTA G

centrifuging at the maximum speed for 30 s and then stored at −70°C.

3.2.2. Purification of Total RNA. QIAGEN RNeasy Kit was used for further extraction and purification of the total RNA. 100 μL RNase-free water was added to dissolve the total RNA, then mixed with 350 μL buffer RLT and 250 μL ethanol. (The preparation of RLT: 14 mL original RLT can be added to 140 μL of β-mercaptoethanol.) Transferred the sample to the RNeasy column, centrifuged at 10000 g for 30 s, and abandoned filtrate. Clean the RNeasy minicolumn twice with 500 μL buffer RPE, centrifuged at 10,000 g for 30 s and 2 min, respectively, and discard the filtrate. Add 40 μL RNase free water to the column, and centrifuge 10000 g for 1 min. Repeat the operation once more; the purified RNA was prepared.

3.2.3. Total RNA Quality Testing. The quality of total RNA can be determined with agarose gel electrophoresis. Prepare the electrophoresis buffer 50x TAE, which was processed with DECP and autoclaves → a 1% agarose gel was prepared after adding on amount of agarose to lx TAE electrophoresis buffer → run on a gel for 15 min, then observe and picture the gel over the gel imager → lab-on-chip.

3.3. Validation of Protein Expression of Specific Genes by Fluorescence Quantitative PCR

3.3.1. Primers and Reaction Conditions. The primers were designed through the 01190 software and synthesized by Sangon Biotech (Shanghai). The primer information of these four genes was shown in Table 1. With the template of sample cDNA, the differentially expressed genes were verified to use SYBR Green by real-time fluorescent quantitative PCR. The conditions of the q-PCR reactions were subjected to 94°C for 10 min, followed by 40 cycles at 94°C for 15 s and 54.5°C for 30 s, and finally 72°C for 45 s. The expression levels of GSK-3β, APC, and β-catenin in test samples were detected with GAPDH as the reference gene and calculated by $2^{-\Delta\Delta CT}$ relative quantification method, which showed the differential expression of different groups compared to the NS group.

3.3.2. RNA Extraction. After isinfecting the reagent bottle, boxes, and gloves under UV light for 30 min, the tissues were homogenized in the trizol reagent. The homogenate was incubated at 15–30°C for 5 min, to which chloroform was added, then vortex them for 15 s, and centrifuged separating the mixture for 15 min in low temperature. Transferred the upper supernatant into another tube, added 0.5 mL isopropanol and mixed them at 15–30°C, incubated them for 10 min, 4°C, then centrifuged them at 12000 g for 10 min, discarded supernatant, and added 1 mL 75% ethanol into the tube, centrifuged them at 7500 g for 5 min, discarded the supernatant, and dried them in the air for 3–5 min. Added 20 μL DEPC deionized water to dissolve the RNA and stored them at −70°C.

3.3.3. RNA Quality Testing

(1) *OD Value Detection.* A260/A280 value was determined by UV with 1 μL extracted from each of RNA which was diluted to 100 μL with TE buffer.

(2) *RNA Formaldehyde Electrophoresis.* The voltage of conditions electrophoresis was 80 V, and running time was 40 min. The RNA samples prepared in Section 3.3.2 were diluted with DEPC water suitably and mixed with an equal volume of sample buffer, then heated for 4 min in boiling water, cooled on ice for 2 min, and then centrifuged in 1200 rpm for 5 s. The sample was spotted on plate to be carried on the electrophoresis.

3.3.4. The Synthesis of cDNA. The RevertAid First Strand cDNA Synthesis Kit was used for reverse transcription. The total reaction volumes of RT-PCR reactions were 20 μL. The system consists of 2 μL RNA, 1 μL Oligo(dT)18 primer, 9 μL RNase-free water, 4 μL 5x reaction buffer, 1 μL Riblock Rnase Inhibitor, 2 μL 10 mM dNTP MIX, and 1 μL RevertAid M-MulV.

The reverse transcription system liquids of the above were subjected to 42°C, 60 min, and 70°C, 5 min, in a PCR instrument. The reaction products were stored at −80°C for long-term preservation.

3.3.5. The Test of RT-PCR Amplification Products. Briefly, the presence or absence of the only bands was observed at 496 bp as the standard showed the quality of cDNA. If there is one and only one band, the PCR product cDNA was qualified, and Q-PCR can be the next. The voltage was 130V, and the analysis time was 25 min.

The RT-PCR amplification system had 25 μL liquid of total reaction volumes, in which consists of 10 μL 2x Taq Master Mix, 2 μL cDNA, 0.75 μL Forward GAPDH primer pair and 0.75 μL Reverse GAPDH primer, and 11.5 μL RNase-free water. PCR reactions were subjected to 94°C for 10 min, followed by 40 cycles at 94°C for 15 s and 54.5°C for 30 s and finally 72°C for 45 s.

3.3.6. Real-Time Fluorescent Quantitative PCR. 1 μL cDNA was diluted to 100 μL with sterile water on standby. Gene

Table 2: The reaction system of q-PCR ($n = 3$).

Composition	Plus the amount
IQ SYBR Green Supermix	10 μL
Forward primer	1 μL
Reverse primer	1 μL
cDNA	2 μL
Nase-free water	6 μL
Total volume	20 μL

primers, F and R, were diluted 20-fold, respectively. This reaction system was shown in Table 2. Each sample should go through the three parallel tests, taking the mean value to calculation.

3.3.7. SYBR Green I Reaction Designed and Optimized

(1) *Optimization of the Annealing Temperature.* By setting a certain temperature range, we can screen the optimal annealing temperature by real-time quantitative PCR reactions. The melting curve can be used to assess the specificity of the reaction in the quantitative PCR instrument. If there are multiple peaks on the melting curve, which indicates nonspecific products such as primer dimer, they are amplified along with specific products simultaneously, which also indicates the primers of the reaction need to be redesigned.

(2) *Construction of the Standard Curve.* cDNA was selected as the template and set eight 10-fold dilution series of points each dilution was repeated three times. The equation of the linear regression line has obtained the logarithmic value of template initial concentration as the abscissa and the CT value as the vertical coordinate. Standard curve correlation coefficient (r) or the coefficient of determination (R^2) can be used to evaluate the degree of linearization with the specific requirements of $r > 0.990$ and $R^2 > 0.980$.

4. Results

4.1. Results of CGA Suppression of the Mice Breast Cancer (EMT-6). See Table 3.

4.2. Electrophoresis Graph and Lab-on-Chip. As is shown in Figure 1, the luminance ratios of 28 s and 18 s are greater than or equal to 2 in electrophoresis graph, which preliminary determines that total RNA was qualified. The result has shown that the quality of RNA extracted from each group of tumor tissue samples meets the requirement of further detection of gene chip. Then the differential genes closely related to the tumor cell suppression in the course of treatment were screened by the time series analysis, GO analysis, and pathway analysis and validated with q-PCR.

4.3. The Quality Results of RNA, cDNA

(1) *The Results of OD Values.* As is shown in Table 4, the A260/A280 value of RNA was from 1.63 to 2.18, which meets the quality requirements of RNA.

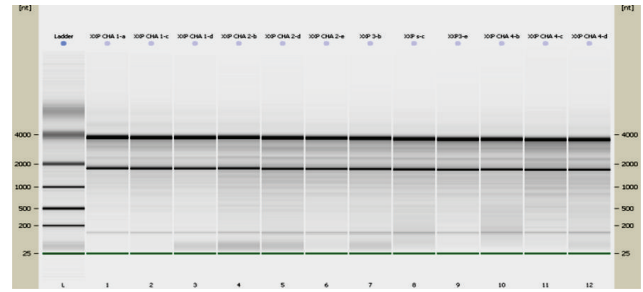

Figure 1: The EC of CGA 1–4.

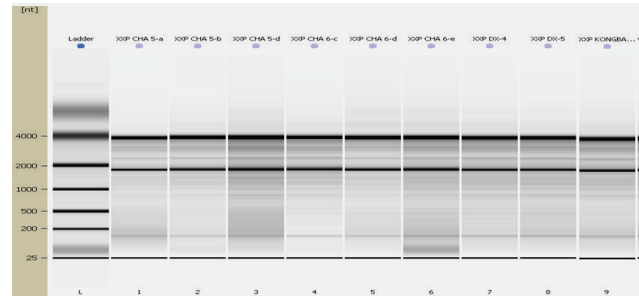

Figure 2: The EC of CGA 5-6, DX, and blank.

(2) *Formaldehyde Electrophoresis of RNA.* As is shown in Figure 4, the formaldehyde denaturing electrophoresis showing the 28S and 18S were clear without DNA impurity band and degradation RNA, which meets the requirements of the experiment.

(3) *Results of cDNA Quality Test.* As is shown in Figure 5, there is only one band at 496 bp, which indicates that the quality of the PCR product meets the requirements.

4.4. PCR Expression of GSK-3β, APC, and β-Catenin. The PCR expression of GSK-3β, APC, and β-catenin was shown in Figure 6 in the tumor tissue of Balc-b/EMT-6 tumor-bearing mice after the treatment of DX (5 mg/kg), IFN (5×10^6 U·kg-1), CGA (20 mg/kg), CGA (10 mg/kg), and CGA (5 mg/kg) for 12 days. Compared with the blank group, the expression of GSK-3β and APC was upregulated in group of 20 mg/kg dosage ($P < 0.05$) and the expression of β-catenin was downregulated in the same dosage group ($P < 0.05$).

5. Discussion

(1) As shown in Table 3, compared to the positive control group of cytotoxic anticancer drugs DX, biological response modifier (BRM) IFN groups, and the negative group of NS, the three dosag of the CGA groups showed better antitumor effect ($P < 0.05$); especially the inhibition rate of the 20 mg·kg^{-1} dose group was more than 50%, which was equivalent to 59.92% of the DX group and 40.80% of the IFN group. It is suggested that chlorogenic acid should be able to be a new good anticancer agent in future clinical application.

(2) According to the data of the different time points in the inhibitory process acquired with the total RNA that was qualified in Figures 1, 2, and 3 the differential genes closely

Table 3: Results of CGA suppression of the mice breast cancer.

Groups	Dose ($mg \cdot kg^{-1}$)	Animals	Average tumor weight (g)	The average tumor inhibition rate (%)
DX	5	5	$0.780 \pm 0.244^{**}$	59.92
IFN	5 million $U \cdot kg^{-1}$	5	$1.152 \pm 0.254^{**}$	40.80
CGA	5	5	$1.326 \pm 0.254^{**}$	31.86
CGA	10	5	$1.222 \pm 0.363^{**}$	37.20
CGA	20	5	$0.968 \pm 0.633^{**}$	50.26
Negative	—	5	1.946 ± 0.233	—

Table 4: OD value of RNA.

No.	Group 1	Group 2	Group 3	Group 4	Group 5	Group 6
1	1.86	2.08	2.18	2.07	2.18	2.15
2	1.95	2.09	2.17	2.09	2.04	2.16
3	2.05	2.12	2.23	2.09	1.90	2.17
4	1.63	2.07	2.14	2.10	1.94	2.19
5	2.15	2.06	2.18	2.13	1.95	2.17

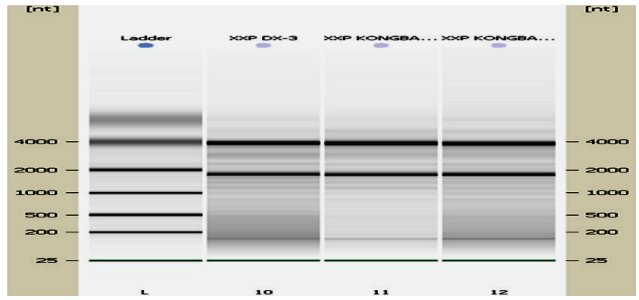

Figure 3: The EC of DX3 and blank.

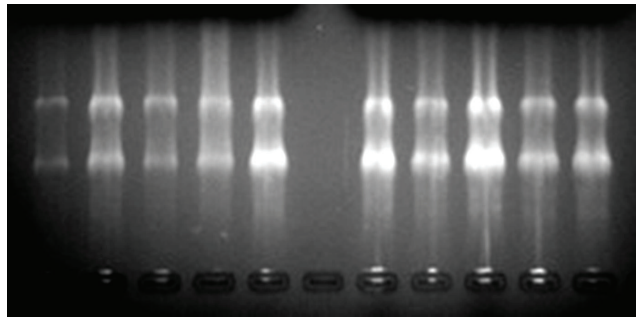

Figure 4: RNA electrophoresis.

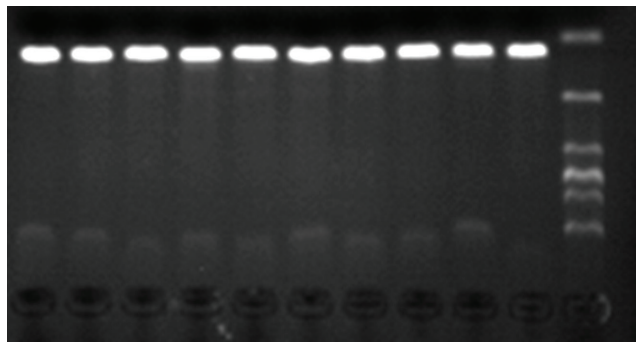

Figure 5: cDNA electrophoresis.

related to the Wnt pathway in the course of treatment were screened by the time series, GO, and pathway. The different genes which were connected with CGA treatment were extracted and were confirmed with q-PCR. The downward trends of the tumor genomes 18 and 21 were screened by the logarithm of standardization and fitting the change course of genes with similar trends; the genetic trend was closer to the fitted values of P smaller, such as Figures 7(a) and 7(b).

(3) As shown in Figure 7(a), the trend of genome 18 was confirmed to the anticancer process of CGA. According to the analysis of KEGG signaling pathway and the characteristics of GO in genome 18, some downregulated genes were found which are related to the tumor suppression pathway, such as BdnF mediated MAPK, Cflar, Cln3 Ddit3 Notch2 Rps6, Sox9, Spn, and Ppp1r13l. The gene 21 time sequence diagram relates to the Wnt pathway, mTOR pathway, the Notch pathway, and some immune-related pathways, such as B cell receptor pathway, T-cell receptor pathway, and metabolic pathway. It was inferred that CGA had a multipathway to inhibit the tumor growing up.

(4) Because our animal model was a breast cancer (EMT-6/BALB-C), we focused on the influence of Wnt pathway (shown in Figure 8) which was a special pathway that the breast cancer had. In particular, the gene glycogen synthase kinase 3(GSK-3β) and downstream gene ubiquitin ligase E3(APC) were upregulated. And the two kinds of genes had closed relationship, in which the gene APC was upregulated by upstream gene GSK-3β. And then, both genes could cause the down-stream gene β-catenin to downregulate directly in the Wnt pathway. As you know, the cancer will be developing when the gene β-catenin expression was upregulated. What is the gene β-catenin? From its GO searching revealed, β-catenin is a multifunctional protein, which can assist the cells react to extracellular signal and changes by interaction with the cytoskeleton. This protein acts as a transcription (transcription) factor in the nucleus to promote cell division genes. The accumulation of β-catenin would lead to abnormal activation of the downstream transcription factors after transferring to the nucleus, which mainly cause tumor.

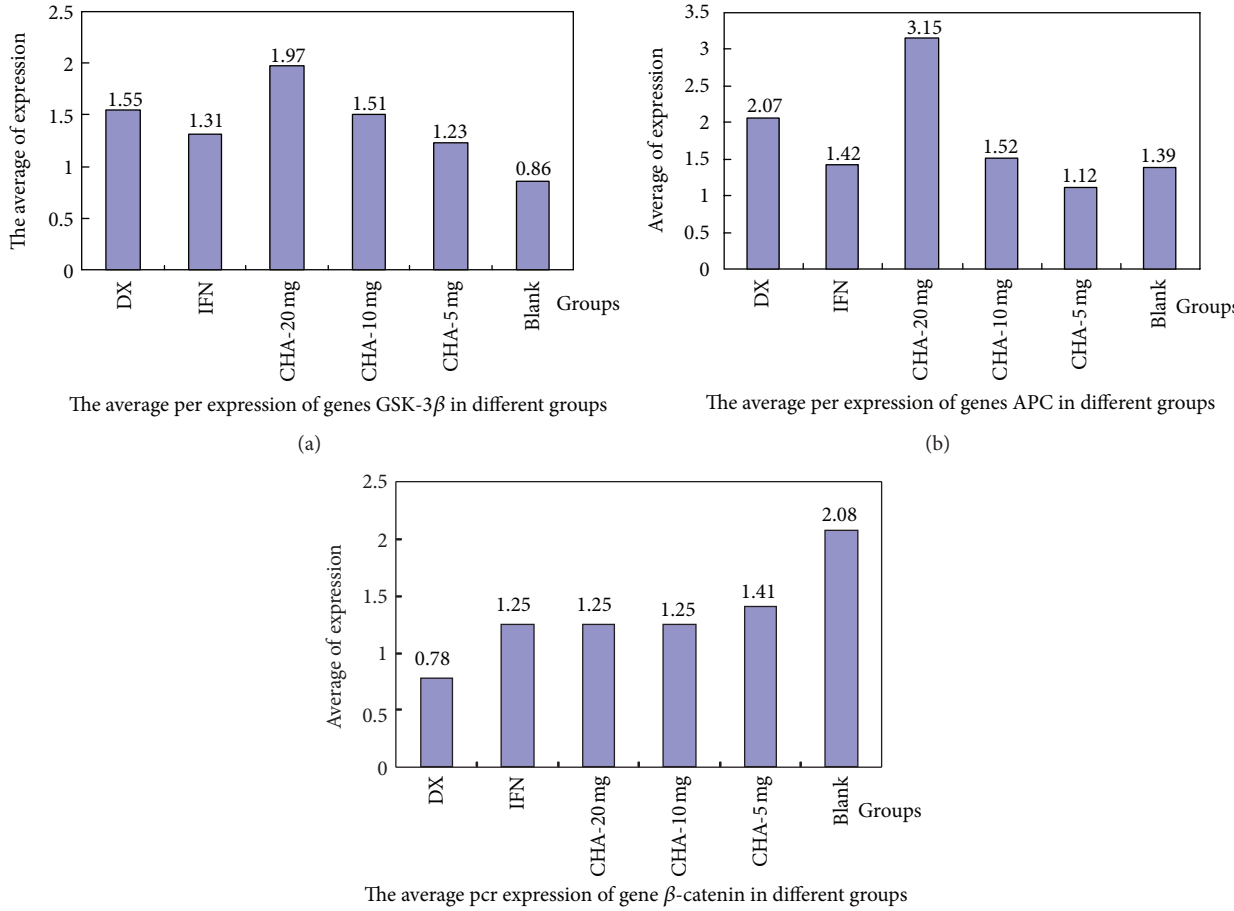

Figure 6: The average PCR expression of different genes in different groups. (a) GSK-3β, (b) gene APC, and (c) gene β-catenin.

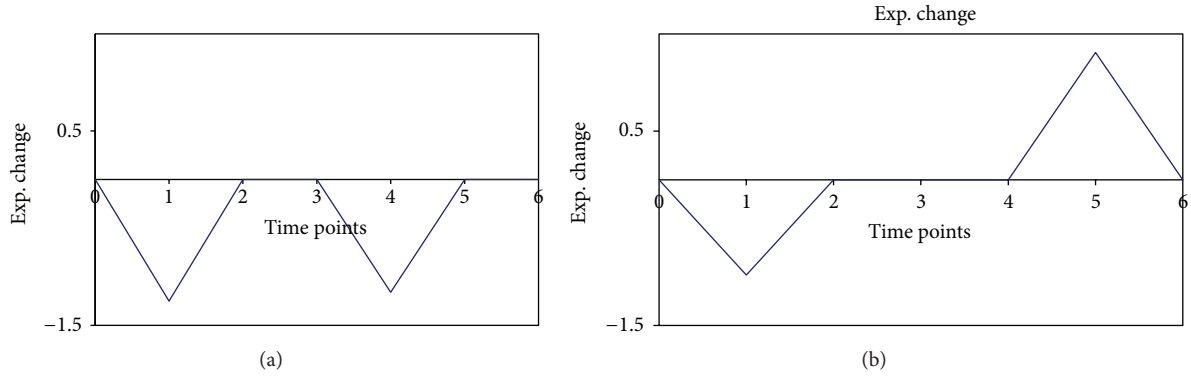

Figure 7: The expression trend graphs of gene 18 and gene 21 ($P = 0$).

So, it is suggested that the β-catenin inhibited was one of the ways to inhibit tumor growth. On the other hand, the upregulation of GSK-3β is a multifunctional serine/threonine class of protein kinase, which plays an important role in the Wnt/wingless, PI3-kinase, and Hedgehog signaling pathway with the physiological functions including transcriptional activation, cell proliferation, and cell differentiation, cell movement. It can phosphorylate shaft protein and β-catenin, cause the degradation of β-catenin protein, and thereby inhibit the activation of the pathway. The activated APC plays an important role in promoting complexes degradation in a fast, efficient, and highly selective way in the anaphase cell cycle, which also can phosphorylate shaft protein and β-catenin, cause the degradation of β-catenin

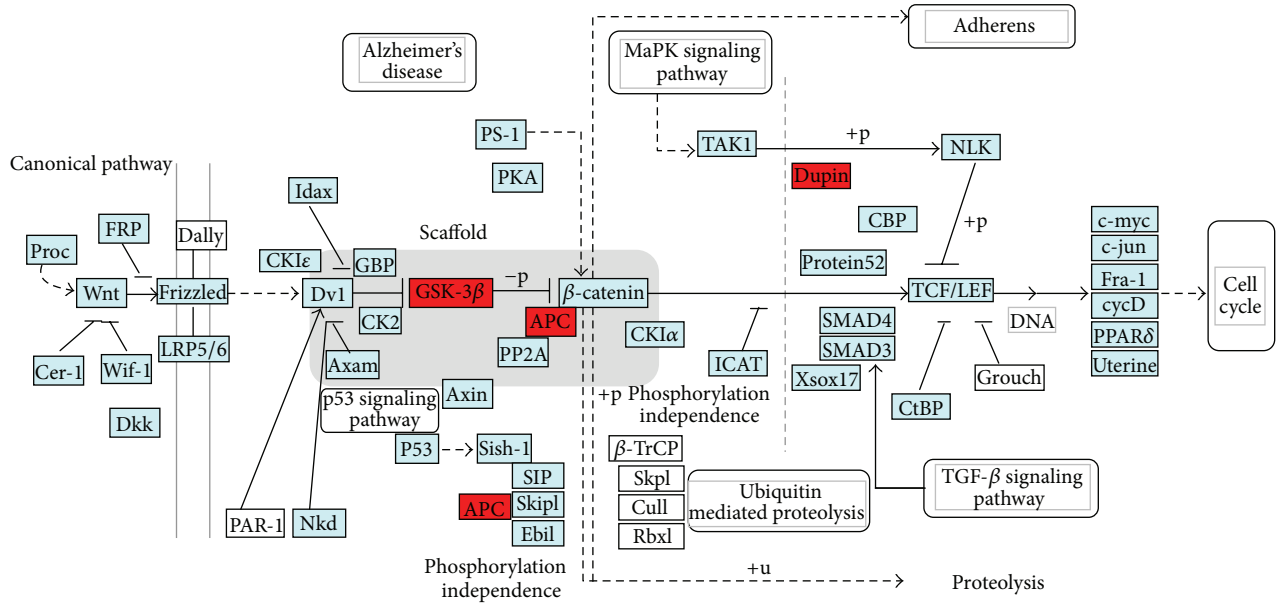

Figure 8: Wnt signaling pathway.

protein, and thereby inhibit the activation of the pathway. So the activation of GSK-3β and APC and downregulation of β-catenin in the group of CGA suggested that CGA could inhibit tumor by activating GSK-3β and APC.

(5) As shown in Figure 6(a), the regulation confirmed by Q-PCR in treatment process of CGA for EMT-6 breast cancer indicates groups of CGA in each dose and DX can activate expression of GSK-3β, especially the CGA 20 mg/kg group and the DX group can significantly upregulate GSK-3β ($P < 0.05$). As shown in Figure 6(b), groups of CGA at 20 mg/kg and 10 mg/kg and DX can activate expression of APC, but groups of CGA at 5 mg/kg dose little to upregulation. As shown in Figure 6(c), DX group, IFN group and CGA 20 mg/kg group was inhibited gene β-catenin.

6. Conclusion

It is suggested that affecting the gene expression of GSK-3β, APC, and β-catenin by chlorogenic acid in Wnt pathway was one of the targets in the multipathway to antitumor of CGA.

Conflict of Interests

All authors are researchers of Sichuan University and have no conflict of interests. Some parts of the experiment were entrusted to the third party but not sponsored by this party. This statement is made in the interest of full disclosure and not because the authors consider this to be a conflict of interests.

Acknowledgments

The Sichuan Province Science and Technology Support Project Fund 2011SZ0131 supported this work. The authors would like to show great thanks to Hongwei Liu for his great help.

References

[1] J.-H. Liu and A.-Y. Qiu, "Chlorogenic acid extraction and purification and application prospects," *Cereals & Oils*, no. 9, pp. 44–446, 2003.

[2] D. G. Dorrell, "Chlorogenic acid content of meal from cultivatial sunflower," *Crop Science*, no. 16, pp. 422–426, 1976.

[3] M. Shimizu, N. Yoshimi, Y. Yamada et al., "Suppressive effects of chlorogenic acid on N-methyl-N-nitrosourea- induced glandular stomach carcinogenesis in male F344 rats," *Journal of Toxicological Sciences*, vol. 24, no. 5, pp. 433–439, 1999.

[4] K. Matsunaga, M. Katayama, K. Sakata et al., "Inhibitory effects of chlorogenic acid on azoxymethane- induced colon carcinogenesis in male F344 rats," *Asian Pacific Journal of Cancer Prevention*, vol. 3, pp. 163–166, 2002.

[5] R. Kurata, M. Adachi, O. Yamakawa, and M. Yoshimoto, "Growth suppression of human cancer cells by polyphenolics from sweetpotato (*Ipomoea batatas L.*) leaves," *Journal of Agricultural and Food Chemistry*, vol. 55, no. 1, pp. 185–190, 2007.

[6] S. N. Rylova, A. Amalfitano, D. A. Persaud-Sawin et al., "The CLN3 gene is a novel molecular target for cancer drug discovery," *Cancer Research*, vol. 62, no. 1, pp. 801–808, 2002.

[7] R. C. Pereira, A. M. Delany, and E. Canalis, "CCAAT/enhancer binding protein homologous protein (DDIT3) induces osteoblastic cell differentiation," *Endocrinology*, vol. 145, no. 4, pp. 1952–1960, 2004.

[8] F. Pellati, S. Benvenuti, L. Magro, M. Melegari, and F. Soragni, "Analysis of phenolic compounds and radical scavenging activity of *Echinacea spp.*," *Journal of Pharmaceutical and Biomedical Analysis*, vol. 35, no. 2, pp. 289–301, 2004.

Hindawi Publishing Corporation
Journal of Analytical Methods in Chemistry
Volume 2013, Article ID 658596, 6 pages
http://dx.doi.org/10.1155/2013/658596

Research Article

Determination of Flavonoids, Phenolic Acids, and Xanthines in *Mate* Tea (*Ilex paraguariensis* St.-Hil.)

Mirza Bojić,[1] Vicente Simon Haas,[2] Darija Šarić,[1] and Željan Maleš[1]

[1] *Faculty of Pharmacy and Biochemistry, University of Zagreb, A. Kovačića 1, 10000 Zagreb, Croatia*
[2] *Universidade Regional Integrada, URI-Farma, Rua Universidade das Missões 464, 98802-470 Santo Ângelo, RS, Brazil*

Correspondence should be addressed to Mirza Bojić; mirza.bojic@gmail.com

Received 25 February 2013; Revised 8 May 2013; Accepted 12 May 2013

Academic Editor: Feng Sun

Raw material, different formulations of foods, and dietary supplements of *mate* demands control of the content of bioactive substances for which high performance thin layer chromatography (TLC), described here, presents simple and rapid approach for detections as well as quantification. Using TLC densitometry, the following bioactive compounds were identified and quantified: chlorogenic acid (2.1 mg/g), caffeic acid (1.5 mg/g), rutin (5.2 mg/g), quercetin (2.2 mg/g), and kaempferol (4.5 mg/g). The results obtained with TLC densitometry for caffeine (5.4 mg/g) and theobromine (2.7 mg/g) show no statistical difference to the content of total xanthines (7.6 mg/g) obtained by UV-Vis spectrophotometry. Thus, TLC remains a technique of choice for simple and rapid analysis of great number of samples as well as a primary screening technique in plant analysis.

1. Introduction

Mate tea (Sp. *yerba mate*, Port. *Erva-mate*) consists of well cut, dried, aerial parts or leaves of *Ilex paraguariensis* St.-Hil. (Aquifoliaceae) shrub. It contains methylxanthines, mainly caffeine, phenolic acids, and saponins and is used as everyday substitution for coffee (psycho stimulant, analeptic) in the south of Brazil, North of Argentina, Oriental Paraguay, and Uruguay. Besides beneficial effects on cardiovascular system, it has significant antioxidant capacity and can be used for the management of weight in obesity [1–3].

Thin layer chromatography (TLC) often represents first-choice technique for samples of plant origin as results can be easily visualized. This technique has been successfully employed for analysis of flavonoids and phenolic acids in wine, propolis, and different medicinal plants [4]. Several studies comparing TLC and HPLC have shown that there is no statistical difference between these methods, and advantage due to lower cost is given to TLC [5, 6].

Determination of xanthines as the main constituents is time consuming titration [7]. Although flavonoids present ubiquitous class of compounds, Bastos et al. [8] did not find any of the analyzed flavonols in *mate* tea using HPLC technique. Thus, the goal of this work was to identify and quantify polyphenolic and xanthine components of *mate* densitometrically using HPTLC plates and compare the results obtained with the content of total polyphenols and xanthines based on UV-Vis spectrophotometry.

2. Experimental Section

2.1. Reagents. All standards were purchased from Sigma Aldrich (Germany) and organic solutions from Kemika (Croatia). The sample of *mate* powder (dried aerial parts) was obtained from Santo Ângelo, RS, Brazil.

2.2. Standard Solutions. Stock solutions of phenolic acids (chlorogenic, caffeic, ferulic, and *p*-coumaric acid), flavonoids (rutin, quercetin, naringenin, and kaempferol), and xanthines (caffeine, theobromine) were prepared by dissolving standards with methanol (polyphenols) or water (xanthines) to obtain concentration of 1.0 mg/mL. Standard solutions were prepared by dissolution with methanol to 0.1 mg/mL.

Table 1: Identification parameters of polyphenolics and xanthines: retention factor, color of band under 366 nm, and spectra after spraying with aluminium chloride (not applicable for caffeine and theobromine).

Bioactive compound	TLC spectra *in situ*	Structure
Chlorogenic acid $R_F = 0.40$ $\lambda_{max} = 328$ nm Colour: blue	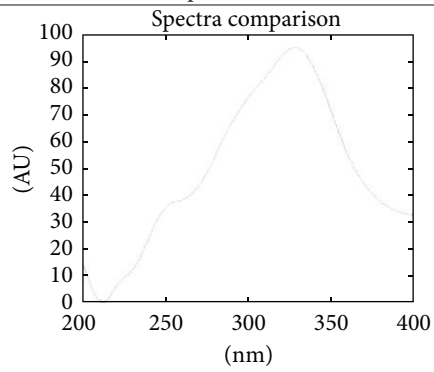	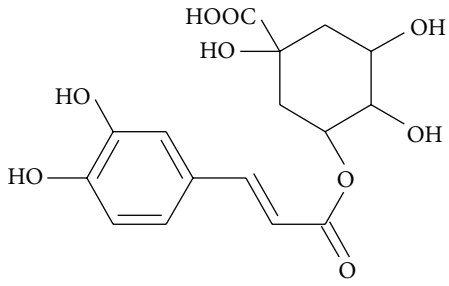
Ferulic acid $R_F = 0.82$ $\lambda_{max} = 330$ nm Colour: blue	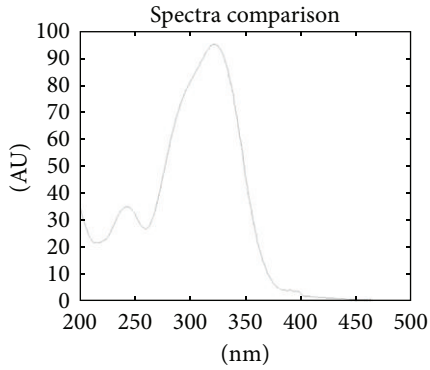	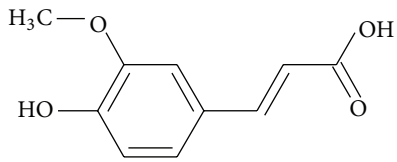
Caffeic acid $R_F = 0.30$ $\lambda_{max} = 330$ nm Colour: intensive blue	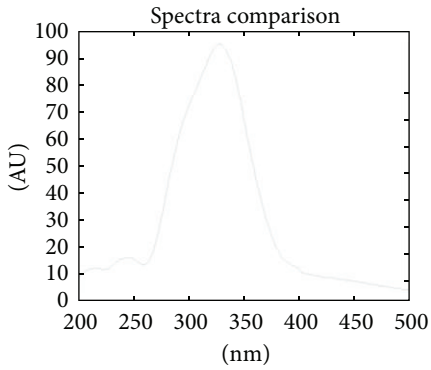	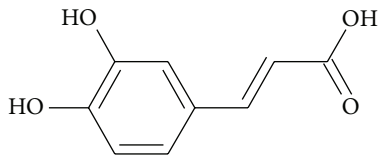
p-Coumaric acid $R_F = 0.77$ $\lambda_{max} = 312$ nm Colour: no colour	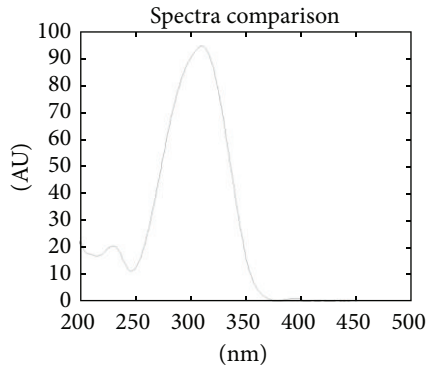	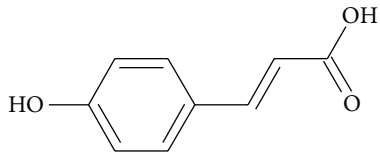

Table 1: Continued.

Bioactive compound	TLC spectra *in situ*	Structure
Naringenin $R_F = 0.75$ $\lambda_{max} = 293$ nm Colour: green	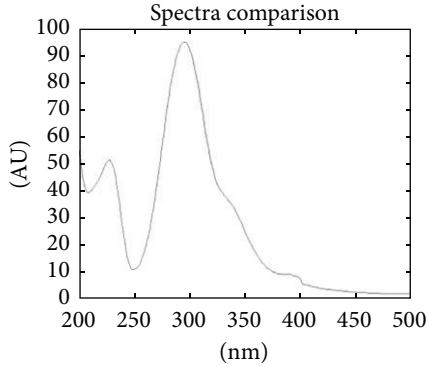	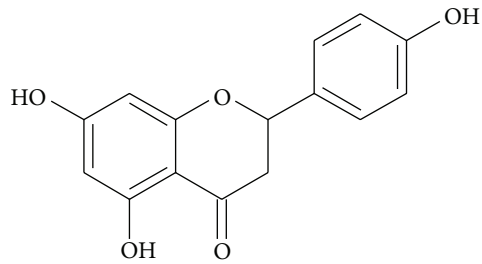
Rutin $R_F = 0.49$ $\lambda_{max} = 329$ nm Colour: green	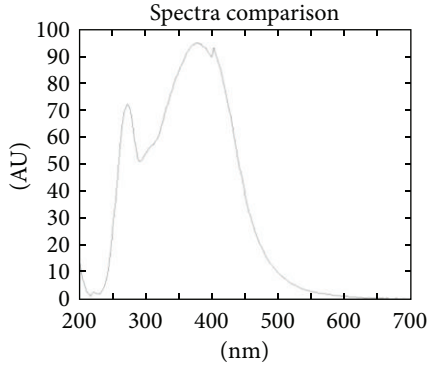	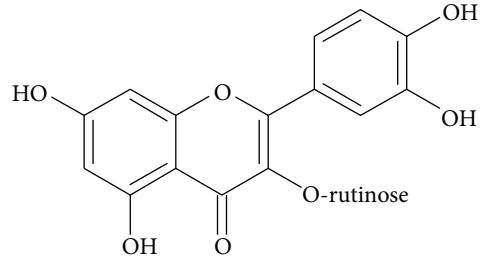
Quercetin $R_F = 0.34$ $\lambda_{max} = 419$ nm Colour: light green	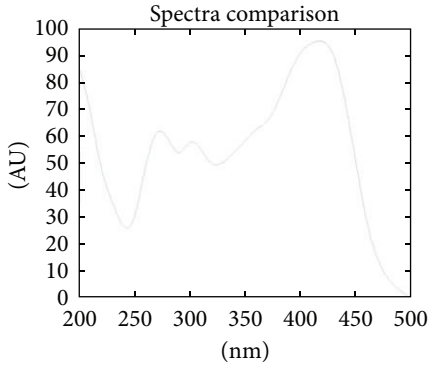	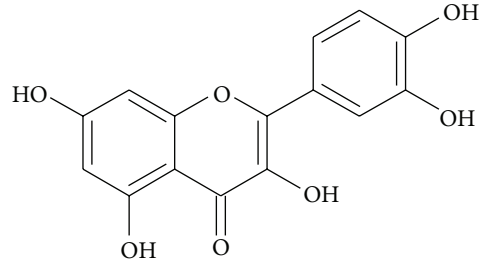
Kaempferol $R_F = 0.65$ $\lambda_{max} = 390$ nm Colour: dark green	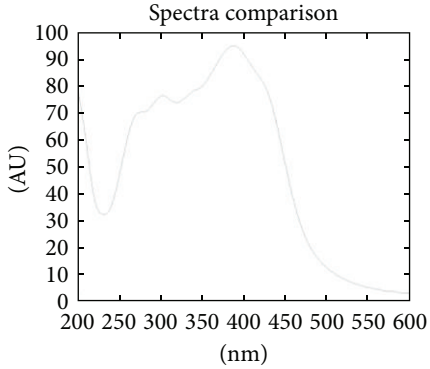	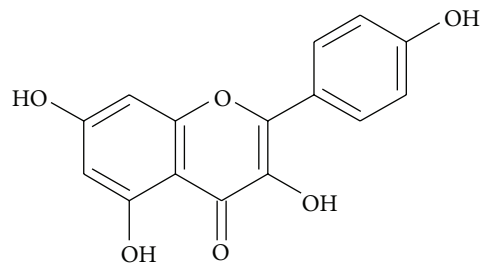

Table 1: Continued.

Bioactive compound	TLC spectra *in situ*	Structure
Caffeine λ_{max} = 275 nm R_F = 0.55	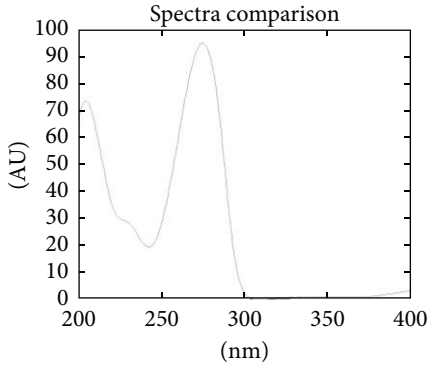	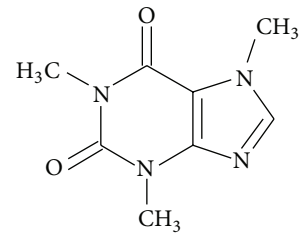
Theobromine λ_{max} = 275 nm R_F = 0.47	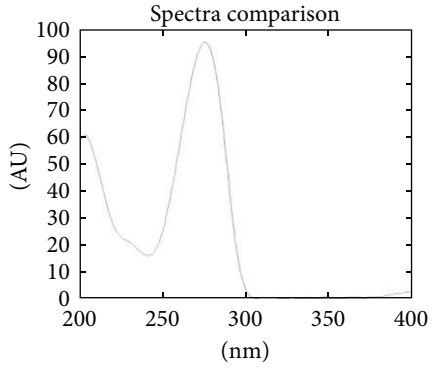	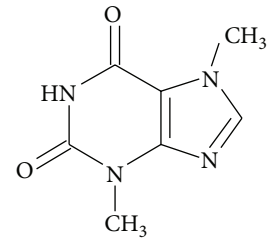

2.3. Aqueous Solution of Yerba Mate. 1.0 g of *erva* was boiled in 100 mL of water for 30 minutes and filtered. 50 mL of this solution was evaporated, and the residues were dissolved in 10 mL of methanol.

2.4. Hydrolyzed Solution of Yerba Mate. 0.5 g of *yerba mate* was refluxed for 30 min. with 20 mL of acetone, 2 mL 25% hydrochloric acid, and 1 mL 0.5% water solution of hexamethylenetetramine. Obtained hydrolyzate was filtered, and crude parts were once again refluxed with acetone for 10 minutes. The filtrates were combined and diluted to 100 mL with acetone. 20 mL of acetone solution was mixed with 20 mL of water and extracted once with 15 mL and 3 times with 10 mL of ethyl acetate. Combined ethylacetate phases were washed with 40 mL of water and filtered through cotton. Filtrate was diluted with ethylacetate to 50 mL. This solution was used for HPTLC analysis and spectrophotometric determination of total flavonoids.

2.5. Spectrophotometric Analysis. Total content of flavonoids was determined by Christ-Müller's method, phenolic acids according to European Pharmacopoeia, and xanthines by the method suggested by International Office of Cocoa, Chocolate and Sugar Confectionery [7, 9, 10]. Briefly flavonoids were determined after acid hydrolysis (see Section 2.4.) as liberated aglycones spectrometrically at 425 nm as a complex with $AlCl_3$ in a methanol-ethyl acetate-acetic acid medium.

For the purpose of phenolic acids determination 0.2 g of *mate* powder was refluxed with 190 mL of 50% ethanol on the water bath. Total phenolic acids were determined by measuring the absorbance at 505 nm of the complex formed between phenolic acids and sodium molybdate—sodium nitrite as an equivalent of rosmarinic acid.

Aqueous solution of *yerba mate* was used for the determination of xanthines. Total xanthines were determined after clarification with lead acetate spectrometrically at 272 nm as an equivalent of theobromine.

2.6. TLC Densitometry. Chloroform : methanol : formic acid in volume ratio 44.1 : 2.5 : 2.15 was used as mobile phase for aglycones, and ethyl acetate : formic acid : acetic acid : water in volume ratio 100 : 11: 11 : 26 was used for glycosides [4, 11]. System used for xanthines development was ethyl acetate, methanol and water in volume ratio 40 : 5.4 : 4 [11]. Merck HPTLC plates (Silica Gel 60 F_{254}, 10 × 20 cm) were used as stationary phase. Samples were applied using CAMAG Linomate V semiautomatic sample applicator. After development the HPTLC plates were dried and sprayed for the analysis of polyphenolics with 1% ethanolic solution of $AlCl_3{\cdot}6H_2O$. Plates were recorded at 254 and 366 nm. Identification and quantification were performed by TLC densitometry using CAMAG TLC Scanner 3 and WinCATS software version 1.3.4.

2.7. Statistical Analysis. The results of TLC densitometry and spectrophotometric analysis were compared using Student's *t*-test. Statistical analysis was performed using Microsoft Office Excel 2003.

Table 2: Results of quantification of individual flavonoids, phenolic acids, and xanthines.

Bioactive compound	Calibration curve	Fraction of flavonoids[1] (mg/g)	Fraction of phenolic acids[2] (mg/g)	Aqueous solution (mg/g)
Chlorogenic acid	$A = 3168.1m + 204.2$ ($r^2 = 0.9865$)	2.1	21.6	3.0
Caffeic acid	$A = 3313.2m - 475.6$ ($r^2 = 0.9955$)	1.5	nd	nd
Rutin	$A = 6223.4m - 649.8$ ($r^2 = 0.9833$)	5.2	6.8	2.3
Quercetin	$A = 6902.1m + 723.7$ ($r^2 = 0.9788$)	2.2	nd	nd
Kaempferol	$A = 9349.3m - 732.7$ ($r^2 = 0.9681$)	4.5	nd	nd
Caffeine	$A = 2328.8m + 6439.2$ ($r^2 = 0.9807$)	na	na	5.4
Theobromine	$A = 3405.5m + 1535.9$ ($r^2 = 0.9667$)	na	na	2.7

[1]Hydrolyzed fraction of flavonoids, [2]nonhydrolyzed fraction of phenolic acids used for the spectrophotometric analysis according to the European pharmacopoeia, and nd: not detected, na: not applicable.

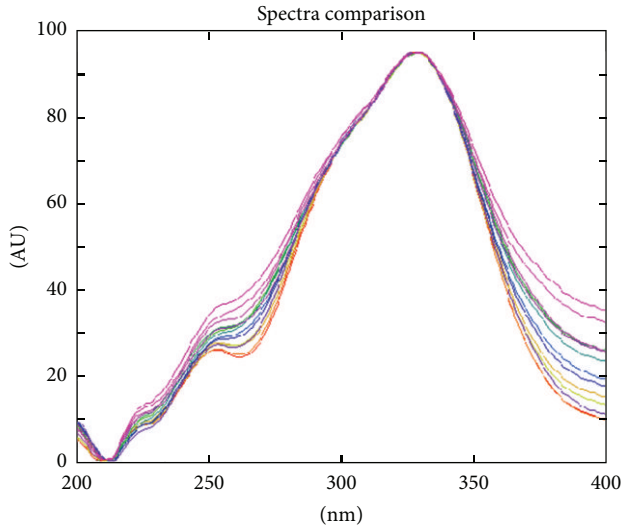

Figure 1: Identification of chlorogenic acid—overlapping spectra of standards and *erva* samples.

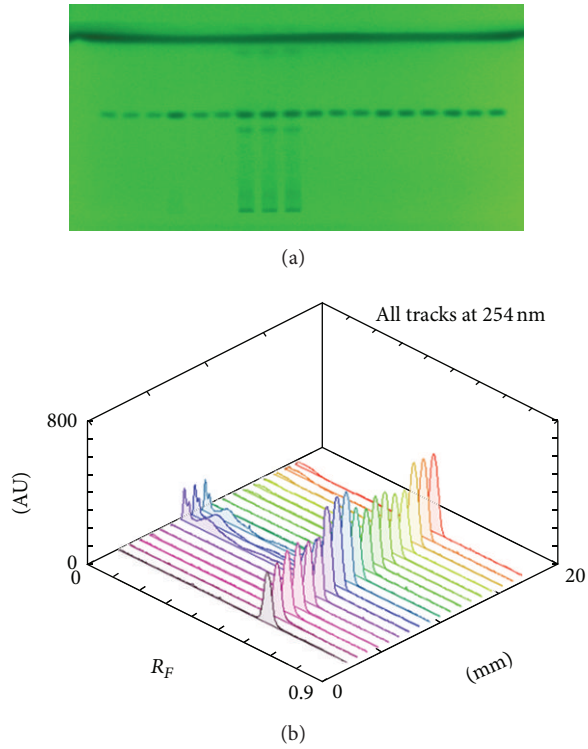

Figure 2: Chromatographic plate (a) and 3D chromatograms (b) of caffeine standard (six tracks from the left and nine from the right) and sample of *mate* (middle part).

3. Results and Discussion

The total content of flavonoids determined by Christ-Müller's method was 3.0 mg/g (RSD = 0.5%, $n = 3$), phenolic acids determined according to Ph. Eur. method 55.1 mg/g (RSD = 0.6%, $n = 3$), and xanthines by IOCCSC method 7.6 mg/g (RSD = 0.7%, $n = 3$).

Identification of bioactive constituents was based on retention factor, absorption spectra *in situ*, and, if applicable, color of the band after spraying with aluminium chloride. The identification parameters are presented in Table 1 and Figure 1.

Times of chromatogram development were 11.5, 24, and 12 min. for aglycones, glycosides, and xanthines, respectively. Out of eight polyphenolics analyzed rutin, and chlorogenic acid, as well as aglycones quercetin, kaempferol, and caffeic acid were identified and quantified. Both xanthines analyzed, caffeine, and theobromine, were determined (Figure 2). Quantification was based on the area under curve using five bands with different amounts of standard in triplicate. The results of quantification are presented in Table 2.

Although in the last few years HPLC has been a major method for the analysis of polyphenolics in *yerba mate* and detailed MS analysis was done [12, 13], we have not encountered TLC method in available primary sources. As the TLC is a rather simple technique, we tried to identify and quantify polyphenolic constituents, primarily flavonoids, and phenolic acids of *mate*. Bastos et al. [8] did not detect quercetin, myricetin, and kaempferol in infusion from dried *mate* leaves using HPLC. This could be caused by inappropriate selection of solvents for extraction, inadequate time of extraction, or poor hydrolysis of glycosides as aglycones were to be determined. As it can be noticed from the result in Table 2 most

commonly employed acid hydrolysis used for the determination of total flavonoids in aglycone form (Christ-Müller's method) did not provide complete degradation of glycoside rutin.

Although advanced techniques for the separation and quantification of individual polyphenols including LC-MS [13, 14] are available, we used simple TLC method with HPTLC plates to determine quercetin and kaempferol in *yerba mate* in the amounts of 2.2 mg/g and 4.5 mg/g, respectively.

The results of TLC analysis concurred with the total content of methylxanthines: 5.4 mg/g for caffeine and 2.7 mg/g for theobromine, while total xanthines were 7.6 mg/g ($t = 0.16$, $\alpha = 0.01$). These results suggest that thin layer chromatography with densitometry could be used for both, identification as well as determination of caffeine and theobromine in *yerba mate* having in mind that the most common method only for determination is time-consuming titration [8].

4. Conclusion

Based on the obtained results, it can be concluded that TLC analysis is an appropriate technique for the analysis of individual polyphenols as well as xanthines. Content of individual methylxanthines corresponds to the spectrophotometric determined total xanthines.

As thin layer chromatography is readily available technique, it could be easily employed for the analysis of polyphenols and xanthines in raw material, different formulations of foods, and dietary supplements of *mate*.

Conflict of Interests

The authors declare no conflict of interests.

Acknowledgment

This work was financially supported by the Ministry of Science, Education and Sports of the Republic of Croatia (Grants nos. 006-0061117-1237 and 006-0061117-1239).

References

[1] D. P. Arçari, W. Bartchewsky, T. W. Dos Santos et al., "Antiobesity effects of yerba maté extract (*ilex paraguariensis*) in high-fat diet-induced obese mice," *Obesity*, vol. 17, no. 12, pp. 2127–2133, 2009.

[2] C. I. Heck and E. G. De Mejia, "Yerba mate tea (*Ilex paraguariensis*): a comprehensive review on chemistry, health implications, and technological considerations," *Journal of Food Science*, vol. 72, no. 9, pp. R138–R151, 2007.

[3] F. H. Reginatto, M. L. Athayde, G. Gosmann, and E. P. Schenkel, "Methylxanthines accumulation in *Ilex* species—caffeine and theobromine in erva-mate (*Ilex paraguariensis*) and other Ilex species," *Journal of the Brazilian Chemical Society*, vol. 10, no. 6, pp. 443–446, 1999.

[4] M. Medić-Šarić, V. Rastija, M. Bojić, and Ž. Maleš, "From functional food to medicinal product: systematic approach in analysis of polyphenolics from propolis and wine," *Nutrition Journal*, vol. 8, no. 33, pp. 1–18, 2009.

[5] R. Jeya Shakila, T. S. Vasundhara, and K. V. Kumudavally, "A comparison of the TLC-densitometry and HPLC method for the determination of biogenic amines in fish and fishery products," *Food Chemistry*, vol. 75, no. 2, pp. 255–259, 2001.

[6] I. N. Urakova, O. N. Pozharitskaya, A. N. Shikov, V. M. Kosman, and V. G. Makarov, "Comparison of high performance TLC and HPLC for separation and quantification of chlorogenic acid in green coffee bean extracts," *Journal of Separation Science*, vol. 31, no. 2, pp. 237–241, 2008.

[7] Council of Europe, *European Pharmacopoeia*, Council of Europe, Strasbourg, France, 6th edition, 2007.

[8] D. H. M. Bastos, A. C. Fornari, Y. S. Queiroz, and E. A. F. S. Torres, "Bioactive compounds content of chimarrão infusions related to the moisture of yerba maté (*Ilex paraguariensis*) leaves," *Brazilian Archives of Biology and Technology*, vol. 49, no. 3, pp. 399–404, 2006.

[9] B. Christ and K. H. Müller, "Zur serienmässigen Bestimmung des Gehaltes an Flavonol-Derivaten in Drogen," *Archiv der Pharmazie*, vol. 293, no. 12, pp. 1033–1042, 1960.

[10] R. Matissek, "Evaluation of xanthine derivatives in chocolate—nutritional and chemical aspects," *Zeitschrift fur Lebensmittel - Untersuchung und -Forschung*, vol. 205, no. 3, pp. 175–184, 1997.

[11] H. Wagner and S. Bladt, *Plant Drug Analysis: A Thin Layer Chromatography Atlas*, Springer, Heidelberg, Germany, 2nd edition, 2009.

[12] M. A. Vieira, M. Maraschin, C. M. Pagliosa et al., "Phenolic acids and methylxanthines composition and antioxidant properties of mate (*ilex paraguariensis*) residue," *Journal of Food Science*, vol. 75, no. 3, pp. C280–C285, 2010.

[13] L. Bravo, L. Goya, and E. Lecumberri, "LC/MS characterization of phenolic constituents of mate (*Ilex paraguariensis*, St. Hil.) and its antioxidant activity compared to commonly consumed beverages," *Food Research International*, vol. 40, no. 3, pp. 393–405, 2007.

[14] C. I. Heck and E. G. De Mejia, "Yerba mate tea (*Ilex paraguariensis*): a comprehensive review on chemistry, health implications, and technological considerations," *Journal of Food Science*, vol. 72, no. 9, pp. R138–R151, 2007.

Hindawi Publishing Corporation
Journal of Analytical Methods in Chemistry
Volume 2013, Article ID 318961, 6 pages
http://dx.doi.org/10.1155/2013/318961

Research Article

Rapid Identification of the Multiple Absorbed Bioactive Components and Metabolites in Rat Serum after Oral Administration of Wu-Jia Sheng-Hua Capsule by UPLC-ESI-MS

Fang Geng,[1] Fashan Wang,[2] Taobo Zou,[3] Kuiyuan Zhu,[3] Wei Ma,[3] Guanghui Tan,[1] and Ning Zhang[3]

[1] *School of Chemistry & Chemical Engineering, Harbin Normal University, Shi Da Nan Road, Harbin 150025, China*
[2] *Duo Duo Pharmaceutical Co. LTD., An Qing Street, Jiamusi 154000, China*
[3] *College of Jiamusi, Heilongjiang University of Chinese Medicine, Guang Hua Road, Jiamusi 154000, China*

Correspondence should be addressed to Ning Zhang; zhang-ning2006@hotmail.com

Received 23 January 2013; Revised 31 March 2013; Accepted 14 April 2013

Academic Editor: Feng Sun

To identify the compounds absorbed in rat serum after the oral administration of Wu-Jia Sheng-Hua (WJSH) capsule, a traditional Chinese medicine (TCM) compound prescription, an ultraperformance liquid chromatography coupled with electrospray ionization mass spectrometry (UPLC/ESI-MS) method, was established. The chromatographic separation of the absorbed compounds and metabolites was achieved with an ACQUITY UPLC BEH C18 column (2.1 mm × 50 mm, 1.7 μm) under a gradient elution. The mobile phase was composed of acetonitrile and water buffered with ammonium acetate (10 mM) and formic acid (0.1%, V/V). Twelve absorbed compounds and four metabolites were found. Seven of the absorbed compounds were identified by ESI-MS. The identification of absorbed compounds might be helpful for the better understanding of the mechanisms underlying the pharmacological effects of WJSH capsule.

1. Introduction

Chinese postpartum care (Zuoyuezi) has been regarded as a crucial rite-to-passage for the woman's recovery and the transition to motherhood after childbirth [1]. The use of Sheng-Hua-Tang, a well-known traditional Chinese medicine (TCM) compound prescription, during the postpartum has been popular in Chinese communities over a long period. Previous study has shown that Sheng-Hua-Tang use during the first month of the postpartum period may have a positive effect on women's health-related quality of life, especially in terms of role limitations due to physical health and emotional problems [2]. Wu-Jia Sheng-Hua capsule (comprising *Radix et Caulis Acanthopanacis Senticosi*, *Radix Angelicae Sinensis*, *Rhizoma Chuanxiong*, *Semen Persicae*, *Radix Glycyrrhizae*, and *Rhizoma Zingiberis Preparata*), derived from Sheng-Hua-Tang, has been used widely in Chinese women to promote blood flow, resolve blood stasis, ease postchildbirth pain, reduce bleeding volume and shorten bleeding duration after induced abortion in Chinese women [3, 4]. The material base, namely the bioactive components, of Wu-Jia Sheng-Hua (WJSH) capsule is still unclear, though the prostaglandin F2alpha ($PGF_{2\alpha}$), prostaglandin E2 (PGE_2), endothelin (ET), and nitrogen monoxide (NO) levels were found to be partially responsible for the curative effects and recovery benefits of WJSH capsule on induced abortion with vaginal haemorrhage [4].

TCM serum pharmacochemistry, based on hypothesis that active compounds should appear in blood after administration of TCM, was proposed by Homma et al. [5, 6]. In the past two decades, it was proved to be helpful in recognizing the real active components in TCM and in gaining a better understanding of the mechanisms under the therapeutic effects of TCM [7–9].

In the present study, an ultraperformance liquid chromatography coupled with electrospray ionization mass

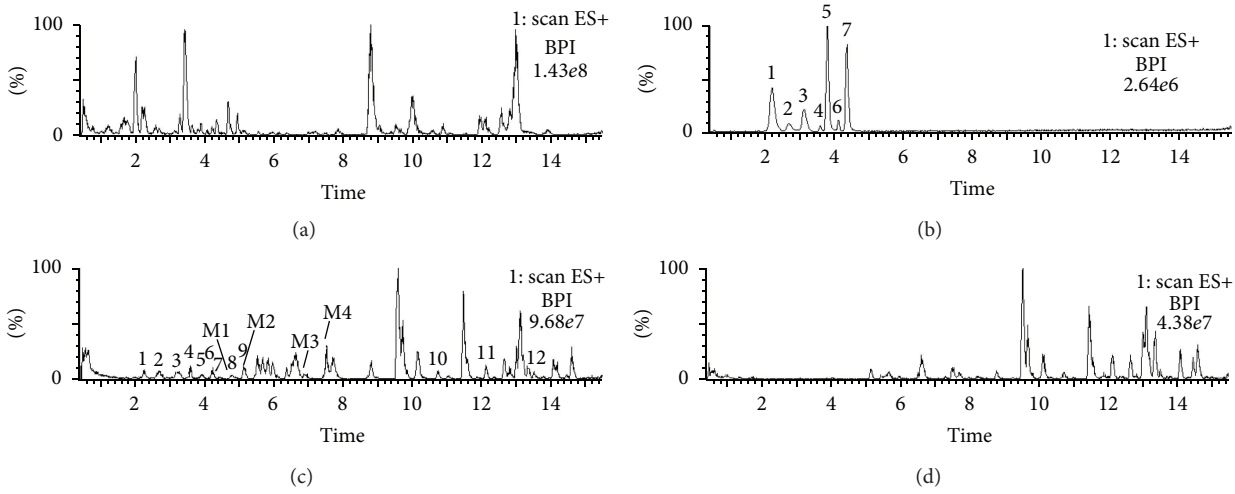

Figure 1: Total ion chromatogram of (a) WJSH capsule extract, (b) mixture of standards, (c) WJSH capsule serum sample, and (d) blank rat serum in positive mode. Peaks: 1, syringin; 2, protocatechuic acid; 3, liguiritin; 4, ferulic acid; 5, isofraxidin; 6, chlorogenic acid; 7, liqustilide; M1, M2, M3, and M4, stand for metabolites 1, 2, 3 and 4, respectively.

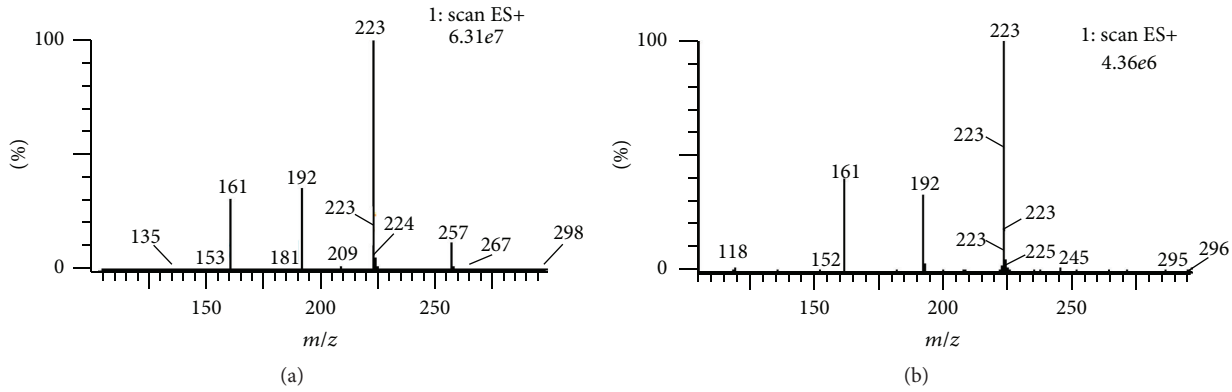

Figure 2: MS/MS spectra of (a) peak 5 in TIC chromatogram of WJSH capsule serum sample; (b) standard of isofraxidine.

spectrometry (UPLC/ESI-MS) method was developed and applied for investigating the serum pharmacochemistry of WJSH capsule. It was thought that TCM expresses its effects through multicomponents with multitargets [10]. The identification of WJSH's multiple absorbed bioactive components and metabolites might be helpful for better understanding the mechanisms under its therapeutic effects.

2. Experimental Method

2.1. Reagents and Chemicals. Syringin, protocatechuic acid, liguiritin, ferulic acid, isofraxidine, chlorogenic acid, and liqustilide (standards) were purchased from National Institute of Control of Pharmaceutical and Biological Products (Beijing, China).

Acetonitrile, methanol, formic acid, and ammonium formate (HPLC grade) were obtained from Merck (Darmstadt, Germany) and Sigma-Aldrich (St. Louis, MO, USA), respectively. Other chemicals are of analytical grade.

Wu-Jia-Sheng-Hua capsule and each single herb in the prescription of Wu Jia Sheng Hua capsule were gifts from Duo Duo Pharmaceutical Co. LTD. (Heilongjiang, China).

2.2. UPLC Conditions. The chromatographic separation of the absorbed components and metabolites were performed on a Waters ACQUITY UPLC system (Waters Corp., Milford, MA, USA) equipped with an UV detector, an autosampler, an ACQUITY UPLC BEH C18 column (2.1 × 50 mm, 1.7 μm), and an automatic thermostatic column oven. The mobile phase consisted of (A) water buffered with ammonium acetate (10 mM) and formic acid (0.1%, V/V) and (B) acetonitrile. The column temperature was kept at 40°C. The elution of the target compounds was conducted in a gradient mode with the volume percentage of B changed from 5% to 50% in the initial 10 minutes and from 50% to 80% in the next 6 minutes. The flow rate was 0.4 mL/min, and the injection volume was 8 μL.

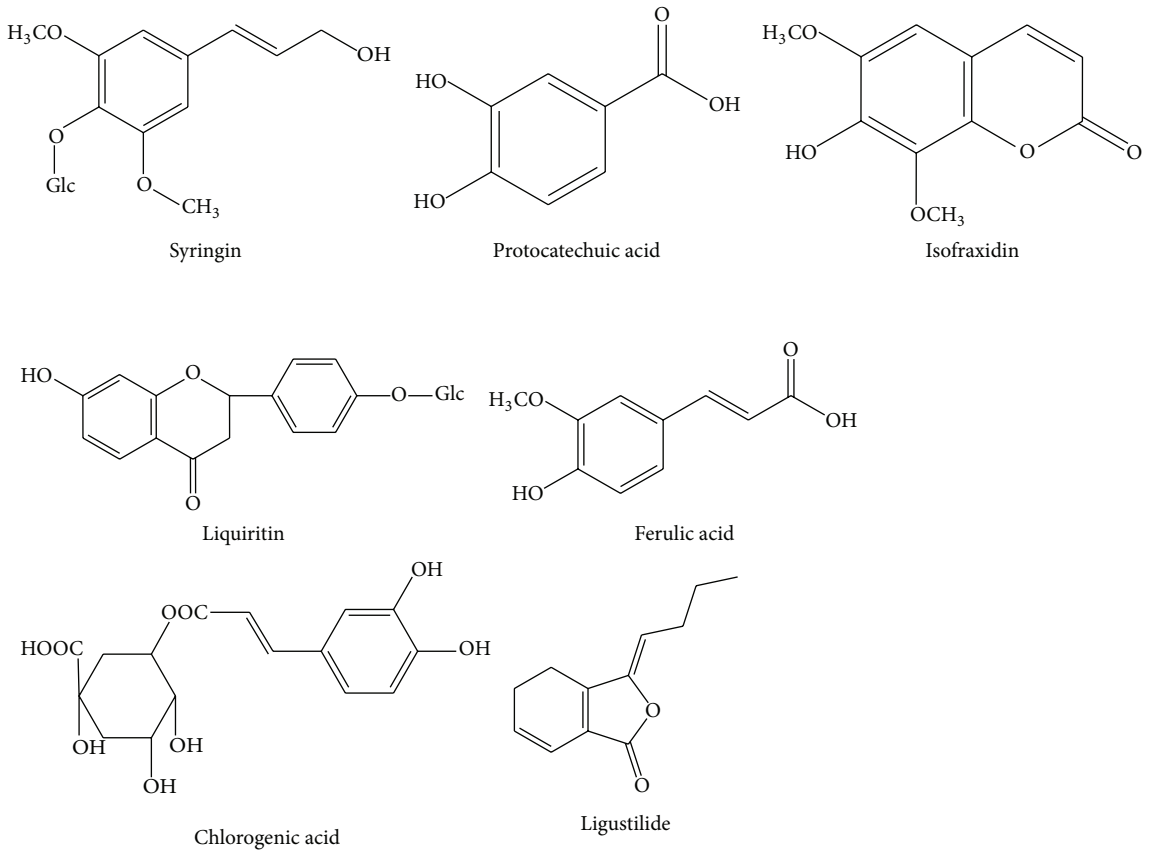

Figure 3: Identified bioactive components of WJSH capsule absorbed into rat plasma after oral administration.

2.3. MS Conditions. To obtain the MS and MS/MS data of the investigated compounds, a Waters Quattro Premiere XE triple-quadrupole mass spectrometer (Micromass MS Technologies) was coupled to the abovementioned UPLC system. Ionization was performed in the positive electrospray (ESI) mode. The mass range was set at *m/z* 100–1000 Da with the scan time being 0.5 s. The ionization parameters were as follows: interval time, 0.2 s; capillary voltage, 3.5 kV; cone voltage, 35 kV; ionization resource temperature, 120°C; desolvation temperature, 380°C, desolvation gas flow rate, 500 L/h (N_2); and cone gas flow rate, 50 L/h (N_2). MassLynx software (version 4.1) and QuanLynx software were used for system control and data processing, respectively.

2.4. Sample Preparation. 5 mL methanol was added to 1 mL blank rat serum sample or WJSH capsule serum sample. The mixture was vortexed for 3 min. and centrifuged for 15 min. (4°C, 5000 rpm). 5 mL supernatant was dried under gentle nitrogen gas stream at 37°C. The residues were kept at −20°C. Before analysis, each residue was reconstituted in 1 mL methanol and centrifuged for 15 min. (4°C, 14,000 rpm). 8 μL supernatant was injected for UPLC-ESI-MS analysis.

2.5. Serum Pharmacochemistry Study of WJSH Capsule. The extracts of WJSH capsule and raw medicinal materials of WJSH capsule were prepared separately. 10 mL methanol was added to 0.4 g WJSH or each raw medicinal material. The suspensions were sonicated for 30 min., centrifuged (3000 rpm) for 15 min., and filtered through 0.45 μm micropore film (Millipore, USA). The supernatants were collected as extracts.

Male Sprague-Dawley rats (230 g ± 10 g, Experimental Animal Center of Heilongjiang University of Traditional Chinese Medicine) were randomly divided into eight groups (six for each): Group A to Group H. All care and handling of animals were performed with the approval of Institutional Authority for Laboratory Animal Care of Heilongjiang University of Traditional Chinese Medicine.

After 12 hours of fasting, normal saline (blank control) and extract of WJSH capsule were given intragastrically to rats in Group A and Group B, separately. Extracts of raw medicinal materials were given intragastrically to rats of the other 6 groups (one extract per group). The dosage was 1.5 mL/100 g body weight, and the administration frequency was once daily in three consecutive days in each group. At forty minutes after the last administration, 5 mL blood was collected *via* hepatic portal vein. The blood samples were centrifugated for 10 min. at 5000 rpm at 4°C to separate serum samples. The residues were kept at −20°C until analysis.

3. Results and Discussions

3.1. Optimization of UPLC-ESI-MS Conditions. To purify the serum sample, the protein precipitation, liquid-liquid extraction, and solid-phase extraction methods were tried. Finally,

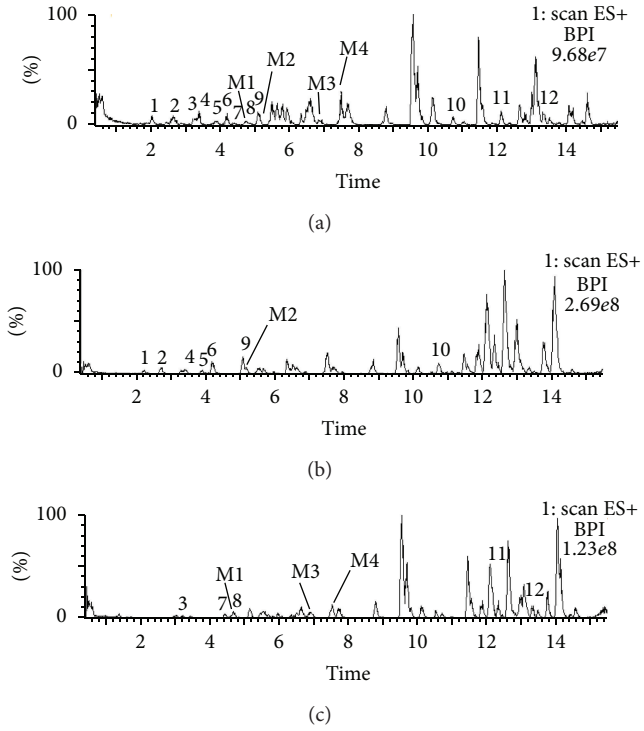

Figure 4: TIC chromatograms of serum samples: (a) WJSH capsule; (b) *Radix et Caulis Acanthopanacis Senticosi* alone; (c) WJSH capsule without *Radix et Caulis Acanthopanacis Senticosi*. Peaks: 1, syringin; 2, protocatechuic acid; 3, liguiritin; 4, ferulic acid; 5, isofraxidine; 6, chlorogenic acid; 7, liqustilide; M1, M2, M3, and M4 stand for metabolites 1, 2, 3, and 4, respectively.

the simple protein precipitation method with methanol was chosen, since most investigated compounds were found in the purified samples.

As compared to methanol-water system, higher resolution, better peak shape, and faster elution of compounds were achieved using acetonitrile-water system buffered with ammonium acetate and formic acid. Therefore, this system was used as mobile phase. The chromatographic separation of the absorbed components and metabolites was conducted in gradient elution mode to overall reduce the retention time of these compounds characterized by different polarities. The timetable of gradient elution was listed in Table 1.

For the ESI-MS conditions, the stronger responses of all compounds were obtained in positive ionization mode than in negative mode. Thus, positive mode was employed in the total ion current (TIC) chromatograms of WJSH capsule serum samples in the *m/z* range of 100 to 1000 Da.

3.2. Identification of Absorbed Components. The multiple bioactive components in TCM could be simultaneously identified using the UPLC-ESI-MS technique. It is generally helpful in better understanding the mechanisms underlying TCM's therapeutic effects.

The serum pharmacochemistry study of WJSH capsule was conducted in rats orally administered with WJSH Capsule. Then, the absorbed bioactive components including

Table 1: The timetable of gradient elution in UPLC conditions.

Time (min.)	Solvent A (%, V/V)	Solvent B (%, V/V)
Initial	95	5
10	50	50
16	20	80

Solvent A: water buffered with ammonium acetate (10 mM) and formic acid.
Solvent B: acetonitrile.

their metabolites were identified by the established UPLC-ESI/MS method. The typical TIC chromatograms of WJSH capsule extract, WJSH capsule serum sample, and blank serum sample were shown in Figure 1. Twelve chemicals of which chromatographic peaks appeared in the TIC chromatograms of WJSH capsule serum sample and WJSH capsule extract, but not in that of the blank serum sample, were presumed to be the absorbed components. Similarly, four chemicals whose chromatographic peaks presented only in the TIC chromatograms of WJSH capsule serum sample, but not in that of the WJSH capsule extract or the blank serum sample, were supposed to be metabolites.

By comparing the MS/MS spectra, the chromatographic peaks in TIC chromatogram of WJSH capsule serum sample versus the standards, respectively, seven absorbed components were identified unequivocally. For instance, the MS/MS spectrum of peak 5 was compared with that of the isofraxidine standard. These MS/MS spectra were shown in Figure 2. Since the quasi-molecular ion at *m/z* 223 $[M + H]^+$, fragmentation ions at *m/z* 192 $[M + H\text{-}OCH_3]^+$, and at *m/z* 161 $[M + H\text{-}OCH_3\text{-}OCH_3]^+$ were found simultaneously in the MS/MS spectra of peak 5 and the standard of isofraxidine; this absorbed component was confirmed to be isofraxidine. The other six components were identified in the same way. The chemical structures of the identified components were shown in Figure 3. The other five absorbed components and the four metabolites were not identified and need further investigation.

By comparing the TIC chromatograms of serum samples, WJSH capsule, WJSH capsule without *Radix et Caulis Acanthopanacis Senticosi,* and *Radix et Caulis Acanthopanacis Senticosi* alone, isofraxidine was confirmed to be originated from *Radix et Caulis Acanthopanacis Senticosi*. Similarly, the original plant(s) of the other absorbed components and metabolites were confirmed. These TIC chromatograms were shown in Figure 4. The retention times, MS/MS data, and original plants of the absorbed components and metabolites were listed in Tables 2 and 3, respectively.

By revealing the bioactive components of TCM compound prescriptions, serum pharmacochemistry studies might be significantly helpful in better understanding the mechanisms under the therapeutic effects of these prescriptions. For instance, WJSH capsule and Danggui-Shaoyao-San have been used extensively in Chinese women to enhance uterine involution after giving birth and alleviate dysmenorrhea, respectively [11, 12]. In pharmacological experiments, the prostaglandins (PG) levels regulation was proved to be partially responsible for the myometrium contraction stimulation and inhibition effects of WJSH capsule and

Table 2: The retention times, +ESI-MS/MS data (m/z), and origins of the absorbed components in rat serum after oral administration of WJSH capsule.

No.	Rt (min.) extract/plasma	Positive ions (m/z)	Origins	Identification
1	2.05/2.04	395 $[M + Na]^+$, 373 $[M + H]^+$	*Radix* et *Caulis Acanthopanacis Senticosi*	Syringing
2	2.71/2.73	155 $[M + H]^+$, 137 $[M + H\text{-}H_2O]^+$, 111 $[M + H\text{-}CO_2]^+$	*Radix* et *Caulis Acanthopanacis Senticosi*, *Radix Glycyrrhizae*, *Rhizoma Chuanxiong*, *Rhizoma Zingiberis Preparata*	Protocatechuic acid
3	3.25/3.28	419 $[M + H]^+$, 441 $[M + Na]^+$, 403 $[M\text{-}CH_3]^+$	*Radix Glycyrrhizae*	Liquiritin
4	3.43/3.40	195 $[M + H]^+$, 180 $[M + H\text{-}CH_3]^+$, 151 $[M + H\text{-}CO_2]^+$,	*Radix* et *Caulis Acanthopanacis Senticosi*, *Radix Angelicae Sinensis*, *Rhizoma Chuanxiong*, *Radix Glycyrrhizae*	Ferulic acid
5	3.89/3.91	223 $[M + H]^+$, 192 $[M + H\text{-}OCH_3]^+$, 161 $[M + H\text{-}OCH_3\text{-}OCH_3]^+$	*Radix* et *Caulis Acanthopanacis Senticosi*	Isofraxidine
6	4.22/4.27	355 $[M + H]^+$, 377 $[M + Na]^+$, 193 $[M\text{-}C_9H_7O_3]^+$, 181 $[M\text{-}C_7H_{11}O_5]^+$, 175 $[M\text{-}C_9H_7O_3\text{-}H_2O]^+$	*Radix* et *Caulis Acanthopanacis Senticosi*, *Radix Glycyrrhizae*	Chlorogenic acid
7	4.44/4.46	191 $[M + H]^+$, 175, 151, 137	*Radix Angelicae Sinensis*	Liqustilide
8	4.73/4.69	223, 205, 195	*Radix Angelicae Sinensis* *Semen Persicae*	—
9	5.10/5.13	237, 222	*Radix* et *Caulis Acanthopanacis Senticosi*	—
10	10.87/10.89	247, 232	*Radix* et *Caulis Acanthopanacis Senticosi*	—
11		194, 176	*Radix Glycyrrhizae*	—
12	13.30/13.27	431, 388, 370	*Rhizoma Chuanxiong*	—

Table 3: The retention times, +ESI-MS/MS data (m/z), and origins of the metabolites in rat serum after oral administration of WJSH capsule.

Peak no.	Rt (min.) extract/plasma	Positive ions (m/z)	Origin
M1	4.78/4.79	207, 229	*Radix Angelicae Sinensis* *Rhizoma Chuanxiong* *Semen Persicae*
M2	5.12/5.14	262, 244	*Radix* et *Caulis Acanthopanacis Santicosi*
M3	6.94/6.92	189, 154	*Radix Angelicae Sinensis* *Rhizoma Chuanxiong* *Semen Persicae*
M4	7.59/7.61	323, 245, 308	*Rhizoma Zingiberis Preparata*

Danggui-Shaoyao-San, separately [4, 12]. In previous and present serum pharmacochemistry investigations, identical (ferulic acid and liqustilide) and different (syringin, protocatechuic acid, liguiritin, isofraxidine, and chlorogenic acid for WJSH capsule; paeoniflorin sulfonate, albiflorin, paeoniflorin, butylidenephthalide, and senkyunolide I for Danggui-Shaoyao-San) bioactive components in WJSH capsule and Danggui-Shaoyao-San were identified [13]. By conducting comparative pharmacokinetic and pharmacological experiments, the major bioactive components in WJSH capsule and Danggui-Shaoyao-San related to the up- and downregulation effect on myometrium contraction might be confirmed, and the influence of other coexisting components on these effected might be revealed. Thus, the mechanisms under WJSH capsule and Danggui-Shaoyao-San's therapeutic effects might be elucidated.

4. Conclusion

In this study, an UPLC-ESI-MS method was established for investigating the serum pharmacochemistry of WJSH capsule. In this way, twelve absorbed bioactive components and four metabolites were found in rat serum. Seven of the absorbed bioactive components were identified. These results might be helpful for better understanding the mechanisms underlying the therapeutic effects of WJSH capsule.

Conflict of Interests

The authors of this paper declear that they have no conflict of interests.

Acknowledgments

This work was financially supported by the Scientific and Technical Research Program of Heilongjiang Education Department (12511167).

References

[1] N. F. Cheung, R. Mander, L. Cheng et al., "'Zuoyuezi' after caesarean in China: an interview survey," *International Journal of Nursing Studies*, vol. 43, no. 2, pp. 193–202, 2006.

[2] P. J. Chang, Y. C. Tseng, C. H. Chuang et al., "Use of Sheng-Hua-Tang and health-related quality of life in postpartum women: a population-based cohort study in Taiwan," *International Journal of Nursing Studies*, vol. 47, no. 1, pp. 13–19, 2010.

[3] P. Chen, S. Xu, L. Chen et al., "Inhibiting effect of Wu-Jia-Sheng-Hua capsule on postpartum haemorrhage: analysis of 159 cases," *Heilongjiang Medicine and Pharmacy*, vol. 30, no. 1, p. 69, 2007.

[4] C. J. Liu, J. P. Lu, and L. L. Pan, "Improvement effects of Wu-Jia-Sheng-Hua capsule on uterine involution following drug-induced abortion," *Chinese Medical Herald*, vol. 7, no. 16, pp. 105–106, 2010.

[5] M. Homma, K. Oka, T. Yamada, T. Niitsuma, H. Ihto, and N. Takahashi, "A strategy for discovering biologically active compounds with high probability in traditional Chinese herb remedies: an application of Saiboku-to in bronchial asthma," *Analytical Biochemistry*, vol. 202, no. 1, pp. 179–187, 1992.

[6] M. Homma, K. Oka, C. Taniguchi, T. Niitsuma, and T. Hayashi, "Systematic analysis of post-administrative saiboku-to urine by liquid chromatography to determine pharmacokinetics of traditional Chinese medicine," *Biomedical Chromatography*, vol. 11, no. 3, pp. 125–131, 1997.

[7] P. Wang, Y. Liang, N. Zhou et al., "Screening and analysis of the multiple absorbed bioactive components and metabolites of Dangguibuxue decoction by the metabolic fingerprinting technique and liquid chromatography/diode-array detection mass spectrometry," *Rapid Communications in Mass Spectrometry*, vol. 21, no. 2, pp. 99–106, 2007.

[8] X. Wang, W. Sun, H. Sun et al., "Analysis of the constituents in the rat plasma after oral administration of Yin Chen Hao Tang by UPLC/Q-TOF-MS/MS," *Journal of Pharmaceutical and Biomedical Analysis*, vol. 46, no. 3, pp. 477–490, 2008.

[9] S. Ni, D. Qian, J. A. Duan et al., "UPLC-QTOF/MS-based screening and identification of the constituents and their metabolites in rat plasma and urine after oral administration of Glechoma longituba extract," *Journal of Chromatography B*, vol. 878, no. 28, pp. 2741–2750, 2010.

[10] P. Wang, Y. Liang, N. Zhou et al., "Screening and analysis of the multiple absorbed bioactive components and metabolites of Dangguibuxue decoction by the metabolic fingerprinting technique and liquid chromatography/diode-array detection mass spectrometry," *Rapid Communications in Mass Spectrometry*, vol. 21, no. 2, pp. 99–106, 2007.

[11] Z. P. He, W. H. Shou, B. R. Gong et al., "Study on pharmacodynamics of Wenjinghuayu mixture," *Chinese Traditional Patent Medicine*, vol. 25, no. 6, pp. 471–473, 2003.

[12] Y. Q. Hua, S. L. Su, J. A. Duan, Q. J. Wang, Y. Lu, and L. Chen, "Danggui-Shaoyao-San, a traditional Chinese prescription, suppresses PGF2α production in endometrial epithelial cells by inhibiting COX-2 expression and activity," *Phytomedicine*, vol. 15, no. 12, pp. 1046–1052, 2008.

[13] L. Chen, J. Qi, Y. X. Chang, D. Zhu, and B. Yu, "Identification and determination of the major constituents in Traditional Chinese Medicinal formula Danggui-Shaoyao-San by HPLC-DAD-ESI-MS/MS," *Journal of Pharmaceutical and Biomedical Analysis*, vol. 50, no. 2, pp. 127–137, 2009.

Hindawi Publishing Corporation
Journal of Analytical Methods in Chemistry
Volume 2013, Article ID 617243, 7 pages
http://dx.doi.org/10.1155/2013/617243

Research Article

The Studies of Chlorogenic Acid Antitumor Mechanism by Gene Chip Detection: The Immune Pathway Gene Expression

Tian Yi Kang,[1] Hua Rong Yang,[2] Jie Zhang,[2] Dan Li,[1] Jie Lin,[1] Li Wang,[1] and XiaoPing Xu[1]

[1] *West China School of Pharmacy, Sichuan University, Chengdu 610041, Sichuan Province, China*
[2] *Jiuzhang Biochemical Engineering Science and Technology Development Co., Ltd, Chengdu 610041, Sichuan Province, China*

Correspondence should be addressed to XiaoPing Xu; xu106@sina.com

Received 31 January 2013; Accepted 4 April 2013

Academic Editor: Yu-Ming Fan

Persistently increasing incident of cancer in human beings has served to emphasize the importance of studies on mechanism of antitumor substances. Chlorogenic acid (CA), extracted from folium cortex eucommiae, has been confirmed to have lots of biological activities encompassing inhibition of tumor. However, the anticancer mechanism of CA remains unclear. Here, we have utilized a whole mouse genome oligo microarray (4∗44K) to analyze gene expression level of female BALB/c mice (implanted with EMT-6 sarcoma cells) after treatment with low, medium, and high-dose CA (5 mg/kg, 10 mg/kg, and 20 mg/kg), docetaxel, interferon, and normal saline separately at 6 time points (3rd, 6th, 9th, 12th, 15th, and 18th days after administration). Differentially expressed genes screened out by time-series analysis, GO analysis, and pathway analysis, and four immune-related genes were selected for further confirmation using RT-qPCR. The results demonstrated that CA is able to change gene expression and that the responsive genes (CaN, NFATC2, NFATC2ip, and NFATC3) involved in immune pathways had been significantly upregulated by CA. Expression of immune factors such as IL-2R and IFN-γ can be improved by CA to promote activation and proliferation of T cells, macrophages, and NK cells, thus enhancing their surveillance and killing abilities, further suppressing the growth rate of tumor cells.

1. Introduction

Cancer dormant cell theory takes the view that activation of resting cells is the key factor causing cancer metastasis. Recent studies indicate that resting cells can be activated through escaping immune surveillance when immune function is weakened and that energy used for cell revivals can be provided by the newborn vessels [1–3]. Therefore, the study on improving body immune surveillance and restraining the energy of tumor growth will be an emergent mission as well as a breakthrough in the field of clinical treatment of cancer.

Chlorogenic acid (CA), extracted from folium cortex eucommiae and the flower bud of *Lonicera confusa*, is a kind of depside formed by caffeic acid and quinic acid. A large number of studies on CA have demonstrated that CA has a wide range of biological activities including inhibition of tumor cells [4]. According to preliminary studies, we recognize that CA is able to inhibit tumor in mouse except for these with T-cells defect, which suggests that immune system can be one of the targets of tumor suppression. Meanwhile, *in vivo* studies of our group indicate that CA also changes the advantage state of Th2 drift of BALB/c EMT-6 mice. It significantly enhance the activities of BALB/c EMT-6 mice cytotoxic T lymphocyte and natural killer cells as well as strengthening macrophage phagocytosis activity and lymphocyte transcription activity, thus boosting specific and nonspecific cellular immune function to tumor cells. Recent studies show that antitumor property of CA may have a connection with its ability of enhancing the activities of aryl hydrocarbon hydroxylase, suppressing formation of 8-OH-dG, carcinogen-DNA adduct, and oxygen radical [5, 6]. Meanwhile, CA can guard against gastric cancer and colon cancer and even suppress related carcinogenic factors [7, 8]. *In vitro* studies revealed that CA can enhance T-cell proliferation caused by influenza virus antigen and can induce the generation of IFN-γ and IFN-α by human lymphocytes and peripheral blood leukocytes [9, 10]. Additionally, we find that CA can also activate neurocalcin to strengthen the activity

of macrophagocyte [11]. Although much evidence has proved the anticancer property of CA, little is known about its exact targets on molecular level.

Base on the principle of complementary base pairing, microarray technology can distinguish particular genes from the mixture of genes by taking advantage of gene probes. Different from normal PCR, RT-qPCR can take quantitative analysis of unknown system. Meanwhile, its sensitivity, accuracy, and specificity are better than those of normal PCR. To explore the expression level of genes in tumor cells, we utilized a microarray technique to detect BALB/c EMT-6 mice after treatment with CA, docetaxel, interferon, normal saline separately, and the differences in expression level were confirmed by RT-qPCR. Time-series analysis, GO analysis, and pathway analysis were used to screen out common genes and analyze the relationship between putative genes and anticancer process of CA. Our data has suggested that CA is able to inhibit the growth of tumor through regulating immune system.

2. Materials and Methods

2.1. Animal Model Construction and CA Treatment. Female SPF mice (BALB/c) used in this experiment weigh 17-18 g on average, provided by the animal center of Sichuan University. EMT-6 sarcoma cells were provided by West China Hospital of Sichuan University Department of Health Engineering Key Laboratory of Transplantation and Transplantation Immunity.

We took EMT-6 cell line out of the −152°C ultra low temperature refrigerator. After thawing, centrifuging, and primary culturing, we used 0.25% trypsin for digestion twice and then subcultured it to a required number. All the collected cells were diluted with phosphate-buffered saline (PBS) in the end. Each BALB/c mouse was injected with 0.2 mL cell solution. The tumor would not transfer until it grew to a certain size. We homogenized the tumor taken from the body of BALB/c tumor-bearing mice to cell suspension and then inoculated the cell suspension to other BALB/c mice. Mice used for microarray analysis were injected with high-dose CA (experimental group), docetaxel (control group), and normal saline (negative control group). Gene expression of experimental group was analyzed at six time points (3rd, 6th, 9th, 12th, 15th, and 18th days, resp., after administration), while the control group and negative control group were both analyzed at the 12th days after administration. RT-qPCR took mice injected with low, medium, and high-dose CA (5 mg/kg, 10 mg/kg, 20 mg/kg) as experimental group, docetaxel and interferon as control group, and normal saline as negative control group. Each of these groups was tested 12 days after administration.

2.2. RNA Extraction and Labeling. Total RNA was extracted using mirVana RNA Isolation Kit (Applied Biosystem p/n AM1556) in 15 min after tissue collection. Quality and concentration of RNA were checked by spectrophotometer analysis and gel electrophoresis. All extracted samples had an A260/280 ratio of between 2.0 and 2.1 and a 28S/18S ratio of 2 [12]. Agilent 2100 Bioanalyzer was used for further verification and qualified RNA had an RIN greater than 7.0. Total RNA was transcribed to double-stranded cDNA using RevertAid First Strand cDNA Synthesis Kit (Fermentas), with T7 Promoter Primer. The aaUTP-labeled cRNA was produced from cDNA by *in vitro* transcription. cRNA was dyed with Cy3 and purified using RNeasy Mini Kit (Qiagen, Valencia, CA, USA) according to the protocol of the RNeasy Plus Mini Kit.

2.3. Hybridization and Scanning. Cy3 cRNA must be fragmented in a buffer of 11 μL 10× blocking agent, 2.2 μL 25× fragmentation buffer and a certain amount of nuclease-free water at 60°C for half an hour before hybridization. We added 55 μL 2× GEx hybridization buffer to the denatured and fragmented cRNA and then transfered them to microarrays at 65°C for 17 h with constant rotation. After hybridization, the microarrays were washed twice with buffer 1 for 1 minute followed by buffer 2 at 37°C for 1 minute too. In the end, the microarrays were autoscanned twice in 100% and 10% PMT, respectively, at 5 μm resolution. The data was analyzed by Agilent Feature Extraction software and the quantile normalization was finished by GeneSpring 10.0.

2.4. Microarray Data Preprocessing. After acquisition of raw data, Agilent Feature Extraction software kit was used to eliminate the effect of background signals through automatic gridding. We took the log 2 of the normalized background adjusted values to narrow the threshold of fluorescence signal strength before quantile normalization by GeneSpring 10.0 and then used a linear model to estimate expression values on the log scale. Both programs were available in the limma package. We chose a standard among the microarray samples thus the whole microarray data varied on it to obtain the same baseline of average density. Unqualified probes should be filtered out. Differentially expressed genes are submitted to Student's t-test and $P \leq 0.05$.

2.5. Interaction Network Analysis. We inputted the data of probes used for gene expressing analysis into SBC Analysis System (V2010.05).

2.6. RT-qPCR. RNA extracted from experimental group of CA, positive control group of docetaxel, and interferon, negative control group were used to measure expression of selected genes of interest by RT-qPCR. Genes CaN, Nfatc2, Nfatc3, and Nfatc2ip showed a different expression level following treatment with low, medium, and high-dose CA, respectively. Primers used for RT-qPCR validation were designed according to each gene sequence and finished by SBC. Primer names, accession numbers, and sequences are listed in Table 1.

Total RNA was isolated using TRIzol reagents. The RNA integrity was verified with RNA formaldehyde electrophoresis and the quality was detected by spectrophotometry. The RNA samples had an A260/280 ratio of greater than 2 and a 20sRNA/18sRNA ratio of greater than 1.1. Single strand cDNA was synthesized using RevertAid First strand cDNA Synthesis

Table 1: Primers used for RT-qPCR validation and additional expression profiling.

Gene	GenBank accession	Forward	Reverse
Nfatc3	NM_010901	CTCCCTATCATAACCCA	CTgAAggCAAATCTgTG
Nfatc2ip	NM_010900	AAAAgCAgAAAgCATACg	gACAggCCCTTCCACTA
Nfatc2	NM_010899	TgAgAAgATCgTAggCAAC	gCTCgATgTCAgCgTTT
CaN	NM_001004025	TgggAAATgAggCgATT	CCACgCTCAAAgAACCAg

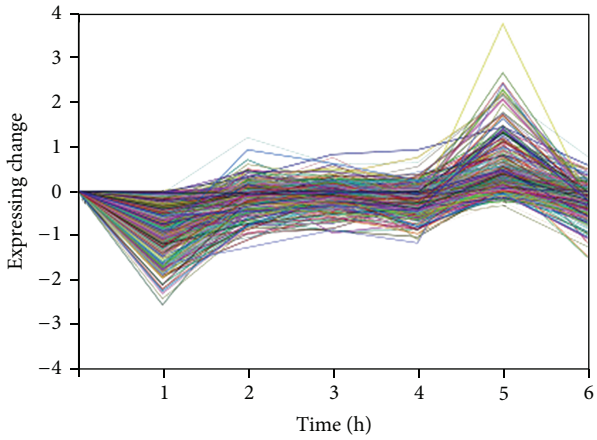

Figure 1: Expressing change of genes covered in NO.21 at 6 time points.

Kit. Reverse transcription reactions were conducted at 42°C for 30 min and at 85°C for 5 min at a 20 μL total reaction volume containing the following reagents: 2 μL RNA, 1 μL oligo, 2 μL (10 mM) dNTP mixture, 1 μL RiboLock RNase Inhibitor, 4 μL 5× reaction buffer, 9 μL water, and 1 μL RevertAid M-MuLV. PCR was performed using a Sino Bio Taq 2× Master Mix. The RT-qPCR products were analyzed by 1.0% agarose gel electrophoresis.

PCR reaction should be taken at a temperature gradient in the range of annealing temperature of CaN, Nfatc2, Nfatc3, and Nfatc2ip. RT-qPCR analysis was conducted to obtain crossing point (Ct) values of each gene and standard curve was established through the linearity between Ct value and log 2 of expression values. Before carrying out RT-qPCR analysis, cDNA and primers should be diluted in 20 μL reagents containing the following: 9 μL MIX, 8 μL H_2O, 1 μL sense primer (F), 1 μL antisense primer (R), and 1 μL cDNA. The same cycling parameters were repeated for 40 times. Relative content of mRNA extracted from experimental group of CA, positive control group of docetaxel, and interferon negative control group was calculated by RT-qPCR detection system BIORAD IQ5.

3. Results and Discussion

3.1. Gene Expression Profiles of Tumor Cell after Being Treated by CA. 34275 probes without repeat were retained after combination and filtration. We carried out a Student's t-test of these probes to select differentially expressed genes ($P \leq 0.05$) and then drew curves reflecting different expression tendency of them at 6 time points. Eighty different curves were obtained after curve fitting. The smaller the P value is, the more similar each gene trend fits the curve. NO.21 fitting curve had a P value close to 0 and the expression profiles of genes covered in this fitting curve were analyzed systematically here. As shown in Figure 1, each inflection point corresponds to gene expression at different time points after administration. Genes covered in this curve were upregulated as seen from the whole time cycle; in other word, CA is capable of upregulating certain genes of tumor-bearing mice.

Data of genes covered in NO.21 was put into SBC Analysis System (V2010.05) and compared with KEGG (Kyoto Encyclopedia of Genes and Genomes) database. As shown in Table 2, 96 pathways are found to be related to upregulated genes and 29 of them are found to be statistically

Table 2: Pathways of upregulated genes.

Pathway name	Hits	Total	Percent (%)
Natural killer cell mediated cytotoxicity—*Mus musculus* (mouse)	4	161	2.48
B-cell receptor signaling pathway—*Mus musculus* (mouse)	5	85	5.88
T-cell receptor signaling pathway—*Mus musculus* (mouse)	6	132	4.55

Table 3: Upregulated genes in T-cell receptor signaling pathway, B-cell receptor signaling pathway, and natural killer cell mediated cytotoxicity.

Pathway name	GeneID	ProbeID	Symbol
Natural killer cell mediated cytotoxicity—*Mus musculus* (mouse)	18019	Nfatc2	NFATC2
	18021	Nfatc3	NFATC3
	19059	CaN	CAN
	22325	Vav2	VAV2
T-cell receptor signaling pathway—*Mus musculus* (mouse)	17973	Nck1	NCK1
	56637	Gsk3b	GSK3B
	18019	Nfatc2	NFATC2
	18021	Nfatc3	NFATC3
	19059	CaN	CAN
	22325	Vav2	VAV2
B-cell receptor signaling pathway—*Mus musculus* (mouse)	56637	Gsk3b	GSK3B
	18019	Nfatc2	NFATC2
	18021	Nfatc3	NFATC3
	19059	CaN	CAN
	22325	Vav2	VAV2

Table 4: GO of statistical significance.

GO ID	Name	Hits	Total	Percent (%)
GO:0009055	Electron carrier activity	7	107	6.54
GO:0003682	Chromatin binding	8	138	5.8
GO:0046906	Tetrapyrrole binding	6	107	5.61
GO:0030528	Transcription regulator activity	28	1053	2.66
GO:0009058	Biosynthetic process	73	3388	2.15
GO:0043167	Ion binding	78	3709	2.1

significant including T-cell receptor signaling pathway, B-cell receptor signaling pathway, and natural killer cell mediated cytotoxicity. Immune-related genes expression is speculated-changed after treatment with CA and probably have a trend of upregulation. Previous studies on CA immune function verified that CA could increase the carbon clearance index and the content of serum hemolysin and enhance the phagocytic function. Expression level of IFN-γ and IL-2 increased whereas that for IL-4, IL-10 decreased. The release of tumor necrosis factor (TFN) was found reduced while the activation of cytotoxic T lymphocyte (CTL) which aimed at Lewis lung cancer was boosted. NK cells activation and lymphocyte transformation rate of Lewis lung cancer bearing mice were both significantly improved through the determination of immune function indexes. To sum up, CA has been proved capable of strengthening cellular immune functions to tumor. When 3 immune related pathways were found including upregulated genes, we inferred that the immunity of mouse had been improved after treatment of CA. GSK3B, NFATC2, NFATC3, CaN, VAV2, and NCK1 were found upregulated in the 3 immune related pathways as listed in Table 3. According to the functions, genes covered in NO.21 can be classified into 312 different GO (Gene Ontology) and 6 of them has a P value less than 0.05 as listed in Table 4. GO of statistical significance includes the following genes: Cyp2a4, Cyp2c37, Cyp2c38, Cyp27b1, Cyp51, E4f1, Fdps, Gata4, Eif2ak1, Myt1l, Rarg, Sod1, Sp1, Taf3, Nr2c2, Hnf4g, Zdhhc3, Phf6, Mynn, Zfp386, Zfp617, Zfp114, Zfp238, Zfp174, Zfp113, Zfp109, Zfp263, Pcdhb6, Pcdhb15, Pcdhb20, Pcdhb21, Cdyl, Nfatc3, Pbx2, Rest, Smarca5, and Nfatc2. After doing some queries on the function of genes covered in statistically significant pathways and GO, we found out immune related genes and common genes of pathway and GO. Nfatc2, Nfatc3, Nfatc2ip, and CaN were found through combing raw analysis data of gene expression profile, as shown in Table 5.

3.2. Validation of Differentially Expressed Genes by Fluorescence Quantitative PCR. Relative expression level of the target genes Nfatc2, Nfatc3, Nfatc2ip, and CaN on average is shown in Table 6. Relative expression level of Nfatc2, Nfatc3, Nfatc2ip, and CaN in high-dose CA group, Nfatc2ip and CaN in medium-dose CA group, and CaN in low-dose CA group significantly improved compared with negative control group. The exact expression quantity is shown in Figure 2.

As shown in Figure 2, relative expression level of Nfatc2ip, Nfatc3, Nfatc2, and CaN in high-dose CA group improved compared with negative control group, which corresponds to the result of microarray analysis.

Table 5: Immune related genes covered in GO and pathway.

GenBank accession	GO ID	Gene symbol
NM_010899	GO:0001816	Nfatc2
NM_010900	GO:0001816	Nfatc2ip
NM_010901	GO:0003677	Nfatc3
NM_001004025	GO:0004723	CaN

3.3. Discussion of Genes Nfatc2ip, Nfatc3, Nfatc2, and CaN. Here, a whole mouse genome oligo microarray (4∗44K) was used to analyze gene expression level of female BALB/c mice and to compare the expression of corresponding target genes of each group on the time series. Systematic error or accidental error can affect the accuracy of microarray analysis to some extent and the errors may come from the processes of RNA extraction, RNA reverse transcription, and hybridization as well as the quality of gene chips and RNA. While the results of microarray analysis can reflect expressing pattern at body's internal gene level quickly, false positive results possibly caused by systematic error or accidental error must be taken into consideration. Verifying experiments like ELISA test, western blot test, and PCR test should be taken for further confirmation. Here, the results of PCR test help completing the study as well as making it more convincing. Through the analysis of genes included in NO.21, expression of critical genes in T-cell receptor signaling pathway, B-cell receptor signaling pathway, and natural killer cell mediated cytotoxicity had changed and immune related genes Nfatc2ip, Nfatc3, Nfatc2, and CaN were found.

NFAT (nuclear factor of activated T cells) which consists of 4 components NFATc1, NFATc2, NFATc3, and NFATc4 has been proved important in lymphocyte activation and development. Nfatc2 existing in cytoplasm translocates to the nucleus upon T-cell receptor stimulation and then becomes a member of the nuclear factor of activating T-cells transcription [13]. When the body lacks NFATc2, lymphocyte apoptosis will be significantly reduced which suggests lymphangiectasia and Th2-type response. Meanwhile, the Th1/Th2 balance will be destroyed which suggests a Th2 polarization. Immune regulatory function will disorder when Th1/Th2 balance is destroyed and tumor occurrence shows the preponderance state tendency of Th2. This state will weaken

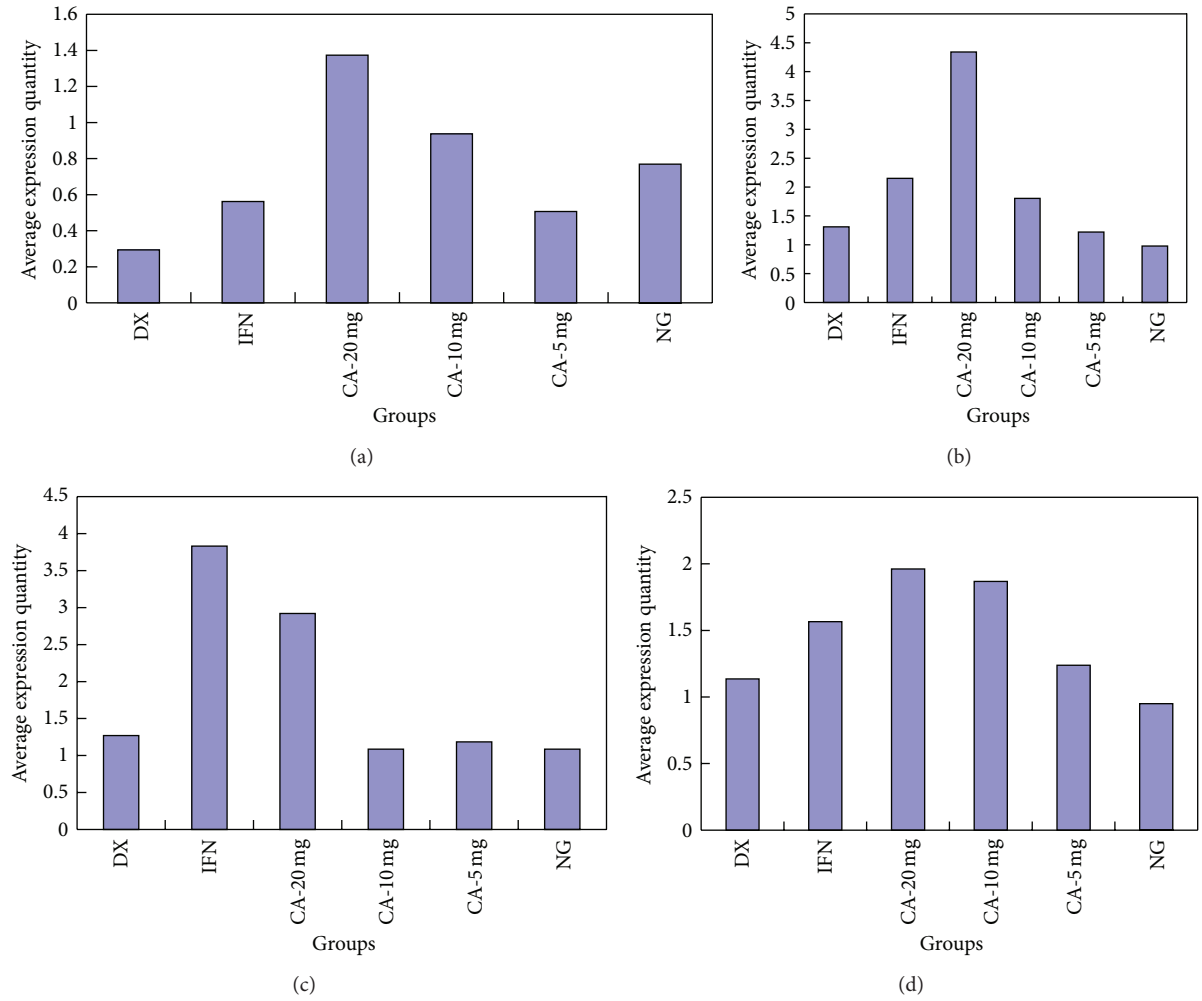

Figure 2: Relative expressing quantity of Nfatc2ip, Nfatc3, Nfatc2, and CaN in each groups. (a) Comparsion of Nfatc2ip expressing quantity among every group. (b) Comparsion of Nfatc3 expressing quantity among every group. (c) Comparsion of Nfatc2 expressing quantity among every group. (d) Comparsion of CaN expressing quantity among every groups.

Table 6: Relative expression level of target genes on average ($\overline{x} \pm s$, $n = 10$).

Group	Gene			
	Nfatc2	Nfatc3	Nfatc2ip	CaN
Docetaxel	1.270 ± 1.216	1.311 ± 0.573	0.294 ± 0.160	1.136 ± 0.544
Interferon	3.831 ± 4.960	2.152 ± 1.089	0.562 ± 0.464	1.566 ± 0.914
High-dose CA	2.920 ± 2.047	4.341 ± 3.961	1.373 ± 1.096	1.961 ± 0.927
Mid-dose CA	1.086 ± 0.367	1.803 ± 1.255	0.937 ± 0.950	1.868 ± 1.160
Low-dose CA	1.185 ± 1.156	1.220 ± 1.303	0.507 ± 0.168	1.238 ± 0.310
Negative	1.085 ± 0.462	0.979 ± 0.839	0.769 ± 1.599	0.950 ± 0.418

antitumor immune function and will induce tumor cells free from immune surveillance and immune attack. This may be one of the immune mechanisms of tumor development and provides a new idea of tumor treating. The reverse of Th1/Th2 abnormal drift is in favor of recovering antitumor immunocompetence and reducing tumor recurrence and metastasis to improve long-term survival rate finally.

NFATc2 and NFATc3 have been proved to synergistically regulate the reaction of T cell receptor, cell division, and Th2 differentiation. Th2-type reaction which suggests the secretion of IL-4, IL-5, and IL-6 is increased whereas the decrease IL-2, IFN-γ, TNF-α, and IL-10 happens when the body lacks NFATc2 and NFATc3 [14–16]. When B cell and T-cell lack NFATc2 and NFATc3 simultaneously, the function

of T cell will be weakened but the ability of T cell receptor mediating cell proliferation still exists, while B cells overactivate and show excessive differentiation [17]. The fact that expression of NFATc2 and NFATc3 is improved after treatment of CA indirectly indicates that CA could reverse Th1/Th2 drift. Meanwhile, secretion of IL-2, IFN-γ, TNF-α, and IL-10 is connected to CA too. High expression of NFATc2 and NFATc3 is in favor of the secretion of these cytokines which have already been used as nonspecific immunity treatment to cancer. NFATc2ip can induce the expression of T-cell cytokines, especially enhancing IL production. Three splice variants existing in NFATc2ip are able to methylate NFATc2ip after its translation to produce NFATc2ip regulatory factor. Expression of Th1-type and Th2-type cell factors will be suppressed when the methylation process is inhibited. Therefore, methylation process of NFATc2ip is an important controlling point of manipulating expression of NFAT-dependent cell factors but it will not have any influence on general transcription factor of Th1 and Th2 nor NFAT activation.

CaN (Calcineurin) is known as the only serine/threonine protein phosphatase regulated by $Ca^{(2+)}$-calmodulin so far and mainly aims at catalyzing dephosphorylation of phosphatidylserine and phosphatidyl threonine. It is a multifunctional signaling enzyme involved in function regulation of many cells and distributes in a wide range of tissues especially nerve tissue, T lymphocytes, heart, and skeletal muscle [18, 19]. NFAT family is the main substrate of CaN. NFAT regulates many genes expression as well as influencing many cells differentiation through CaN/NFAT signaling pathway. CaN is able to make NFAT existing in cytoplasm move into cell nucleus after dephosphorylation to finish following transcription and translation, and then Nfatc can combine with AP-1 family members alone or in groups to stimulate secretion of cell factors in certain areas such as IL-2. Transcription induction of IL-2 is a sign of T-cells activation. As mentioned above, NFAT is very important in regulating immunoreaction; meanwhile, NFATc3 and NFATc2 play a particularly key role in correcting body's immune function. Thus, high expression of CaN is a benefit to dephosphorylation of NFAT and indirectly has an effect upon immune system.

4. Conclusion

The result of microarray analysis of differentially expressed genes of female BALB/c EMT-6 mice has indicated that the antitumor mechanism of CA is closely related to body's immune system. Through upregulating, the expression of CaN, NFATC2, NFATC2ip, and NFATC3, CA is able to improve the transcription of immune factors like IL-2R and IFN-γ, stimulate proliferation and activation of T cells, NK cells, and macrophage, strengthen monitoring and killing abilities of cancer cells, and inhibit growth of tumor finally. The understanding of the anticancer mechanism of CA has provided a reliable evidence of taking advantage of CA to fight against cancer.

Disclosure

Hua Rong Yang and Jie Zhang, employed by Jiuzhang Biochemical Engineering Science and Technology Development Co., Ltd, are cooperators of this project. All of the other authors are researchers of West China School of Pharmacy, Sichuan University, and have no conflict of interests. Reagents were supported by the fund (The Sichuan Province Science and Technology Support Project Fund 2011SZ0131) of this project. Some parts of the experiment were entrusted to the third party but not sponsored by it. This statement is made in the interest of full disclosure and not because the authors consider this to be a conflict of interests.

Acknowledgments

The Sichuan Province Science and Technology Support Project Fund 2011SZ0131 supported this work. The authors would like to thank Hongwei Liu (Shanghai Biochip Co., Ltd.) for his great help in microarray analysis.

References

[1] R. McKallip, R. Li, and S. Ladisch, "Tumor gangliosides inhibit the tumor-specific immune response," *Journal of Immunology*, vol. 163, no. 7, pp. 3718–3726, 1999.

[2] S. A. Rosenberg, "Progress in human tumour immunology and immunotherapy," *Nature*, vol. 411, no. 6835, pp. 380–384, 2001.

[3] S. Ostrand-Rosenberg, "Animal models of tumor immunity immunotherapy and cancer vaccines," *Current Opinion in Immunology*, vol. 16, no. 2, pp. 1430–1450, 2004.

[4] A. L. Zhang, Q. Ma, and J. M. Gao, "Studies on bioactivities of chlorogenic acid and its analogues," *Chinese Traditional and Herbal Drugs*, vol. 32, no. 2, pp. 173–176, 2001.

[5] H. Kasai, S. Fukada, Z. Yamaizumi et al., "Action of chlorogenic acid in vegetables and fruits as an inhibitor of 8-hydroxy-deoxyguanseine formation in vitro and in a rat carcinogenesis model," *Food and Chemical Toxicology*, vol. 38, no. 5, pp. 467–471, 2000.

[6] E. Ignatowicz, B. Balana, S. V. Vulimiri et al., "The effect of plant Phenolics on the formaiton of 7, 12-dimethylbenz[a] anthracene-DNA adducts and TPA- stimulated polymorphonuclear neutrophifls chemiluminescence in vitro," *Toxicology*, vol. 189, no. 3, pp. 199–209, 2003.

[7] M. Shimizu, N. Yoshimi, Y. Yamach et al., "Suppressive effects of chlorogenic acid on N-methyl-N-nitrosourea-indueed glandular stomach carcinogenesis in male F344 rats," *Toxicological Sciences*, vol. 24, no. 5, pp. 433–439, 1999.

[8] K. Matsunaga, M. Katayama, K. Sakata et al., "Inhibitory effects of chlorogenic acid on azoxymethane-induced colon carcinogenesis in male F344 rats," *Asian Pacific Organization for Cancer Prevention*, vol. 3, no. 2, pp. 163–166, 2002.

[9] L. C. Chiang, L. T. Ng, W. Chiang et al., "Immunomodulatory activities of flavonoids, monoterponoids, triterpenoids, iridoid glycosides and phenolic compounds of Plantago species," *Planta Medica*, vol. 69, no. 7, pp. 600–604, 2003.

[10] K. J. Hu, F. J. Qu, Z. L. Wang et al., "Experimental study on the induction of a-tinterferon of human leucocyte in vitro by chlorogenic acid," *Journal of Harbin Medical University*, vol. 38, pp. 120–122, 2004.

[11] H. Z. Wu, J. Luo, Y. X. Yin et al., "Effects of chlorogenic acid, an active compound activating calcineurin, purified from Flos

Lonicerce on macrophage," *Acta Pharmacologica Sinica*, vol. 25, no. 12, pp. 1685–1689, 2004.

[12] P. D. Rogers and K. S. Barker, "Evaluation of differential gene expression in fluconazole-susceptible and -resistant isolates of Candida albicans by cDNA microarray analysis," *Antimicrobial Agents and Chemotherapy*, vol. 46, no. 11, pp. 3412–3417, 2002.

[13] S. Baksh, H. R. Widlund, A. A. Frazer-Abel et al., "NFATc2-mediated repression of cyclin-dependent kinase 4 expression," *Molecular Cell*, vol. 10, no. 5, pp. 1071–1081, 2002.

[14] M. R. Hodge, A. M. Ranger, F. C. de la Brousse, T. Hoey, M. J. Grusby, and L. H. Glimcher, "Hyperproliferation and dysregulation of IL-4 expression in NF-ATp-deficient mice," *Immunity*, vol. 4, no. 4, pp. 397–405, 1996.

[15] A. Kiani, J. P. B. Viola, A. H. Lichtman, and A. Rao, "Down-regulation of IL-4 gene transcription and control of Th2 cell differentiation by a mechanism involving NFAT1," *Immunity*, vol. 7, no. 6, pp. 849–860, 1997.

[16] A. M. Ranger, M. R. Hodge, E. M. Gravallese et al., "Delayed lymphoid repopulation with defects in IL-4-driven responses produced by inactivation of NF-ATc," *Immunity*, vol. 8, no. 1, pp. 125–134, 1998.

[17] K. Schuh B Kneitz J Heyer et al., "Retarded thymic involution and massive germinal center formation in NF-ATp-deficient mice," *The European Journal of Immunology*, vol. 28, no. 8, pp. 2456–2466, 1998.

[18] H. Mukai, C. D. Chang, H. Tanaka, A. Ito, T. Kuno, and C. Tanaka, "cDNA cloning of a novel testis-specific calcineurin B-like protein," *Biochemical and Biophysical Research Communications*, vol. 179, no. 3, pp. 1325–1330, 1991.

[19] K. L. Dodge and J. D. Scott, "Calcineurin anchoring and cell signaling," *Biochemical and Biophysical Research Communications*, vol. 311, no. 4, pp. 1111–1115, 2003.

Hindawi Publishing Corporation
Journal of Analytical Methods in Chemistry
Volume 2013, Article ID 827361, 9 pages
http://dx.doi.org/10.1155/2013/827361

Research Article

Simultaneous Quantification of Limonin, Two Indolequinazoline Alkaloids, and Four Quinolone Alkaloids in *Evodia rutaecarpa* (Juss.) Benth by HPLC-DAD Method

Pei-ting Zhang,[1] Bi-yan Pan,[2] Qiong-feng Liao,[3] Mei-cun Yao,[1] Xin-jun Xu,[1] Jin-zhi Wan,[1] Dan Liu,[1] and Zhi-yong Xie[1]

[1] *School of Pharmaceutical Sciences, Sun Yat-sen University, Guangzhou 510006, China*
[2] *Guangzhou Baiyun Shan Ming Xing Pharmaceutical Co. Ltd., Guangzhou 510250, China*
[3] *College of Chinese Traditional Medicine, Guangzhou University of Chinese Medicine, Guangzhou 510006, China*

Correspondence should be addressed to Zhi-yong Xie; xiezy2074@yahoo.com

Received 23 January 2013; Accepted 16 April 2013

Academic Editor: Yu-Ming Fan

A simple and efficient HPLC-DAD (225 nm) method was developed and validated for the simultaneous determination of limonin and six key alkaloids (evodiamine, rutaecarpine, 1-methyl-2-undecyl-4(1H)-quinolone, evocarpine, 1-methy-2-[(6Z,9Z)]-6,9-pentadecadienyl-4-(1H)-quinolone, and dihydroevocarpine) in *Evodia rutaecarpa* (Juss.) Benth, which has been widely used as one of the Traditional Chinese Medicines. The chromatographic separation was carried out on a Hypersil BDS C18 column, and gradient elution was employed with a mobile phase containing acetonitrile and water. Contents of the analytes in 18 batches of samples were analyzed by ultrasonic extraction with ethanol and water mixture (80 : 20, v/v) followed by HPLC analysis. Separation of the seven analytes was achieved within 60 min with good linearity ($r > 0.999$). The RSD of both the intraday and interday precision was below 1.85%. The accuracy at different concentrations was within the range of 97.91 to 100.49%. Hierarchical clustering analysis was performed to differentiate and classify the samples based on the contents of the seven constituents. This study indicated that the quality control of *E. rutaecarpa* could be simplified to the measurement of four constituents, and that limonin, 1-methyl-2-undecyl-4(1H)-quinolone, and dihydroevocarpine should also be served as the chemical markers together with evodiamine for the quality control of *Evodia rutaecarpa* (Juss.) Benth.

1. Introduction

The dried fruit of *Evodia rutaecarpa* (Juss.) Benth (*E. rutaecarpa*, Chinese name, Wu-zhu-yu) has been used as one of the Traditional Chinese Medicines (TCM) for more than 2000 years and is officially listed in the Chinese Pharmacopoeia [1]. It has been proven to be effective in the treatment of gastrointestinal disorders, headache, postpartum hemorrhage, amenorrhea, and chill limbs. Up to now, *E. rutaecarpa* is known to contain a large number of compounds including limonoids, indolequinazoline and quinolone alkaloids, essential oils, carboxylic acids, and flavonoids [2].

Extensive studies have been conducted since the discovery of *E. rutaecarpa* and many pharmacological activities has been reported for alkaloids. Evodiamine (Evo) and rutaecarpine (Rut), two indolequinazoline alkaloids, are the characteristic chemical constituents and responsible for the beneficial effects on the human health. Several studies have shown that Rut has a variety of intriguing biological properties, such as cardioprotective [3–8], antihypertensive [8–11], antithrombotic [8, 11], antiatherosclerosis [8, 12], anti-inflammatory [8, 13], antiobesity [8, 14], and uterotonic activity [15], by modulating drug metabolizing enzymes and receptors [8, 16–18]. Recent studies demonstrated that Evo had anticancer activity and induction of apoptosis in several types of cancer cells [19–26]. In addition, pharmacological studies indicated that quinolone alkaloids of *E. rutaecarpa* could inhibit leukotriene biosynthesis in human granulocytes [27] and the nuclear factor of activated T cells [28] and had a highly selective antibacterial activity against *Helicobacter pylori* [29].

Lee et al. [30] found three quinolone alkaloids as blockers of angiotensin II receptor which modulate blood pressure. Furthermore, it was reported that limonin (Lim) had anti-HIV [31, 32], antinociceptive, and anti-inflammatory effects [33, 34], and it could inhibit P-glycoprotein activity and induce carcinogenesis [35, 36].

Unlike the synthetic drugs, herbal medicines have more complicated compositions. The effectiveness of herbal medicines may be attributed to the overall effect of all the components rather than a single component. Besides, the interactions among different components in different herbs are always a concern. Thus, the quality evaluation of herbal medicine should contain the information of as much bioactive components as possible.

To date, there have already been some preliminary researches about the quantitative analysis of *E. rutaecarpa*. Analytical techniques such as TLC [37, 38], CE [39], HPLC [40–44], UPLC [45], and LC-MS [46–48] have been applied for the determination of indoloquinazoline and/or quinolone alkaloids in *E. rutaecarpa*. GC-MS has been used to detect the volatile oils in Evodia species [49]. Meanwhile, Huang et al. found that three species of Fructus Evodiae revealed 20 major common peaks, and the similarities of internal transcribed spacer (ITS) sequences were 97% in *E. rutaecarpa*, but only Evo and Rut were identified and quantitative analyzed [42]. Zhao et al. developed an HPLC method for the determination of wuchuyuamide-I, quercetin, Lim, Evo, and Rut within 55 min [44]. Although only a little pharmacological effect of quinolone alkaloids has been reported so far, it is possible that these compounds may play a vital role in comprehensive effect of *E. rutaecarpa*. The determination of quinolone alkaloids may provide additional information for the overall quality control. Zhou et al. [48] developed an LC-ESI-MS^n method purposed for the analysis and characterization of indolequinazoline and quinolone alkaloids in the extract of *E. rutaecarpa*. Though 15 peaks were identified by MS data, the method focused on chromatographic fingerprint study and could not be used to quantitative determination of Lim, Evo, and Rut, the contents of which were defined in Chinese Pharmacopoeia.

However, to the best of our knowledge, there has been no method for simultaneous quantitation of limonin, indolequinazoline, and quinolone alkaloids in *Evodia rutaecarpa* (Juss.) Benth by HPLC-DAD by now. Since DAD can offer peak purity analysis and absorption spectrum of analyte for qualitative analysis, it is a very useful tool in identifying the different compounds simultaneously. The present study is proposed aiming to develop a simple HPLC-DAD method for the simultaneous determination of limonin, two indolequinazoline alkaloids (Evo and Rut), and four quinolone alkaloids (1-methyl-2-undecyl-4(1H)-quinolone (Q1), evocarpine (Q2), 1-methy-2-[(6Z,9Z)]-6,9-pentadecadienyl-4-(1H)-quinolone (Q3), and dihydroevocarpine (Q4)) in 18 batches of *E. rutaecarpa* (the chemical structures of them are shown in Figure 1). As a result, the method provides a rapid, simple, and accurate simultaneous quantification of Lim and six alkaloids in *E. rutaecarpa*, which could provide a more suitable method and significantly improve the quality evaluation of the raw material of *E. rutaecarpa*.

2. Experimental

2.1. Reagents and Materials. Lim, Evo, and Rut standards were purchased from the National Institute for Food and Drug Control (Beijing, China). 1-methyl-2-undecyl-4(1H)-quinolone (Q1), evocarpine (Q2), 1-methy-2-[(6Z,9Z)]-6,9-pentadecadienyl-4-(1H)-quinolone (Q3), and dihydroevocarpine (Q4) were isolated by high-speed counter-current chromatography (HSCCC). Their structures (shown in Figure 1) were confirmed on the basis of spectral analysis comprising ultraviolet spectrometry (UV), ^{1}H Nuclear Magnetic Resonance (NMR), ^{13}C NMR, and electrospray ionisation tandem mass spectrometry (ESI-MS/MS). The purities calculated by normalization of the peak areas were 94.3%, 95.2%, 96.8%, and 98.3%, respectively. Acetonitrile (ACN) used for HPLC was of chromatographic grade (Tedia Company Inc, Beijing, China), and water used was distilled water. Other reagent solutions were of analytical grade. Eighteen batches of samples collected from different regions and time were investigated and authenticated as *E. rutaecarpa* (Table 1). Voucher specimens were stored away from light and water in sealed dryer before use in order to avoid moisture and chemical changes.

2.2. Standard Solution Preparation. Lim, Evo, Rut, Q1, Q2, Q3, and Q4 were weighed accurately and dissolved in ACN in a 10 mL volumetric flask to make a stock solution (800, 250, 250, 150, 250, 250, and 150 μg/mL, resp.). Working standard solutions were prepared from the stock solution by further dilution with the appropriate volume of methanol. These solutions were stored protected from light at −20°C.

2.3. Sample Solution Preparation. Pulverized sample (120 mesh, 0.5 g) was weighed accurately into a 100 mL conical flask with cover and dipped in 20 mL of ethanol-water (80 : 20, v/v) for 1 h, and then extracted in an ultrasonic bath (35°C, 40 Hz) for 1 h. The extracts were then filtrated through a 0.22 μm membrane filter and diluted with ethanol-water (80 : 20, v/v) to 20 mL for analysis. Each sample was prepared with the previous protocol for HPLC analysis.

2.4. Instrumentation and Chromatographic Conditions. A Waters HPLC instrument equipped with a 1525 QuatPump, a 2996 UV-Vis photodiode array detector, a 717 autosampler, and an Empower workstation was used. Chromatographic separations were carried out on an Hypersil BDS C18 column (200 mm × 4.6 mm, id 5 μm) protected by a guard column (4.0 mm × 3.0 mm, id 5 μm). The mobile phase consisted of water (A) and ACN (B). The gradient program was as follow: 0–30 min, linear gradient 40–50% B; 30–35 min, linear gradient 50–75% B; 35–55 min, linear gradient 75–80% B; 55–60 min, isocratic 80% B. The column temperature was maintained at 25°C. The flow rate of the mobile phase was 1.0 mL/min. The effluents were monitored at 225 nm by a photodiode array detector. A typical injection volume was 20 μL.

2.5. Hierarchical Clustering Analysis (HCA) of 18 Samples Based on Chemical Markers. HCA is a statistical method for

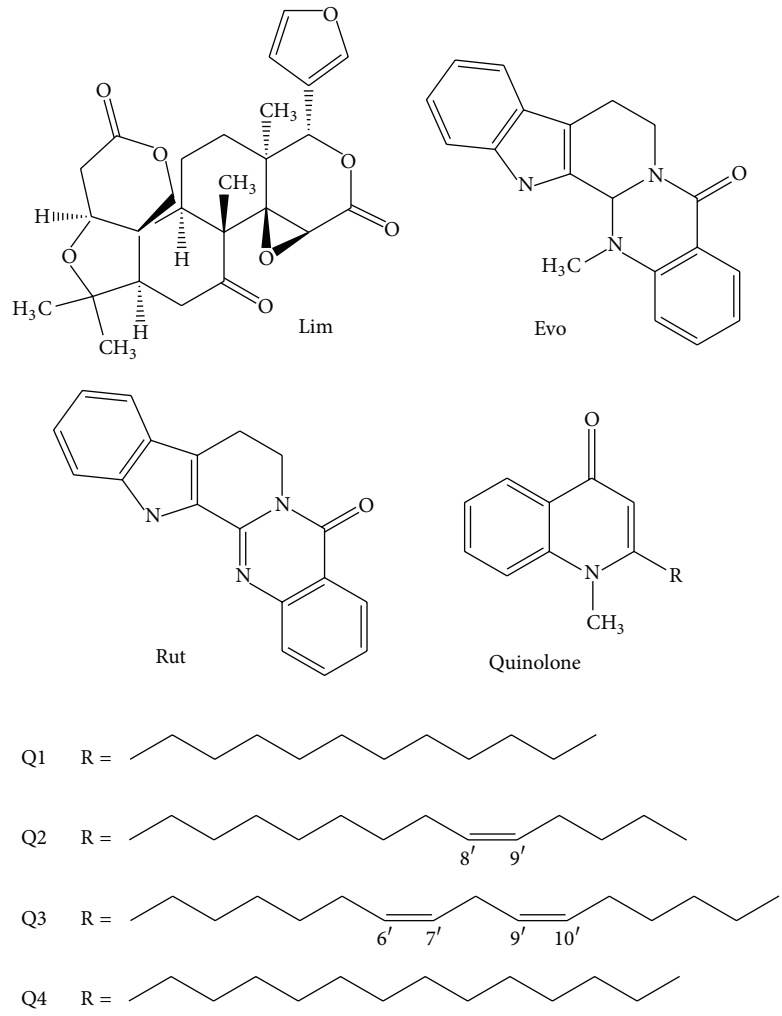

Figure 1: Chemical structures of seven constituents from *E. rutaecarpa*. Lim: limonin; Evo: evodiamine; Rut: rutaecarpine; Q1: 1-methyl-2-undecyl-4(1H)-quinolone; Q2: evocarpine; Q3: 1-methy-2-[(6Z,9Z)]-6,9-pentadecadienyl-4-(1H)-quinolone; Q4: dihydroevocarpine.

finding relatively homogeneous clusters of cases based on measured characteristics. It starts with each case in a separate cluster and then combines the clusters sequentially, reducing the number of clusters at each step until only one cluster is left. When there are N cases, this involves $N - 1$ clustering steps or fusions. This hierarchical clustering process can be represented as a tree or dendrogram, where each step in the clustering process is illustrated by a joint of the tree. HCA method was used in our study to find relatively homogeneous clusters of the 18 batches of *E. rutaecarpa* based on the contents of the seven markers as the measured characteristics, which was operated in Minitab 15.0 software.

Ward's method, which is a very efficient method for the analysis of variance between clusters, was applied, and Euclidean distance was selected as a measurement.

3. Results and Discussion

3.1. Selection and Identification of Markers. Alkaloids and limonoids are the major active compounds in *E. rutaecarpa*. In the present study, the selected markers, which contained one limonoid (Lim), two indolequinazoline alkaloids (Evo and Rut), and four quinolone alkaloids (Q1, Q2, Q3, and Q4), are the main constituents of *E. rutaecarpa* and have significant pharmacological effect reported before. Peaks of these seven chemical markers were assigned in HPLC by comparing individual peak retention times and UV spectra with those of the standards. Peaks at retention times 10.2, 14.7, 17.7, 43.5, 44.9, 46.8, and 52.8 min were determined to be Lim, Evo, Rut, Q1, Q2, Q3, and Q4, respectively (Figure 2).

3.2. Optimization of Chromatographic Conditions. The optimization of the chromatographic conditions was performed by using the solution of sample number 11. To obtain good resolution and peaks sharp, different compositions of mobile phases (ACN-water or methanol-water) and different gradient elution programs were tried. The results showed that sharp and symmetrical peaks were obtained by using ACN as organic phases. Because the analytes had a great difference in polarity, the ratio of organic phases was changed rapidly in 30–35 min. According to the UV spectra of seven markers recorded by DAD full scan in the range from 210 to 400 nm,

Table 1: Collected information and contents of the seven markers of the samples ($n = 3$).

Sample number	Sources	Acquisition time	Contents (%)* ± SD						
			Lim	Evo	Rut	Q1	Q2	Q3	Q4
1	Guangxi	Mar 2007	1.756 ± 0.0282	0.224 ± 0.0042	0.308 ± 0.0049	0.591 ± 0.0115	0.245 ± 0.0019	0.153 ± 0.0003	0.137 ± 0.0017
2	Guangxi	Sep 2007	1.129 ± 0.0107	0.238 ± 0.0009	0.440 ± 0.0026	0.122 ± 0.0009	0.459 ± 0.0015	0.449 ± 0.0028	0.173 ± 0.0003
3	Guangxi	Jan 2010	2.141 ± 0.0155	0.267 ± 0.0037	0.211 ± 0.0016	0.537 ± 0.0105	0.215 ± 0.0035	0.214 ± 0.0657	0.126 ± 0.0015
4	Guangxi	Apr 2010	2.161 ± 0.0342	0.471 ± 0.0077	0.447 ± 0.0078	0.110 ± 0.0016	0.499 ± 0.0078	0.512 ± 0.0088	0.185 ± 0.0028
5	Guizhou	Nov 2006	1.747 ± 0.0288	0.078 ± 0.0008	0.157 ± 0.0030	0.571 ± 0.0046	0.100 ± 0.0019	0.163 ± 0.0020	0.113 ± 0.0016
6	Guizhou	Mar 2007	1.603 ± 0.0129	0.775 ± 0.0118	0.742 ± 0.0084	0.408 ± 0.0034	0.740 ± 0.0085	0.688 ± 0.0089	0.337 ± 0.0047
7	Guizhou	Jan 2010	1.362 ± 0.0181	0.231 ± 0.0027	0.188 ± 0.0032	0.055 ± 0.0009	0.221 ± 0.0008	0.171 ± 0.0032	0.083 ± 0.0008
8	Guizhou	Mar 2010	6.111 ± 0.0529	2.070 ± 0.0251	1.019 ± 0.0121	0.375 ± 0.0056	1.326 ± 0.0198	1.273 ± 0.0251	0.487 ± 0.0092
9	Guizhou	Jun 2010	3.212 ± 0.0536	1.189 ± 0.0058	0.818 ± 0.0043	0.250 ± 0.0013	1.000 ± 0.0067	0.811 ± 0.0029	0.333 ± 0.0021
10	Guizhou	Jul 2010	1.344 ± 0.0210	0.380 ± 0.0058	0.496 ± 0.0027	0.180 ± 0.0020	0.697 ± 0.0098	0.500 ± 0.0010	0.204 ± 0.0035
11	Hunan	Apr 2009	2.621 ± 0.0433	0.407 ± 0.0063	0.387 ± 0.0065	0.213 ± 0.0008	0.437 ± 0.0048	0.412 ± 0.0010	0.217 ± 0.0023
12	Hunan	Apr 2010	1.822 ± 0.0344	0.324 ± 0.0030	0.430 ± 0.0058	0.118 ± 0.0018	0.497 ± 0.0045	0.533 ± 0.0096	0.198 ± 0.0027
13	Jiangxi	Mar 2007	1.635 ± 0.0235	1.053 ± 0.0199	0.817 ± 0.0122	0.138 ± 0.0027	0.646 ± 0.0126	0.632 ± 0.0074	0.224 ± 0.0042
14	Jiangxi	Nov 2008	1.514 ± 0.0290	0.078 ± 0.0012	0.200 ± 0.0035	0.064 ± 0.0012	0.321 ± 0.0013	0.385 ± 0.0032	0.152 ± 0.0020
15	Jiangxi	Mar 2010	1.695 ± 0.0146	0.825 ± 0.0116	0.690 ± 0.0037	0.194 ± 0.0013	0.740 ± 0.0052	0.605 ± 0.0038	0.236 ± 0.0015
16	Shanxi	Mar 2007	1.135 ± 0.0046	0.335 ± 0.0031	0.477 ± 0.0070	0.126 ± 0.0017	0.472 ± 0.0086	0.419 ± 0.0078	0.171 ± 0.0022
17	Shanxi	Jul 2010	13.478 ± 0.2313	1.967 ± 0.0350	1.127 ± 0.0174	0.543 ± 0.0028	1.881 ± 0.0358	1.151 ± 0.0211	0.592 ± 0.0062
18	Sichuan	Mar 2010	1.624 ± 0.0028	0.235 ± 0.0007	0.386 ± 0.0021	0.104 ± 0.0016	0.409 ± 0.0068	0.454 ± 0.0037	0.174 ± 0.0026

*Content (%) means the content (g) of marker in 100 g crude drug. Content (%) = [found amount (μg) $*$ 20 mL/(20 μL $*$ 0.5 g)] $\times$ 100%; 20 mL is the volume of sample solution; 20 μL is the injection volume, and 0.5 g is the weight of pulverized crude drug.

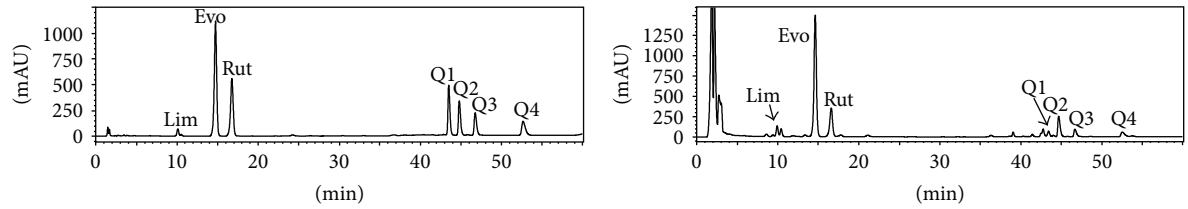

Figure 2: Representative HPLC chromatograms of mixed standards and the extract of *E. rutaecarpa* at 225 nm. (a) Mixed standards of the seven chemical constituents; (b) extract of *E. rutaecarpa* (sample number 11). Peaks: Lim: limonin; Evo: evodiamine; Rut: rutaecarpine; Q1: 1-methyl-2-undecyl-4(1H)-quinolone; Q2: evocarpine; Q3: 1-methy-2-[(6Z,9Z)]-6,9-pentadecadienyl-4-(1H)-quinolone; Q4: dihydroevocarpine.

Table 2: Linear regression data, LOD and LOQ of investigated compounds.

Analytes	Linear regression data[a]			LOD (ng)	LOQ (ng)
	Regressive equation	r	Linear range[b] (μg)		
Lim	$Y = 264926X - 79642$	0.9991	0.80–16	5.962	19.873
Evo	$Y = 1119030X - 176315$	0.9997	0.25–5.0	0.199	0.664
Rut	$Y = 57966X - 388805$	0.9990	0.25–5.0	0.454	1.514
Q1	$Y = 2563591X - 59536.5$	0.9999	0.15–3.0	0.809	2.696
Q2	$Y = 2605282X - 79116$	0.9999	0.25–5.0	0.580	1.935
Q3	$Y = 1253639X - 56012$	0.9999	0.25–5.0	1.773	5.909
Q4	$Y = 2749144X - 68371$	0.9999	0.15–3.0	1.553	4.615

[a]In the linear regression data, Y refers to the peak area, X is the concentration, and r is the correlation coefficient of equation.
[b]Linear range (μg) means the content of marker in injection volume (20 μL).

225 nm was selected for monitoring the seven markers, which provided the optimum S/N and the highest value of the marker with the lowest content for simultaneously quantitative analysis of all the markers. Compared with [44, 48], the usage of single-wavelength UV detection instead of multiwavelength and MS detection was essential to the popular application of the method.

3.3. Optimization of Extraction Method. The constituents of *E. rutaecarpa* could be extracted by reflux [41–43], ultrasonic water bath [46–48], and supercritical fluid [45]. To simplify the extraction process, ultrasonic extraction was chosen, and the efficiency of extraction procedure was evaluated by using different solvents, such as methanol, ethanol, ethyl acetate, and chloroform. The best solvent was found to be ethanol-water, which was less poisonous and provided the highest values in the contents of the seven markers.

A method involving four-factor-three-level orthogonal array design (OAD) including composition of extraction solvent (ethanol-water 70 : 30, 80 : 20, and 90 : 10, v/v), volume of extraction solvent (10, 15, and 20 mL), and duration of extraction (30, 45, and 60 min) was developed for the optimization of the extraction. The results demonstrated that the established extraction method without the procedure of concentration was adequate and appropriate for the analysis. Therefore, the sample preparation method was optimized as in "Section 2.3. Sample Solution Preparation."

3.4. Method Validation. Specificity was investigated by comparing the chromatograms of mixed standards and the extract of *E. rutaecarpa* (Figure 2). Furthermore, according to the three-dimensional plot of the absorbance as a function of retention time and wavelength in the HPLC-DAD data for sample number 11, no evidence of peak of impurity which overlapped with those of markers was found.

The stock solution containing the seven markers was prepared and diluted to appropriate concentration ranges for the establishment of calibration curves. The calibration graphs were plotted after linear regression of the peak areas versus the corresponding concentrations, and good linear behaviors were observed with the values of r higher than 0.999 for all the analytes. LOD and LOQ were determined at S/N of about 3 and 10, respectively (data shown in Table 2).

Precision was evaluated with the solution of sample number 11 under the selected optimal conditions six times in 1 day for intraday variation and twice a day on 3 consecutive days for interday variation. Repeatability was confirmed with six different working solutions prepared from sample number 11 and, one of them was injected into the apparatus in 0, 2, 4, 8, 12, 24, and 36 h to evaluate the stability of the solution. All the results were expressed as RSDs which were shown in Table 3.

The recovery was performed by adding known amounts of the seven standards at low (80% of the known amounts), medium (same as the known amounts), and high (120% of the known amounts) levels. The spiked samples were then extracted, processed, and quantified in accordance with the methods mentioned above. The recoveries measured at three levels varied from 97.91 to 100.49% with RSDs from 0.13 to 1.94% (data shown in Table 4).

The comparison with those previous study [42, 46, 48] demonstrates that our proposed method has many

Table 3: Precision, repeatability, and stability of the HPLC method for determination of the seven markers.

Analytes	Nominal amount (μg)	Precision[a]						Repeatability[b]		Stability[b]	
		Intraday (n = 6)			Interday (n = 6)			Mean (%)	RSD (%)	Mean (%)	RSD (%)
		Mean (μg)	RSD (%)	RE (%)[c]	Mean (μg)	RSD (%)	RE (%)				
Lim	8.0	7.88	0.54	−1.54	7.85	1.57	−1.82	2.62	1.93	2.62	0.97
Evo	2.0	1.97	0.29	−1.49	2.03	1.85	1.68	0.40	1.94	0.40	1.34
Rut	2.0	1.96	0.23	−1.79	2.04	1.53	1.96	0.39	1.19	0.39	1.63
Q1	1.2	1.18	0.18	−1.26	1.21	0.87	1.16	0.21	1.71	0.20	1.80
Q2	2.0	1.98	0.22	−1.00	2.03	0.73	1.53	0.44	1.16	0.44	0.76
Q3	2.0	1.97	0.14	−1.49	2.04	1.48	2.02	0.41	0.87	0.41	1.05
Q4	1.2	1.19	0.21	−0.48	1.22	1.85	1.37	0.22	1.29	0.22	1.12

[a]Tested by standard mixture solution.
[b]Tested by sample number 11 solution.
[c]RE (%) is short for relative error. RE (%) = [(mean − nominal amount)/nominal amount] × 100%.

Table 4: Recovery of the extraction method for determination of the seven markers.

Analytes	Amount			RSD (%)	Recovery (%)[c]
	Original (μg)[a]	Add (μg)[b]	Found (μg)		
Lim	13.12	10.49	23.41	1.80	98.18
	13.12	13.12	26.06	0.64	98.64
	13.12	15.74	28.56	1.50	98.12
Evo	2.04	1.63	3.65	0.71	98.96
	2.04	2.04	4.03	1.06	98.14
	2.04	2.44	4.45	0.13	99.02
Rut	1.94	1.55	3.46	0.89	98.52
	1.94	1.94	3.85	0.79	98.76
	1.94	2.32	4.22	1.61	98.14
Q1	1.05	0.84	1.87	1.76	97.91
	1.05	1.05	2.09	0.75	98.60
	1.05	1.26	2.29	0.68	98.34
Q2	2.19	1.75	3.94	0.46	100.49
	2.19	2.19	4.34	1.04	98.78
	2.19	2.62	4.76	0.13	98.14
Q3	2.06	1.65	3.71	1.71	100.29
	2.06	2.06	4.11	1.64	99.51
	2.06	2.47	4.51	1.16	99.35
Q4	1.09	0.87	1.94	1.46	98.68
	1.09	1.09	2.15	0.98	98.53
	1.09	1.30	2.36	1.94	97.98

[a]Tested by sample number 11 solution.
[b]The samples added known amounts of standards at low, medium, and high levels (80%, 100%, and 120% of the known amounts, resp.).
[c]Recovery (%) = [(found − original)/added] × 100%. The results indicated that the developed method was reliable and accurate for the measurement of the seven analytes.

advantages. It is the first time that limonin, two indolequinazoline alkaloids, and four quinolone alkaloids were analyzed simultaneously with acceptable performance of linearity, precision, repeatability, and accuracy. In addition, the developed method can offer better precision (RSDs < 1.9%) compared with HPLC-MS method [46] (RSDs < 6.6%), so that it can be an economic alternative for experiments in which a higher degree of sensitivity is not required.

3.5. Quantitative Determination of Seven Markers. The contents of seven markers in 18 batches of *E. rutaecarpa* were measured with the developed method. The representative HPLC chromatograms of mixed standards and the extract of *E. rutaecarpa* (sample number 11) are shown in Figure 2. The contents of seven markers were calculated from the regression equations obtained from calibration curves, and the results are shown in Table 1, expressed as the percentage of each constituent in crude drug. Among these markers, it was defined in the newest Chinese Pharmacopoeia that the total content of Evo and Rut in *E. rutaecarpa* should not be less than 0.15%, and the content of Lim should not be less than 1.0%, otherwise it would not be used as the raw material and is regarded as substandard herb. Based on this definition, all samples met the requirement of Chinese Pharmacopoeia and could be put into production, but the content of each marker differed greatly, which might cause serious waste of the herbs.

Moreover, eight samples were stored for several years at a dry and good ventilation place under ambient temperature in order to evaluate storage stability. The results showed that the similarities within samples from the same location were high. It proved that the raw materials could be stored steadily for three years in the previous conditions.

3.6. HCA of 18 Samples Based on 7 Chemical Markers. A dendrogram of HCA was generated (Figure 3), which revealed the relationships among the samples. Using this method, 18 samples were classified into two broad categories. Samples numbers 8 and 17 were in category I, and the other samples were in category II, which was further divided into two clusters. Samples numbers 1, 3, and 5 were in cluster A, and the others were in cluster B. The result indicated that samples with similar chemical profiles could be divided into one group.

The results obtained from the HCA statistical methods accorded well with those of Zhao et al. [44], because we

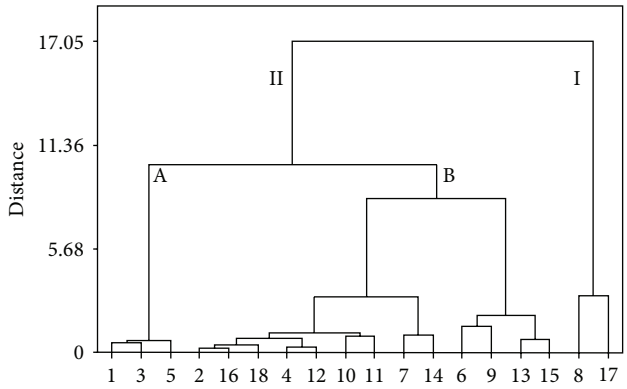

Figure 3: Dendrogram of HCA for the 18 tested samples of *E. rutaecarpa*. The hierarchical clustering was done by Minitab 15.0 software. Ward's method was applied, and Euclidean distance was selected as a measurement. 18 batches of *E. rutaecarpa* were divided into two broad categories. Samples numbers 8 and 17 were in category I, and the other samples were in category II, which was divided into two clusters again. Samples numbers 1, 3, and 5 were in cluster A, and the others were in cluster B.

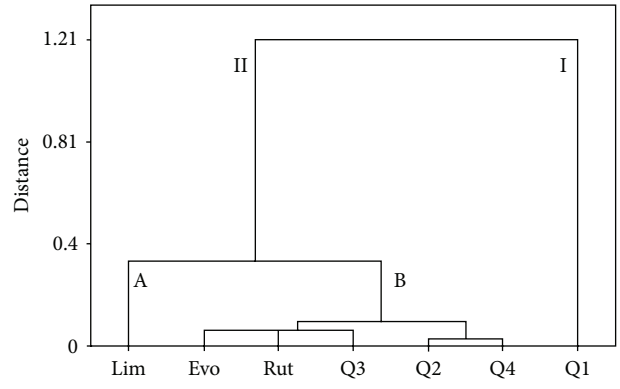

Figure 4: Dendrogram of HCA for the seven chemical constituents of *E. rutaecarpa*. The hierarchical clustering was done by Minitab 15.0 software. Ward's method was applied, and Euclidean distance was selected as a measurement. Seven chemical constituents of *E. rutaecarpa* were divided into two categories. Q1 was in category I, and the other samples were in category II, which was divided into two clusters again. Lim was in cluster A, and the others were in cluster B.

also found that some samples could be classified to the main domain. Generally speaking, 18 samples could be classified into three groups. Samples numbers 8 and 17 were in Group I, which had high contents of seven markers; samples numbers 1, 3, and 5 were in Group II, which had high relative content of Q1; and the other samples were in Group III. The similarities of the herbs were relative to their collecting locations, but the relative content of Q1 was significantly high in three samples (samples numbers 1, 3, and 5) originating from Guangxi and Guizhou Provinces. These results indicated that Q1 played a significant role in HCA. The samples from Guizhou Province showed relatively high contents of all markers; however, the differences between samples came from Guizhou, and other provinces were not obvious. In addition, sample number 17 was found to have extraordinary high contents of all markers, and it might due to the degree of drying of the herb.

At the beginning of manufactory, the content of key constituents in TCMs should be determined in order to adjust the ratio of the prescription, so that the quality of medicine could be controlled easily. According to Zhao et al. [44], blending the low-content samples with the high-content ones is a conductive way to save resources and to guide rational herb use. Actually, it is not encouraged to mix different material in industry. Because the content of key constituents may not have the same trends, the result of mixture is hard to control. As a result, further study should be paid on the quality evaluation of *E. rutaecarpa*.

3.7. HCA of 18 Samples Based on Lim, Evo, Q1, and Q4. The contents of the seven markers were defined as seven variables in the analysis so as to analyze, differentiate, and classify the seven chemical constituents.

A dendrogram was generated (Figure 4), which revealed the relationships among the chemical constituents. It was noticeable that seven variables were divided into two main clusters. Q1 was in cluster I, and the other samples were in cluster II, which was divided into two subgroups again. Lim was in subgroup A, and the others were in subgroup B.

As shown in the results, Q1 and Lim were essential markers in quality control, and Evo, Rut, and Q3 had similar effect, so as Q2 and Q4. The results indicated that there was no need to analyze all markers to evaluate the quality of *E. rutaecarpa*. Then several combinations were tried. It was found that the HCA result was mostly accordant with that obtained from seven markers, when the contents of Lim, Evo, Q1, and Q4 were chosen as markers to analyze, differentiate, and classify the 18 samples. Samples numbers 8 and 17 were in category I, and the other samples were in category II, which was divided into two clusters again. Samples numbers 1, 3, and 5 were in cluster A, and the others were in cluster B. Compared with the results attained from seven markers (Figure 3), a little difference occurred in cluster A, and the other samples had the same classification. The results indicated that the quality evaluation of *E. rutaecarpa* could be simplified to the measurement of Lim, Evo, Q1, and Q4, and it will be of great use in reasonable application of *E. rutaecarpa*.

4. Conclusions

In the present study, the limonoid of Lim, the alkaloids of Evo and Rut, and four quinolone alkaloids in *E. rutaecarpa* were simultaneously determined by the developed HPLC-DAD method. It was the first time that these seven chemical constituents were analyzed by HPLC simultaneously with acceptable performance of linearity, precision, repeatability, accuracy, and robustness. The method also met the requirements of convenience and time efficiency for evaluating the markers content of large quantities of raw materials. More importantly, the optimized method was successfully applied to analyze 18 batches of *E. rutaecarpa*. HCA was utilized to differentiate and classify the 18 samples for guiding reasonable herb use and controlling its quality better. Further

study showed that the quality control of *E. rutaecarpa* could be simplified to the measurement of Lim, Evo, Q1, and Q4. It is proposed that the determination of key biomarkers may be useful standards to adopt for the quality control of *E. rutaecarpa*.

Conflict of Interests

The authors declare that they do not have conflict of interests.

Acknowledgments

Financial support was provided by the National Natural Science Foundation of China (Grant nos. 81173564 and 81274028).

References

[1] Pharmacopoeia of People's Republic of China, *The State Pharmacopoeia Committee of People's Republic of China*, vol. 1, Chemical Industry Press, Beijing, China, 2010.

[2] Q. Z. Wang and J. Y. Liang, "Studies on the chemical constituents of *Evodia rutaecarpa* (Juss.) Benth," *Acta Pharmaceutica Sinica*, vol. 39, no. 8, pp. 605–608, 2004.

[3] C. P. Hu, L. Xiao, H. W. Deng, and Y. J. Li, "The cardioprotection of rutaecarpine is mediated by endogenous calcitonin related-gene peptide through activation of vanilloid receptors in guinea-pig hearts," *Planta Medica*, vol. 68, no. 8, pp. 705–709, 2002.

[4] H. H. Yi, W. Q. Rang, P. Y. Deng et al., "Protective effects of rutaecarpine in cardiac anaphylactic injury is mediated by CGRP," *Planta Medica*, vol. 70, no. 12, pp. 1135–1139, 2004.

[5] C. P. Hu, N. S. Li, L. Xiao, H. W. Deng, and Y. J. Li, "Involvement of capsaicin-sensitive sensory nerves in cardioprotection of rutaecarpine in rats," *Regulatory Peptides*, vol. 114, no. 1, pp. 45–49, 2003.

[6] Z. Dai, J. Xiao, S. Y. Liu, L. Cui, G. Y. Hu, and D. J. Jiang, "Rutaecarpine inhibits hypoxia/reoxygenation-induced apoptosis in rat hippocampal neurons," *Neuropharmacology*, vol. 55, no. 8, pp. 1307–1312, 2008.

[7] D. Li, X. J. Zhang, L. Chen et al., "Calcitonin gene-related peptide mediates the cardioprotective effects of rutaecarpine against ischaemia-reperfusion injury in spontaneously hypertensive rats," *Clinical and Experimental Pharmacology and Physiology*, vol. 36, no. 7, pp. 662–667, 2009.

[8] S. Jia and C. Hu, "Pharmacological effects of rutaecarpine as a cardiovascular protective agent," *Molecules*, vol. 15, no. 3, pp. 1873–1881, 2010.

[9] Z. Chen, G. Hu, D. Li et al., "Synthesis and vasodilator effects of rutaecarpine analogues which might be involved transient receptor potential vanilloid subfamily, member 1 (TRPV1)," *Bioorganic and Medicinal Chemistry*, vol. 17, no. 6, pp. 2351–2359, 2009.

[10] J. S. Ding, R. Gao, D. Li, J. Peng, L. L. Ran, and Y. J. Li, "Solid dispersion of rutaecarpine improved its antihypertensive effect in spontaneously hypertensive rats," *Biopharmaceutics and Drug Disposition*, vol. 29, no. 9, pp. 495–500, 2008.

[11] D. Li, J. Peng, H. Y. Xin et al., "Calcitonin gene-related peptide-mediated antihypertensive and anti-platelet effects by rutaecarpine in spontaneously hypertensive rats," *Peptides*, vol. 29, no. 10, pp. 1781–1788, 2008.

[12] S. K. Heo, H. J. Yun, H. S. Yi, E. K. Noh, and S. D. Park, "Evodiamine and rutaecarpine inhibit migration by LIGHT via suppression of NADPH oxidase activation," *Journal of Cellular Biochemistry*, vol. 107, no. 1, pp. 123–133, 2009.

[13] H. C. Ko, Y. H. Wang, K. T. Liou et al., "Anti-inflammatory effects and mechanisms of the ethanol extract of *Evodia rutaecarpa* and its bioactive components on neutrophils and microglial cells," *European Journal of Pharmacology*, vol. 555, no. 2-3, pp. 211–217, 2007.

[14] S. J. Kim, S. J. Lee, S. Lee et al., "Rutecarpine ameliorates bodyweight gain through the inhibition of orexigenic neuropeptides NPY and AgRP in mice," *Biochemical and Biophysical Research Communications*, vol. 389, no. 3, pp. 437–442, 2009.

[15] C. L. King, Y. C. Kong, N. S. Wong, H. W. Yeung, H. H. S. Fong, and U. Sankawa, "Uterotonic effect of *Evodia rutaecarpa* alkaloids," *Journal of Natural Products*, vol. 43, no. 5, pp. 577–582, 1980.

[16] P. L. Yu, H. L. Chao, S. W. Wang, and P. S. Wang, "Effects of evodiamine and rutaecarpine on the secretion of corticosterone by zona fasciculata-reticularis cells in male rats," *Journal of Cellular Biochemistry*, vol. 108, no. 2, pp. 469–475, 2009.

[17] E. H. Han, H. G. Kim, J. H. Im, T. C. Jeong, and H. G. Jeong, "Up-regulation of CYP1A1 by rutaecarpine is dependent on aryl hydrocarbon receptor and calcium," *Toxicology*, vol. 266, no. 1–3, pp. 38–47, 2009.

[18] T. Haarmann-Stemmann, J. Sendker, C. Götz et al., "Regulation of dioxin receptor function by different beta-carboline alkaloids," *Archives of Toxicology*, vol. 84, no. 8, pp. 619–629, 2010.

[19] M. C. Chen, C. H. Yu, S. W. Wang et al., "Anti-proliferative effects of evodiamine on human thyroid cancer cell line ARO," *Journal of Cellular Biochemistry*, vol. 110, no. 6, pp. 1495–1503, 2010.

[20] G. Dong, C. Sheng, S. Wang, Z. Miao, J. Yao, and W. Zhang, "Selection of evodiamine as a novel topoisomerase i inhibitor by structure-based virtual screening and hit optimization of evodiamine derivatives as antitumor agents," *Journal of Medicinal Chemistry*, vol. 53, no. 21, pp. 7521–7531, 2010.

[21] J. Jiang and C. Hu, "Evodiamine: a novel anti-cancer alkaloid from *Evodia rutaecarpa*," *Molecules*, vol. 14, no. 5, pp. 1852–1859, 2009.

[22] S. F. Kan, C. H. Yu, H. F. Pu, J. M. Hsu, M. J. Chen, and P. S. Wang, "Anti-proliferative effects of evodiamine on human prostate cancer cell lines DU145 and PC3," *Journal of Cellular Biochemistry*, vol. 101, no. 1, pp. 44–56, 2007.

[23] C. Zhang, X. Fan, X. Xu, X. Yang, X. Wang, and H. P. Liang, "Evodiamine induces caspase-dependent apoptosis and S phase arrest in human colon lovo cells," *Anti-Cancer Drugs*, vol. 21, no. 8, pp. 766–776, 2010.

[24] Z. G. Yang, A. Q. Chen, and B. Liu, "Antiproliferation and apoptosis induced by evodiamine in human colorectal carcinoma cells (COLO-205)," *Chemistry and Biodiversity*, vol. 6, no. 6, pp. 924–933, 2009.

[25] X. N. Wang, X. Han, L. N. Xu et al., "Enhancement of apoptosis of human hepatocellular carcinoma SMMC-7721 cells through synergy of berberine and evodiamine," *Phytomedicine*, vol. 15, no. 12, pp. 1062–1068, 2008.

[26] C. Wang, S. Li, and M. W. Wang, "Evodiamine-induced human melanoma A375-S2 cell death was mediated by PI3K/Akt/caspase and Fas-L/NF-κB signaling pathways and augmented by ubiquitin-proteasome inhibition," *Toxicology In Vitro*, vol. 24, no. 3, pp. 898–904, 2010.

[27] M. Adams, O. Kunert, E. Haslinger, and R. Bauer, "Inhibition of leukotriene biosynthesis by quinolone alkaloids from the fruits of *Evodia rutaecarpa*," *Planta Medica*, vol. 70, no. 10, pp. 904–908, 2004.

[28] H. Z. Jin, J. H. Lee, D. Lee et al., "Quinolone alkaloids with inhibitory activity against nuclear factor of activated T cells from the fruits of *Evodia rutaecarpa*," *Biological and Pharmaceutical Bulletin*, vol. 27, no. 6, pp. 926–928, 2004.

[29] N. Hamasaki, E. Ishii, K. Tominaga et al., "Highly selective antibacterial activity of novel alkyl quinolone alkaloids from a Chinese herbal medicine, Gosyuyu (Wu-Chu-Yu), against Helicobacter pylori *in vitro*," *Microbiology and Immunology*, vol. 44, no. 1, pp. 9–15, 2000.

[30] H. S. Lee, W. K. Oh, H. C. Choi, and J. W. Lee, "Inhibition of angiotensin II receptor binding by quinolone alkaloids from *Evodia rutaecarpa*," *Phytotherapy Research*, vol. 12, no. 3, pp. 212–214, 1998.

[31] L. Battinelli, F. Mengoni, M. Lichtner et al., "Effect of limonin and nomilin on HIV-1 replication on infected human mononuclear cells," *Planta Medica*, vol. 69, no. 10, pp. 910–913, 2003.

[32] A. Roy and S. Saraf, "Limonoids: overview of significant bioactive triterpenes distributed in plants kingdom," *Biological and Pharmaceutical Bulletin*, vol. 29, no. 2, pp. 191–201, 2006.

[33] H. Matsuda, M. Yoshikawa, M. Iinuma, and M. Kubo, "Antinociceptive and anti-inflammatory activities of limonin isolated from the fruits of *Evodia rutaecarpa* var. *bodinieri*," *Planta Medica*, vol. 64, no. 4, pp. 339–342, 1998.

[34] W. Kim, Y. Y. Fan, R. Smith et al., "Dietary curcumin and limonin suppress CD4+ T-cell proliferation and Interleukin-2 production in mice," *Journal of Nutrition*, vol. 139, no. 5, pp. 1042–1048, 2009.

[35] M. Z. El-Readi, D. Hamdan, N. Farrag, A. El-Shazly, and M. Wink, "Inhibition of P-glycoprotein activity by limonin and other secondary metabolites from Citrus species in human colon and leukaemia cell lines," *European Journal of Pharmacology*, vol. 626, no. 2-3, pp. 139–145, 2010.

[36] T. Tanaka, M. Maeda, H. Kohno et al., "Inhibition of azoxymethane-induced colon carcinogenesis in male F344 rats by the citrus limonoids obacunone and limonin," *Carcinogenesis*, vol. 22, no. 1, pp. 193–198, 2001.

[37] J. Z. Zhang, Y. Wang, H. Chen, and H. B. Shao, "TLC-SERS study on evodiamine in *Evodia rutaecarpa*," *Spectroscopy and Spectral Analysis*, vol. 27, no. 5, pp. 944–947, 2007.

[38] H. J. Kim, E. H. Jee, K. S. Ahn, H. S. Choi, and Y. P. Jang, "Identification of marker compounds in herbal drugs on TLC with DART-MS," *Archives of Pharmacal Research*, vol. 33, no. 9, pp. 1355–1359, 2010.

[39] M. C. Lee, W. C. Chuang, and S. J. Sheu, "Determination of the alkaloids in *Evodiae fructus* by capillary elctrophoresis," *Journal of Chromatography A*, vol. 755, no. 1, pp. 113–119, 1996.

[40] W. C. Chuang, C. M. Cheng, H. C. Chang, Y. P. Chen, and S. J. Sheu, "Contents of constituents in mature and immature fruits of *Evodia species*," *Planta Medica*, vol. 65, no. 6, pp. 567–571, 1999.

[41] M. Y. Zhao and X. W. Yang, "Optimization of the extraction conditions and simultaneous quantification by RP-LC of six alkaloids in *Evodiae fructus*," *Chromatographia*, vol. 67, no. 7-8, pp. 543–550, 2008.

[42] D. Huang, S. X. Li, G. X. Cai, C. H. Yue, L. J. Wei, and P. Zhang, "Molecular authentication and quality control using a high performance liquid chromatography technique of *Fructus Evodiae*," *Biological and Pharmaceutical Bulletin*, vol. 31, no. 2, pp. 312–315, 2008.

[43] Y. Zhao, X. Zhou, H. G. Chen, X. J. Gong, Z. W. Cai, and C. Y. Zhou, "Determination of dehydroevodiamine in *Evodia rutaecarpa* (Juss.) Benth by high performance liquid chromatography and classification of the samples by using hierarchical clustering analysis," *Fitoterapia*, vol. 80, no. 7, pp. 415–420, 2009.

[44] Y. Zhao, Z. Li, X. Zhou, Z. Cai, X. Gong, and C. Zhou, "Quality evaluation of *Evodia rutaecarpa* (Juss.) Benth by high performance liquid chromatography with photodiode-array detection," *Journal of Pharmaceutical and Biomedical Analysis*, vol. 48, no. 4, pp. 1230–1236, 2008.

[45] X. Gao, X. W. Yang, and P. J. Marriott, "Simultaneous analysis of seven alkaloids in Coptis-Evodia herb couple and Zuojin pill by UPLC with accelerated solvent extraction," *Journal of Separation Science*, vol. 33, no. 17-18, pp. 2714–2722, 2010.

[46] Y. Zhou, S. H. Li, R. W. Jiang et al., "Quantitative analyses of indoloquinazoline alkaloids in *Fructus Evodiae* by high-performance liquid chromatography with atmospheric pressure chemical ionization tandem mass spectrometry," *Rapid Communications in Mass Spectrometry*, vol. 20, no. 20, pp. 3111–3118, 2006.

[47] X. Luo, B. Chen, and S. Yao, "Simultaneous analysis of protoberberine, indolequinoline and quinolone alkaloids in coptis-evodia herb couple and the Chinese herbal preparations by high-performance liquid chromatography-electrospray mass spectrometry," *Talanta*, vol. 66, no. 1, pp. 103–110, 2005.

[48] X. Zhou, Y. Zhao, P. Lei, Z. Cai, and H. Liu, "Chromatographic fingerprint study on *Evodia rutaecarpa* (Juss.) Benth by HPLC/DAD/ESI-MSn technique," *Journal of Separation Science*, vol. 33, no. 15, pp. 2258–2265, 2010.

[49] J. Teng, X. W. Yang, H. Y. Tao, and H. X. Liu, "GC-MS analysis of constituents of volatile oil from fruits of *Erutaecarpa* var. *bodinieri*," *Chinese Traditional and Herbal Drugs*, vol. 34, no. 6, pp. 504–505, 2003.

Hindawi Publishing Corporation
Journal of Analytical Methods in Chemistry
Volume 2013, Article ID 479056, 8 pages
http://dx.doi.org/10.1155/2013/479056

Research Article

Cloud-Point Extraction Combined with Liquid Chromatography for the Determination of Ergosterol, a Natural Product with Diuretic Activity, in Rat Plasma, Urine, and Faeces

Dan-Qian Chen,[1] Jun-Min An,[2] Ya-Long Feng,[1] Ting Tian,[1] Xiang-Yang Qin,[3] and Ying-Yong Zhao[1]

[1] *Key Laboratory of Resource Biology and Biotechnology in Western China, Ministry of Education, The College of Life Sciences, Northwest University, No. 229 Taibai North Road, Xi'an, Shaanxi 710069, China*
[2] *Department of Nephrology, Xi'an No. 4 Hospital, No. 21 Jiefang Road, Xi'an, Shaanxi 710004, China*
[3] *Department of Chemistry, School of Pharmacy, Fourth Military Medical University, Xi'an, Shaanxi 710032, China*

Correspondence should be addressed to Ying-Yong Zhao; zyy@nwu.com.cn

Received 23 January 2013; Accepted 7 March 2013

Academic Editor: Feng Wei

Ergosterol from many medicinal fungi has been demonstrated to possess a variety of pharmacological activities *in vivo* and *in vitro*. A new method based on cloud-point extraction has been developed, optimized and validated for the determination of ergosterol in rat plasma, urine and faeces by liquid chromatography. The non-ionic surfactant Triton X-114 was chosen as the extract solvent. The chromatographic separation was performed on an Inertsil ODS-3 analytical column with a mobile phase consisting of methanol and water (98 : 2, v/v) at a flow rate of 1 mL/min. The methodology was validated completely. The results indicated good performance in terms of specificity, linearity, detection and quantification limits, precision and accuracy. The method was successfully applied to the pharmacokinetic studies of ergosterol in rats. The results indicate that the ergosterol levels in feces are much higher than those in plasma and urine of the rat.

1. Introduction

Ergosterol is one of the best-known steroids, which exists widely in many medicinal fungi such as *Polyporus umbellatus*, *Cordyceps sinensis*, and *Hypsizigus marmoreus* [1–3]. We have recently reported the ergosterol has diuretic activity from *Polyporus umbellatus* [4]. Ergosterol has also been reported to possess cytotoxic activity [5] and anti-inflammatory activity [3]. Despite the fact that ergosterol showed multiple pharmacological activities, several pharmacokinetic and biochemical aspects of this compound remain unclear. However, the final effect of the drug *in vivo* might be influenced by many factors, such as body-and/or cell-compartment distribution, drug metabolism, lipophilicity, membrane permeability, and protein binding. So, these multiple pharmacological activities of ergosterol make it worth carrying out further study on pharmacokinetic properties and elimination pathway of ergosterol.

A number of methods have been reported for the quantification of ergosterol in raw materials, such as high performance liquid chromatography-ultraviolet detection (HPLC-UV) [1, 6–11], high performance liquid chromatography-tandem mass spectrometry (HPLC-MS/MS) [12, 13], and gas chromatography-mass spectrometry (GC-MS) [14–16]. To the best of our knowledge, there is no information describing the quantification of ergosterol in biological samples such as rat or human plasma, urine, and faeces. In addition, the effects on the elimination pathway of ergosterol have not been

reported. In general, preclinical research including metabolism and pharmacokinetics of herbal medicine components are of great importance in understanding their biological effects and safety [17, 18]. In order to investigate the pharmacokinetic properties and elimination pathway of ergosterol, a simple and reproducible analytical method for quantification of ergosterol in rat plasma, urine, and faeces is required. Recently, the cloud-point extraction (CPE) method has aroused much attention as a convenient alternative to the conventional extraction systems. Compared with classical organic solvents, it offers the advantages of safety, low cost, high-concentration efficiency, easy disposal of surfactants, low toxicity, less environmental pollution, and simple procedure. CPE has been increasingly applied for the selective extraction of various analytes from biological and environmental samples (proteins, vitamins, and metal ions) [19], but only a few reports involve the extraction of drugs from plasma for pharmacokinetic studies [20, 21]. In this paper, a simple, specific, and reproducible HPLC-UV method with a simple protein precipitation procedure was described to determine ergosterol in rat plasma, urine, and faeces for the first time. The method was validated and successfully applied to the pharmacokinetic study of ergosterol in rat plasma, urine, and faeces after oral administration of ergosterol at a dose of 100 mg/kg.

2. Experimental

2.1. Chemicals and Reagents. The standard of ergosterol (Figure 1(a)) was isolated by the authors from *Polyporus umbellatus*. The procedure isolation and purification of ergosterol was published in our previous paper [22]. Its structure was characterized by chemical and spectroscopic methods (^{1}H NMR, ^{13}C NMR, and MS) and compared with those found in the literature [23]. Ergosta-4,6,8(14),22-tetraen-3-one (ergone, Figure 1(b)) was used as internal standard (IS) which was one of the components of *Polyporus umbellatus* purified in our laboratory with 99% purity as determined by HPLC. HPLC-grade methanol was purchased from Baker Company (Baker Inc., USA). Ultrahigh purity water was prepared by a Millipore-Q SAS 67120 MOLSHEIM (France).

2.2. Preparation of Standards and Quality Control Samples. Standard stock solutions of ergosterol (5 μg/mL) and ergone (1, 5, and 100 μg/mL) were prepared by dissolving suitable amounts of pure substance in acetone and were stored in darkness at 4°C.

Faecal samples were homogenized with acetone in the ratio 1 : 10 (g : vol = faeces : acetone) to obtain faecal homogenate. For HPLC determination, calibration standards of ergosterol at concentration levels of 0.09, 0.25, 0.50, 0.75, 1.00, 2.00, and 2.50 μg/mL were prepared by spiking appropriate amount of the standard solutions in blank plasma and urine obtained from healthy rats. Calibration standards of ergosterol at concentrations of 0.08, 0.25, 5, 25, 50, 100, and 125 μg/mL were also prepared by spiking appropriate amount of the standard solutions in faecal homogenate obtained from healthy rats. The quality control (QC) samples were separately prepared in a similar manner as those used for the calibration curve. Concentrations of 0.25, 0.75, and 2.00 μg/mL were used for plasma and urine calibration standards, whereas concentrations of 0.25, 25, and 100 μg/mL were used for faecal homogenate corresponding to the low QC, medium QC, and high QC, respectively.

2.3. Chromatographic Conditions. HPLC was performed with a Waters 2695 instrument composed of a quaternary pump, a column oven, and a Waters 2487 dual wavelength absorbance detector, and Empower was used for data collection. The chromatographic separation was performed on an Inertsil ODS-3 analytical column (250 mm × 4.6 mm i.d., 5 μm, Japan) with the column temperature set at 30°C. An isocratic elution of methanol (A) and water (B) was 98 : 2 (v/v) in 23 min. The flow rate was 1.0 mL/min with detector wavelength set at 283 nm (maximum absorption wavelength of ergosterol), and the injection volume was 20 μL.

2.4. Extraction Procedures for Plasma and Urine Sample. The plasma or urine was prepared by a cloud-point extraction method. In a 1.5 mL capped centrifugal tube, 50 μL of plasma or urine was spiked with 15 μL (5 μg/mL for plasma, 1 μg/mL for urine) of IS working solution and 135 μL of 0.3 mol/L sodium chloride solution. The contents were mixed for 2 min, and then followed by the addition of 100 μL of 5% Triton X-114 (v/v) aqueous solution. After that, the obtained contents were well mixed again for 5 min and then incubated in the thermostatic bath at 40°C for 20 min. After the phase separation was formed by centrifugation at 5000 rpm for 10 min, the surfactant-rich phase was obtained in the bottom of the tube by the removal of the water phase. 100 μL of mobile phase was spiked to the surfactant-rich phase. Then, the contents were mixed and centrifuged at 16,000 rpm for 5 min, respectively. Most of the surfactants and coextractants such as hydrophobic proteins were precipitated in the bottom of the tube, and 20 μL of supernatant fluid was injected into the HPLC system for analysis.

2.5. Extraction Procedures for Faeces Sample. A 100 μL volume of faecal homogenate standard or sample was transferred to a 1.5 mL centrifuge tube, and then 30 μL of IS working solution was spiked and vortex-mixed for 1 min. 70 μL of acetone was added to the solution and vortex again for 2 min. The mixture was centrifuged at 10,000 ×g for 10 min. A 20 μL of supernatant of the solution was injected into the HPLC for analysis.

2.6. Linearity, Limit of Detection, and Lower Limit of Quantification. HPLC-UV method was applied for the quantification of ergosterol from rat plasma, urine, and faeces. Calibration standards of seven concentrations of ergosterol for plasma and urine (0.09, 0.25, 0.50, 0.75, 1.00, 2.00, and 2.50 μg/mL) and calibration standards for faecal homogenate (0.08, 0.25, 5, 25, 50, 100, and 125 μg/mL) were extracted and assayed. The linearity of the calibration curve was confirmed by plotting the peak-area ratios of ergosterol to IS versus the ergosterol concentrations with a $1/x$-weighted least-squares linear regression analysis. The limit of detection (LOD) was

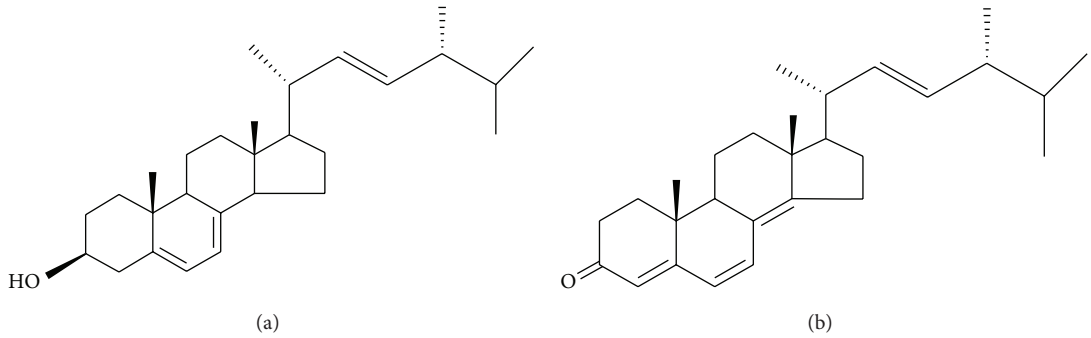

(a) (b)

Figure 1: Chemical structures of ergosterol (a) and ergone (b).

considered as the final concentration producing a signal-to-noise ratio of 3. The lower limit of quantification (LLOQ) was considered as the lowest concentration on the calibration curve where precision was within 20% and accuracy was within 100 ± 20% [24].

2.7. Precision and Accuracy. The accuracy and intra- and interday precisions of the method were determined for ergosterol according to FDA guidance for bioanalytical method validation [24]. Accuracy and precision were assessed by the determination of QC samples at three concentration levels in three different validation assays. Accuracy was calculated by the percentage difference between the concentration of drug measured from calibration curve and that of drug added to the blank plasma, urine, and faecal homogenate. Precision was expressed by the relative standard deviation (RSD).

2.8. Selectivity. Selectivity of the method was assessed by analyzing five independent sources of blank plasma, urine, and faecal homogenate or plasma, urine, and faecal homogenate samples spiked with ergosterol and the IS, and observing the extent to which interferent from plasma, urine, and faecal homogenate may interfere with the analyte or IS.

2.9. Recovery. The extraction recovery for plasma, urine, and faecal homogenate at three different concentrations of ergosterol was determined. The analyte/IS peak-area ratios were compared to those obtained from the direct injection of the compounds dissolved in the solutions at the same theoretical concentrations.

2.10. Stability. The stability of ergosterol and IS stock solutions was evaluated. Short-term stability was assessed by analyzing QC plasma, urine, and faecal homogenate samples kept at room temperature for 6 h that exceeded the routine preparation time of samples. Long-term stability was determined by assaying QC plasma, urine, and faecal homogenate samples after storage at −20°C for 30 days. Freeze-thaw stability was investigated after three freeze-(−20°C) thaw (room temperature) cycles.

2.11. Application to Pharmacokinetics of Ergosterol. To validate the method with real samples, a trial was undertaken to determine ergosterol in the plasma and excretion samples of healthy rats, which were administered a single dose of ergosterol orally. The study was conducted in accordance with the Regulations of Experimental Animal Administration issued by the State Committee of Science and Technology of China. All procedures and the care of the rats were in accordance with institutional guidelines for animal use in research. Rats were housed in individual metabolic cages on standard laboratory food bedding in a temperature controlled room (22 ± 2°C) with a 12 h light/dark cycle.

Male Sprague-Dawley (SD) rats, 200 ± 10 g, fasted overnight with free access to water for at least 12 h, were dosed orally by gavages with 100 mg/kg body weight of ergosterol dissolved in plant oil as a vehicle. Rats were divided into three groups ($n = 6$) based on the time of blood sampling with two animals each. The control groups received the vehicle only. The blood samples (approximately 300 μL) were collected from vena orbitalis in heparinized tubes at control and 1, 2, 3, 4, 5, 6, 8, 10, 12, 14, 16, 24, and 36 h after the administration. Samples were immediately centrifuged at 5,000 ×g for 10 min and the plasma was frozen at −20°C and stored until analysis. The estimation of ergosterol in all the samples was undertaken within 36 h of blood collection by the method described previously.

Excretion was studied in another four groups ($n = 6$) based on the time of urine and faeces sampling with three animals each. The control groups received the vehicle only. Rats were housed with free access to food and water in individual metabolic cages, except for the final 12 h before a single oral administration of 100 mg/kg of ergosterol (access to water was ad libitum during the experiment). Faeces and urine were collected after administration in different periods (0–2, 2–4, 4–6, 6–8, 8–10, 10–12, 12–14, 14–16, 16–18, 18–24, and 24–36 h). The amount of faeces and urine collected over each period was recorded, respectively, and then urine and faeces were stored at −20°C until analysis.

Pharmacokinetics analysis was carried out by noncompartmental method with the aid of the software DAS 2.0 (issued by the State Food and Drug Administration of China for pharmacokinetic study) and pharmaceutical parameters were obtained.

The percentage of ergosterol eliminated in faeces was calculated with the accumulated ergosterol eliminated in all periods divided by administration amount (ergosterol eliminated over each period was calculated using the amount of faeces multiplied by the concentration of ergosterol in it).

3. Results and Discussion

3.1. ^1H NMR and ^{13}C NMR Data of Ergosterol. The characteristics of ergosterol are ^1H NMR ($CDCl_3$, 500 MHz) 3.63 (1H, m, H-3), 5.39 (1H, m, H-6), 5.58 (1H, m, H-7), 0.63 (3H, s, H-18), 0.95 (3H, s, H-19), 1.04 (3H, d, J = 6.6 Hz, H-21), 5.18 (1H, dd, J = 15.2, 8.0 Hz, H-22), 5.22 (1H, dd, J = 15.2, 8.0 Hz, H-23), 0.83 (3H, d, J = 6.7 Hz, H-26), 0.84 (3H, d, J = 6.4 Hz, H-27), 0.92 (3H, d, J = 6.8 Hz, H-28); ^{13}C NMR ($CDCl_3$, 125 MHz) 38.3 (C-1), 32.1 (C-2), 70.6 (C-3), 40.8 (C-4), 139.9 (C-5), 119.7 (C-6), 116.4 (C-7), 141.5 (C-8), 46.4 (C-9), 37.1 (C-10), 21.3 (C-11), 39.0 (C-12), 42.8 (C-13), 54.7 (C-14), 23.1 (C-15), 28.4 (C-16), 55.8 (C-17), 12.2 (C-18), 17.7 (C-19), 40.5 (C-20), 21.2 (C-21), 135.5 (C-22), 132.1 (C-23), 42.9 (C-24), 33.2 (C-25), 19.8 (C-26), 20.1 (C-27), 16.4 (C-28). The data of mass spectrum was published in our previous paper [25, 26].

3.2. Optimization of Chromatographic Conditions and Sample Preparation. Chromatographic optimisation of HPLC conditions was carried out with respect to mobile phase conditions (methanol-water or acetonitrile-water), stationary phase (Inertsil ODS-3 column, 250 mm × 4.6 mm i.d., 5 μm or Diamonsil C18 column, 250 mm × 4.6 mm i.d., 5 μm), temperature (30 or 35°C), and peak shape. The test results showed that the peak shapes of ergosterol were improved by the solvent system of methanol and water.

The previously-mentioned method was demonstrated by comparing chromatograms of six independent biological samples (plasma, urine, and faecal homogenate) from blank rats, each as a blank sample and a spiked sample. The chromatograms of ergosterol and the IS are showed in Figures 2(a1)–2(a3), 2(b1)–2(b3), and 2(c1)–2(c3), respectively. Figures 2(b1)–2(b3) indicate no significant interferences at the retention times of ergosterol and the IS. The ergosterol and the IS of the retention times were 18.8 and 15.7 min, respectively, with a total run time of less than 23 min. System suitability parameters for the method were as follows: the theoretical plates for ergosterol and the IS were 4900 and 5400, respectively. Tailing factor was less than 1.1 for all ergosterol and the IS and resolution among ergosterol and the IS was more than 1.5. Ergosterol was chosen as IS because of its similarity to the analytes with respect to polarity, high recovery, and suitable retention time.

3.3. Linearity. Calibration curves of ergosterol were linear over the concentration range of 0.09–2.50 μg/mL for plasma and urine and 0.08–125 μg/mL for faecal homogenate. The typical equation was $Y = 0.8251\ X + 0.0357$ ($r = 0.9996$) for plasma, $Y = 2.9189\ X + 0.1265$ ($r = 0.9995$) for urine, and $Y = 0.0262\ X + 0.0104$ ($r = 0.9994$) for faecal homogenate. Y = peak-area ratio (ergosterol/IS) and X = ergosterol concentration. During routine analysis, each analytical run included a set of calibration samples, a set of QC samples, and the unknowns. The LOD of ergosterol in rat plasma, urine, and faecal homogenate were 42, 50, and 49 ng/mL, respectively. The LOQ of ergosterol in rat plasma, urine, and faecal homogenate was 90, 90, and 80 ng/mL respectively.

Table 1: Summary of precision and accuracy of ergosterol in rat plasma, urine, and faeces.

Added concentration (μg/mL)	Found concentration (mean ± SD, μg/mL)	Recovery (%)	Intraday (RSD %)	Interday (RSD %)
Plasma				
0.25	0.259 ± 0.012	103.6	9.6	7.8
0.75	0.713 ± 0.030	95.1	3.7	5.4
2.00	2.001 ± 0.072	100.1	3.9	4.8
Urine				
0.25	0.254 ± 0.009	101.6	4.2	7.1
0.75	0.736 ± 0.038	98.1	5.5	5.8
2.00	1.956 ± 0.090	97.8	3.3	3.1
Faeces				
0.25	0.247 ± 0.010	98.8	4.8	3.6
25	25.1 ± 0.7	100.4	2.8	5.1
100	99.5 ± 1.9	99.5	3.1	1.6

3.4. Accuracy and Precision. Table 1 shows the intra- and interday precision and accuracy for ergosterol from biological matrices QC samples. The intra- and interday precisions were measured below 9.6% and 7.8%, respectively, with relative recovery from 95.1% to 103.6%. The results indicated that the method showed good precision and accuracy.

3.5. Selectivity. The selectivity of the method was demonstrated by comparing chromatograms of five independent biological samples (plasma, urine, and faecal homogenate) from blank rats, each as a blank sample and a spiked sample. Figure 2 indicates no significant interferences at the retention times of ergosterol and IS in plasma, urine, and faeces samples. The ergosterol and IS of the retention times were 18.8 and 15.7 min, respectively.

3.6. Extraction Recovery. The mean extraction recovery of ergosterol from plasma, urine, and faecal homogenate was 90.9 ± 2.9%, 92.4 ± 2.6%, and 93.7 ± 3.3%, respectively. The mean relative recovery for IS was 94.5 ± 3.2% ($n = 5$). Recovery data are shown in Table 2. The results indicated that the method showed high recovery.

3.7. Stability. Table 3 shows the results of short-term, long-term, and freeze-thaw stability of ergosterol in plasma, urine, and faeces. Ergosterol was found to be stable in frozen plasma, urine, and faeces after three freeze-thaw cycles. The relative standard deviations were within ±15%. Long-term stability studies of ergosterol in three rat matrices showed appreciable stability over 30 days. Furthermore, ergosterol in three rat matrices was found to be stable at room temperature for a period of 6 h. All the results well met the criterion for stability measurements.

3.8. Application of the Method. The diuretic activity of ergosterol was reported in our previous publication [4]. Pharmacokinetic studies of this drug are important for further biological and biochemical research and for future clinical trials. After a single oral administration of ergosterol (100 mg/kg) to rats, the concentrations of ergosterol in plasma, urine,

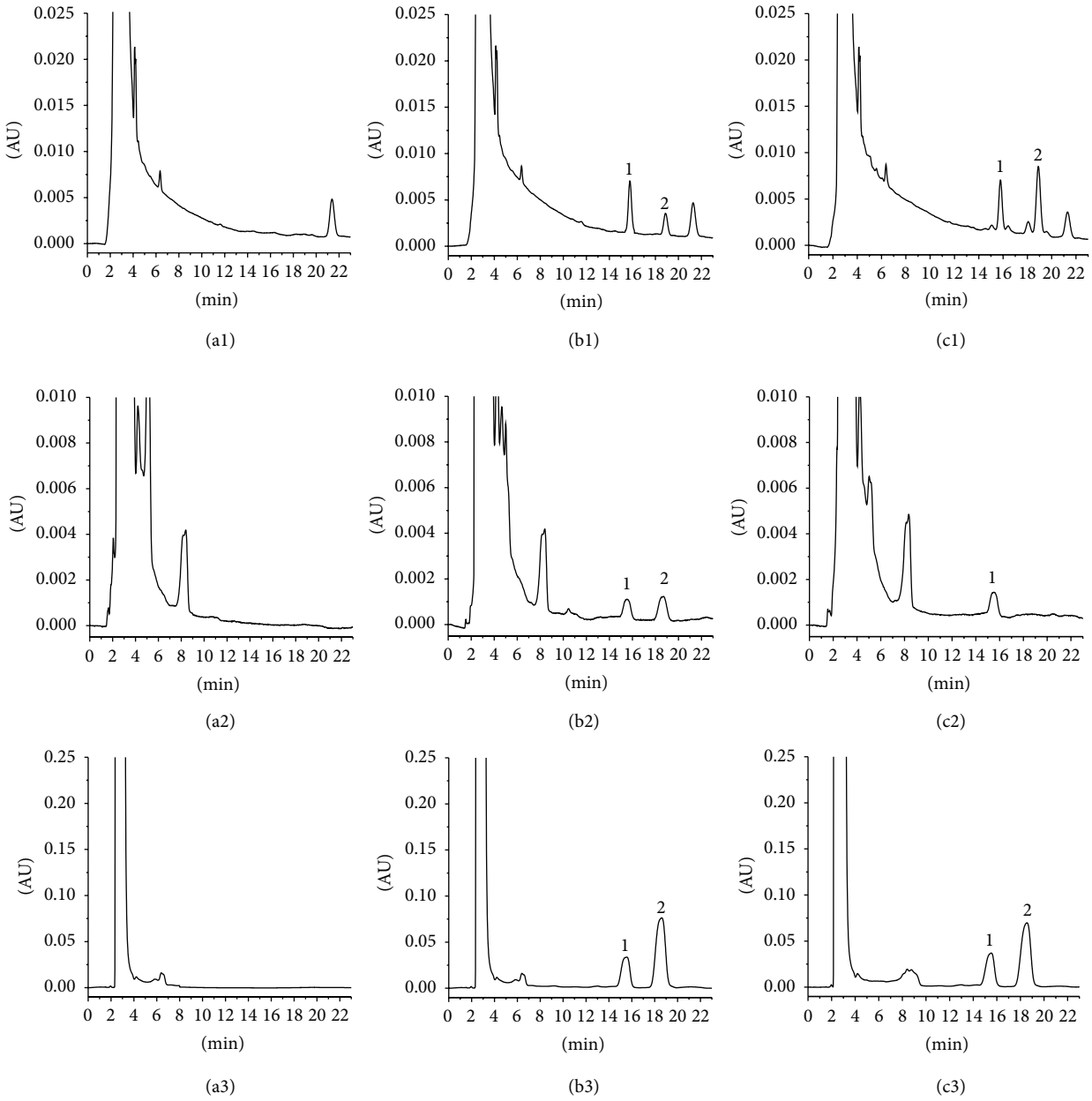

Figure 2: Chromatograms of ergosterol and IS in rat plasma, urine, and faecal homogenate—(a1) blank rat plasma, (a2) blank urine, (a3) blank faecal homogenate, (b1) blank plasma spiked with ergosterol and IS, (b2) blank urine spiked with ergosterol and IS, (b3) blank faecal homogenate spiked with ergosterol and IS, (c1) a rat plasma sample after oral administration, (c2) a urine sample after oral administration, and (c3) a faecal homogenate sample after oral administration (1, IS; 2, ergosterol).

and faecal homogenate were determined by the HPLC-UV method. Figure 3 shows mean plasma concentration-time curves of ergosterol after administration. Pharmacokinetic parameters are listed in Table 4.

The ergosterol was detected in rat plasma, urine, and faeces samples collected from 0 to 36 h after an oral administration. The results indicate that the ergosterol levels in faeces are much higher than those in plasma and urine of the rat (Figure 4(a)). Almost 62.5% of loading dose is cumulative in the faeces within 36 h after an oral dose with a dosage of 100 mg/kg (Figure 4(a)), but the lower level of ergosterol was found in urine (Figure 4(b)).

4. Conclusions

The cloud-point extraction technique has been successfully applied for the first time as an effective method for the extraction and preconcentration of ergosterol from rat plasma samples. It was shown that this method is suitable for the analysis of ergosterol in rat plasma samples collected for

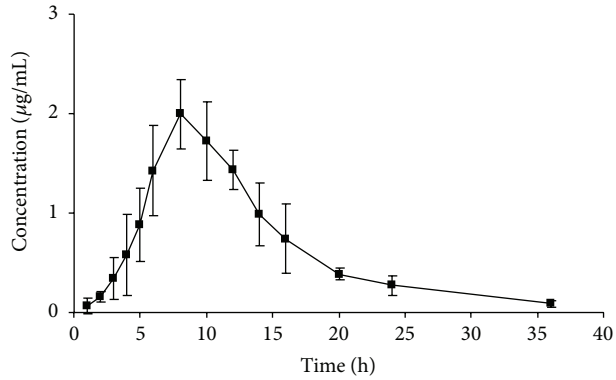

Figure 3: Mean (±S.D.) plasma concentration-time profile of ergosterol in the plasma of healthy rats ($n = 6$) that were administered a single oral dose of 100 mg/kg of ergosterol.

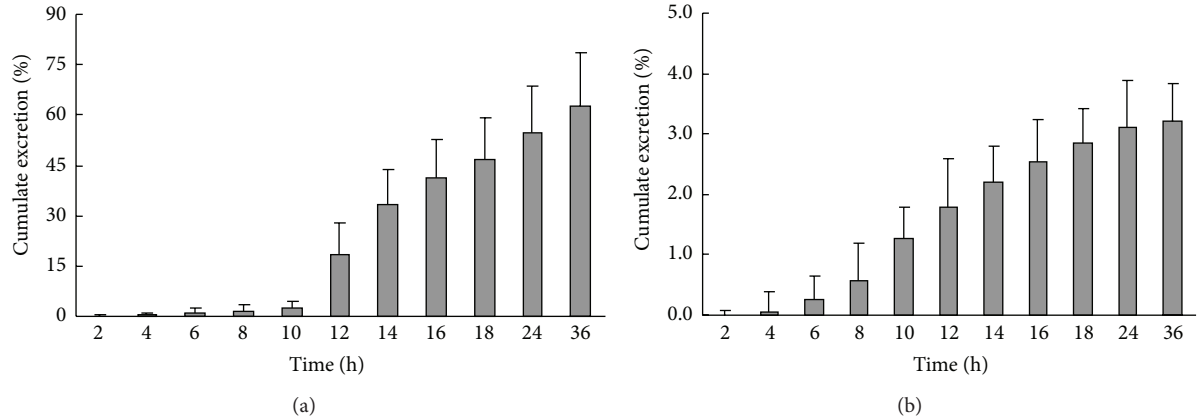

Figure 4: Cumulative excretion of ergosterol in faeces (a) and urine (b) of rats after an oral dose with a dosage of 100 mg/kg. Faeces were collected after administration in different periods (0–2, 2–4, 4–6, 6–8, 8–10, 10–12, 12–14, 14–16, 16–18, 18–24, and 24–36 h).

Table 2: Absolute recoveries of ergosterol in rat plasma, urine, and faeces.

Added concentration (μg/mL)	Found concentration (mean ± SD, μg/mL)	Recovery (%)	RSD %
Plasma			
0.25	0.227 ± 0.008	90.8	5.2
0.75	0.678 ± 0.078	90.4	2.8
2.00	1.832 ± 0.102	91.6	3.4
Urine			
0.25	0.231 ± 0.006	92.4	3.5
0.75	0.703 ± 0.065	93.7	3.8
2.00	1.825 ± 0.131	91.3	2.4
Faeces			
0.25	0.233 ± 0.009	93.2	4.7
25	23.4 ± 1.3	93.6	2.2
100	94.3 ± 3.2	94.3	2.8

pharmacokinetic study. The HPLC-UV method is simple, specific, and reproducible for quantitative determination of ergosterol in rat plasma, urine, and faeces. The small amount of biological matrices required (0.3 mL per determination) made this method suitable for routine analysis in preclinical pharmacokinetic studies, and the method was helpful in clinical pharmacokinetic studies. It can also be used as a reference for therapeutic drug monitoring of ergosterol.

Conflict of Interests

There is no conflict of interests to declare.

Authors' Contribution

Dan-Qian Chen and Jun-Min An contributed to this paper as co-first authors.

Acknowledgments

This study was supported in part by Grants from the National Natural Scientific Foundation of China (nos. J1210063, 81001622, and 81073029) and China Postdoctoral Science Foundation (2012M521831) and Innovative Research Team in

Table 3: Summary of stability studies of ergosterol in rat plasma, urine, and faeces under various storage conditions.

Biological matrix	Added concentration (μg/mL)	Found concentration (μg/mL)	Recovery (%)	RSD %
		Short-term stability		
	0.25	0.249 ± 0.010	99.6	4.1
Plasma	0.75	0.714 ± 0.043	95.2	6.7
	2.00	1.90 ± 0.080	95.0	1.9
	0.25	0.252 ± 0.011	100.8	4.6
Urine	0.75	0.717 ± 0.039	95.6	1.4
	2.00	1.91 ± 0.01	95.5	1.6
	0.25	0.243 ± 0.007	97.2	2.9
Faeces	25	24.8 ± 0.63	98.8	2.5
	100	99.4 ± 2.1		2.1
		Three freeze-thaw cycles		
	0.25	0.262 ± 0.021	104.8	7.8
Plasma	0.75	0.738 ± 0.027	98.4	4.2
	2.00	1.92 ± 0.08	96.0	2.1
	0.25	0.251 ± 0.011	100.4	4.6
Urine	0.75	0.759 ± 0.032	101.2	3.5
	2.00	1.93 ± 0.04	96.5	2.2
	0.25	0.251 ± 0.007	100.4	3.2
Faeces	25	24.7 ± 0.6	98.8	2.6
	100	98.9 ± 3.3	98.9	3.3
		Long-term stability		
	0.25	0.250 ± 0.013	100.0	4.6
Plasma	0.75	0.723 ± 0.045	96.4	2.9
	2.00	1.95 ± 0.12	97.5	1.8
	0.25	0.238 ± 0.009	95.2	4.0
Urine	0.75	0.759 ± 0.007	101.2	3.1
	2.00	2.06 ± 0.15	103.0	5.2
	0.25	0.249 ± 0.011	99.6	4.5
Faeces	25	24.6 ± 0.5	98.4	2.1
	100	100.1 ± 2.4	100.1	2.4

Table 4: Pharmacokinetic parameters obtained after administration of ergosterol in SD rats ($n = 6$).

Pharmacokinetic parameters	mean ± SD
$AUC_{0-36\,h}$ ($\mu g\,h\,mL^{-1}$)	22.23 ± 5.04
C_{Max} ($\mu g\,mL^{-1}$)	2.18 ± 0.21
$t_{1/2}$ (h)	5.90 ± 1.43
T_{Max} (h)	8.00 ± 1.26

University of Ministry of Education of China (no. IRT1174). In this work, Pharmacokinetics parameter was analyzed by the software DAS 2.0. Methanol was purchased from Baker Company.

References

[1] Y. Y. Zhao, X. L. Cheng, Y. Zhang, Y. Zhao, R. C. Lin, and W. J. Sun, "Simultaneous determination of eight major steroids from *Polyporus umbellatus* by high-performance liquid chromatography coupled with mass spectrometry detections," *Biomedical Chromatography*, vol. 24, no. 2, pp. 222–230, 2010.

[2] J. W. Bok, L. Lermer, J. Chilton, H. G. Klingeman, and G. H. N. Towers, "Antitumor sterols from the mycelia of *Cordyceps sinensis*," *Phytochemistry*, vol. 51, no. 7, pp. 891–898, 1999.

[3] K. Yasukawa, T. Aoki, M. Takido, T. Ikekawa, H. Saito, and T. Matsuzawa, "Inhibitory effects of ergosterol isolated from the edible mushroom *Hypsizigus marmoreus* on TPA-induced inflammatory ear oedema and tumour promotion in mice," *Phytotherapy Research*, vol. 8, no. 1, pp. 10–13, 1994.

[4] Y. Y. Zhao, R. M. Xie, X. Chao, Y. Zhang, R. C. Lin, and W. J. Sun, "Bioactivity-directed isolation, identification of diuretic

compounds from *Polyporus umbellatus*," *Journal of Ethnopharmacology*, vol. 126, no. 1, pp. 184–187, 2009.

[5] H. Matsuda, J. Akaki, S. Nakamura et al., "Apoptosis-inducing effects of sterols from the dried powder of cultured mycelium of *Cordyceps sinensis*," *Chemical and Pharmaceutical Bulletin*, vol. 57, no. 4, pp. 411–414, 2009.

[6] Y. Y. Zhao, Y. Zhao, R. C. Lin, and W. J. Sun, "HPLC determination of ergosta-4, 6, 8(14), 22-tetraen-3-one in *Polyporus umbellatus*," *Chinese Journal of Pharmaceutical Analysis*, vol. 29, no. 9, pp. 1579–1581, 2009.

[7] D. Abramson and D. M. Smith, "Determination of ergosterol in canola (*Brassica napus* L.) by liquid chromatography," *Journal of Stored Products Research*, vol. 39, no. 2, pp. 185–191, 2002.

[8] J. P. Yuan, J. H. Wang, X. Liu, H. C. Kuang, and S. Y. Zhao, "Simultaneous determination of free ergosterol and ergosteryl esters in *Cordyceps sinensis* by HPLC," *Food Chemistry*, vol. 105, no. 4, pp. 1755–1759, 2007.

[9] L. M. Seitz and Y. Pomeranz, "Ergosterol, ergosta-4,6,8(14),22-tetraen-3-one, ergosterol peroxide, and chitin in ergoty barley, rye, and other grasses," *Journal of Agricultural and Food Chemistry*, vol. 31, no. 5, pp. 1036–1038, 1983.

[10] S. P. Li, P. Li, C. M. Lai et al., "Simultaneous determination of ergosterol, nucleosides and their bases from natural and cultured Cordyceps by pressurised liquid extraction and high-performance liquid chromatography," *Journal of Chromatography A*, vol. 1036, no. 2, pp. 239–243, 2004.

[11] C. Arnezeder, W. Koliander, and W. A. Hampel, "Rapid determination of ergosterol in yeast cells," *Analytica Chimica Acta*, vol. 225, no. 1, pp. 129–136, 1989.

[12] M. Varga, T. Bartók, and Á. Mesterházy, "Determination of ergosterol in Fusarium-infected wheat by liquid chromatography-atmospheric pressure photoionization mass spectrometry," *Journal of Chromatography A*, vol. 1103, no. 2, pp. 278–283, 2006.

[13] J. V. Headley, K. M. Peru, B. Verma, and R. D. Robarts, "Mass spectrometric determination of ergosterol in a prairie natural wetland," *Journal of Chromatography A*, vol. 958, no. 1-2, pp. 149–156, 2002.

[14] Z. Parsi and T. Górecki, "Determination of ergosterol as an indicator of fungal biomass in various samples using non-discriminating flash pyrolysis," *Journal of Chromatography A*, vol. 1130, no. 1, pp. 145–150, 2006.

[15] B. O. Axelsson, A. Saraf, and L. Larsson, "Determination of ergosterol in organic dust by gas chromatography-mass spectrometry," *Journal of Chromatography B*, vol. 666, no. 1, pp. 77–84, 1995.

[16] F. Q. Yang, K. Feng, J. Zhao, and S. P. Li, "Analysis of sterols and fatty acids in natural and cultured Cordyceps by one-step derivatization followed with gas chromatography-mass spectrometry," *Journal of Pharmaceutical and Biomedical Analysis*, vol. 49, no. 5, pp. 1172–1178, 2009.

[17] K. Kobashi and T. Akao, "Relation of intestinal bacteria to pharmacological effects of glycoside," *Bioscience and Microflora*, vol. 16, no. 1, pp. 1–7, 1997.

[18] D. H. Kim, K. W. Yu, E. A. Bae, H. J. Park, and J. W. Choi, "Metabolism of kalopanaxsaponin B and H by human intestinal bacteria and antidiabetic activity of their metabolites," *Biological and Pharmaceutical Bulletin*, vol. 21, no. 4, pp. 360–365, 1998.

[19] J. Shen and X. Shao, "Cloud point extraction and its applications to the separation and analysis of organic components," *Progress in Chemistry*, vol. 18, no. 4, pp. 482–487, 2006.

[20] H. Ma, J. You, and Y. Liu, "Cloud-point extraction combined with HPLC for determination of larotaxel in rat plasma: a pharmacokinetic study of liposome formulation," *Journal of Separation Science*, vol. 35, no. 12, pp. 1439–1446, 2012.

[21] M. D. Rukhadze, S. K. Tsagareli, N. S. Sidamonidze, and V. R. Meyer, "Cloud-point extraction for the determination of the free fraction of antiepileptic drugs in blood plasma and saliva," *Analytical Biochemistry*, vol. 287, no. 2, pp. 279–283, 2000.

[22] Y. Y. Zhao, L. B. Yang, M. C. Wang et al., "1β-hydroxylfriedelin, a new natural pentacylic triterpene from the sclerotia of *Polyporus umbellatus*," *Journal of Chemical Research*, no. 11, pp. 699–701, 2009.

[23] J. X. Li, J. Li, L. Z. Xu, S. L. Yang, and Z. M. Zou, "Studies on chemical constituents of *Cordyceps sinensis* (Berk) Sacc," *Chinese Pharmaceutical Journal*, vol. 38, no. 7, pp. 499–501, 2003.

[24] U.S. Department of Health and Human Services, Food and Drug Administration, Center for Drug Evaluation and Research (CDER), and Center for Veterinary Medicine (CVM), *Guidance for Industry-Bioanalytical Method Validation*, Center for Drug Evaluation and Research (CDER), Rockville, Md, USA, 2001.

[25] Y. Y. Zhao, X. L. Cheng, Y. Zhang et al., "A fast and sensitive HPLC-MS/MS analysis and preliminary pharmacokinetic characterization of ergone in rats," *Journal of Chromatography B*, vol. 878, no. 1, pp. 29–33, 2009.

[26] Y. Y. Zhao, X. L. Cheng, F. Wei et al., "Ultra performance liquid chromatography coupled with electrospray and atmospheric pressure chemical ionization-quadrupole time-of-flight mass spectrometry with novel mass spectrometry$^{\text{Elevated Energy}}$ data collection technique: determination and pharmacokinetics, tissue distribution and biliary excretion study of ergone in rat," *Journal of Separation Science*, vol. 35, no. 13, pp. 1619–1629, 2012.

Hindawi Publishing Corporation
Journal of Analytical Methods in Chemistry
Volume 2013, Article ID 389390, 7 pages
http://dx.doi.org/10.1155/2013/389390

Research Article

Exploring the Relationship between the Inhibition Selectivity and the Apoptosis of Roscovitine-Treated Cancer Cells

Chunying Cui,[1] Yaonan Wang,[2] Yuji Wang,[1] Ming Zhao,[1] and Shiqi Peng[1]

[1] *College of Pharmaceutical Sciences, Capital Medical University, Beijing 100069, China*
[2] *Medical Experiment and Test Center, Capital Medical University, Beijing 100069, China*

Correspondence should be addressed to Ming Zhao; mingzhao@bjmu.edu.cn and Shiqi Peng; sqpeng@bjmu.edu.cn

Received 22 February 2013; Accepted 18 March 2013

Academic Editor: Shuang-Qing Zhang

The antitumor activity of roscovitine was tested in four cervical carcinoma cells: C33A, HCE-1, HeLa, and SiHa. The effects of roscovitine on ATP Lite assay, cell cycle, and apoptosis were assessed. The Sub-G_1 DNA content occurred great increasing, and this indicates that apoptosis was induced quickly in HeLa cells, but slowly in the other cells. The morphological observation results showed that roscovitine induced apoptosis and cell death in the cervical carcinoma cells. Results revealed that roscovitine exhibited selective cytotoxicity towards 4 cervical carcinoma cells, and the cells showed different morphologic and apoptotic changes at the same concentration. It was estimated that cervical carcinoma cells responded differently to roscovitine because of differences in apoptotic and genetic background in different cervical carcinoma cells. This study suggested that roscovitine had the potential to be a chemotherapeutic agent against cervical carcinoma.

1. Introduction

Cyclin-dependent kinase inhibitors have the potential to induce cell cycle arrest and apoptosis in cancer cells [1]. Roscovitine, a potent and selective inhibitor of Cdk2 and Cdc2, has demonstrated selective inhibition of Cdk enzymes over related kinases. It has been reported that roscovitine does cause not only cell cycle arrest, but also apoptosis in cancer cells [2, 3]. In in vitro study, it has been shown that roscovitine has cytotoxic activity against a lot of human tumor cells, as well as in tumor xenograft models [4, 5]. Roscovitine is currently undergoing phase II clinical trials as a treatment for nonsmall cell lung cancer and nasopharyngeal cancer [6, 7].

In this study, we investigated whether roscovitine could inhibit the tumor growth and exhibit cytotoxicity in cervical carcinoma cell lines: C33A, HCE-1, HeLa, and SiHa. In addition, we are interested in elucidating the biochemistry of apoptosis of roscovitine on these cell lines. Our data showed that roscovitine can inhibit tumor cell proliferation in dose- and time-dependent manner in cervical carcinoma cells. Roscovitine can induce cell cycle arrest and apoptosis in 4 cervical cells but showed selective sensitivity. We estimated that cervical carcinoma cells responded differently to roscovitine because of differences in apoptotic and genetic background. These results also suggest that roscovitine may be a selective and effective chemotherapeutic agent against cervical carcinoma.

2. Materials and Methods

Roscovitine was purchased from Sigma-Aldrich (CAS: 186692466, USA). C33A, HCE-1, HeLa, and SiHa cell lines were purchased from the Institute of Basic Medical Sciences Chinese Academy of Medical Sciences and Shanghai Sanqiang Analysis Company. Dulbecco's modified Eagle medium (DMEM), fetal bovine serum (FBS), and trypsin were purchased from Hyclone Laboratories Inc. (USA). Penicillin and streptomycin were purchased from Sigma Chemical Company (USA). Dimethyl sulfoxide (DMSO) was purchased from AppliChem GmbH Company (Germany). 3-(4,5-Dimethylthiazol-2-yl)-2,5-diphenyl-tetrazolium bromide (MTT) and acridine orange were purchased from

Amresco company (USA). Protease inhibitor cocktail (1%, Cat No: 539134) was purchased from Merck (USA). All reagents were of chemical grade unless otherwise specified.

2.1. Cell Culture and Reagents. A 10 mmol/L roscovitine stock solution of the compound was prepared in DMSO and diluted to a different concentration. The final concentration of DMSO in culture medium was ≤0.3%. Four cervical carcinoma cells (C33A, HCE-1, HeLa, and SiHa) were maintained in RPMI-1640 media containing 10% fetal bovine serum, 2 mmol/L L-glutamine, 100 U/mL penicillin, and 100 μg/mL streptomycin. Cells were cultured in an incubator at 37°C under 5% CO_2 in air.

2.2. Assessment of Cell Viability (Dose and Time Relationship). C33A, HCE-1, HeLa, and SiHa cells (5×10^4/well) were grown in 24-well plates and treated with roscovitine (0–30 μmol/L) or DMSO (0.3%, final concentration) for 48 and 72 h. Attached cells were released by trypsin and combined with nonadherent cells. After centrifugation, cells were resuspended in PBS and treated with 0.2% trypan blue. Experiments were performed in five replicates independently. For cell growth inhibition experiment, cells were seeded in 24-well culture plates at a density of 5×10^4/well. After 0, 2, 4, 6, 12, 24, and 72 h, 20 μmol/L of roscovitine was added into the wells. Cell number and cell viability were determined using haemocytometer and trypan blue dye exclusion test.

2.3. MTT Assay. C33A, HCE-1, HeLa, and SiHa cells were seeded into 96-well plates and incubated overnight at 37°C. Roscovitine was added to cells (in 5 replicates) and incubated for 72 h at 37°C. 3-[4,5-Dimethylthiazol-2-yl]-2,5-diphenyltetrazolium bromide (MTT) was made up as a stock of 2 mg/mL in cell media and filter sterilized. Media were removed from cells, and MTT solution was then added at 50 μL per well and incubated in the dark at 37°C for 4 h. MTT solution was removed, and MTT dye was solubilised with 50 μL/well of DMSO with agitation. Measure the absorbance at 562 nm and then determine the IC_{50} (concentration of roscovitine which inhibits cell growth by 50%).

2.4. Flow Cytometry. Apoptotic effects of roscovitine on cervical carcinoma cells were detected by flow cytometry. Cervical carcinoma cells in logarithmic phase of 5×10^5/mL were incubated into 6-well cell culture plate and were cultured at 37°C in an incubator with 5% CO_2 for 24 h. With the culture medium removed, the volume of 2 mL containing 20 μmol/L roscovitine was added into each well. The cells were cultured at 37°C in an incubator with 5% CO_2 for 0, 6, 12, 24, 48, and 72 h, respectively, collected, respectively, and then centrifuged at 2000 g for 5 min. With the supernatant removed, the cell concentration was diluted to 1×10^6/mL. The media binding reagent with 10 μL of AnnexinV-FITC was added. The cells were incubated in darkness for 15 min and centrifuged at 3000 g for 5 min, and then the supernatant was removed. The cells were resuspended in the 0.5 mL binding buffer. The cell suspension was added with 10 μL PI on ice. The cells were protected from light and detected by flow cytometry.

2.5. ATP Lite Assay. ATP is a sign of cell viability, and it exists in all living cells with metabolism. As cells undergo necrosis or apoptosis, the ATP concentration decreases rapidly. The Luciferase and D-luciferin contained in the ATP Lite kit react with ATP to produce fluorescence. The reaction formula is as follows:

$$\text{ATP} + \text{D-Luciferin} + O_2 \longrightarrow \text{Oxyluciferin} + \text{AMP} + \text{PPi} + CO_2 + \text{Light} \quad (1)$$

Fluorescence intensity was measured by PerckinElmer 2030 Multilabel Reader. 100 μL cells suspension were seeded at 3×10^5/mL in 96-well culture plate. After 24 h, the cells were added with 100 μL culture medium containing roscovitine 10, 20, 30, 40, 50, and 60 μmol/L, respectively. The blank group was added with media, and the control group was added with 0.5% DMSO. Each group had 5 repeats. The cells of C33A and HeLa were cultured for 48 h. Temperatures of ATP Lite buffer, cell lysis solution, and lyophilized substrate solution were balanced to room temperature (RT). ATP Lite buffer with the volume of 5 mL was added into the lyophilized substrate solution. Cell lysis solution with the volume of 50 μL was added into each well. The mixture was vibrated at 1000 g for 5 min by microvibration to dissolve the cells and to stabilize ATP. The prepared matrix solution with the volume of 50 μL was added into each well. The mixture was vibrated at 1000 g for 5 min and was protected from light for 10 min to measure its fluorescence intensity.

2.6. Morphological Observation. The concentration of C33A and HeLa cells in logarithmic phase was diluted to around 5×10^4/mL. 2 mL of the C33A and HeLa cell suspension was placed into 6-well culture plate and covered by the cover slips. The cells were cultured at 37°C in an incubator with 5% CO_2 for 24 h. Then the culture medium was removed. 20 μmol/L roscovitine was added into each well, respectively, with the group of 0.3% DMSO as the control group. Two groups were cultured for 0 and 24 h, respectively. The cover slip with growing cells was selected, washed with PBS for 3 times to remove serum, fixed with 95% ethanol for 15 min, treated by 1% acetic acid for 30 s, then stained by 2×10^{-4} mol/L acridine orange for 30–60 s, processed by 1 mol/L $CaCl_2$ for 30–120 s, and washed by PBS for 3 times. A slide dropped with 200 μL glycerol was covered lightly, as the excess liquid was sucked by filter paper. The picture was taken by Confocal microscope at the excitation wavelength of 488 nm and the emission wavelength of 561 nm.

2.7. Statistics. All experiments were performed at least 5 times. Data are expressed as means ± SD. A $^*P$ value of <0.05 was considered statistically significant, and $^{**}P$ value of <0.01 was considered very significant.

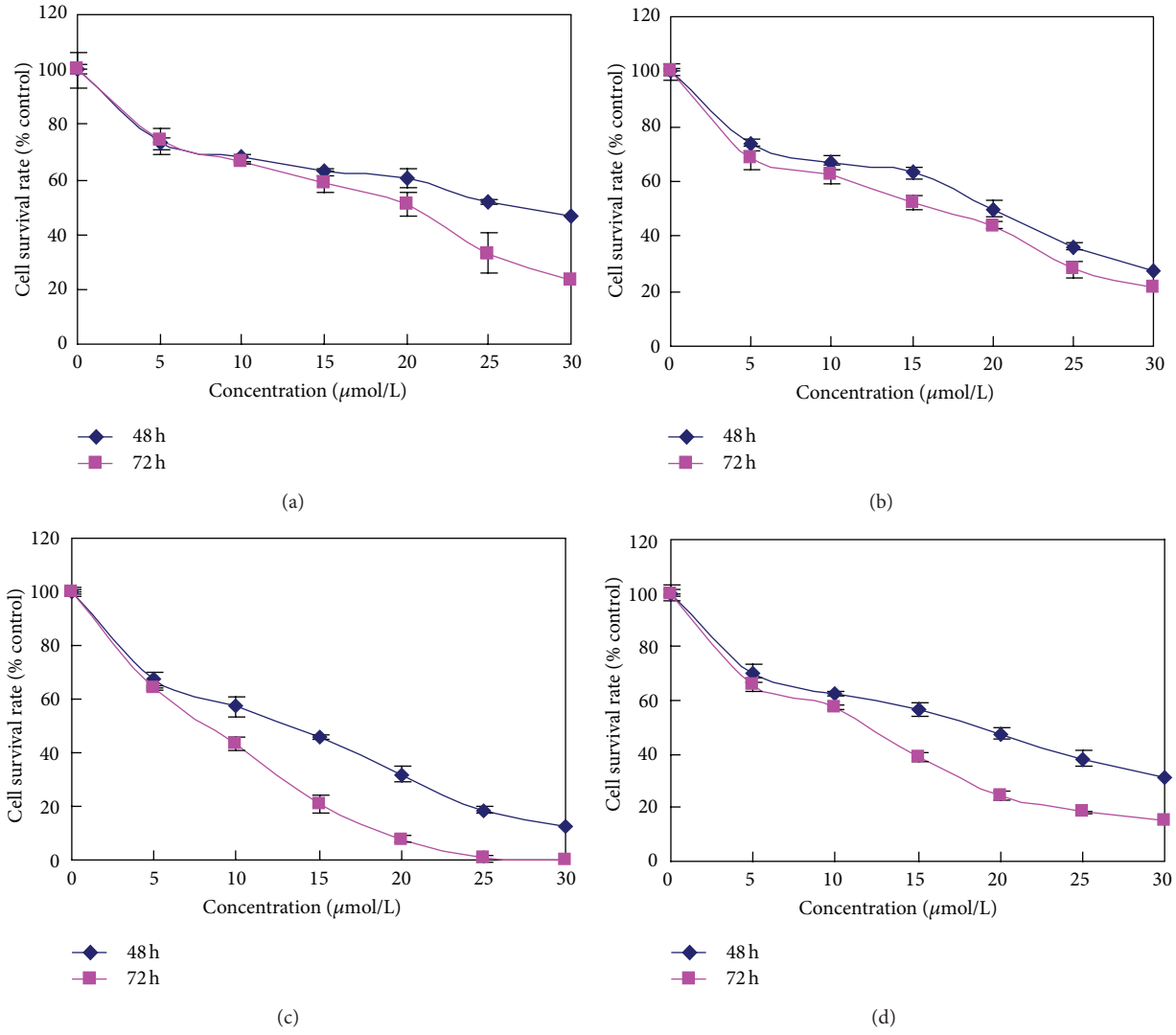

Figure 1: Survival rates (%) after 4 cervical carcinoma cell lines were incubated with various concentrations of roscovitine. (a), (b), (c), and (d) represent C33A, HCE-1, HeLa, and SiHa cell lines. Data are presented as the mean ± SD. ($n = 5$).

3. Results

3.1. The Effect of Roscovitine on Viability and Growth. The growth of cells was inhibited in dose-dependent manner after exposure to roscovitine for 48 h and 72 h ranging from 0 to 30 μmol/L (Figure 1). HeLa cells were most sensitive. The antiproliferation effect of roscovitine was evaluated by measuring the growth rates and treated with 20 μmol/L roscovitine. Treatment with roscovitine caused a time-dependent inhibition of cell growth in accordance with the cell viability assay during 72 h as compared with control (Figure 2).

3.2. Cytotoxicity Assay. Cytotoxicity was determined by MTT assay following 72 h incubation with roscovitine. The IC_{50} values of C33A, HCE-1, HeLa, and SiHa cells were 22.09±3.29, 21.21±1.96, 13.79±3.30, and 16.88±7.39 μmol/L, respectively, as shown in Figure 3.

3.3. Cell Cycle Effects. We analyzed the cell cycle profiles of growing cervical cell lines exposed to 20 μmol/L roscovitine. In C33A, HCE-1, and SiHa cell lines, the Sub-G_1 DNA content was remarkable and apparently increased during 24–48 h, indicating that apoptosis occurred (Figure 4). In HeLa cell lines, we found that the Sub-G_1 DNA content occurred great increase within 12 h. The results indicated that roscovitine induced apoptosis in four cervical carcinoma cells, and HeLa is the most sensitive to roscovitine.

3.4. ATP Lite Assay. To understand the reason of the cancer cells exhibiting different sensitivity to roscovitine, the most sensitive HeLa cells and the most resistant C33A cells were used as the representatives to do the ATP Lite and morphological study. With ATP assay, it was confirmed that roscovitine significantly inhibited the growth of both C33A and HeLa cells. The intracellular ATPase activity decreased significantly as the concentration of roscovitine increased,

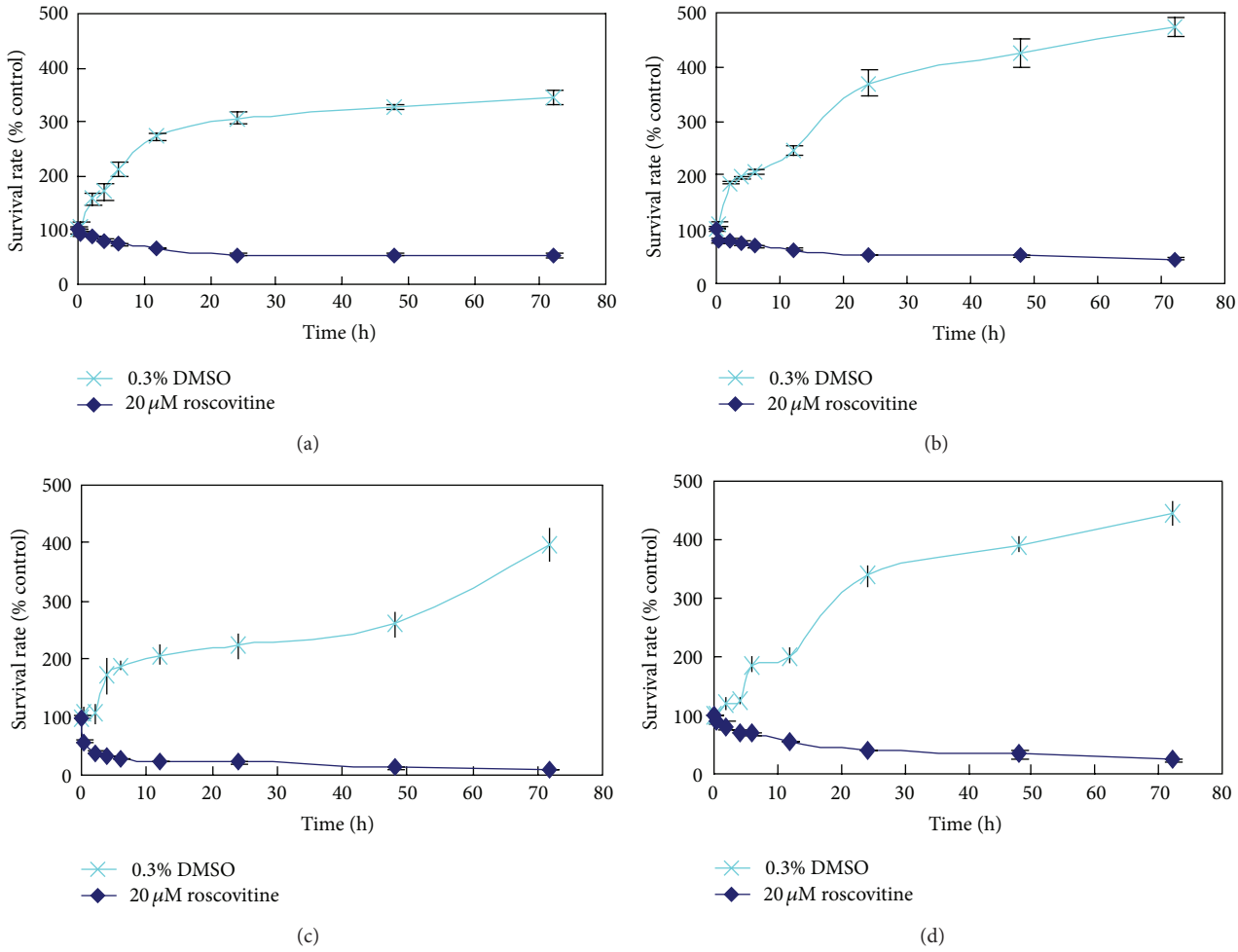

Figure 2: Survival rates (%) after 4 cervical carcinoma cell lines were incubated with 0.3% DMSO or 20 μmol/L roscovitine at various time points. (a), (b), (c), and (d) represent C33A, HCE-1, HeLa, and SiHa cell lines. Data are presented as the mean ± SD. (n = 5).

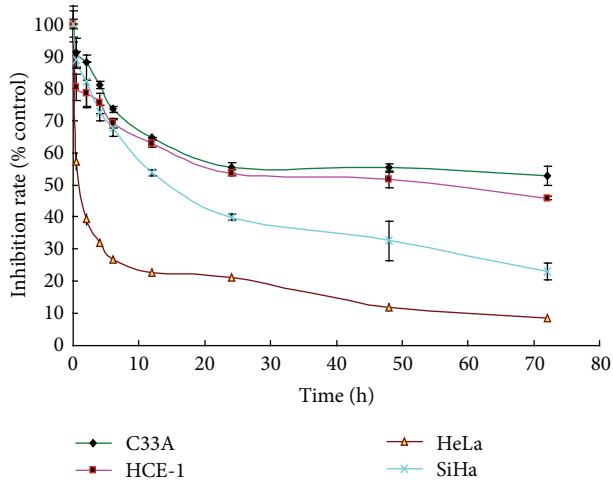

Figure 3: Inhibition rates (%) of cervical carcinoma cells treated with 20 μmol/L roscovitine at various time points. The results are expressed as the mean ± S.D. (n = 5).

as shown in Figure 5. The inhibition effect of roscovitine in HeLa cells is higher than that in C33A cell lines in a dose-dependent manner.

3.5. Morphological Observation. The C33A and HeLa cells stained with acridine orange fluorescence were observed by Confocal microscopy. Their nuclei presented homogeneous fluorescence of green light while in the apoptotic cells, due to the chromatin pyknosis or the broken fragments of unequal size, the apoptotic body was formed. They were stained with acridine orange and presented the deep and dense fluorescence or the granular fluorescence of green. The fluorescence in necrotic cells decreased or even disappeared. C33A and HeLa cells treated with roscovitine were taken pictures at 0, 24 h, the apoptosis feature was demonstrated clearly, as shown in Figure 6. The results indicated that the cells treated with roscovitine showed cell membrane blister, cell shrinkage, and apoptosis. Those indicated that roscovitine induced apoptosis in both two cell lines, and HeLa cells were more sensitive to roscovitine.

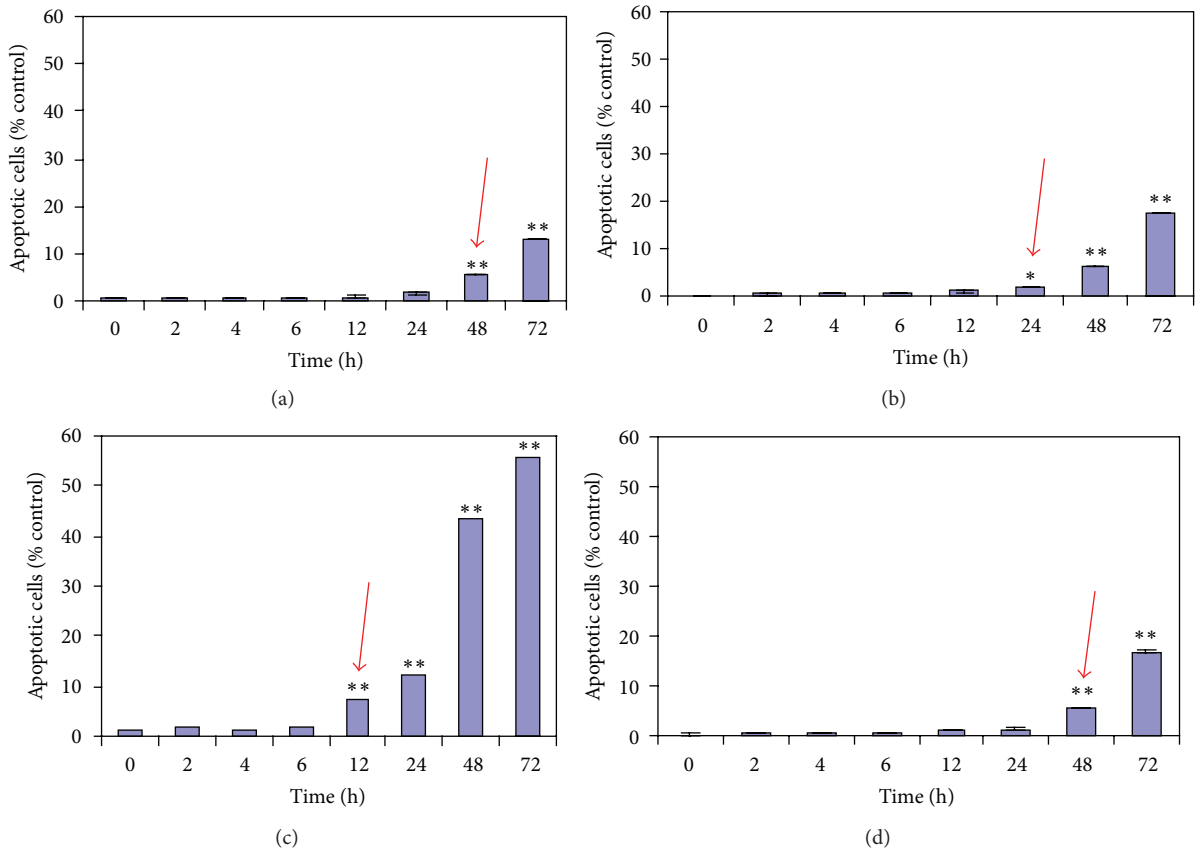

Figure 4: Effect of 20 μmol/L of roscovitine on the apoptosis of C33A, HCE-1, HeLa, and SiHa cancer cells. Data are expressed with mean ± SD. ($n = 5$).

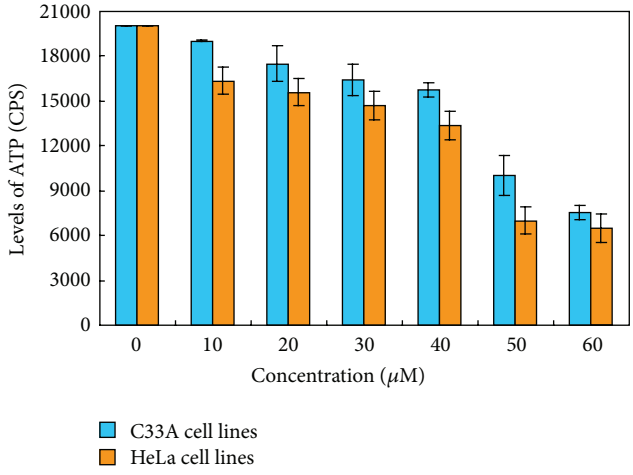

Figure 5: Cytotoxicity assay using ATP Lite approach: CPS changes of cervical cells treated with various concentrations of roscovitine. Data are presented as the mean ± SD ($n = 5$).

4. Discussion

Roscovitine, an olomoucine-related purine analogue derived from 6-DMAP and isopentenyladenine that competes with ATP for its binding site on Cdks, has been developed as a Cdk inhibitor [8, 9]. Roscovitine treatment induced not only cell cycle arrest, but also apoptosis in various type cell lines [4, 10, 11]. In this study, we showed for the first time that the novel CDK inhibitor roscovitine inhibits cervical tumor cell proliferation in dose- and time-dependent manner and induced apoptosis rapidly *in vitro* in cervical carcinoma cells by a mechanism that involved apoptosis.

We found that roscovitine exhibited selective cytotoxicity towards cervical cells, and the cells showed different morphologic and apoptotic changes at the same concentration. This observation was confirmed by flow cytometry and indicating the apoptotic mechanism of roscovitine. Published paper using roscovitine on head and neck squamous carcinoma cells also showed two possible results [12–14]. Firstly, cells may show apoptosis concurrently with cell cycle arrest. This significance is not entirely clear but would suggest chemosensitivity. Secondly, it showed a prolonged cell cycle arrest preceding apoptosis. The results suggest that cervical carcinoma cells may respond differently to roscovitine because of the mechanism and relationship of apoptosis and cell cycle arresting. From our study, roscovitine can inhibit tumor cell proliferation in dose-dependent and time-dependent manner and exhibited difference cytotoxicity in different cervical cell lines. Cervical carcinoma cells occurred apoptosis with cell cycle arrest concurrently. As such, roscovitine will be a selective and effective chemosensitivity drug for cervical carcinoma therapy.

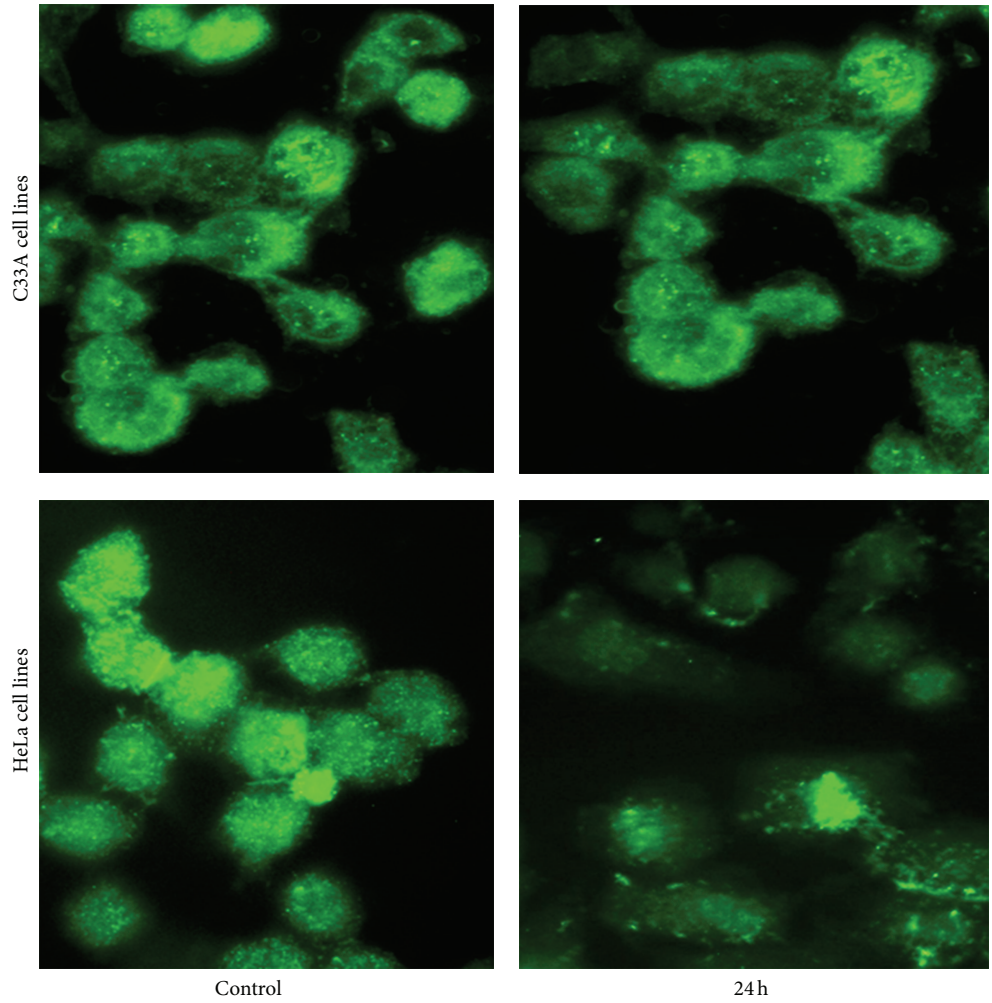

Figure 6: The apoptotic cell photos were taken by fluorescence microscope after C33A and HeLa cells were incubated with 20 μmol/L roscovitine at 0 (control) and 24 h.

Conflict of Interests

The authors report no conflict of interests related to this work.

Acknowledgments

This work was finished in Beijing Area Major Laboratory of Peptide & Small Molecular Drugs, supported by the Importation and Development of High-Caliber Talents Project of Beijing Municipal Institutions and Basic-clinical Key Research Grant (11JL02) from Capital Medical University.

References

[1] J. Węsierska-Gądek, D. Gritsch, N. Zulehner, O. Komina, and M. Maurer, "Roscovitine, a selective CDK inhibitor, reduces the basal and estrogen-induced phosphorylation of ER-α in human er-positive breast cancer cells," *Journal of Cellular Biochemistry*, vol. 112, no. 3, pp. 761–772, 2011.

[2] O. P. Mgbonyebi, J. Russo, and I. H. Russo, "Roscovitine induces cell death and morphological changes indicative of apoptosis in MDA-MB-231 breast cancer cells," *Cancer Research*, vol. 59, no. 8, pp. 1903–1910, 1999.

[3] J. Węsierska-Gądek, A. Borza, O. Komina, and M. Maurer, "Impact of roscovitine, a selective CDK inhibitor, on cancer cells: bifunctionality increases its therapeutic potential," *Acta Biochimica Polonica*, vol. 56, no. 3, pp. 495–501, 2009.

[4] S. J. McClue, D. Blake, R. Clarke et al., "In vitro and in vivo antitumor properties of the cyclin dependent kinase inhibitor CYC202 (R-roscovitine)," *International Journal of Cancer*, vol. 102, no. 5, pp. 463–468, 2002.

[5] J. Węsierska-Gądek, A. Borza, E. Walzi et al., "Outcome of treatment of human HeLa cervical cancer cells with roscovitine strongly depends on the dosage and cell cycle status prior to the treatment," *Journal of Cellular Biochemistry*, vol. 106, no. 5, pp. 937–955, 2009.

[6] V. Yarotskyy and K. S. Elmslie, "Roscovitine inhibits CaV3.1 (T-type) channels by preferentially affecting closed-state inactivation," *Journal of Pharmacology and Experimental Therapeutics*, vol. 340, no. 2, pp. 463–472, 2012.

[7] C. Le Tourneau, S. Faivre, V. Laurence et al., "Phase I evaluation of seliciclib (R-roscovitine), a novel oral cyclin-dependent kinase inhibitor, in patients with advanced malignancies," *European Journal of Cancer*, vol. 46, no. 18, pp. 3243–3250, 2010.

[8] M. Gallorini, A. Cataldi, and V. di Giacomo, "Cyclin-dependent kinase modulators and cancer therapy," *BioDrugs*, vol. 26, no. 6, pp. 377–391, 2012.

[9] J. Vesely, L. Havlicek, M. Strnad et al., "Inhibition of cyclin-dependent kinases by purine analogues," *European Journal of Biochemistry*, vol. 224, no. 2, pp. 771–786, 1994.

[10] T. David-Pfeuty, "Potent inhibitors of cyclin-dependent kinase 2 induce nuclear accumulation of wild-type p53 and nucleolar fragmentation in human untransformed and tumor-derived cells," *Oncogene*, vol. 18, no. 52, pp. 7409–7422, 1999.

[11] L. Meijer, A. Borgne, O. Mulner et al., "Biochemical and cellular effects of roscovitine, a potent and selective inhibitor of the cyclin-dependent kinases cdc2, cdk2 and cdk5," *European Journal of Biochemistry*, vol. 243, no. 1-2, pp. 527–536, 1997.

[12] N. Raje, S. Kumar, T. Hideshima et al., "Seliciclib (CYC202 or R-roscovitine), a small-molecule cyclin-dependent kinase inhibitor, mediates activity via down-regulation of Mcl-1 in multiple myeloma," *Blood*, vol. 106, no. 3, pp. 1042–1047, 2005.

[13] O. M. Tirado, S. Mateo-Lozano, and V. Notario, "Roscovitine is an effective inducer of apoptosis of Ewing's sarcoma family tumor cells in vitro and in vivo," *Cancer Research*, vol. 65, no. 20, pp. 9320–9327, 2005.

[14] M. Mihara, S. Shintani, A. Kiyota, T. Matsumura, and D. T. Wong, "Cyclin-dependent kinase inhibitor (roscovitine) suppresses growth and induces apoptosis by regulating Bcl-x in head and neck squamous cell carcinoma cells," *International Journal of Oncology*, vol. 21, no. 1, pp. 95–101, 2002.

Hindawi Publishing Corporation
Journal of Analytical Methods in Chemistry
Volume 2013, Article ID 706723, 11 pages
http://dx.doi.org/10.1155/2013/706723

Research Article

Effects of Borneol on Pharmacokinetics and Tissue Distribution of Notoginsenoside R1 and Ginsenosides Rg1 and Re in *Panax notoginseng* in Rabbits

Shixiang Wang,[1,2] Weijin Zang,[1] Xinfeng Zhao,[1,2] Weiyi Feng,[3] Ming Zhao,[1] Xi He,[1] Qinshe Liu,[4] and Xiaohui Zheng[1,2]

[1] *Department of Pharmacology, School of Medicine, Xi'an Jiaotong University, Xi'an 710061, China*
[2] *Key Laboratory of Resource Biology and Biotechnology in Western China, Ministry of Education/College of Life Science, Northwest University, Xi'an 710069, China*
[3] *First Affiliated Hospital, School of Medicine, Xi'an Jiaotong University, Xi'an 710061, China*
[4] *Shaanxi Provincial People's Hospital, Xi'an 710068, China*

Correspondence should be addressed to Weijin Zang; zwj@xjtu.edu.cn and Xiaohui Zheng; zhengxh@nwu.edu.cn

Received 16 January 2013; Accepted 5 March 2013

Academic Editor: Ying-Yong Zhao

The purpose of this study is to investigate the effects of Borneol on the pharmacokinetics of notoginsenoside R1 (NGR1) and the ginsenosides Rg1 (GRg1) and Re (GRe) in *Panax notoginseng*. Reversed phase high-performance liquid chromatography coupled with electrospray ion trap mass spectrometry was employed to determine the concentrations of the three compounds in rabbit plasma. In comparison with rabbits administrated *Panax notoginseng* extract alone, animals simultaneously taking *Panax notoginseng* extract and Borneol exhibited significant differences in pharmacokinetic parameters of NGR1, GRg1, and GRe, such as increasing their bioavailability. Quantities of NGR1, GRg1, and GRe in rabbit tissues were also increased after combining administration of Borneol. In addition, the apparent permeability coefficients (P_{app}) of NGR1, GRg1, and GRe were raised by Borneol significantly in Caco-2 cells. However, no significant changes were observed in the efflux ratio (Er) of NGR1, GRg1 and GRe. These data indicate that Borneol has the properties of enhancing the intestinal absorption, increasing the distribution, and inhibiting the metabolism of NGR1, GRg1, and GRe. The underlying mechanism might be attributed to the loosening of the intercellular tight junction.

1. Introduction

Panax notoginseng, also known as sanchi ginseng, is famous in China and other countries for its obvious therapeutic effects on the cardiovascular system [1, 2]. Previous studies have shown that *Panax notoginseng* mainly contained dammarane-type saponins (ginsenosides) including sanchinoside or notoginsenoside which is unique to *Panax notoginseng* [3–6]. Recent researches have revealed various pharmacological effects of notoginsenosides such as blocking Ca^{2+} influx through the receptor, enhancing astrocyte differentiation, and inhibiting vessel restenosis and antifibrotic effects [7–10].

Various methods for the quality control of *Panax notoginseng* and its complex prescription have been reported previously in the literature [11–15]. Among these analytical assays, high-performance liquid chromatography coupled with an ultraviolet visible (UV-Vis) detector or a diode array detector was a common choice for the detection of saponins in *Panax notoginseng*. Setting the detecting wavelength at 190~205 nm due to low absorbance of these compounds in the regular UV region, however, greatly increased the baseline noise and decreased the sensitivity of detection. To address this issue, an evaporative light-scattering detector has been employed for the detection of saponins, resulting in a stable baseline even with a gradient elution [16, 17]. In addition, recent researches

have shown that high-performance liquid chromatography coupled with mass spectrometry is a favorable and useful alternative for the detection of saponins in *Panax notoginseng* [18–20].

Borneol, a monoterpenoid component of the medicinal plant such as *Blumea martiniana* and *Clausena dentata* [21–23], is usually used as "Guide drug" in the prescription to guide the bioactive components of herbs to the proper organs to exert a harmonizing effect. A better therapeutic effect has been observed for the combined administration of other herbs, *Panax notoginseng* and *Radix Salvia miltiorrhiza*, and Borneol than the single use of other herbs for the patients with cardiovascular diseases in practice [24, 25]. However, the mechanism underlying the synergistic effect of *Panax notoginseng* and Borneol is still an enigma. In most of the previous studies, pharmacokinetics of saponins in *Panax notoginseng* and its prescriptions were investigated [25–29]. However, little attention has been paid to pharmacokinetics of notoginsenoside R1 (NGR1), ginsenosides Rg1 (GRg1), and Re (GRe), the main active components of *Panax notoginseng*, especially the interactive effects of *Panax notoginseng* and Borneol.

The current study is to investigate the effect of Borneol on the pharmacokinetics of NGR1, GRg1, and GRe in *Panax notoginseng* in rabbits. A sensitive and accurate SPE-HPLC-MS method was established and applied to the pharmacokinetic study of NGR1, GRg1, and GRe via determining their concentrations in rabbit plasma after oral administration of *Panax notoginseng* or *Panax notoginseng* combined with Borneol. In addition, the mechanism underlying the effect of borneol on NGR1, GRg1, and GRe was investigated by vinblastine-selected Caco-2 cells *in vitro*.

2. Materials and Methods

2.1. Materials and Reagents. NGR1, GRg1, and GRe (purity > 95%) were purchased from the National Institute for the Control of Pharmaceutical and Biological Products of China (Lots nos. 110754-200322; 110703-200322; and 110745-200414, resp.). Borneol (purity > 98%) was supplied by Tianjin Tasly Pharm. Co., Ltd. Caco-2 cells were acquired from Institute of Biochemistry and Cell Biology, Shanghai institute for Biological Sciences, CAS. Transwell plates (pore size 0.4 μm, 24 mm diameter) were purchased from Corning Costar Co. Foetal bovine serum and nonessential amino acids were bought from Gibco-BRL Life Technologies (Paisley, Scotland). Penicillin, streptomycin, trypsin, dimethylsulfoxide (DMSO), and ammonium formate were bought from Sigma Chemical Co. HPLC grade solvents and reagents were obtained from Fisher Scientific Company (Pittsburgh, PA, USA). Ultrapure water (18.2 MΩ) was obtained through a Milli-Q water purification system.

2.2. Preparation of Herb Extract. 250 grams of *Panax notoginseng* were immersed in an 8-fold ethanol/water (V : V, 70 : 30) solution for 30 min and refluxed twice (1.5 h each time). The suspension was then filtered followed by concentrating to 50 mL to obtain the *Panax notoginseng* extract. The *Panax notoginseng* extract combined with Borneol was prepared by adding 1.42 g Borneol to 50 mL *Panax notoginseng* extract. The concentrations of NGR1, GRg1, and GRe in the extract were determined to be 87.5, 124.6, and 40.2 mg·mL^{-1}, respectively, by the HPLC method.

2.3. Animals. The ethical use of animals in this study was approved by the Advisory Board on Animal Experiments of the Xi'an Jiaotong University in China. New Zealand rabbits (weight 1.7–2.3 kg) were provided by the Animal Center of Xi'an Jiaotong University. The rabbits were maintained in air-conditioned animal quarters at a temperature of 22 ± 2°C and a relative humidity of 50 ± 10%. The cannula (Terumo, 22 G × 1, i.d. 0.60 × 20 mm) was placed in the central ear artery and used for blood collection. The animals were acclimatized to the facilities for 5 days, and then fasted and had free access to water for 12 h prior to experiment.

2.4. Liquid Chromatographic and Mass Spectrometric Conditions. Liquid chromatography was carried out on an Agilent 1100 HPLC system with an auto sampler, a quaternary pump and a vacuum degasser (Waldoboro, Frankfurt, Germany). Operations were controlled by Agilent Chemstation 4.2 software (Littleforts, Philadelphia, USA). Separations were achieved on a reversed-phase HPLC column (Zorbax SB-C_{18} 150 × 2.1 mm, 5.0 μm particle size). A solution of acetonitrile and water (V : V, 20 : 80) with 0.1% (V : V) ammonium formate was used as the mobile phase. The flow rate was set at 0.3 mL·min^{-1} and the column temperature was 25°C. Under these conditions, NGR1, GRg1, and GRe in plasma samples were separated efficiently without any interferences.

MS^n detection was performed on an Agilent SL trap MS system (Waldoboro, Frankfurt, Germany). The ion source-dependent (electrospray ionization) conditions were the same for all analyses with a spraying voltage of −4500 V in the negative ion mode. The pressure of the nebulizing gas (nitrogen) was set at 35 p.s.i. The flow rate of the drying gas (nitrogen) was set at 7.0 L·min^{-1} with the temperature of 325°C. The collision gas (He) for the MS^n mode at trap was set at flow of 4 (instrument unit). The voltage of the capillary was set at 4000 V, and its end plate offset was −500 V. Scan range was from 500 to 1500 *m/z*.

2.5. Preparation of Calibration Standard Working Solutions. Primary stock solutions of 0.28 mg·min^{-1} NGR1, 0.30 mg·min^{-1} GRg1 and 0.72 mg·min^{-1} GRe were prepared in methanol. Working standard solutions of NGR1, GRg1, and GRe were prepared by diluting the aliquots of the primary solution with methanol. The solutions were stored at 4°C in glass tubes until further use.

2.6. Extraction of Sample. Frozen plasma and tissue samples were thawed in a water bath at 37°C and were then vortexed followed by centrifuging at 5000 r·min^{-1} for 5 min. An aliquot of 1.0 mL of the supernatant from each sample was loaded onto C_{18} Bond Elute Solid phase extraction (SPE) cartridges (1000 mg, 1 cc reservoir, Varian, Harbor City, CA, USA) pretreated with 2.0 mL hexane, isopropanol,

methanol, and water, sequentially. The SPE cartridges were then washed with 1.0 mL water, 20% methanol/water solution, 40% methanol/water solution, and 60% methanol/water solution, sequentially. Finally, analytes were eluted twice with 1.0 mL of 70% methanol/water solution. The eluant was evaporated to dryness under nitrogen. The residues were then reconstituted in 1.0 mL mobile phase. An aliquot of 10 μL was injected into the LC-MS system.

2.7. Calibration Procedure. Samples calibration standards containing 0.28, 0.56, 2.8, 5.6, 14.0, 28.0, and 56.0 $\mu g \cdot min^{-1}$ of NGR1, 0.30, 0.60, 3.0, 6.0, 15.0, 30.0, and 60.0 $\mu g \cdot min^{-1}$ of GRg1, and 0.36, 0.72, 3.6, 7.2, 18.0, 36.0, and 72.0 $\mu g \cdot min^{-1}$ of GRe were freshly prepared daily by diluting the working standard solution with blank sample. The calibration curve was then obtained by plotting the peak areas of the extracted ion current versus the concentrations of the standards using weighted linear regression. The results showed that the linear range of NGR1, GRg1, and GRe was 0.28–56.0, 0.30–60.0, and 0.36–72.0 $\mu g \cdot min^{-1}$, respectively.

2.8. Method Validation. Validation of the proposed method included assessment of the calibration curve performance, as well as accuracy and precision of the method, and stability of the analytes at various test conditions.

The precision of the assay was determined for the quality control (QC) plasma and tissue samples by replicate analyses of three levels of concentration at 0.5, 5.0, and 35.0 $\mu g \cdot min^{-1}$ for NGR1, 0.4, 3.0, and 40.0 $\mu g \cdot min^{-1}$ for GRg1, and 0.8, 8.0, and 48.0 $\mu g \cdot min^{-1}$ for GRe. Intraday precision and accuracy were determined via repeated analysis of the QC plasma and tissue samples within one day ($n = 5$). Interday precision and accuracy were determined via repeated analysis on five consecutive days. The concentration of each sample was determined using the prepared calibration curve and analyzed on the same day. All stabilities were evaluated at different concentration levels. Short-term stability of NGR1, GRg1, and GRe were assessed by analyzing QC samples kept at 4°C for 4–24 h. Freeze-thaw stability was evaluated at three consecutive freeze-thaw cycles. Long-term stability was studied by analyzing samples during a period of 8 weeks of storage at −70°C.

2.9. Pharmacokinetics Study. Eighteen rabbits were randomly divided into three groups of 6 subjects and were orally given 3.0 $mL \cdot kg^{-1}$ normal saline, 3.0 $mL \cdot kg^{-1}$ *Panax notoginseng* extract, and 3.0 $mL \cdot kg^{-1}$ *Panax notoginseng* extract combined with Borneol, respectively. Plasma samples were collected in heparinized tubes from the central ear artery at 0.0, 5.0, 10.0, 20.0, 30.0, 45.0, 60.0, 75.0, 90.0, 120.0, 180.0, 300.0 and 480.0 min after dose. After each sampling, the same volume of 0.9% saline solution was injected from the ear vein to compensate the loss of blood. The plasma obtained was frozen at −70°C for storage and was processed prior to analysis with the proposed method as described in Section 2.6.

2.10. Tissue Distribution Study. One group of rabbits ($n = 18$) was orally administered a dose of 3.0 $mL \cdot kg^{-1}$ *Panax notoginseng* extract, while another group of rabbits ($n = 18$) was orally given 3.0 $mL \cdot kg^{-1}$ *Panax notoginseng* extract combined with Borneol. At 0.5, 1, and 3 h after administration, blood samples were collected from the central ear artery of six rabbits from each group, and the heart, liver, lung, kidney, and brain were immediately removed after animals were sacrificed by decapitation. An accurately weighed amount of tissue (1 g) was collected to be rinsed, dried, minced, and homogenized (400 $r \cdot min^{-1}$) in normal saline (1.5 mL). All of the samples were stored at −70°C and were processed prior to analysis with the proposed method as described in Section 2.6.

2.11. Transport Studies. The Caco-2 cells were cultured in Dulbecco's modified Eagle's medium (DMEM) supplemented with 20% foetal bovine serum, 1% nonessential amino acids and penicillin-streptomycin, at 37°C in an atmosphere with a relative humidity of 95% and a CO_2 flow of 5%. Medium was replaced every 2-3 days. When the cell monolayer reached 80% confluence, the cells were detached with a solution of 0.02% EDTA and 0.25% trypsin. The vinblastine-selected Caco-2 cells were cultivated in the presence of 10 nM vinblastine to induce P-glycoprotein (P-gp) expression. The culture medium was changed to a fresh medium without vinblastine 24 h before experiments, and the cells were used between passages 25 and 46. Prior to the transport study, cytotoxicity of NGR1, GRg1, GRe, and Borneol toward Caco-2 cells was determined using MTT assays. Noncytotoxic concentrations of 500 μM NGR1, GRg1, GRe, and 200 μM Borneol (dissolved in DMSO) were chosen for transport study.

In transport studies, vinblastine-selected Caco-2 cells were seeded on polycarbonate filter of transwells for 18–21 days before starting transport study, and the monolayers with the transepithelial electrical resistance (TEER) values greater than 300 Ωcm^2 were used. Caco-2 monolayers were rinsed twice with Hanks' balanced salt solution (HBSS) and preincubated in HBSS at 37°C for 30 min before starting experiments. To start the experiments, 500 μM of NGR1, GRg1, and GRe in final concentrations were added to the donor side with or without 200 μM Borneol and then incubated at 37°C. An aliquot of 0.1 mL samples were withdrawn from receiver chambers at 0, 30, 60, 90, and 120 min after the loading. After each sampling, 0.1 mL of HBSS was added to the receiver chamber to maintain a constant volume. All the experiments were performed five times in duplicate. The collected samples were stored at −20°C until HPLC analysis. During the above transport studies, the TEER values were also monitored before and at the end of each experiment. Apparent permeability coefficients (P_{app}) were then calculated according to the following equation:

$$P_{app} = \frac{(dC/dt \times V)}{(A \times C_0)}, \quad (1)$$

where dC/dt is the rate of the test compound appearing in the receiver chamber, V is the volume of the solution in the receiver chamber, A is the cell monolayer surface area, and C_0 is the initial concentration of the test compound added in the donor chamber.

The efflux ratio (Er) was calculated using the following equation:

$$\mathrm{Er} = \frac{P_{\mathrm{app}}\,(\text{basolateral-apical})}{P_{\mathrm{app}}\,(\text{apical-basolateral})}. \quad (2)$$

2.12. Statistical Analysis. Statistical analysis of the biological data was performed using the Student's t-test. The drug analysis system 2.0 (DAS 2.0, T.C.M., Shanghai, China) was used to calculate the pharmacokinetic parameters, such as the area under curve (AUC), the maximum plasma concentration ($C_{\max}$), the time needed to reach the maximum plasma concentration ($t_{\max}$) and the half-life of absorption, and distribution and elimination ($t_{1/2K_a}$, $t_{1/2\alpha}$, $t_{1/2\beta}$).

3. Results and Discussion

3.1. Method Validation

3.1.1. Specificity. The base peaks of each mass spectrum for NGR1, GRg1, and GRe were observed during the infusion of the standard solution in negative mode. Three $[M\text{-}H]^-$ precursor ions, *m/z* 931.6 $[M\text{-}H]^-$ for NGR1, *m/z* 799.5 $[M\text{-}H]^-$ for GRg1, and *m/z* 945.1 $[M\text{-}H]^-$, were subjected to collision-induced dissociation (CID). The product ions were recorded as *m/z* 799.4 $[M\text{-}H\text{-}Xyl]^-$, 637.3 $[M\text{-}H\text{-}Glc]^-$, and *m/z* 799.2 $[M\text{-}H\text{-}Rha]^-$, respectively. Mass transition patterns, *m/z* 931.6 → 799.4, *m/z* 799.5 → 637.3, and *m/z* 945.1 → 799.2, were selected to monitor NGR1, GRg1, and GRe. Representative HPLC-MS ion chromatograms of blank plasma samples, plasma standard solutions of 5.0 μg·mL^{-1} NGR1, 3.0 μg·mL^{-1} GRg1 and 8.0 μg·mL^{-1} GRe as well as plasma samples after administration of *Panax notoginseng* extract at a dose volume of 3.0 mL·kg^{-1} are shown in Figure 1. No endogenous peaks were found to be coeluted with the analytes, indicating high specificity of the proposed method.

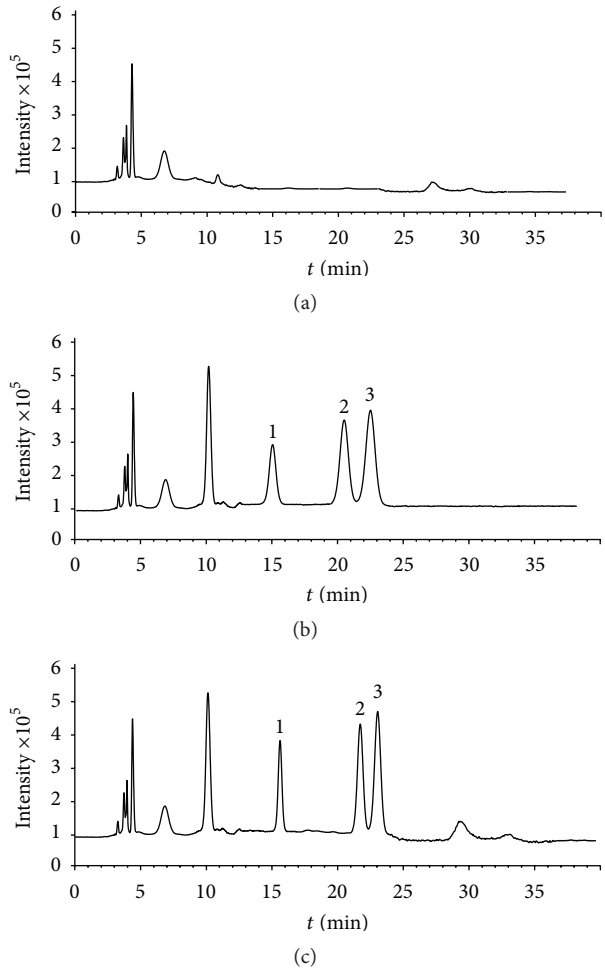

Figure 1: HPLC-MS ion chromatograms of plasma samples. (a) blank plasma samples; (b) plasma standard solutions of 5.0 μg·mL^{-1} NGR1, 3.0 μg·mL^{-1} GRg1, and 8.0 μg·mL^{-1} GRe; (c) plasma samples after administration of *Panax notoginseng* extract at a dose volume of 3.0 mL·kg^{-1}.

3.1.2. Calibration Curve Performance. The calibration curves were created by plotting the peak areas of NGR1, GRg1, and GRe to their various concentrations in the spiked plasma and tissue standards. A weighted (1/[nominal concentration]) least-squares linear regression of the type $y = bx + a$ was used to fit the curves (Table 1). The lowest correlation coefficient of determination (r^2) among the five calibration curves of NGR1, GRg1, and GRe were between 0.9982 and 0.9996. Thus, the calibration curves exhibited good linearity within the chosen range.

3.1.3. Limit of Detection and Quantitation. The limit of detection (LOD) was estimated as the amount of NGR1, GRg1, and GRe, which caused a signal three times that of noise ($S/N = 3/1$). The LOD was determined to be 0.57, 0.30, and 0.24 ng·mL^{-1} in lung and liver, and 0.28, 0.15, and 0.12 ng·mL^{-1} in plasma and other tissues, respectively. The lower limit of quantitation (LLOQ) was defined as the lowest concentration with the accuracy and precision better than 20% and a signal to noise ratio of >10. The LLOQ for NGR1, GRg1, and GRe were determined to be 1.8, 1.0, and 0.8 ng·mL^{-1} in lung and liver and 1.0, 0.5, and 0.4 ng·mL^{-1} in plasma and other tissues, respectively.

3.1.4. Accuracy and Precision. Data for intraday and interday precision and accuracy assessed by analyzing QC samples at different concentrations are presented in Table 2. The results suggested that the method was adequately accurate and reproducible for the determination of NGR1, GRg1, and GRe in rabbit plasma and tissues.

3.1.5. Extraction Recovery and Stability. The extraction recovery analysis was conducted with NGR1, GRg1, and GRe spiked biosamples at three QC levels and calculated by comparing the NGR1, GRg1, and GRe peak areas in extracted biosamples with those found by direct injection of standard solutions at the same concentration. The mean recoveries of

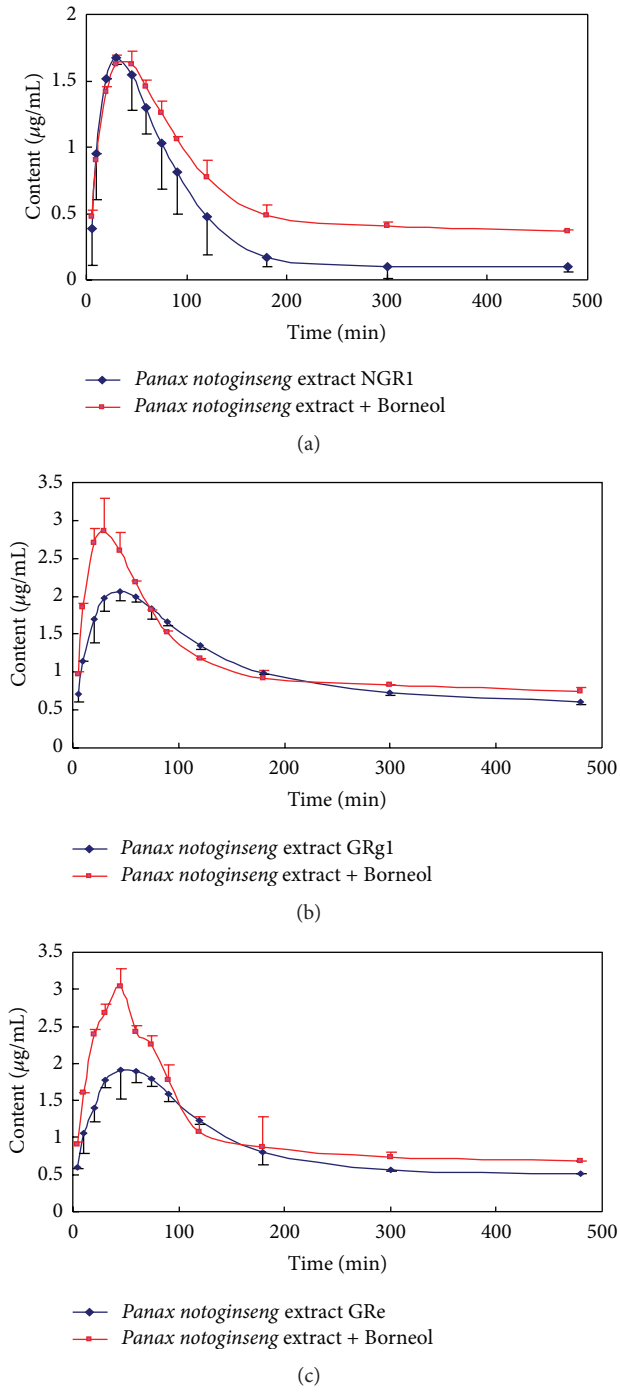

Figure 2: Plasma concentration-time curves of NGR1 (a), GRg1 (b), and GRe (c) after administration of *Panax notoginseng and Panax notoginseng* combined with Borneol extracts in rabbit, respectively. The dose volume was 3.0 mL·kg^{-1} and the fitted curves were obtained by analyzing the plasma concentration-time data with the Program DAS 2.0. ♦ rabbits administered *Panax notoginseng* extract; ■ rabbits administered *Panax notoginseng* combined with Borneol.

NGR1, GRg1, and GRe in plasma and tissue samples at three different concentrations were above 90.0% (Table 2).

The stability studies were performed by evaluating small variations in three different conditions. The results were expressed as the percentage of initial content of NGR1, GRg1, and GRe in the freshly treated samples, suggesting that NGR1, GRg1, and GRe showed no significant change in plasma and tissue samples (Table 3).

Table 1: Calibration curves for the analysis of NGR1, GRg1, and GRe in rabbit plasma and tissue.

Biosample	Calibration curves	Correlation coefficient (r^2)	Linear range (μg/mL)
NGR1			
Plasma	$Y = 356948X + 1.0076$	0.9990	0.280–56.0
Heart	$Y = 397087X - 9.5861$	0.9992	
Liver	$Y = 389965X - 9.4869$	0.9990	
Brain	$Y = 390069X - 8.4391$	0.9996	
Lung	$Y = 379924X - 8.5585$	0.9992	
Kidney	$Y = 386942X - 9.2368$	0.9996	
GRg1			
Plasma	$Y = 358992X - 3.0221$	0.9988	0.307–60.4
Heart	$Y = 356409X - 2.6782$	0.9982	
Liver	$Y = 367748X - 3.4734$	0.9986	
Brain	$Y = 362745X - 2.9939$	0.9996	
Lung	$Y = 359638X - 4.1365$	0.9990	
Kidney	$Y = 364720X - 4.5526$	0.9990	
GRe			
Plasma	$Y = 293769X - 1.605$	0.9996	0.362–54.3
Heart	$Y = 284093X + 3.8607$	0.9988	
Liver	$Y = 279365X + 3.9834$	0.9992	
Brain	$Y = 287562X + 4.1262$	0.9986	
Lung	$Y = 285328X + 3.9967$	0.9988	
Kidney	$Y = 294563X + 4.0062$	0.9990	

3.2. Pharmacokinetics Study. After oral administration of *Panax notoginseng* or *Panax notoginseng* combined with Borneol, the plasma concentrations of NGR1, GRg1, and GRe were determined by the described LC/MS/MS method. Figure 2 showed the plasma concentration-time curves of NGR1, GRg1, and GRe following ingestion of *Panax notoginseng* or *Panax notoginseng* combined with Borneol (n = 6). The statistical results through DAS 2.0 indicated that the plasma drug concentration-time course of the three compounds in rabbits confirmed the 2-compartment open models. The corresponding regression pharmacokinetic parameters were shown in Table 4.

It can be noted that the highest values of GRg1 were approximately the same as the values of GRe. This partly ascribed to the similar chemical properties of the two compounds. In addition, the increasing tendency of total distribution volume (V/F) for NGR1 was similar to that for GRg1 and GRe. However, the highest values of NGR1 parameters were different from the values of GRg1 and GRe.

Combined with Borneol, the values of $t_{1/2\alpha}$ decreased but the AUC values increased obviously, which indicated that

Table 2: The interday and intraday precision and accuracy of the method for the determination of NGR1, GRg1, and GRe ($n = 5$).

Biosample	QC conc ($\mu g \cdot mL^{-1}$)	Intraday		Interday		Extraction recovery	
		Precision (R.S.D %)	Accuracy (mean %)	Precision (R.S.D %)	Accuracy (mean %)	Mean ± S.D.	R.S.D %
NGR1							
Plasma	0.5	10.4	96.0	13.0	92.0	93.5 ± 4.7	5.1
	5.0	6.7	102.0	11.1	94.0	91.7 ± 3.5	3.8
	35.0	4.2	97.4	5.4	103.7	95.7 ± 7.5	7.9
Heart	0.5	6.3	92.5	8.4	104.9	97.8 ± 6.8	7.0
	5.0	8.3	91.8	9.3	98.9	107.4 ± 14.6	8.4
	50.0	4.9	100.3	5.3	106.1	96.9 ± 9.8	10.6
Liver	0.5	8.7	98.1	10.6	95.8	92.7 ± 7.8	8.4
	5.0	7.5	91.4	8.3	96.6	102.1 ± 5.0	4.9
	50.0	7.1	99.6	7.8	105.6	95.5 ± 7.1	7.4
Brain	0.5	9.5	90.0	6.3	108.3	92.3 ± 9.3	10.4
	5.0	4.2	108.3	9.7	95.7	99.2 ± 7.7	7.8
	50.0	3.7	103.5	7.9	95.6	92.7 ± 4.8	5.3
Lung	0.5	7.4	94.2	13.1	103.7	105.3 ± 8.9	8.5
	5.0	12.1	98.6	4.8	105.5	95.0 ± 8.2	8.6
	50.0	6.7	105.8	10.2	95.4	90.9 ± 9.2	10.1
Kidney	0.5	8.2	90.2	5.4	90.8	101.7 ± 8.5	6.2
	5.0	11.1	91.4	3.8	98.4	92.7 ± 3.7	4.0
	50.0	5.9	90.5	7.8	91.3	90.5 ± 5.1	5.6
GRg1							
Plasma	0.4	14.3	105.1	13.5	92.5	103.2 ± 4.6	4.5
	3.0	4.4	90.0	9.0	103.3	92.4 ± 7.5	8.1
	40.0	4.6	95.3	4.1	98.3	93.2 ± 5.0	5.4
Heart	0.4	10.2	97.4	6.4	96.3	95.7 ± 9.8	10.2
	3.0	4.4	93.9	7.5	94.7	99.2 ± 7.7	7.8
	40.0	6.2	101.3	10.4	104.6	106.3 ± 8.7	8.2
Liver	0.4	9.9	97.2	12.3	98.4	90.5 ± 7.1	7.9
	3.0	12.4	92.5	7.8	96.2	95.7 ± 10.0	10.5
	40.0	6.3	90.9	6.8	102.5	91.8 ± 11.3	12.3
Brain	0.4	8.9	108.9	13.2	90.4	104.8 ± 6.8	6.5
	3.0	6.1	96.3	8.4	94.3	98.2 ± 5.6	5.7
	40.0	7.3	101.8	9.3	103.1	97.9 ± 8.1	8.3
Lung	0.4	11.8	91.9	8.8	92.8	93.4 ± 8.0	8.6
	3.0	8.4	98.0	7.5	91.9	96.1 ± 4.7	4.9
	40.0	6.2	104.7	5.4	108.2	96.8 ± 7.0	7.3
Kidney	0.4	5.4	92.8	10.2	98.7	93.3 ± 9.8	10.5
	3.0	7.2	91.5	5.4	90.4	95.1 ± 3.6	3.8
	40.0	6.1	99.2	6.7	92.5	90.5 ± 6.9	7.6
GRe							
Plasma	0.8	8.4	103.7	11.5	97.5	91.2 ± 6.1	6.7
	8.0	6.6	92.5	6.2	107.5	90.8 ± 7.2	7.9
	48.0	4.2	104.7	3.8	102.9	98.1 ± 7.7	7.8
	0.8	5.4	95.8	5.8	92.6	105.3 ± 9.8	9.3

Table 2: Continued.

Biosample	QC conc ($\mu g \cdot mL^{-1}$)	Intraday		Interday		Extraction recovery	
		Precision (R.S.D %)	Accuracy (mean %)	Precision (R.S.D %)	Accuracy (mean %)	Mean ± S.D.	R.S.D %
Heart	8.0	6.8	99.4	8.3	101.5	99.2 ± 5.7	5.8
	48.0	5.5	109.1	6.7	103.8	93.1 ± 8.2	8.8
	0.8	9.1	96.8	10.8	98.3	97.2 ± 10.2	10.5
Liver	8.0	6.8	94.5	9.6	96.1	94.4 ± 6.2	6.6
	48.0	9.1	96.8	8.4	98.0	106.2 ± 7.7	7.3
	0.8	12.1	91.0	7.7	99.5	93.3 ± 6.3	6.7
brain	8.0	8.2	109.5	13.2	104.3	95.8 ± 8.9	9.3
	48.0	7.3	104.8	9.4	93.9	94.5 ± 6.4	6.8
	0.8	7.8	92.6	9.8	96.3	102.9 ± 9.7	9.4
Lung	8.0	8.5	96.4	11.4	101.6	95.7 ± 7.3	7.7
	48.0	4.7	95.9	7.8	94.8	101.7 ± 7.0	6.9
	0.8	6.1	91.8	8.5	92.8	98.1 ± 7.9	8.1
Kidney	8.0	3.3	92.2	9.0	90.6	90.2 ± 4.2	4.7
	48.0	8.9	96.4	4.5	95.4	97.4 ± 5.8	6.0

Borneol improved the absorption rate and bioavailability of NGR1, GRg1, and GRe. In addition, the decreased value of K_{10} and the increased value of K_{12} indicated that Borneol slowed down the clearance speed of NGR1, GRg1, and GRe, but increased the transferring speed of these compounds from the central compartment to the peripheral compartment. The increase in *V/F* indicated that NGR1, GRg1, and GRe transferred from the blood to the tissues, but the transfer speed was different.

In contrast to the pharmacokinetics of NGR1 in the *Panax notoginseng* group and the *Panax notoginseng* combined with Borneol group, the value of K_a was reduced, $t_{1/2K_a}$ was increased, β was reduced, and $t_{1/2\beta}$ was increased, indicating that the absorption and the clearance speed of NGR1 in the *Panax notoginseng* combined with Borneol group were reduced. Compared with the pharmacokinetic parameters of GRg1 and GRe in these two groups, the absorption rate was increased and the absorption time was reduced, while the clearance speed was constant in the *Panax notoginseng* group and the *Panax notoginseng* combined with Borneol group. In these comparisons, Borneol had different effects on the values of K_a, $t_{1/2K_a}$, β, $t_{1/2\beta}$, and K_{12} of NGR1, GRg1, and GRe.

3.3. Tissue Distribution Study. As listed in Table 5, compared with other organs, NGR1 and GRe levels in heart as well as GRg1 level in lung were high, but NGR1 and GRg1 levels in brain as well as GRe level in lung were low at 0.5, 1.0, and 3.0 h in *Panax notoginseng* group. The highest levels of NGR1, GRg1, and GRe were observed at 1.0 h in heart, liver, lung, and brain, meanwhile the drug concentration in kidney decreased at 1.0 h. For Borneol combined with *Panax notoginseng*, the three saponins levels were all increased markedly in the tissues with peak levels observed at 1.0 h in the tissues except kidney. The levels of NGR1 in heart, liver, brain, lung and kidney were 3.90-, 6.36-, 3.82-, 6.82-, and 2.3-fold higher than the plasma concentrations, respectively. The GRg1 levels in these tissues were 12.40-, 27.09-, 11.77-, 8.17-, and 7.77-fold higher than the plasma concentrations, respectively. The GRe levels in these tissues were 1.35-, 1.97-, 1.14-, 1.24-, and 1.0-fold higher than the plasma concentrations, respectively. These data indicate that Borneol could increase the levels of NGR1, GRg1, and GRe in the tissues.

3.4. Transport Studies. According to the classification method proposed by Yee [30], the permeabilities less than 10^{-6} cm/s correspond to substances with low absorption (<30%), permeabilities between 10^{-6} cm/s and 10^{-5} cm/s correspond to substances with moderate absorption (30–70%), and permeabilities more than 10^{-5} cm/s correspond to substances with high absorption (>70%). As showed in Table 6, the P_{app} values of NGR1, GRg1, and GRe were less than 10^{-6} cm/s, indicating that NGR1, GRg1, and GRe presented the poor membrane permeabilities and low bioavailabilities in Caco-2 monolayers. The efflux ratios (Er) of NGR1, GRg1, and GRe were within the range of 1.0-1.1, suggesting that there was no significant difference between the permeability in apical-to-basolateral and that in basolateral-to-apical directions, and implying that NGR1, GRg1, and GRe seemed not to be substrates of P-gp. However, it was reported that metabolic inhibitor KCN and P-gp inhibitor verapamil could increase GRg1 concentration within the cells, and the efflux of Rg1 was energy-dependent and P-gp was likely to be involved [31]. Its precise mechanism still needs to be investigated in further work.

Borneol is used as a "Guide drug" in traditional Chinese medicine, enhancing the expected functions of bioactive components from other herbs in the complex prescription through increasing bioavailability. Other research groups

Table 3: Stability of of NGR1, GRg1, and GRe in plasma samples and tissue homogenates of rabbits ($n = 6$).

Biosample	QC conc ($\mu g \cdot mL^{-1}$)	Remaining (mean ± S.D.) Short-term stability	Long-term stability	Freeze-thaw stability
NGR1				
Plasma	0.5	98.0 ± 6.2	100.0 ± 8.7	90.4 ± 5.9
	5.0	96.0 ± 8.4	94.0 ± 6.8	92.8 ± 6.4
	35.0	99.8 ± 3.3	97.0 ± 5.3	96.6 ± 5.5
Heart	0.5	98.2 ± 6.7	103.6 ± 6.5	92.8 ± 6.8
	5.0	94.8 ± 9.5	92.9 ± 4.2	102.5 ± 10.6
	50.0	100.3 ± 7.5	96.6 ± 6.7	96.7 ± 8.7
Liver	0.5	95.1 ± 3.1	92.6 ± 9.1	98.9 ± 7.9
	5.0	94.3 ± 6.7	96.6 ± 6.4	103.8 ± 8.2
	50.0	95.4 ± 8.6	100.9 ± 5.6	99.0 ± 5.0
Brain	0.5	92.3 ± 9.4	101.8 ± 6.8	92.8 ± 6.9
	5.0	98.4 ± 4.4	90.0 ± 9.5	92.2 ± 8.5
	50.0	103.5 ± 9.2	99.0 ± 5.3	95.2 ± 11.4
Lung	0.5	91.2 ± 5.4	97.6 ± 6.8	95.8 ± 9.8
	5.0	96.8 ± 8.3	89.8 ± 4.6	91.9 ± 9.3
	50.0	95.6 ± 5.9	91.6 ± 9.8	96.9 ± 7.5
Kidney	0.5	92.4 ± 4.3	91.1 ± 5.4	92.2 ± 7.5
	5.0	95.8 ± 5.6	94.3 ± 2.8	95.4 ± 8.9
	50.0	90.8 ± 3.7	96.8 ± 9.5	80.9 ± 6.7
GRg1				
Plasma	0.4	102.0 ± 5.7	92.0 ± 5.7	96.0 ± 3.9
	3.0	94.0 ± 5.9	86.0 ± 9.7	91.1 ± 8.2
	40.0	102.8 ± 9.6	104.6 ± 5.5	103.6 ± 7.0
Heart	0.4	97.8 ± 8.2	98.3 ± 4.4	91.3 ± 6.1
	3.0	96.3 ± 8.4	95.1 ± 5.2	90.8 ± 9.7
	40.0	92.5 ± 4.8	103.2 ± 6.4	102.3 ± 6.6
Liver	0.4	92.5 ± 7.2	95.6 ± 9.7	93.5 ± 8.9
	3.0	94.8 ± 6.4	92.8 ± 6.8	91.9 ± 2.4
	40.0	93.8 ± 8.4	94.7 ± 5.8	93.8 ± 3.8
Brain	0.4	97.5 ± 5.6	90.2 ± 8.3	95.6 ± 5.7
	3.0	93.7 ± 7.2	105.4 ± 8.7	90.9 ± 6.4
	40.0	90.6 ± 6.4	98.7 ± 7.8	98.3 ± 6.1
Lung	0.4	96.1 ± 4.9	90.5 ± 9.8	96.2 ± 4.5
	3.0	99.0 ± 7.9	92.4 ± 3.7	92.3 ± 4.8
	40.0	92.4 ± 9.2	98.9 ± 5.4	98.0 ± 6.7
Kidney	0.4	91.5 ± 6.5	90.8 ± 6.1	90.5 ± 7.8
	3.0	95.9 ± 4.5	91.6 ± 11.2	94.7 ± 3.7
	40.0	102.1 ± 5.7	95.7 ± 4.6	91.2 ± 10.6
GRg1				
Plasma	0.4	101.6 ± 9.2	96.0 ± 7.9	105.0 ± 5.8
	3.0	91.8 ± 7.8	86.0 ± 7.2	103.7 ± 8.5
	40.0	97.3 ± 9.5	104.6 ± 6.3	103.1 ± 7.9
Heart	0.4	98.4 ± 3.9	92.4 ± 5.5	91.9 ± 7.8
	3.0	102.5 ± 6.7	95.3 ± 4.2	95.5 ± 8.3
	40.0	92.8 ± 4.9	93.6 ± 6.8	97.8 ± 5.2
Liver	0.4	95.5 ± 6.1	95.9 ± 8.4	97.2 ± 5.7
	3.0	100.5 ± 3.7	92.4 ± 9.2	93.9 ± 6.5
	40.0	95.8 ± 6.3	96.1 ± 4.5	96.7 ± 7.9

Table 3: Continued.

Biosample	QC conc ($\mu g \cdot mL^{-1}$)	Remaining (mean ± S.D.) Short-term stability	Long-term stability	Freeze-thaw stability
Brain	0.4	92.2 ± 3.8	93.7 ± 6.4	90.5 ± 6.8
	3.0	96.7 ± 5.3	96.0 ± 3.5	92.9 ± 5.4
	40.0	93.8 ± 8.5	97.0 ± 6.8	95.4 ± 6.7
Lung	0.4	96.2 ± 3.9	92.4 ± 6.4	90.9 ± 5.9
	3.0	91.7 ± 5.8	93.5 ± 5.3	97.2 ± 5.8
	40.0	96.4 ± 7.3	97.7 ± 8.7	93.8 ± 7.3
Kidney	0.8	93.6 ± 5.7	96.3 ± 4.2	90.7 ± 3.4
	8.0	95.2 ± 4.2	98.3 ± 7.2	93.8 ± 12.2
	48.0	92.8 ± 3.8	92.9 ± 9.0	92.3 ± 5.8

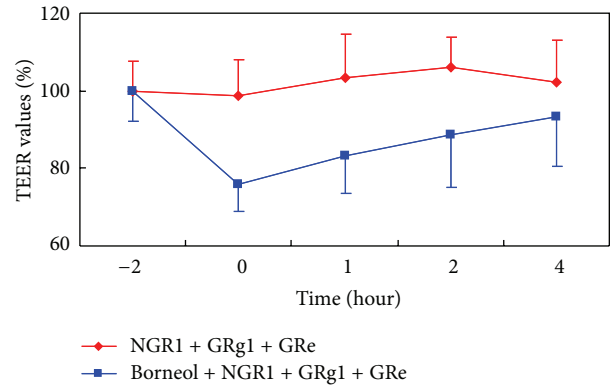

Figure 3: Effect of Borneol on TEER values of the Caco-2 cell monolayers. The Caco-2 cell monolayers were pretreated 2 h with 500 μM of NGR1, GRg1, and GRe, or the three saponins plus 200 μM Borneol. At time point 0, the monolayers were washed with buffered DMEM (pH 7.4), and then incubated at 37°C for 4 h.

have found that Borneol could obviously loosen the intercellular tight junction, increase the number and volume of pinocytosis vesicles [32, 33], promote the fluidity of membrane and the permeability of bilayer lipid membrane *in vitro* [34], and inhibit the function of P-gp on cell membrane [35]. In this experiment, we found that Borneol increased the P_{app} (apical-to-basolateral) and P_{app} (basolateral-to-apical) values of NGR1, GRg1 and GRe significantly, by 2.9-, 2.6-, and 2.3-fold and 2.9-, 2.6-, and 2.4-fold, respectively. Meanwhile, TEER values of the monolayers decreased reversibly to about 23% (Figure 3). These data imply that Borneol may open the paracellular spaces between cells and enhance permeability of NGR1, GRg1, and GRe. However, no significant changes in Er of NGR1, GRg1, and GRe were observed, indicating that the three saponins are not substrates of P-gp. We may therefore suppose that Borneol could loosen the intercellular tight junction and enhance permeability of NGR1, GRg1, and GRe, which is probably the main reason why Borneol enhances the bioavailability of NGR1, GRg1, and GRe.

Table 4: The statistical parameters of NGR1, GRg1, and GRe after administration of *Panax notoginseng* and *Panax notoginseng* combined with Borneol.

Parameters	*Panax notoginseng*			*Panax notoginseng* with Borneol		
	NGR1	GRg1	GRe	NGR1	GRg1	GRe
α (min^{-1})	0.018 ± 0.008	0.018 ± 0.005	0.020 ± 0.004	0.024 ± 0.005	0.031 ± 0.011	0.027 ± 0.008
β (min^{-1})	0.014 ± 0.003	0.010 ± 0.007	0.010 ± 0.002	0.010 ± 0.003*	0.010 ± 0.001	0.010 ± 0.001
$t_{1/2\alpha}$ (min)	38.5 ± 4.5	38.5 ± 2.5	35.0 ± 1.9	28.4 ± 3.2**	22.3 ± 3.1**	25.2 ± 2.4**
$t_{1/2\beta}$ (min)	47.9 ± 8.1	69.3 ± 12.0	69.3 ± 5.8	69.3 ± 5.2**	69.3 ± 10.7	69.3 ± 15.2
V/F ($L \cdot kg^{-1}$)	27.3 ± 8.6	24.5 ± 4.5	20.0 ± 4.7	58.8 ± 6.9**	35.9 ± 8.7*	31.1 ± 6.9*
CL/F ($L \cdot min^{-1} \cdot kg^{-1}$)	0.488 ± 0.091	0.123 ± 0.067	0.150 ± 0.030	0.506 ± 0.027	0.119 ± 0.040	0.143 ± 0.054
AUC_{0-t} ($mg \cdot L^{-1} \cdot min^{-1}$)	162.1 ± 42.7	494.8 ± 46.5	424.9 ± 79.6	306.3 ± 82.9**	545.1 ± 51.7	525.1 ± 101.3
$AUC_{0-\infty}$ ($mg \cdot L^{-1} \cdot min^{-1}$)	164.0 ± 51.8	651.9 ± 73.9	534.7 ± 123.8	395.3 ± 101.4**	1674.6 ± 148.2**	1400.6 ± 251.9**
K_{10} (min^{-1})	0.018 ± 0.005	0.005 ± 0.001	0.007 ± 0.003	0.009 ± 0.002*	0.003 ± 0.00	0.005 ± 0.001
K_{12} (min^{-1})	0.000 ± 0.000	0.011 ± 0.003	0.012 ± 0.004	0.015 ± 0.005**	0.025 ± 0.005**	0.022 ± 0.005**
K_{21} (min^{-1})	0.014 ± 0.007	0.012 ± 0.003	0.011 ± 0.005	0.011 ± 0.002	0.013 ± 0.001	0.011 ± 0.003
K_a (min^{-1})	0.060 ± 0.004	0.039 ± 0.004	0.025 ± 0.004	0.037 ± 0.005**	0.051 ± 0.010*	0.034 ± 0.003**
C_{max} ($mg \cdot L^{-1}$)	2.12 ± 0.46	2.36 ± 0.15	1.92 ± 0.22	1.62 ± 0.30	2.87 ± 0.34**	3.04 ± 0.24**
T_{max} (min)	45.0 ± 9.8	30.0 ± 5.2	45.0 ± 0.0	30.0 ± 8.0*	30.0 ± 0.0	45.0 ± 13.4
$t_{1/2Ka}$ (min)	11.6 ± 2.4	17.8 ± 2.4	27.7 ± 3.7	18.8 ± 3.1**	13.5 ± 4.6	20.3 ± 4.2**
T_{lag} (min)	2.38 ± 0.49	0 ± 0	0 ± 0	1.04 ± 0.21**	1.25 ± 0.34**	0.61 ± 0.47*

* $P < 0.05$, ** $P < 0.01$ compared with *Panax notoginseng*.

Table 5: Drug concentrations in rabbit tissues after administration of *Panax notoginseng* and *Panax notoginseng* combined with Borneol ($n = 6$).

Time (h)	Biosample	Concentration ($\mu g \cdot g^{-1}$)					
		Panax notoginseng			*Panax notoginseng* with Borneol		
		NGR1	GRg1	GRe	NGR1	GRg1	GRe
0.5	Heart	3.90 ± 0.53	2.21 ± 0.76	1.65 ± 0.53	4.68 ± 0.21**	22.65 ± 0.36**	2.81 ± 0.74**
	Liver	1.38 ± 0.54	8.48 ± 0.53	0.99 ± 0.33	8.24 ± 0.42**	50.10 ± 1.95**	3.60 ± 0.46**
	Brain	0.65 ± 0.24	0.75 ± 0.11	1.05 ± 0.42	4.02 ± 0.46**	20.57 ± 1.36**	1.80 ± 0.42*
	Lung	1.77 ± 0.46	14.30 ± 0.43	0.70 ± 0.41	5.79 ± 0.29**	15.09 ± 3.24**	2.48 ± 0.69**
	Kidney	2.85 ± 0.45	4.05 ± 0.26	1.63 ± 0.18	3.98 ± 0.12**	27.54 ± 0.17**	2.84 ± 0.53**
	Plasma ($\mu g \cdot mL^{-1}$)	1.67 ± 0.05	1.97 ± 0.16	1.78 ± 0.11	1.62 ± 0.07	2.87 ± 0.06**	2.68 ± 0.13**
1.0	Heart	4.26 ± 0.27	2.94 ± 0.24	2.11 ± 0.28	5.55 ± 0.31**	27.03 ± 0.31**	3.28 ± 0.43**
	Liver	1.66 ± 0.28	8.85 ± 0.51	1.30 ± 0.25	9.29 ± 0.72**	59.05 ± 3.74**	4.77 ± 0.42**
	Brain	0.81 ± 0.26	0.91 ± 0.89	1.21 ± 0.28	5.58 ± 0.68**	25.66 ± 2.69**	2.76 ± 0.63**
	Lung	1.82 ± 0.20	15.32 ± 0.64	0.92 ± 0.13	9.96 ± 0.66**	17.80 ± 1.25**	2.99 ± 0.17**
	Kidney	2.74 ± 0.33	3.67 ± 0.38	1.53 ± 0.22	3.38 ± 0.34**	16.93 ± 0.81**	2.43 ± 0.29**
	Plasma ($\mu g \cdot mL^{-1}$)	1.29 ± 0.20	1.99 ± 0.06	1.90 ± 0.15	1.46 ± 0.05	2.18 ± 0.09**	2.42 ± 0.08**
3.0	Heart	3.31 ± 0.32	1.53 ± 0.45	1.14 ± 0.13	4.59 ± 0.52**	19.07 ± 1.16**	2.24 ± 0.54**
	Liver	0.89 ± 0.12	6.18 ± 0.59	0.69 ± 0.11	6.87 ± 0.61**	37.78 ± 3.43**	2.63 ± 0.81**
	Brain	0.48 ± 0.14	0.57 ± 0.20	0.63 ± 0.12	3.69 ± 0.84**	17.86 ± 2.60**	1.65 ± 0.23**
	Lung	1.51 ± 0.16	11.87 ± 0.71	0.31 ± 0.44	4.56 ± 0.75**	12.31 ± 1.46	1.53 ± 0.45**
	Kidney	1.94 ± 0.24	3.03 ± 0.23	1.15 ± 0.13	2.27 ± 0.28	10.16 ± 2.77**	1.61 ± 0.45
	Plasma ($\mu g \cdot mL^{-1}$)	0.16 ± 0.06	0.98 ± 0.01	0.79 ± 0.02	0.49 ± 0.02	0.92 ± 0.01	0.87 ± 0.04

** $P < 0.01$ compared with *Panax notoginseng*.

4. Conclusion

In summary, the present study showed that after combined oral administration to rabbits with *Panax notoginseng,* Borneol significantly changed the pharmacokinetic parameters of NGR1, GRg1, and GRe, the main active compounds in *Panax notoginseng*. The possible mechanism was that Borneol could loosen the intercellular tight junction and enhance permeability of NGR1, GRg1, and GRe. Our results might help in guiding the clinic use of Borneol and other herbs in traditional Chinese medicine.

Table 6: Apparent permeability coefficients (P_{app}) of NGR1, GRg1, and GRe with or without the addition of 200 μM Borneol on the Caco-2 Model.

Compound	P_{app} (apical to basolateral) ($\times 10^{-7}$ cm/s)	P_{app} (basolateral to apical) ($\times 10^{-7}$ cm/s)	E_r
NGR1	0.64 ± 0.08	0.68 ± 0.12	1.06
GRg1	3.48 ± 0.42	3.64 ± 0.29	1.05
GRe	5.46 ± 0.40	5.73 ± 0.37	1.05
NGR1 + Borneol	1.87 ± 0.23**	1.95 ± 0.34**	1.04
GRg1 + Borneol	9.05 ± 0.67**	9.51 ± 0.62**	1.05
GRe + Borneol	12.67 ± 1.01**	13.65 ± 1.59**	1.08

* $P < 0.05$, ** $P < 0.01$ compared with corresponding single compound such as NGR1, GRg1, or GRe.

Conflict of Interests

There is no conflict of interests to declare.

Acknowledgments

This work was supported by grants from the National Natural Science Foundation of China (Major International (Regional) Joint Research Project; Key Program, no. 81120108002; General Program, nos. 30930105 and 81071765), Program for Changjiang Scholars and Innovative Research Team in University of China (IRT1174), the Eleventh Five-Year National Science and Technology Support Program of China (no. 2008BAI51B01), and Natural Science Foundation of Shaanxi Province (nos. 2010JM4047 and 2012JZ4001), and The Education Department of Shaanxi Province (nos. 09JS086 and 11JK0661).

References

[1] W. H. Park, S. K. Lee, and C. H. Kim, "A Korean herbal medicine, *Panax notoginseng*, prevents liver fibrosis and hepatic microvascular dysfunction in rats," *Life Sciences*, vol. 76, no. 15, pp. 1675–1690, 2005.

[2] S. K. Lam and T. B. Ng, "A xylanase from roots of sanchi ginseng (*Panax notoginseng*) with inhibitory effects on human immunodeficiency virus-1 reverse transcriptase," *Life Sciences*, vol. 70, no. 25, pp. 3049–3058, 2002.

[3] G. H. Lu, Q. Zhou, S. Q. Sun, K. S. Y. Leung, H. Zhang, and Z. Z. Zhao, "Differentiation of Asian ginseng, American ginseng and *Notoginseng* by Fourier transform infrared spectroscopy combined with two-dimensional correlation infrared spectroscopy," *Journal of Molecular Structure*, vol. 883-884, no. 1–3, pp. 91–98, 2008.

[4] Q. Du, G. Jerz, R. Waibel, and P. Winterhalter, "Isolation of dammarane saponins from *Panax notoginseng* by high-speed counter-current chromatography," *Journal of Chromatography A*, vol. 1008, no. 2, pp. 173–180, 2003.

[5] P. Zhao, Y. Q. Liu, and C. R. Yang, "Minor dammarane saponins from *Panax notoginseng*," *Phytochemistry*, vol. 41, no. 5, pp. 1419–1422, 1996.

[6] S. K. Lam and T. B. Ng, "Isolation of a novel thermolabile heterodimeric ribonuclease with antifungal and antiproliferative activities from roots of the sanchi ginseng *Panax notoginseng*," *Biochemical and Biophysical Research Communications*, vol. 285, no. 2, pp. 419–423, 2001.

[7] Y. Y. Guan, J. G. Zhou, Z. Zhang et al., "Ginsenoside-Rd from *Panax notoginseng* blocks Ca^{2+} influx through receptor- and store-operated $^{Ca2+}$ channels in vascular smooth muscle cells," *European Journal of Pharmacology*, vol. 548, no. 1–3, pp. 129–136, 2006.

[8] Q. Shi, Q. Hao, J. Bouissac, Y. Lu, S. Tian, and B. Luu, "Ginsenoside-Rd from *Panax notoginseng* enhances astrocyte differentiation from neural stem cells," *Life Sciences*, vol. 76, no. 9, pp. 983–995, 2005.

[9] L. Wu, W. Zhang, Y. H. Tang et al., "Effect of total saponins of "*Panax notoginseng* root" on aortic intimal hyperplasia and the expressions of cell cycle protein and extracellular matrix in rats," *Phytomedicine*, vol. 17, no. 3-4, pp. 233–240, 2010.

[10] X. D. Peng, L. L. Dai, C. Q. Huang, C. M. He, B. Yang, and L. J. Chen, "Relationship between anti-fibrotic effect of *Panax notoginseng* saponins and serum cytokines in rat hepatic fibrosis," *Biochemical and Biophysical Research Communications*, vol. 388, no. 1, pp. 31–34, 2009.

[11] Y. H. Li, X. L. Li, G. Hong, J. Y. Liu, and M. Y. Zhang, "Determination of panoxadiol and panoxatriol in *Panax notoginseng* and Yunnan White Powder by supercritical fluid chromatography," *Acta Pharmacologica Sinica*, vol. 26, pp. 764–767, 1991.

[12] M. Vanhaelen and R. Vanhaelen-Fastre, "Quantitative determination of biologically active constituents in crude extracts of medicinal plants by thin-layer chromatography-densitometry. II. Eleutherococcus senticosus Maxim., Panax ginseng Meyer and Picrorrhiza kurroa Royle," *Journal of Chromatography*, vol. 312, pp. 497–503, 1984.

[13] A. D. Lang, T. Y. Zhang, and A. L. Sekhavat, "GC/MS/DS analysis of fatty acid of *Panax notoginseng*," *Journal of Beijing Normal University*, vol. 32, pp. 257–259, 1996.

[14] Y. H. Wang, C. Y. Hong, C. F. Chen, and T. H. Tsai, "Determination of triacylglycerols in Panax pseudo-ginseng by HPLC polymeric column," *Journal of Liquid Chromatography and Related Technologies*, vol. 19, no. 15, pp. 2497–2503, 1996.

[15] M. Wang, Y. G. Fan, and W. F. Gao, "Quantitative determination of notoginsenoside R_1 and ginsenoside Rg_1, Rb_1 content in total notoginsenosides of *Panax notogineseng* and Xuesaitong Injection by HPLC gradient elution method," *Chinese Journal of Pharmaceutical Analysis*, vol. 20, pp. 410–413, 2000.

[16] Y. J. Wei, L. W. Qi, P. Li, H. W. Luo, L. Yi, and L. H. Sheng, "Improved quality control method for Fufang Danshen preparations through simultaneous determination of phenolic acids, saponins and diterpenoid quinones by HPLC coupled with diode array and evaporative light scattering detectors," *Journal of Pharmaceutical and Biomedical Analysis*, vol. 45, no. 5, pp. 775–784, 2007.

[17] J. B. Wan, F. Q. Yang, S. P. Li, Y. T. Wang, and X. M. Cui, "Chemical characteristics for different parts of *Panax notoginseng* using pressurized liquid extraction and HPLC-ELSD," *Journal of Pharmaceutical and Biomedical Analysis*, vol. 41, no. 5, pp. 1596–1601, 2006.

[18] G. C. Kite, E. A. Porter, and M. S. J. Simmonds, "Chromatographic behaviour of steroidal saponins studied by high-performance liquid chromatography-mass spectrometry," *Journal of Chromatography A*, vol. 1148, no. 2, pp. 177–183, 2007.

[19] L. Li, R. Tsao, J. Dou, F. Song, Z. Liu, and S. Liu, "Detection of saponins in extract of *Panax notoginseng* by liquid

chromatography-electrospray ionisation-mass spectrometry," *Analytica Chimica Acta*, vol. 536, no. 1-2, pp. 21–28, 2005.

[20] H. Zhang and Y. Cheng, "Solid-phase extraction and liquid chromatography-electrospray mass spectrometric analysis of saponins in a Chinese patent medicine of formulated *Salvia miltiorrhizae* and *Panax notoginseng*," *Journal of Pharmaceutical and Biomedical Analysis*, vol. 40, no. 2, pp. 429–432, 2006.

[21] L. Zhu and Y. J. Tian, "Chemical composition and larvicidal effects of essential oil of *Blumea martiniana* against *Anopheles anthropophagus*," *Asian Pacific Journal of Tropical Medicine*, vol. 4, no. 5, pp. 371–374, 2011.

[22] S. Rajkumar and A. Jebanesan, "Chemical composition and larvicidal activity of leaf essential oil from *Clausena dentata* (Willd) M. Roam. (Rutaceae) against the chikungunya vector, *Aedes aegypti* Linn. (Diptera: Culicidae)," *Journal of Asia-Pacific Entomology*, vol. 13, no. 2, pp. 107–109, 2010.

[23] P. J. Dunlop, C. M. Bignell, J. F. Jackson, and D. B. Hibbert, "Chemometric analysis of gas chromatographic data of oils from *Eucalyptus species*," *Chemometrics and Intelligent Laboratory Systems*, vol. 30, no. 1, pp. 59–67, 1995.

[24] Chinese Pharmacopeia Commission, *Pharmacopeia of the People's Republic of China*, vol. 1, China Medical Science Publisher, Beijing, China, 2010.

[25] S. S. Yang, K. R. Zhang, X. Lin et al., "Pharmacokinetic comparisons of single herb extract of Fufang Danshen preparation with different combinations of its constituent herbs in rats," *Journal of Pharmaceutical and Biomedical Analysis*, vol. 67-68, pp. 77–85, 2012.

[26] Q. F. Xu, X. L. Fang, and D. F. Chen, "Pharmacokinetics and bioavailability of ginsenoside Rb1 and Rg1 from *Panax notoginseng* in rats," *Journal of Ethnopharmacology*, vol. 84, no. 2-3, pp. 187–192, 2003.

[27] L. Li, J. L. Zhang, Y. X. Sheng, G. Ye, H. Z. Guo, and D. A. Guo, "Liquid chromatographic method for determination of four active saponins from *Panax notoginseng* in rat urine using solid-phase extraction," *Journal of Chromatography B*, vol. 808, no. 2, pp. 177–183, 2004.

[28] M. Song, S. Zhang, X. Xu, T. Hang, and L. Jia, "Simultaneous determination of three *Panax notoginseng* saponins at sub-nanograms by LC-MS/MS in dog plasma for pharmacokinetics of compound Danshen tablets," *Journal of Chromatography B*, vol. 878, no. 32, pp. 3331–3337, 2010.

[29] H. Liu, J. Yang, F. Du et al., "Absorption and disposition of ginsenosides after oral administration of *Panax notoginseng* extract to rats," *Drug Metabolism and Disposition*, vol. 37, no. 12, pp. 2290–2298, 2009.

[30] S. Yee, "*In vitro* permeability across Caco-2 cells (colonic) can predict *in vivo* (small intestinal) absorption in man—fact or myth," *Pharmaceutical Research*, vol. 14, no. 6, pp. 763–766, 1997.

[31] Z. Meng, H. Zhang, Y. Zhao, J. Lan, and L. Du, "Transport behavior and efflux of Rg1 in rat pulmonary epithelial cells," *Biomedical Chromatography*, vol. 21, no. 6, pp. 635–641, 2007.

[32] R. Liu, L. Zhang, X. Lan et al., "Protection by borneol on cortical neurons against oxygen-glucose deprivation/reperfusion: involvement of anti-oxidation and anti-inflammation through nuclear transcription factor κappaB signaling pathway," *Neuroscience*, vol. 176, pp. 408–419, 2011.

[33] Y. M. Chen and N. S. Wang, "Effect of borneol on the intercellular tight junction and pinocytosis vesicles *in vitro* blood-brain barrier model," *Chinese Journal of Integrated Traditional and Western Medicine*, vol. 24, no. 7, pp. 632–634, 2004.

[34] L. Li, Y. Yuan, and X. H. Jiang, "Absorption mechanism of liposoluble components of Salvia miltiorrhiza with Caco-2 cell model," *Chinese Pharmaceutical Journal*, vol. 41, no. 2, pp. 108–112, 2006.

[35] Y. M. Chen and N. S. Wang, "Effect of borneol on P-glycoprotein," *Traditional Chinese Drug Research & Clinical Pharmacology*, vol. 14, pp. 96–99, 2003.

Hindawi Publishing Corporation
Journal of Analytical Methods in Chemistry
Volume 2013, Article ID 439039, 7 pages
http://dx.doi.org/10.1155/2013/439039

Research Article

Rapid Screening of Drug-Protein Binding Using High-Performance Affinity Chromatography with Columns Containing Immobilized Human Serum Albumin

Ying-Fei Li,[1] Xiao-Qiong Zhang,[1,2] Wei-Yu Hu,[3] Zheng Li,[1] Ping-Xia Liu,[1,4] and Zhen-Qing Zhang[1]

[1] *Beijing Institute of Pharmacology and Toxicology, Beijing 100850, China*
[2] *Institute of Pharmacy, Medical School of Xiang Ya, Central South University, Changsha 410013, China*
[3] *Hepatobiliary Surgery Department, The Affiliated Hospital of Medical College, Qingdao University, Qingdao 266003, China*
[4] *Department of Pharmacy, Lushan Sanitarium of PLA, Jiujiang 332000, China*

Correspondence should be addressed to Zhen-Qing Zhang; zqzhang55@yahoo.com

Received 25 January 2013; Accepted 28 February 2013

Academic Editor: Shuang-Qing Zhang

For drug candidates, a plasma protein binding (PPB) more than 90% is more meaningful and deserves further investigation in development. In the study, a high-performance liquid chromatography method employing column containing immobilized human serum albumin (HSA) to screen in vitro PPB of leading compounds was established and successfully applied to tested compounds. Good correlation (a coefficient correlation of 0.96) was attained between the reciprocal values (X) of experimentally obtained retention time of reference compounds eluted through HSA column and the reported PPB values (Y) with a correlation equation of $Y = 92.03 - 97.01X$. The method was successfully applied to six test compounds, and the result was confirmed by the conventional ultrafiltration technique, and both yielded equal results. However, due to the particular protein immobilized to column, the method cannot be applied for all compounds and should be exploited judiciously based on the value of the logarithmic measure of the acid dissociation constant (pKa) as per the requirement. If α1-acid glycoprotein and other plasma proteins could be immobilized like HSA with their actual ratio in plasma to column simultaneously, the result attained using immobilized column may be more accurate, and the method could be applied to more compounds without pKa limitation.

1. Introduction

When entering into plasma, most compounds bind rapidly to blood constituents. While the phenomenon of plasma protein binding (PPB) of a chemical is considered, it usually means the protein binding of drug molecules to blood components, such as albumin and α1-acid glycoprotein [1]. The concentration of a free drug is primarily responsible for its pharmacological activity, safety, and tissue distribution. The extent of protein binding in plasma is, therefore, considered one of the important physiological factors affecting pharmacokinetic characteristics, such as clearance, volume of distribution, half-life, drug-drug interaction, and the pharmacological efficacy of a drug [2–6].

Conventionally, during the lead characterization stage, protein binding is investigated in rat, dog, monkey, and human plasma. these in vitro studies will help to characterize the therapeutic index for the selection of dose range in clinical trials. However, over the past decade, with the rapid rise in new molecular entities (NMEs) arising from computational lead discovery or modification of natural products, combinatorial chemistry, and high-throughput biological screening, an urgent need has arisen for the determination of the absorption, disposition, metabolism, and excretion properties of these NMEs or even "hit" at earlier stages in the drug discovery pipeline to speed up the selection of "ideal" drug candidates for further development. Back integration of key studies into the discovery phase enables earlier identification

of potential drug metabolites/pharmacokinetics and safety liabilities [7]. This information increases the effectiveness of discovery scientists in lead selection, optimization, and enhancement of discovery biology and in many instances has been incorporated into criteria for compound advancement into the development phase [8, 9]. As one of important pharmacokinetic parameters, PPB of lead compounds should be screened at earlier stage.

There are several in vitro methods for measuring the unbound drug concentration in plasma, including equilibrium dialysis, ultrafiltration, gel filtration, and albumin column [10]. Among them, equilibrium dialysis and ultrafiltration are the two most commonly used for determining the unbound drug concentrations in plasma or serum. However, given the need for earlier and more rapid evaluation of a larger number of lead compounds, it is necessary to establish a faster, higher-throughput, and less compound amount consuming approach to screen compound protein binding.

Compared with the conventional methods, chromatography-based methods employing columns immobilized with plasma proteins have been more and more popular over the years for the simplicity, specificity, and speed. Although plasma contains >60 different soluble proteins, among these, the major proteins that bind drug are albumin, the richest protein in plasma, and α1-acid glycoprotein. The work in the area of immobilized HSA chromatography was initiated from Noctor and Wainer [11]. Henceforth, various strategies used to investigate the drug-protein interactions for the development of columns immobilized with HSA, including frontal analysis (frontal affinity chromatography), zonal elution, equilibrium dialysis combined with high-performance liquid chromatography (HPLC), and micellar liquid chromatography, have been reported [12–19]. However, all methods could not estimate the PPB of compounds accurately due to compounds binding to other proteins of plasma, in this way the PPB of compounds was often underestimated. Hence, that underestimation, the PPB of compounds was usually attained.

Being a quick means of in vitro PPB estimation based on human serum albumin-HPLC (HSA-HPLC), the method especially suits rapid screening of PPB for numerous leading compounds in early drug discovery phase. The present investigation reports an HSA-based HPLC method for drug-protein binding rapid screening of UV active compounds. An application of the method to six test compounds, was made and the results confirmed by ultrafiltration have also been applied.

2. Experimental

2.1. Chemicals and Reagents. A set of commercially available reference compounds with a wide range of pKa was selected for this study. Caffeic acid, caffeine, catechuic acid, chlorphenamine maleate, chuanxiongzine hydrochloride, clomifene citrate, diazepam, diphenhydramine hydrochloride, ferulic acid, fluconazole, hydrocortisone acetate, nefopam hydrochloride, ranitidine hydrochloride, phenacetin, phenytoin sodium, praziquantel, propranolol hydrochloride, progesterone, reserpine, rutoside, salicylic acid, sulfadiazine, quercetin, sulfadimidine, sulfamethoxazole, testosterone propionate, tolbutamide, vanillic acid, and warfarin sodium with purity of more than 98.6% (except rutin (92.5%) and warfarin sodium (92.6%)) were all supplied by the National Institutes for Food and Drug Control (Beijing, China). Compounds A, B, C, D, E, and F (Figure 1), with purity of more than 99%, were test compounds which experienced nonclinical pharmacokinetics evaluation as a new drug in our lab. A, B, and D were semisynthetic natural compounds.

Sodium chloride of analytical grade was purchased from Beijing Chemical Works (Beijing, China). HPLC grade methanol (USA) and acetonitrile (Trinidad) were purchased from Fisher Scientific Inc., and the other chemicals used were all of analytical reagent grade. HPLC grade water was prepared with a Direct-Q 3 UV water purifying system (Millipore, Bedford, MA, USA).

All solutions were kept in the refrigerator at 4°C. The solutions were filtrated through 0.22 μm membrane (Millipore) before injection.

2.2. Instruments. The assay was performed on an Agilent 1100 series HPLC system (Agilent Technologies, Waldbronn, Germany) consisting of a quaternary pump, an autosampler, a vacuum degasser, and a UV absorbance detector set at 210 nm.

2.3. Chromatographic Methods for Drug-Protein Binding Screening Using Immobilized HSA Columns. Compounds were dissolved with water or water-ethanol (with different ratio) to a concentration of 100 μg/mL. The chromatographic peak was attained on a 5 μm Chiral-HSA, 50 × 3 mm column (Chrom Tech, France), which was preceded by an on-line filter. The ChemStation for LC 3D software was used for data acquiring and handling. As a generic rapid method, an isocratic mobile phase was selected. To simulate physiology environment, a mobile phase consisting of 0.9% NaCl (pH 7.0) at a flow rate of 0.5 mL/min was used. 10 μL aliquot of analyte solution was injected to HPLC to be analyzed.

2.4. PPB Experiment for Test Compounds by Ultrafiltration. The stock solution (1.0 or 2 mg/mL) of test compounds was prepared by dissolving appropriate amount of compounds in water-methanol (50 : 50, v/v) mixture. Working solution (1, 10 or 100 μg/mL) was attained by diluted stock solution with water. A different volume of the working solution was added to a 2 mL eppendorf vial and evaporated to dryness under a stream of nitrogen in the thermostatically controlled water bath maintained at 55°C for about 20 min. Drug-free plasma (0.5 mL) was then added to it and vortexed for 5 min to get the final concentration of 10, 40, 200, 100, 2000, and 100 ng/mL for compounds A, B, C, D, E, and F, respectively. The mixture was incubated at 37°C for 30 min. Thereafter, 400 μL aliquot of the sample was loaded into the preheated sample reservoir of Microcon YM-30 filter device (filter pore size 30 kDa) and centrifuged for 45 min at 5000 g and 37°C. The filtrate was analyzed for the drug content by HPLC-MS.

To estimate the nonspecific binding of the test drugs to the filter membrane, 500 μL of the solution of each compound

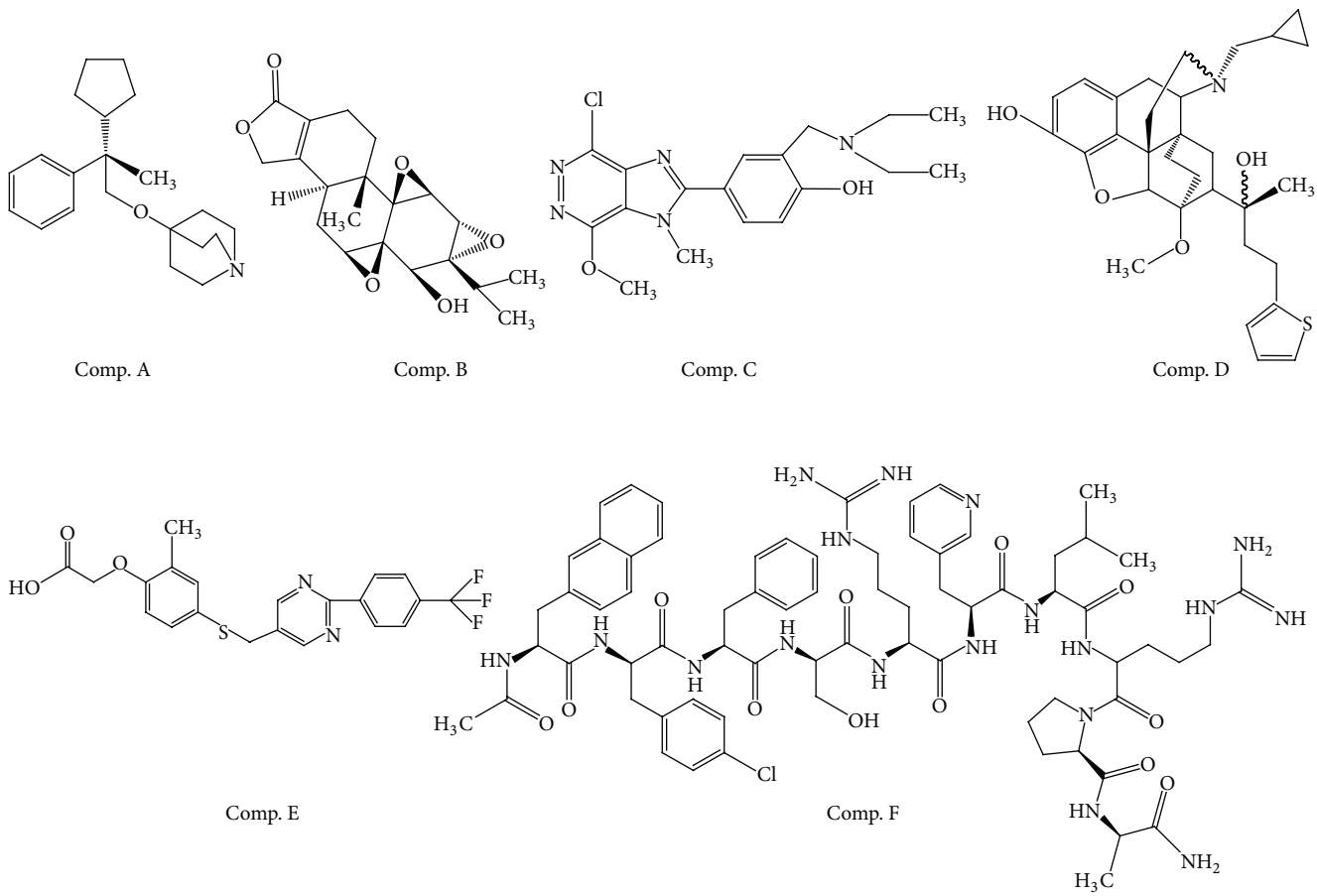

Figure 1: Chemical structures of six test compounds.

tested was centrifuged for 45 min at 5000 g in a Microcon YM-30 filter device. The concentration of the filtrate was analyzed by HPLC-MS. The nonspecific binding was <5% for each compound. The PPB by ultrafiltration was performed in triplicates for all the compounds studied.

2.5. pKa Calculation and Correlation Analysis. The pKa for all compounds except progesterone was calculated using ACD/labs 6.0. The pKa of progesterone was calculated by Pallas. Origin 6.0 was used to perform the plot and statistical analysis of the linear regressions.

3. Results and Discussion

Around 30 different compounds with PPB ranging from 11.5 to 98.0% were analyzed using immobilized HSA-HPLC. Most compounds with low PPB eluted at a lower retention time and exhibited sharp peak shapes as compared with the high protein bound compounds. Representative chromatograms are shown in Figure 2. There is one compound, clomifene citrate, that did not elute from HSA column to 240 min due to the strong binding. The related information about the reference compounds was listed in Table 1.

Every compound binds to all the plasma proteins to a certain extent. Hence that for the data of all reference compounds, there is no manifest relationship between retention time (RT) and reported PPB of compounds as showed in Figure 3. Because albumin generally binds acidic drugs better while α1-acid glycoprotein preferentially binds to basic drugs [1, 6], pKa less than 7.0 was used as a criterion for the drug binding to HSA mainly. However, for numerous leading compounds, it is difficult to know their actual pKa values. So the pKa values (Table 1) for drugs were predicted by ACD/Labs, one of the most accurate softwares to predict the pKa as reported [20]. Obviously, there is a hyperbola relationship for compounds with pKa less than 7.0 which mainly binds to HSA. A good linear correlation was attained between the reciprocal value of retention time and the reported PPB with a correlation equation of $Y = 92.03–97.01X$ and coefficient correlation of 0.96 using linear regression fit of Origin 6.0 (Figure 4).

Some understanding of the possible binding characteristics of candidate molecules could supply valuable information in the strategies of the design process, so the linear relationship established above was used to rapidly predict the protein binding. An interaction is likely, and a clinical study should be performed to quantify the effects if the drug of interest has

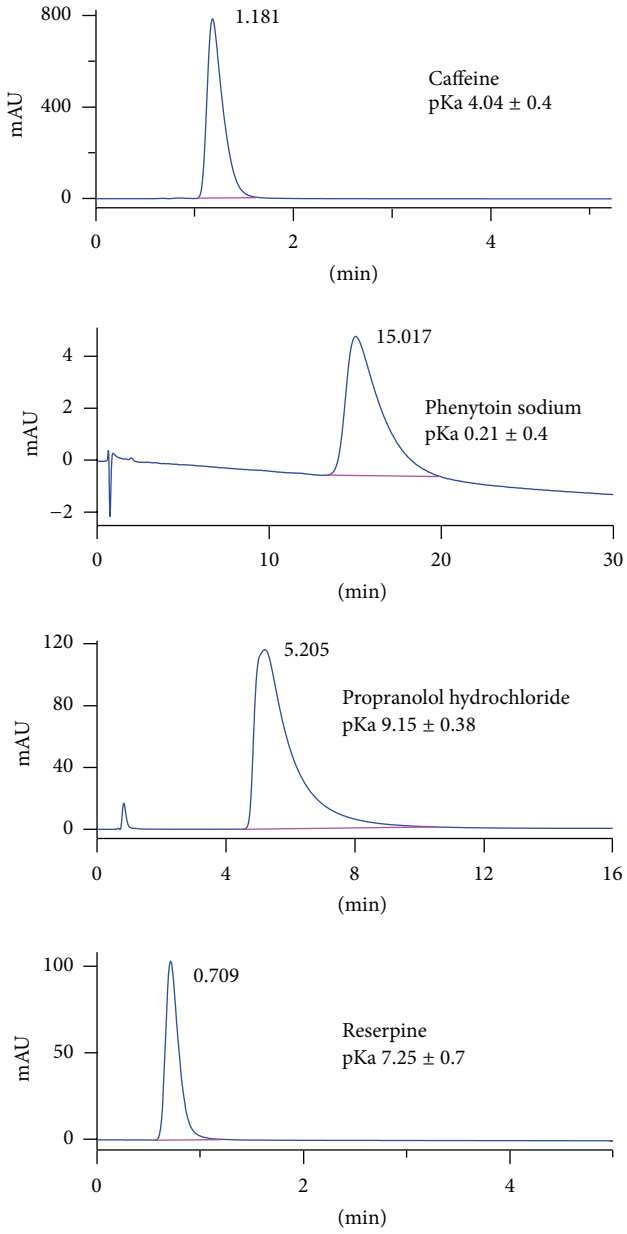

Figure 2: Representative chromatograms of some reference compounds analysed on HSA column.

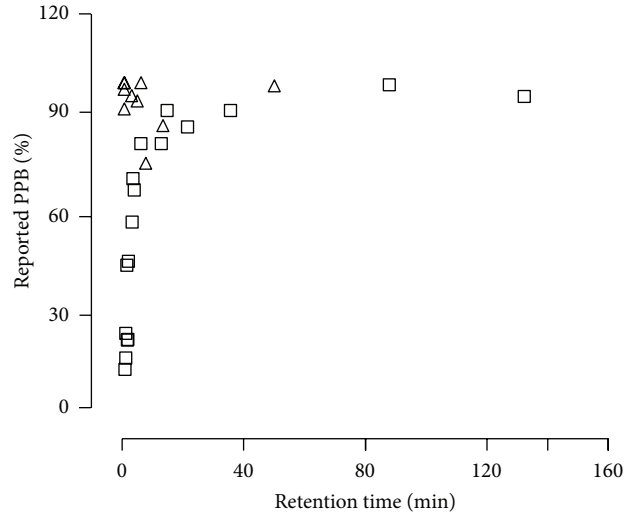

Figure 3: Scatter plot of retention time of reference compounds using immobilized HAS-HPLC and the corresponding reported PPB values. △: compounds with pKa < 7.0; □: compounds with pKa > 7.0.

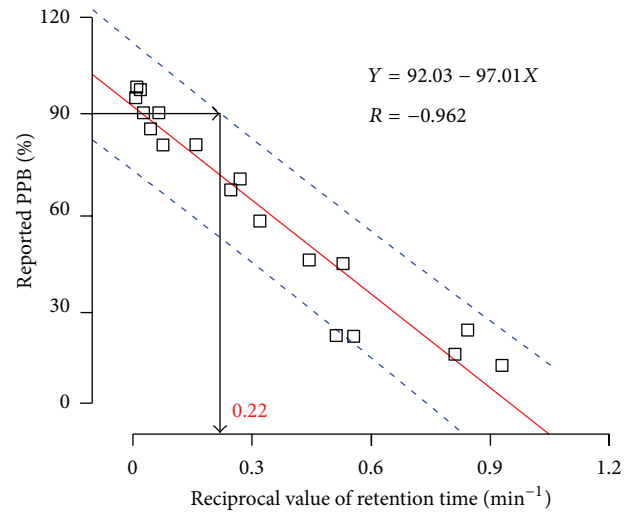

Figure 4: Correlation between reciprocal values of retention time of reference compounds (pKa < 7.0) by immobilized HAS-HPLC and the reported PPB values. The solid line was linear ship achieved by Origin 6.0 linear regression fit. The dash line represents 95% prediction limits.

a PPB above 90%, and narrow therapeutic index, high hepatic extraction ratio, and especially intravenous administration will increase the possibility [21]. For leading compounds, PPB of 90% is an appropriate index to decide whether the PPB of a drug needs to be investigated using the method of equilibrium dialysis or ultrafiltration in the following development phase.

Based on the upper prediction limit with 95% confidence interval, the reciprocal value of retention time for the compound in the HSA column should be less than 0.22 when its protein binding was more than 90% (Figure 4). This means that the retention time of the drug was more than 4.55 min in the HSA column if its PPB was more than 90%. Although the pKa of diphenhydramine hydrochloride, rutoside, nefopam hydrochloride, progesterone, and propranolol hydrochloride is 8.76, 13.85, 9.16, 15.00, and 9.15, respectively, far more than 7.0, the retention time of the drugs in the HSA column was 6.23, 13.43, 7.87, 50.02, and 5.21 min, respectively, later than 4.50 min. The reported PPB of diphenhydramine hydrochloride, progesterone, and propranolol hydrochloride is 98%, 97%, and 90–95%, respectively. And the value for rutoside and nefopam was 80–90% and 71–76% close to 90%. Therefore, the compounds with retention time in the HSA column later than 4.55 min were potentially more than 90% regardless of the pKa value and need the further investigation.

Table 1: The retention time, reported PPB, and predicted pKa of reference compounds.

Compound	Retention time (min)	PPB from literature (%)	pKa based on ACD/labs
Caffeic acid	4.02	66.0	4.04 ± 0.40
Caffeine	1.18	22.5	0.63 ± 0.70
Catechuic acid	1.94	20.7	4.45 ± 0.10
Chlorphenamine maleate	5.93	37.5 (25–50)	3.77 ± 0.19
Chuanxiongzine hydrochloride	2.23	44.3	2.88 ± 0.50
Diazepam	132.21	94.5 (90–99)	3.40 ± 0.10
Ferulic acid	1.79	20.6	4.04 ± 0.40
Fluconazole	1.07	11.5 (11-12)	2.56 ± 0.12
Ranitidine hydrochloride	1.23	15.0 (12–18)	2.38 ± 0.70
Phenytoin sodium	15.02	90.0	0.21 ± 0.40
Praziquantel	12.97	80.0	−0.79 ± 0.20
Salicylic acid	21.81	85.0 (80–90)	3.01 ± 0.10
Sulfadiazine	1.88	43.0 (38–48)	1.57 ± 0.10
Sulfadimidine	6.22	80.0	1.55 ± 0.10
Sulfamethoxazole	3.68	69.5 (69-70)	1.39 ± 0.10
Tolbutamide	35.82	90.0	5.12 ± 0.50
Vanillic acid	3.11	56.3	4.45 ± 0.10
Warfarin	87.85	98.0	4.50 ± 1.00
Bendroflumethiazide	3.27	94.0	8.63 ± 0.40
Diphenhydramine hydrochloride	6.23	98.0	8.76 ± 0.28
Hydrocortisone acetate	0.73	90.0	13.46 ± 0.70
Rutoside	13.43	85.0 (80–90)	13.85 ± 0.70
Nefopam hydrochloride	7.87	73.5 (71–76)	9.16 ± 0.70
Phenacetin	3.19	30.0	14.57 ± 0.70
Progesterone	50.02	97.0	19.28*
Propranolol hydrochloride	5.21	92.5 (90–95)	9.15 ± 0.38
Quercetin	0.72	98.0	8.14 ± 0.60
Reserpine	0.71	96.0	7.25 ± 0.70
Testosterone propionate	0.74	98.0	9.63 ± 0.65

*Calculated by software of Pallas.

Table 2: Retention time, predicted pKa, experimental PPB, and result by HSA-HPLC of test compounds

Compound	Retention time (min)	pKa based on ACD/labs	PPB by ultrafiltration (%)	Screening result by HSA-HPLC (%)
Comp. A	0.76	9.49 ± 0.12	78.2	—
Comp. B	1.70	14.24 ± 0.60	21.6	—
Comp. C	1.75	1.17 ± 0.50	51.0	<90
Comp. D	4.87	9.46 ± 0.60	95.0	>90
Comp. E	>5.00	3.17 ± 0.10	99.5	>90
Comp. F	0.81	15.06 ± 0.46	97.2	—

—: compound is not appropriate for the method of HSA-HPLC.

The PPB attained by ultrafiltration was 78.2 ± 1.67%, 21.6 ± 2.30%, 51.0 ± 2.52%, 94.86 ± 0.56%, 99.5 ± 0.24%, and 97.2 ± 0.60% for test compounds A, B, C, D, E, and F, respectively. The PPB of six compounds experienced nonclinical evaluation which was rapidly screened (Table 2) by the immobilized HSA-HPLC, and a confirmation with the result of the ultrafiltration was made. There were two compounds, D and E, with retention time more than 4.55 min which indicated that the PPB of these two compounds was more than 90%. The result of the ultrafiltration confirmed that the PPB was 95.0% and 99.5% for compounds D and E, respectively. For the left four compounds, only the pKa of compound C is less than 7.0 and the retention time of which is 1.75 min less than 4.55 min. So the PPB of compound C based on the HSA column was less than 90% and the PPB of compound C using ultrafiltration was 51.5%. The results were consistent with each other. However, the pKa of compounds A, F, and B was 9.49, 15.06, and 14.24, respectively, which is all

more than 7.0. Due to binding to other constitutes of blood, the PPB of these drugs couldnot be predicted based on the retention time attained using the method of the HSA column.

Every compound binds to all the plasma proteins to a certain extent. The percentage protein binding obtained by the ultrafiltration method measures all the specific and nonspecific binding to all of the plasma components. Although the HSA-HPLC method measures both the specific and nonspecific binding to one particular protein and cannot reflect the binding to the other plasma proteins, it is still a quick means of in vitro PPB screening for lead compounds. If α1-acid glycoprotein and other plasma proteins could be immobilized like HSA with their actual ratio in plasma to column simultaneously, the result attained using immobilized column may be more accurate, and the method could be applied to more compounds without pKa limitation. A further validation of the method is under way.

4. Conclusions

In accordance with the result of ultrafiltration, the HSA-HPLC method described in the present investigation could be applied in rapid screening lead compounds within 5 min in early drug discovery programs. It can be concluded that HSA-HPLC is suitable for the compounds that are designed to specifically or to some extent bind to HSA. The current commercial available HSA columns can be used in drug-protein binding screening while AGP columns are not as appropriate for such work. Further, using more analysis capacity HPLC-MS technique instead of HPLC, higher throughput for such studies will be acquired.

Authors' Contribution

Y.-F. Li and X.-Q. Zhang contributed equally in this work.

Acknowledgment

The authors thank the financial support from the National Natural Science Foundation of China (Grant no. 81202578) for this work.

References

[1] Y. Kwon, *Handbook of Essential Pharmacokinetics, Pharmacodynamics, and Drug Metabolism For Industrial Scientists*, Kluwer Academic/Plenum Publishers, New York, NY, USA, 2001.

[2] S. L. Rodgers, A. M. Davis, N. P. Tomkinson, and H. Van De Waterbeemd, "QSAR modeling using automatically updating correction libraries: application to a human plasma protein binding model," *Journal of Chemical Information and Modeling*, vol. 47, no. 6, pp. 2401–2407, 2007.

[3] H. van de Waterbeemd, "Which in vitro screens guide the prediction of oral absorption and volume of distribution?" *Basic and Clinical Pharmacology and Toxicology*, vol. 96, no. 3, pp. 162–166, 2005.

[4] H. van de Waterbeemd, "High-throughput and in silico techniques in drug metabolism and pharmacokinetics," *Current Opinion in Drug Discovery & Development*, vol. 5, no. 1, pp. 33–43, 2002.

[5] P. R. Chaturvedi, C. J. Decker, and A. Odinecs, "Prediction of pharmacokinetic properties using experimental approaches during early drug discovery," *Current Opinion in Chemical Biology*, vol. 5, no. 4, pp. 452–463, 2001.

[6] C. Han, C. B. Davis, and B. Wang, *Evaluation of Drug Candidates for Preclinical Development: Pharmacokinetics, Metabolism, Pharmaceutics, and Toxicology*, John Wiley & Sons, Hoboken, NJ, USA, 2010.

[7] E. H. Kerns and L. Di, *Drug-Like Properties: Concepts, Structure Design and Methods: From ADME to Toxicity Optimization*, Academic Press, Amsterdam , The Netherlands, 2008.

[8] A. F. Nassar, P. F. Hollenberg, and J. Scatina, *Drug Metabolism Handbook: Concepts and Applications*, Wiley, Hoboken, NJ, USA, 2009.

[9] R. T. Borchardt, *Optimizing the, "Drug-Like" Properties of Leads in Drug Discovery*, Springer, New York, NY, USA, 2006.

[10] J. Oravcova, B. Bohs, and W. Lindner, "Drug-protein binding studies new trends in analytical and experimental methodology," *Journal of Chromatography B*, vol. 677, no. 1, pp. 1–28, 1996.

[11] T. A. Noctor and I. W. Wainer, "The in situ acetylation of an immobilized human serum albumin chiral stationary phase for high-performance liquid chromatography in the examination of drug-protein binding phenomena," *Pharmaceutical Research*, vol. 9, no. 4, pp. 480–484, 1992.

[12] P. R. Tiller, I. M. Mutton, S. J. Lane, and C. D. Bevan, "Immobilized human serum albumin: liquid chromatography/mass spectrometry as a method of determining drug-protein binding," *Rapid Communications in Mass Spectrometry*, vol. 9, no. 4, pp. 261–263, 1995.

[13] Y. C. Guillaume, E. Peyrin, and A. Berthelot, "Chromatographic study of magnesium and calcium binding to immobilized human serum albumin," *Journal of Chromatography B*, vol. 728, no. 2, pp. 167–174, 1999.

[14] M. C. Millot, S. Servagent-Noinville, N. L. Taleb, M. H. Baron, M. Revault, and B. Sébille, "Structural changes of human serum albumin immobilized on chromatographic supports: a high-performance liquid chromatography and Fourier-transform infrared spectroscopy study," *Journal of Chromatography B*, vol. 753, no. 1, pp. 101–113, 2001.

[15] Y. Cheng, E. Ho, B. Subramanyam, and J. L. Tseng, "Measurements of drug-protein binding by using immobilized human serum albumin liquid chromatography-mass spectrometry," *Journal of Chromatography B*, vol. 809, no. 1, pp. 67–73, 2004.

[16] R. Mallik, M. J. Yoo, C. J. Briscoe, and D. S. Hage, "Analysis of drug-protein binding by ultrafast affinity chromatography using immobilized human serum albumin," *Journal of Chromatography A*, vol. 1217, no. 17, pp. 2796–2803, 2010.

[17] R. Matsuda, J. Anguizola, K. S. Joseph, and D. S. Hage, "Analysis of drug interactions with modified proteins by high-performance affinity chromatography: binding of glibenclamide to normal and glycated human serum albumin," *Journal of Chromatography A*, vol. 1265, pp. 114–122, 2012.

[18] Z. Tong, K. S. Joseph, and S. D. Hage, "Detection of heterogeneous drug-protein binding by frontal analysis and high-performance affinity chromatography ," *Journal of Chromatography A*, vol. 1218, no. 49, pp. 8915–8924, 2011.

[19] R. Matsuda, J. Anguizola, K. S. Joseph, and D. S. Hage, "High-performance affinity chromatography and the analysis of drug interactions with modified proteins: binding of gliclazide with

glycated human serum albumin ," *Analytical and Bioanalytical Chemistry*, vol. 401, no. 9, pp. 2811–2819, 2011.

[20] Z. Tong, J. E. Schiel, E. Papastavros, C. M. Ohnmacht, Q. R. Smith, and D. S. Hage, "Kinetic studies of drug-protein interactions by using peak profiling and high-performance affinity chromatography: examination of multi-site interactions of drugs with human serum albumin columns," *Journal of Chromatography A*, vol. 1218, no. 15, pp. 2065–2071, 2011.

[21] C. Bertucci, V. Andrisano, R. Gotti, and V. Cavrini, "Use of an immobilised human serum albumin HPLC column as a probe of drug-protein interactions: the reversible binding of valproate," *Journal of Chromatography B*, vol. 768, no. 1, pp. 147–155, 2002.

Hindawi Publishing Corporation
Journal of Analytical Methods in Chemistry
Volume 2013, Article ID 380705, 6 pages
http://dx.doi.org/10.1155/2013/380705

Research Article

Headspace Single-Drop Microextraction Gas Chromatography Mass Spectrometry for the Analysis of Volatile Compounds from Herba Asari

Guan-Jie Wang,[1] Li Tian,[1] Yu-Ming Fan,[1] and Mei-Ling Qi[2]

[1] *National Institutes for Food and Drug Control, No. 2, Tiantan Xili, Beijing 100050, China*
[2] *Beijing Institute of Technology, No. 5, Zhongguancun South Street, Haidian District, Beijing 100081, China*

Correspondence should be addressed to Yu-Ming Fan; fanyuming@nifdc.org.cn and Mei-Ling Qi; mlqi@bit.edu.cn

Received 7 January 2013; Revised 18 February 2013; Accepted 5 March 2013

Academic Editor: Shuang-Qing Zhang

A rapid headspace single-drop microextraction gas chromatography mass spectrometry (SDME-GC-MS) for the analysis of the volatile compounds in Herba Asari was developed in this study. The extraction solvent, extraction temperature and time, sample amount, and particle size were optimized. A mixed solvent of n-tridecane and butyl acetate (1 : 1) was finally used for the extraction with sample amount of 0.750 g and 100-mesh particle size at 70°C for 15 min. Under the determined conditions, the pound samples of Herba Asari were directly applied for the analysis. The result showed that SDME-GC–MS method was a simple, effective, and inexpensive way to measure the volatile compounds in Herba Asari and could be used for the analysis of volatile compounds in Chinese medicine.

1. Introduction

Single-drop micro-extraction (SDME), a new sample preparation technique introduced by Jeannot and Cantwell [1], has attracted increasing attentions. In this straightforward technique, a microdrop of solvent is suspended at the tip of a conventional microsyringe and then exposed in the sample headspace. Since only the volatile or semivolatile compounds can be volatilized into headspace and extracted to a single drop, interferences from the complex matrix will be decreased greatly. Other advantages of this method are the small amount of organic solvent required and the simple experimental and sampling equipment, while extraction, concentration, and sample introduction are integrated into a single step [2]. Several papers have been published using this sample preparation approach for the determination of environmental specimen [3–8], food [9, 10], biological products [11–14], engine oil samples [15], and pesticide residue [10, 16]. In SDME process, it is very important to use a suitable extraction solvent to achieve a good selectivity for the analytes, especially for complicated samples. In the above-mentioned papers, only one extraction solvent for several substances was employed [3–16], but there is little reported for complex extraction solvent. In our previous investigations, a single extraction solvent was successfully used to analyze traditional Chinese medicine (TCM) [17, 18]. However, these methods based on a single extraction still had the following drawbacks that amount and categories of extracted compounds almost depended on the polarity of the single extraction solvent.

To overcome the shortcomings of single solvent extraction in the present study, mixed solvent extraction based on SDME was developed for analysis of volatile components in TCM, Herba Asari. Herba Asari was used to dispel wind heat, headache, toothache, snuffling, and rheumatism [19]. The method precision and the parameters of SDME were studied.

2. Experimental

2.1. Reagents and Materials. The extraction solvents (benzyl alcohol, n-tridecane, n-tetradecane, 1,4-butanediol, butyl acetate, n-dodecane, methylbenzene, 1-octanol, decane, decanol, isobutyl alcohol, and n-tridecane) were purchased from our Chem Company (of GC grade or minimum purity

of 99%) and used without any further purification. One-microliter SGE microsyringe and water bath were purchased for the SDME procedure. A manual SPME holder and 100 μm PDMS fibers from Supelco (Bellefonte, PA, USA) were used for the SPME procedure. Fibers were conditioned prior to use according to the supplier's instructions.

The dry root samples of Herba Asari were purchased from An'guo traditional Chinese medicine market in Hebei province of China and were authenticated by the Institute of Medicinal Plants, Academy of Medical Science of China. The samples were dried in air, cut, milled, and then sieved via 40, 60, 80, 100, and 120 mesh, respectively, to obtain different particle size samples. Finally, the pound samples were stored in tightly sealed weighing bottles until analysis.

2.2. GC-MS Conditions. Chromatographic separation was performed on an Agilent 6890 GC (USA) with a PEG-20W Innowax (Agilent) capillary column (30 m × 0.25 mm × 0.25 μm). The oven temperature program was 7.0 min at 50°C 20°C/min to 130°C (keeping 130°C for 1 min), 1°C/min to 150°C, and 8°C/min to 190°C (keeping 190°C for 5 min). The injector and detector temperatures were 230°C and 260°C, respectively. Nitrogen of high purity was used as the carrier gas at a flow rate of 1.0 mL/min. The split ratio was 1 : 100. The mass spectrometer was fitted with an EI source operated at 70 eV, and mass spectra were recorded in the range of *m/z* 50 to 450 amu in the full-scan acquisition mode. The interface temperature and the ion source temperature were fixed at 240°C and 230°C, respectively. Volatile compounds were identified by comparing the obtained mass spectra of the analytes with those of authentic standards from the NIST and Hist 98 libraries with a resemblance percentage above 85%.

2.3. SDME Procedure. A 15 mL vial (Supclo, USA) with PTFE septum containing the powdered sample was placed at a fixed position in a water bath. Then a 1 μL GC micro-syringe was pierced into the headspace of the vial, which was clamped at a fixed position for improving precision of the method. The microsyringe was washed at least 20 times by extraction solvent between runs. After a preset extraction time, the extraction solvent was retracted into the needle and swiftly injected onto GC-MS for the analysis.

SDME parameters including the type of the extracting solvent, extraction temperature and time, headspace volume (sample amount), solvent volume, and particle size of the pound sample were investigated.

3. Results and Discussion

3.1. Selection of SDME Conditions. Selecting a proper extraction solvent is especially crucial for the analysis of volatile compounds of TCMs because of the great differences of the compounds in polarity and volatility. Mass transfer of the analytes from the pound sample to the microdrop continues until thermodynamic equilibrium is attained or the extraction is stopped according to the considerations of SDME. The principle "like dissolves like" can become the basis of the solvent selection. Different solvents were tested to find a suitable one that meets such requirements as high extraction efficiency in terms of the compounds and yields especially those of low volatility, less toxicity, and satisfactory chromatographic resolution for the analytes. Low volatility is helpful to keep the solvent micro-drop at the tip of the micro-syringe needle sustainable over the extraction time period. If possible, the front/end solvent peak is preferred to avoid the solvent problem with GC-MS. The decane, n-tridecane, n-tetradecane, butyl acetate, methylbenzene, 1-octanol benzyl alcohol, decanol, and isobutyl alcohol were selected and benzyl alcohol offered a better extraction. Then a mixture of two solvents was selected and after a detailed comparison of the peak areas of the seven main compounds (shown in Figure 1), n-tridecane mixed with butyl acetate was found to be the optimal combination and was finally adopted as the extraction solvent.

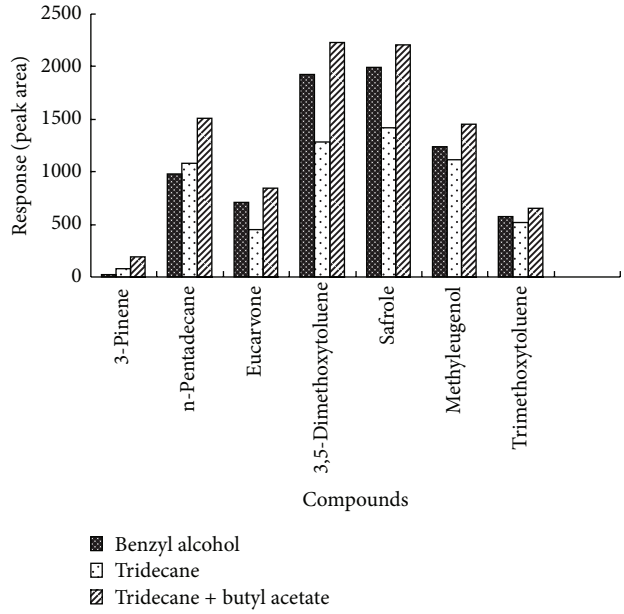

Figure 1: Comparison among different extraction solvents on the relative peak area of the seven main compounds from Herba Asari. Powdered sample, 0.500 g; extraction solvent volume, 0.6 μL; particle size, 100 mesh; extraction time, 20 min, extraction temperature, 70°C; the percent between two mixed solvent, 1 : 1 (volume).

3.2. Percent of Mixed Extraction Solvent. Selecting a proper percent of mixed extraction solvent is also important for the analysis of volatile compounds. The volume scale of the mixed solvent of n-tridecane and butyl acetate was investigated in the ranges of 1 : 0, 3 : 1, 1 : 1, 1 : 3, and 0 : 1, while keeping the other parameters under the following conditions: powdered sample, 0.500 g; extraction solvent volume, 0.6 μL; particle size, 100 mesh; extraction time, 20 min; extraction temperature, 70°C. The results showed that the peak area ratios of analytes of interest to benzyl alcohol (internal standard 0.2%) rapidly increased with the elevated percent of n-tridecane from 0 to 50 but decreased slowly after 50% n-tridecane. As a result, 50% was chosen as the extraction percent for the analysis (show in Figure 2).

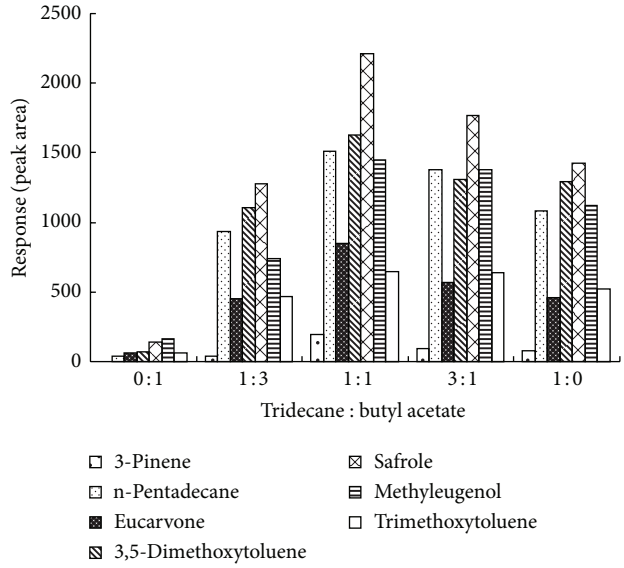

Figure 2: Comparison among different scales of n-tridecane in the extracting solvent on the relative peak area of the seven main compounds from Herba Asari. Powdered sample, 0.500 g; extraction solvent volume, 0.6 μL; particle size, 100 mesh; extraction time, 20 min, extraction temperature, 70°C; the percent between two mixed solvent, 1 : 1 (volume).

The solvent volume was investigated by setting the volume of the solvent at the volume of the solvent in the range of 0.30 to 0.90 μL. It can be known that the amount of the extracted analytes in the solvent drop increased with the solvent volume. However, the results also showed that when the volume exceeded 0.60 μL, the chromatographic peak of the solvent broadened and even overlapped the peaks of analytes of interest. In light of this, the solvent volume of 0.60 μL was finally used in the present study.

3.3. Extraction Time. The extraction time was determined by varying the exposure time of the microdrop in the headspace of a sample from 5 to 25 min while keeping the other parameters under the same conditions as Section 3.2. The peak areas of the seven main chosen compounds to the peak areas of benzyl alcohol were different from 5 to 25 min, but their sum peak areas were the largest at 15 min. So the extraction time of 15 min was chosen for the present work.

3.4. Extraction Temperature. The extraction efficiency of SDME procedure was temperature dependent. The effect of sample temperature on the extraction efficiency was investigated in the range of 50–90°C while keeping the other parameters under the same conditions as Section 3.3. The results showed that the peak areas of the seven main compounds in Herba Asari and their sum peak areas to benzyl alcohol (internal standard 0.2%) increased significantly with the temperature from 50°C to 70°C but deceased dramatically after 70°C. As a result, 70°C was chosen as the extraction temperature for the analysis.

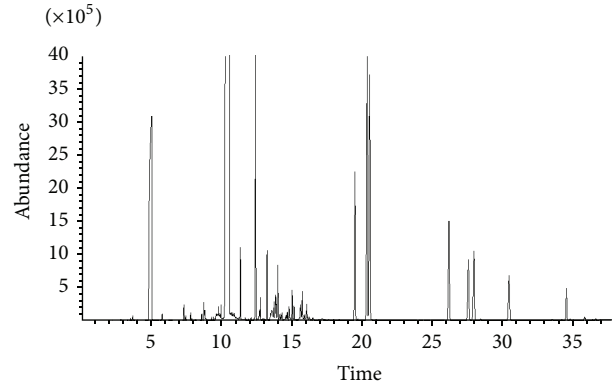

Figure 3: Typical chromatograms of volatile components from Herba Asari by SDME-GC-MS.

3.5. Particle Size of Sample. For a solid sample, particle size plays an important part in the extraction. Particle size of the sample was tested from 40 to 120 mesh at 70°C for 15 min with powdered sample 0.500 g. The results showed that the amount of volatile compounds increased with the decrease of particle size from 40 to 100 mesh but deceased after 100 mesh. As a result, 100 mesh was chosen as the optimal extraction particle size of the sample.

3.6. Sample Amount. Sample amount was determined by varying the amount of the powdered sample in a 15 mL vial. Increasing sample amount led to an increase of the analytes concentrations in the headspace which chanced the extracted amount of the analytes in the drop and a decrease of headspace volume. The extracted amount of the analytes increased continuously with the sample amount from 0.25 to 0.75 g and then decreased at 1.25 g. This observation could be explained by the fact that the powdered sample matrix could not be stirred during the process; consequently, with the increase of the sample amount, both the convection in the matrix and the mass transfer became slow. So 0.75 g was chosen as the optimal sample amount.

3.7. Repeatability. Under the determined conditions, the repeatability of the SDME method was determined by performing six replicate experiments. Relative standard deviations (RSD) of the seven main peak areas of the analytes of interest to the internal standard were 2.3% for 3-Pinene, 8.7% for eucarvone, 7.5% for 3,5-dimethoxytoluene, 9.2% for n-pentadecane, 9.8% for safrole, and 9.0% for methyleugenol. The RSD values for the seven compounds were all below 9.8%, indicating a satisfactory repeatability of the SDME method compared with the above-mentioned papers 10.8% [17].

3.8. SDME-GC-MS Results. The typical total ion chromatograms of SDME-GC-MS methods are shown in Figure 3 and the corresponding volatile compounds identified are listed in Table 1. The retention index of every compound was calculated under the same temperature process. The number of the volatile compounds identified was 61 for SDME-GC-MS. In general, SDME-GC-MS can be used as a good method

Table 1: Components of Herba Asari obtained by SDME-GC-MS.

No	Retention time (min)	Compounds	RI	SDME- (mixed-) GC-MS RA%
1	3.60	Acetic acid, 2-methylpropyl ester	1047	0.07
2	3.76	1R-.alpha.-Pinene	1052	0.21
3	5.85	beta.-Pinene	1099	0.34
4	7.40	3-Carene	1158	0.83
5	7.88	.alpha.-Phellandrene	1172	0.28
6	7.94	beta.-Phellandrene	1174	0.01
7	8.65	D-Limonene	1192	0.21
8	8.88	Eucalyptol	1193	0.55
9	9.36	1,3,6-Octatriene, 3,7-dimethyl-, (E)-	1230	0.08
10	9.50	1,4-Cyclohexadiene, 1-methyl-4-(1-methylethyl)-	1240	0.10
11	9.61	1,3,6-Octatriene, 3,7-dimethyl-, (Z)-	1248	0.08
12	9.67	Nonane, 3-methyl-	1253	0.32
13	9.73	Tridecane, 7-methyl-	1257	0.51
14	9.85	Tridecane, 7-methyl-	1265	0.86
15	9.96	Benzene, 1-methyl-2-(1-methylethyl)-	1272	0.31
16	10.03	Cyclohexene, 1-methyl-4-(1-methylethylidene)-	1277	0.45
17	10.86	Cyclohexene, 1-methyl-4-(1-methylethylidene)-	1598	0.21
18	11.40	Tetradecane	1397	2.23
19	11.74	Benzene, 1-methyl-4-(1-methylethenmethylethyl)-	1428	0.08
20	12.16	1,3-Cyclohexadiene, 1-methyl-4-(1-methylethyl)-	1467	0.08
21	12.49	Pentadecane	1496	12.80
22	12.74	1-Hexadecanol	1516	0.20
23	12.77	Bicyclo[2.2.1]heptan-2-one, 1,7,7-trimethyl-, (1R)-	1518	0.34
24	12.82	Cyclopentadecane	1522	0.65
25	13.29	Eucarvone	1556	2.33
26	13.55	Aristolene	1574	0.43
27	13.63	1,6,10-Dodecatriene, 7,11-dimethyl-3-methylene-, (Z)-	1580	0.75
28	13.68	4,7-Methanoazulene,1,2,3,4,5,6,7,8-octahydro-1,4,9,9-tetramethyl-,[1S-(1.alpha.,4.alpha.,7.alpha.)]-	1584	0.31
29	13.80	Azulene,1,2,3,4,5,6,7,8-octahydro-1,4-dimethyl-7-(1-methylethenyl)-,[1S-(1.alpha.,4.alpha.,7.alpha.)]-	1592	1.07
30	13.90	1H-Cyclopropa[a]naphthalene,1a,2,3,5,6,7,7a,7b-octahydro-1,1,7,7a-tetramethyl-,[1aR-(1a.alpha.,7.alpha.,7a.alpha.,7b.alpha.)]-	1599	1.26
31	13.94	3-Cyclohexen-1-ol,4-methyl-1-(1-methylethyl)-, (R)-	1601	0.66
32	14.06	2H-2,4a-Methanonaphthalene,1,3,4,5,6,7-hexahydro-1,1,5,5-tetramethyl-, (2S)-	1608	0.32
33	14.20	1H-Cyclopenta[1, 3]cyclopropa[1, 2]benzene,octahydro-7-methyl-3-methylene-4-(1-methylethyl)-,[3aS-(3a.alpha.,3b.beta.,4.beta.,7.alpha.,7 aS*)]-	1616	0.27
34	14.29	Benzene, 1,3,5-tris(1-methylethyl)	1620	0.27
35	14.37	Thujopsene	1625	0.39
36	14.60	Benzoic acid, 2,4-bis[(trimethylsilyl) oxy]-, trimethylsilyl ester	1637	0.07
37	14.65	1H-3a,7-Methanoazulene,2,3,6,7,8,8a-hexahydro-1,4,9,9-tetramethyl-, (1.alpha.,3a.alpha.,7.alpha.,8a.beta.)-	1640	0.23
38	14.74	Androsta-1,4-dien-3-one,17-hydroxy-17-methyl-, (17.alpha.)-	1644	0.41
39	14.86	Cyclohexane, 1,4-bis(methylene)-	1651	0.83

Table 1: Continued.

No	Retention time (min)	Compounds	RI	SDME- (mixed-) GC-MS RA%
40	14.98	1,6,10-Dodecatriene,7,11-dimethyl-3-methylene-, (Z)-	1657	0.05
41	15.08	Estragole	1662	1.40
42	15.22	Naphthalene,1,2,3,5,6,8a-hexahydro-4,7-dimethyl-1-(1-methylethyl)-, (1S-cis)-	1669	0.65
43	15.60	Heptadecane	1688	0.15
44	15.67	1H-3a,7-Methanoazulene,octahydro-3,8,8-trimethyl-6-methylene-,[3R-(3.alpha.,3a.beta.,7.beta.,8a.alpha.)]-	1692	1.11
45	15.69	3-Cyclohexene-1-methanol,.alpha.,.alpha.4-trimethyl-	1693	0.21
46	15.80	Borneol	1698	1.41
47	15.98	Azulene,1,2,3,3a,4,5,6,7-octahydro-1,4-dimethyl-7-(1-methylethenyl)-,[1R-(1.alpha.,3a.beta.,4.alpha.,7.beta.)]-	1706	0.31
48	16.11	Azulene,1,2,3,5,6,7,8,8a-octahydro-1,4-dimethyl-7-(1-methylethenyl)-,[1S-(1.alpha.,7.alpha.,8a.beta)]-.	1711	0.84
49	16.30	cis-.alpha.-Bisabolene	1719	0.17
50	16.55	1H-Cyclopropa[a]naphthalene,1a,2,3,5,6,7,7a,7b-octahydro-1,1,7,7a-tetramethyl-,[1aR-(1a.alpha.,7.alpha.,7a.alpha.,7b.alpha.)]-	1729	0.18
51	19.54	3,5-Dimethoxytoluene	1845	10.50
52	20.41	Safrole	1878	20.39
53	26.21	Benzene, 1,2-dimethoxy-4-(2-propenyl)-	2070	9.94
54	27.59	Methyleugenol	2110	6.29
55	27.99	Benzene, 1,2,3-trimethoxy-5-methyl	2121	7.33
56	30.48	1,3-Benzodioxole,4-methoxy-6-(2-propenyl)-	2188	5.11
57	33.58	Patchouli alcohol	2264	0.10
58	34.56	1,3-Benzodioxole,4- methoxy-6-(2-propenyl)-	2286	2.31
59	35.83	Benzene, 1,2,3-trimethoxy-5-(2-propenyl)-	2313	0.05
60	35.89	3-(4-N,N-Dimethylaminophenyl)propenoic acid, 2-(diethoxyphosphinyl)-, ethyl ester	2314	0.07
	SUM			60

for the analysis of volatile compounds in TCMs. SDME-GC-MS has a much lower cost (only using negligible volume of a solvent) and wider availability of extraction solvents.

4. Conclusions

SDME-GC-MS has a lower cost, more choices of extraction solvents, requires a smaller amount of sample, and directly utilizes the ground powder of traditional Chinese medicines for the analysis. SDME-GC-MS method is a simple, cheap, and effective method for the analysis of volatile compounds in TCM.

Acknowledgments

The research work was supported by the National Natural Science Foundation of China (Grant no. 20475007). The authors would like to thank Professor Bao-Lin Guo (Institute of Medicinal Plants, Academy of Medicinal Science of China) for authentication of Herba Asari.

References

[1] M. A. Jeannot and F. F. Cantwell, "Solvent microextraction into a single drop," *Analytical Chemistry*, vol. 68, no. 13, pp. 2236–2240, 1996.

[2] D. A. Lambropoulou, I. K. Konstantinou, and T. A. Albanis, "Recent developments in headspace microextraction techniques for the analysis of environmental contaminants in different matrices," *Journal of Chromatography A*, vol. 1152, no. 1-2, pp. 70–96, 2007.

[3] S. Shariati-Feizabadi, Y. Yamini, and N. Bahramifar, "Headspace solvent microextraction and gas chromatographic determination of some polycyclic aromatic hydrocarbons in water samples," *Analytica Chimica Acta*, vol. 489, no. 1, pp. 21–31, 2003.

[4] M. Kaykhaii, S. Nazari, and M. Chamsaz, "Determination of aliphatic amines in water by gas chromatography using headspace solvent microextraction," *Talanta*, vol. 65, no. 1, pp. 223–228, 2005.

[5] L. Vidal, A. Canals, N. Kalogerakis, and E. Psillakis, "Headspace single-drop microextraction for the analysis of chlorobenzenes in water samples," *Journal of Chromatography A*, vol. 1089, no. 1-2, pp. 25–30, 2005.

[6] H. F. Wu, J. H. Yen, and C. C. Chin, "Combining drop-to-drop solvent microextraction with gas chromatography/mass spectrometry using electronic ionization and self-ion/molecule reaction method to determine methoxyacetophenone isomers in one drop of water," *Analytical Chemistry*, vol. 78, no. 5, pp. 1707–1712, 2006.

[7] A. Przyjazny and J. M. Kokosa, "Analytical characteristics of the determination of benzene, toluene, ethylbenzene and xylenes in water by headspace solvent microextraction," *Journal of Chromatography A*, vol. 977, no. 2, pp. 143–153, 2002.

[8] G. Shen and H. K. Lee, "Headspace liquid-phase microextraction of chlorobenzenes in soil with gas chromatography-electron capture detection," *Analytical Chemistry*, vol. 75, no. 1, pp. 98–103, 2003.

[9] R. Batlle and C. Nerín, "Application of single-drop microextraction to the determination of dialkyl phthalate esters in food simulants," *Journal of Chromatography A*, vol. 1045, no. 1-2, pp. 29–35, 2004.

[10] D. A. Lambropoulou and T. A. Albanis, "Liquid-phase microextraction techniques in pesticide residue analysis," *Journal of Biochemical and Biophysical Methods*, vol. 70, no. 2, pp. 195–228, 2007.

[11] A. Besharati-Seidani, A. Jabbari, and Y. Yamini, "Headspace solvent microextraction: a very rapid method for identification of volatile components of Iranian Pimpinella anisum seed," *Analytica Chimica Acta*, vol. 530, no. 1, pp. 155–161, 2005.

[12] P. R. Sudhir, H. F. Wu, and Z. C. Zhou, "Identification of peptides using gold nanoparticle-assisted single-drop microextraction coupled with AP-MALDI mass spectrometry," *Analytical Chemistry*, vol. 77, no. 22, pp. 7380–7385, 2005.

[13] Y. C. Fiamegos, C. G. Nanos, and C. D. Stalikas, "Ultrasonic-assisted derivatization reaction of amino acids prior to their determination in urine by using single-drop microextraction in conjunction with gas chromatography," *Journal of Chromatography B*, vol. 813, no. 1-2, pp. 89–94, 2004.

[14] N. Li, C. Deng, X. Yin, N. Yao, X. Shen, and X. Zhang, "Gas chromatography-mass spectrometric analysis of hexanal and heptanal in human blood by headspace single-drop microextraction with droplet derivatization," *Analytical Biochemistry*, vol. 342, no. 2, pp. 318–326, 2005.

[15] J. M. Kokosa and A. Przyjazny, "Headspace microdrop analysis—an alternative test method for gasoline diluent and benzene, toluene, ethylbenzene and xylenes in used engine oils," *Journal of Chromatography A*, vol. 983, no. 1-2, pp. 205–214, 2003.

[16] E. C. Zhao, L. J. Han, S. R. Jiang, Q. X. Wang, and Z. Q. Zhou, "Application of a single-drop microextraction for the analysis of organophosphorus pesticides in juice," *Journal of Chromatography A*, vol. 1114, no. 2, pp. 269–273, 2006.

[17] J. Cao, M. L. Qi, Y. Zhang et al., "Analysis of volatile compounds in Curcuma wenyujin Y.H. Chen et C. Ling by headspace solvent microextraction-gas chromatography-mass spectrometry," *Analytica Chimica Acta*, vol. 561, no. 1-2, pp. 88–95, 2006.

[18] L. H. Fang, M. L. Qi, T. L. Li, Q. Shao, and R. Fu, "Headspace solvent microextraction-gas chromatography-mass spectrometry for the analysis of volatile compounds from Foeniculum vulgare Mill," *Journal of Pharmaceutical and Biomedical Analysis*, vol. 41, no. 3, pp. 791–797, 2006.

[19] C. H. Deng, N. Yao, B. Wang, and X. G. Zhang, "Development of microwave-assisted extraction followed by headspace single-drop microextraction for fast determination of paeonol in traditional Chinese medicines," *Journal of Chromatography A*, vol. 1103, no. 1, pp. 15–21, 2006.

Hindawi Publishing Corporation
Journal of Analytical Methods in Chemistry
Volume 2013, Article ID 473649, 10 pages
http://dx.doi.org/10.1155/2013/473649

Research Article

Liquid Chromatography/Quadrupole Time-of-Flight Mass Spectrometry for Identification of In Vitro and In Vivo Metabolites of Bornyl Gallate in Rats

Wei Lan, Liujiao Bian, Xinfeng Zhao, Pu Jia, Xue Meng, Yizhen Wu, Shixiang Wang, Sha Liao, Jie Yu, and Xiaohui Zheng

College of Life Sciences, Northwest University, Xi'an, Shaanxi 710069, China

Correspondence should be addressed to Xiaohui Zheng; zhengxh@nwu.edu.cn

Received 23 January 2013; Accepted 27 February 2013

Academic Editor: Feng Wei

Bornyl gallate (BG) is a potential drug candidate synthesized by the reaction of two natural products, gallic acid and borneol. Previous studies have strongly suggested that BG is worthy of further investigation due to antioxidant, antiatherosclerosis activities, and obvious activity of stimulating intersegmental vessel growth in zebrafish. This work was designed to elucidate the metabolic profile of BG through analyzing its metabolites in vitro and in vivo by a chromatographic separation coupled with a mass spectrometry. The metabolites of BG were characterized from the rat liver microsome incubation solution, as well as rat urine and plasma after oral administration. Chromatographic separation was performed on an Agilent TC-C_{18} column (250 mm × 4.6 mm, 5 μm) with gradient elution using methanol and water containing 0.2% (V : V) formic acid as the mobile phase. Metabolites identification involved analyzing the retention behaviors, changes of molecular weights and MS/MS fragment patterns of BG and the metabolites. Five compounds were identified as isomers of hydroxylated BG metabolites in vitro. The major metabolites of BG in rat urine and plasma proved to be BG-O-glucuronide and O-methyl BG-O-glucuronide. The proposed method confirmed to be a reliable and sensitive alternative for characterizing metabolic pathways of BG.

1. Introduction

Traditional Chinese medicine (TCM), which serves as a resource of bioactive compounds for drug discovery, is attracting increasing global attention [1]. In practice, it is generally prescribed as a combination of several herbal species and/or minerals to improve therapeutic effects. So far, there have been 12,806 medical resources found in China, including 11,145 medicinal plants, 1581 medicinal animals, and 80 medicinal minerals [2]. Such ample Chinese natural medicinal resources provide valuable materials for the discovery and development of new drugs. More importantly, the clinic medicinal experience of more than 2000 years made the TCM-derived active compounds better lead compounds for further chemical improvements.

Gallic acid (3,4,5-trihydroxybenzoate) (Figure 1(a)), an endogenous plant phenol, is found abundantly in tea, grapes, different berries, and other fruits as well as wine. It is also isolated from various TCMs such as *Galla Chinensis*, *Choerospondiatis Fructus*, *Radix Paeoniae Rubra*, and many others [3, 4]. Plenty of studies demonstrate that gallic acid has strong antioxidant, anti-inflammatory, and anticancer activities [5, 6]. In particular, the protective effects of gallic acid on cardiovascular diseases have attracted increasing attention in recent studies [7–9]. Borneol (endo-1,7,7-trimethylbicyclo[2.2.1]heptan-2-ol) (Figure 1(b)), as an adjuvant drug in many formulae of TCMs, is believed to play assisting roles in facilitating the delivery of principal components, increasing bioavailability, and helping active compounds penetrate the biological barriers [10, 11]. For the purpose of developing new drugs for treatment of cardiovascular diseases, we synthesized bornyl gallate [1,7,7-trimethylbicyclo[2.2.1]heptan-2-yl 3,4,5-trihydroxybenzoate (BG)] (Figure 1(c)) through the dehydration reaction of gallic acid and borneol. Bornyl gallate will not only keep the bioactivities from gallic acid but also get higher penetrability for the existence of borneol moiety.

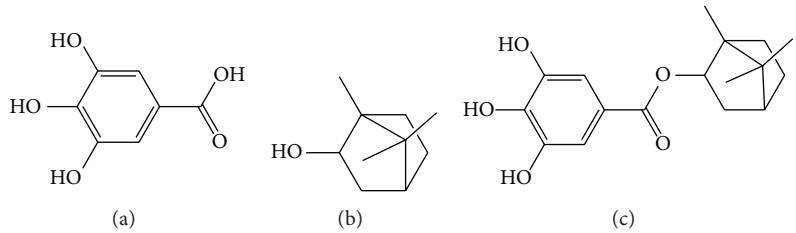

Figure 1: Chemical structures of gallic acid (a), borneol (b), and bornyl gallate (c).

Besides the reported antioxidant activity of bornyl gallate [12], previous studies in our laboratory also showed that BG has obvious activity of stimulating intersegmental vessel growth in zebrafish and potential for antiatherosclerosis by suppressing monocyte activation and foam cell formation [13]. These results strongly suggest that BG is worthy of further investigation.

Metabolite identification is becoming increasingly important in the early stage of drug discovery as a basis for judging whether or not a drug candidate merits further development [14]. Through metabolite identification, we are able to get a quick look at the metabolic fate of a parent drug, determine the major metabolic pathways, and also find whether or not any potentially reactive or toxic metabolites are formed. A great deal of the structural information of metabolites can be obtained using the state-of-art liquid chromatography-mass spectrometry (LC-MS) strategies available now. In several different LC/MS platforms, quadrupole time-of-flight mass spectrometry (Q-TOF/MS) is adopted in this paper because it provides elemental composition from accurate mass measurement and metabolite structures can be proposed with high degrees of certainty without the need of standards for each metabolite [15, 16].

In order to predict the safety and efficacy of BG, it is extremely important to identify its metabolites and thoroughly understand its metabolic fate. Therefore, we firstly analyzed the in vitro metabolites of BG after incubating with rat liver microsome (RLM), subsequently investigated the metabolic profiles of BG in rat plasma and urine, and tentatively identified in vivo metabolites by comparing MS/MS fragment patterns and change of molecular mass with those of the parent drug.

2. Experimental

2.1. Chemicals and Reagents. Bornyl gallate (purity: >99%, HPLC) was synthesized and identified by ^{1}HNMR, IR, and LC/Q-TOF/MS in our laboratory. HPLC grade methanol was purchased from Fisher Chemical Co., Inc. (CA, USA). HPLC grade formic acid was purchased from Kermel Chemical Reagent Co., Ltd. (Tianjin, China). β-NADP, D-glucose 6-phosphate and glucose-6-phosphate dehydrogenase were from Sigma-Aldrich Chemical Co. (MO, USA). Water was double distilled in the laboratory. All other reagents used are analytical grade unless stated specially.

2.2. Animals. Male Sprague-Dawley rats (200–220 g) were purchased from the Laboratory Animal Research Center of Xi'an Jiaotong University (Shaanxi, China). The rats were kept in metabolic cages in a breeding room with temperature at 23 ± 2°C, relative humidity of 55 ± 10%, and a 12 h light-dark cycle. They were fed with standard laboratory food and water for at least 3 days before experimentation. All experiments on animals were performed in accordance with the university guideline and approved by the Ethical Committee for Animal Care and Use of Northwest University, China.

2.3. In Vitro Sample Preparation. Rats were starved overnight before sacrificed. Minced livers were homogenized in 4 × volume of microsome buffer (pH 7.4) containing 0.1 M potassium phosphate, 10% sucrose, 0.1 mM EDTA, 2 mM dithiothreitol, and 1 mM phenylmethylsulfonyl fluoride prior to be centrifuged at 9,000 ×g for 30 min (4°C). Then, the supernatant was further centrifuged at 100,000 ×g for 60 min (4°C). The resulted microsomal pellet was resuspended in fresh microsome buffer and centrifuged again (100,000 ×g, 60 min, 4°C). The collected RLM was dissolved in fresh microsome buffer and immediately stored at −80°C until next use.

Incubations were performed at 37°C in a system containing 3.06 mg/L BG, 0.5 mg/mL rat liver microsomal protein in 0.5 mL of 0.1 mol/L phosphate buffer (pH 7.4). After preincubation at 37°C for 3 min, the reaction between BG and RLM was started by adding a NADPH-regenerating buffer consisting of 1.3 mM β-NADP, 3.3 mM D-glucose-6-phosphate, 3.3 mM $MgCl_2$, and 0.4 U/mL glucose-6-phosphate dehydrogenase. Incubation was terminated after 30 min by adding ice-cold acetonitrile. Then, 1.0 mL ethyl acetate was used to extract the reacting products from the incubating solution. After being swirled for 60 s and centrifuged at 10,000 ×g for 10 min at 4°C, the supernatant was transferred into a clean tube and evaporated under a gentle stream of nitrogen. The residue was dissolved in 50 μL of 50% methanol water and centrifuged at 10,000 ×g for 10 min. A 25 μL aliquot of the supernatant was injected for LC/MS analysis. Negative control samples were prepared in the same way besides the step of adding ice-cold acetonitrile before the NADPH-regenerating buffer.

2.4. In Vivo Sample Preparation. Five male Sprague-Dawley rats were starved overnight with free access to water. Blank

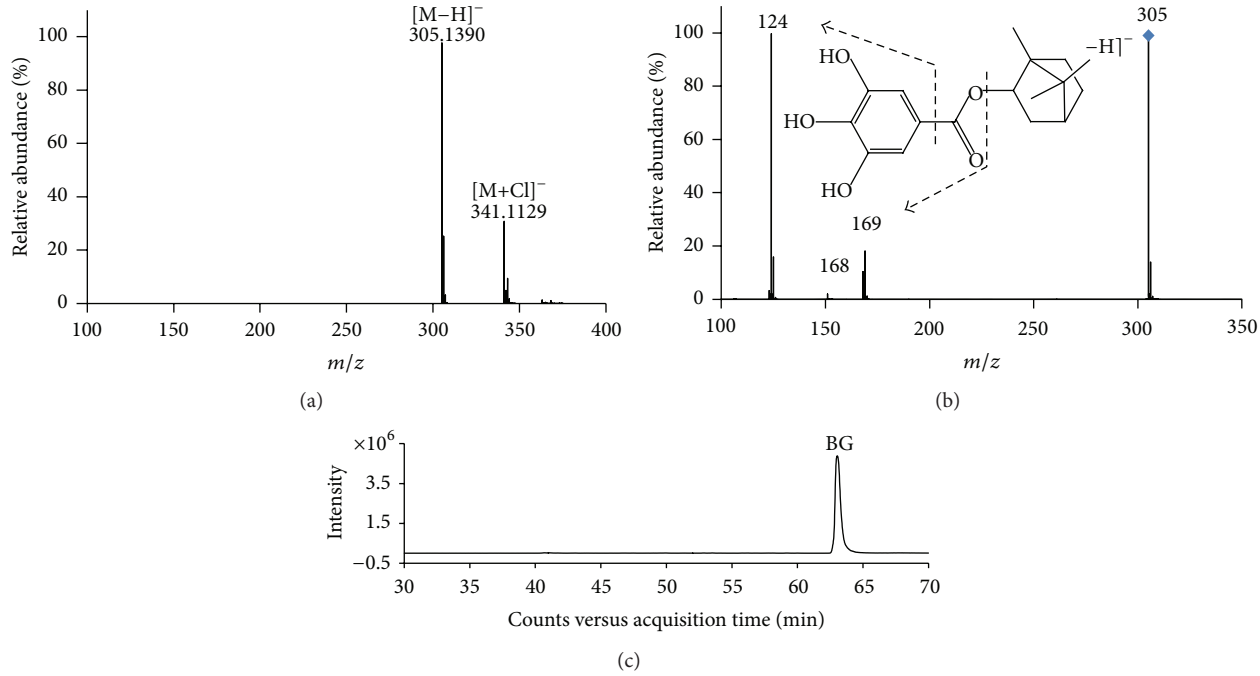

Figure 2: MS, MS/MS spectrum, and total ion chromatogram (TIC) of reference BG (a) MS spectrum; (b) MS/MS spectrum, and the predominant fragmentation pattern; (c) TIC of BG. The chromatographic separation is performed on an Agilent TC-C_{18} column (250 mm × 4.6 mm, 5 μm) with gradient elution using methanol and water containing 0.2% (V : V) formic acid as the mobile phase. Under the proposed condition, the retention time of BG was determined to be 63.0 min.

blood and urine from each rat were collected prior to dosing. The BG was suspended in 0.5% CMC-Na and orally administered to rats at a dose of 50 mg/kg. 0.5 mL blood samples were collected through ophthalmic veins using heparinized tubes under anesthesia at 1 h after dose. Plasma was prepared by centrifuging the blood for 10 min at 8,000 ×g. Urine samples were collected individually during the time period 0–12 h. The plasma and urine samples were stored at −20°C before further preparation.

All the samples were thawed at room temperature. 0.2 mL acetonitrile containing 0.5% formic acid was added into 0.2 mL plasma or urine. The mixture was thoroughly swirled for 2 min and then centrifuged at 8,000 ×g for 10 min to remove protein in the sample. The supernatant was filtered by 0.45 μm membrane and a 25 μL aliquot was injected into LC/MS system for on-line analysis.

2.5. HPLC/Q-TOF/MS Conditions. Chromatographic experiments were performed on an Agilent 1200 series HPLC system, equipped with binary pump, autosampler, on-line degasser and automatic thermostatic column oven (CA, USA). HPLC separation was achieved on an Agilent TC-C_{18} column (4.6 mm × 250 mm, 5 μm) protected by an Agilent TC-C_{18} guard column (4.6 mm × 12.5 mm, 5 μm) with the column temperature set at 30°C. The mobile phase consisted of water containing 0.2% (V:V) formic acid (pH 2.2) (A) and methanol (B) using a gradient elution of 10% B at 0–15 min, 10% to 85% B at 15–60 min, and 95% B at 60–65 min. The flow rate was 0.7 mL/min with an injection volume of 25 μL.

To identify the metabolites in the elution, the HPLC system was coupled online to an Agilent 6500 series quadrupole-time of flight mass spectrometer (Q-TOF/MS), equipped with a dual electrospray ionization source (Dual-ESI) (CA, USA). The LC effluent was introduced into the ESI source in a postcolumn splitting ratio of 3 : 1. Mass spectra were acquired in negative ion mode with the mass range set at m/z 100–1000. The conditions used for the ESI source included a capillary voltage of 4000 V, a drying gas temperature of 350°C, a drying gas flow of 10 L/min, and a nebulizer pressure of 35 psi as well as a fragmentor voltage of 125 V. Internal reference masses in negative mode were set at m/z 112.9855 and 966.0007. MassHunter Workstation software from Agilent Technologies (CA, USA) was used for data acquisition and processing in full-scan and targeted MS/MS modes.

3. Results and Discussion

3.1. LC-MS Analysis of Bornyl Gallate. The HPLC-MS conditions were optimized to provide a full overview of the pattern of the metabolites in rat plasma and urine after oral administration of BG. Ionization of the parent drug BG was much better in the negative mode than that in the positive mode, and the difference between the chromatograms of blank samples and those of samples after oral dosing was more noticeable in the negative mode. Therefore, metabolite identification was performed in the negative ionization mode. Under the proposed condition, the retention time of BG was determined to be 63.0 min (Figure 2(c)). Full-scan analysis generated a mass spectrum of BG (Figure 2(a)) attributing to

a negative deprotonated ion $[M-H]^-$ at m/z 305.1390 and an adduct ion $[M+Cl]^-$ at m/z 341.1129. Precursor ion at m/z 305 gave daughter ions at m/z 169, m/z 168, m/z 124, and m/z 125 (Figure 2(b)). Directly loss of borneol moiety produced the ion at m/z 168. The daughter ion at m/z 169 was generated due to the McLafferty rearrangement cleavage based on gallic acid group. Ions at m/z 124 and m/z 125 attributed to the loss of CO_2 from the above two ions, respectively. The four ions were subsequently used as diagnostic product ions to ensure whether an unknown metabolite is formed from BG through comparing difference of mass lost between BG and the metabolite.

3.2. Identification of In Vitro Metabolites in RLM. Compared with the negative control sample, five new compounds (M1a, M1b, M1c, M1d, and M1e) and the parent drug BG were detected in RLM incubation solution. The full-scan mass spectrum analysis revealed that the five compounds had molecular ions $[M-H]^-$ at m/z 321.1339, 321.1341, 321.1340, 321.1338, and 321.1335, respectively. All ions had identical calculated formula of $C_{17}H_{22}O_6$ ($mass_{calc.}$ = 321.1344, error <2.7 ppm), representing the notable difference of a single oxygen atom from BG. This interesting result indicated that the new compounds found in vitro should be isomers of monohydroxylated BG. Further MS/MS spectra of each compound at m/z 321 provided same product ions at m/z 169, 168, 124 and 125, which remains same as the MS^2 fragment ions of the parent drug. The full-scan mass spectrum, MS/MS spectrum, and the predominant fragmentation pattern of M1a are shown in Figure 3(a) and Figure 3(b) as the representative spectra of five metabolites, which exhibited almost identical spectrum. It is accordingly believed that the compounds are metabolites of BG. The data above strongly suggests that hydroxylation of BG took place in borneol moiety while the gallic acid moiety was not modified by enzymes present in RLMs.

The retention times of the five metabolites were determined to be 49.0, 51.8, 54.0, 56.8, and 57.5 min from the extracted ion chromatogram of m/z 321.1339 (Figure 3(c)). It is found that the retention times were all shorter than those of BG, suggesting stronger polarity of the metabolite than BG. For the isomers themselves, the polarities decreased as the order of M1a, M1b, M1c, M1d, and M1e. Among the isomers, M1a, M1b, and M1c should be main metabolites of hydroxylation based on the ion abundance.

3.3. Analysis of In Vivo Metabolites of BG. Drug metabolism involves chemical conversion to reduce pharmacological activity of a drug candidate and to facilitate its elimination from the body. Metabolic processes can also produce metabolites that are more pharmacologically active. These metabolic reactions are generally divided into two cases called phase I and phase II reactions. According to the rules of metabolic reactions and the results from in vitro experiments, we predict that the probable metabolic reactions of BG involve in phase I reactions including hydroxylation and hydrolysis as well as phase II reactions such as glucuronidation, O-methylation, and sulfation plus acetylation. The possible structures of metabolites in vivo have been analyzed based on the above theory. Additionally, the calculated molecular formulas and mass values (m/z) of corresponding metabolites have been generated by a tool of Mass Calculator in software Qualitative Analysis B.04.00 (MassHunter Workstation, Agilent, USA).

3.3.1. Metabolic Profile of BG. The total ion chromatograms (TICs) of blank samples and samples after oral dosing in negative ion mode are shown in Figure 4. In order to increase sensitivity and to eliminate the endogenous interferences from complex biological matrices, the extracted ion chromatograms (EICs) were used to confirm the existence of potential metabolites by comparing the EICs of the samples after oral dosing with those of blank samples (Figure 5). As a result, the parent drug BG (M0) was detected in both urine and plasma. 9 kinds of potential metabolites were detected in urine. These metabolites have deprotonated ions $[M-H]^-$ of m/z 321 (M1), 169 (M2), 345 (M3), 183 (M4), 497 (M5), 657 (M6), 481 (M7), 495 (M8), and 319 (M9), respectively. Among them, M3, M5, M6, M7, M8, and M9 were detected in plasma after oral administration. Most of the potential metabolites, except M1, M2, M3, and M6, have two or three isomers due to the existence of 3 phenolic hydroxyl groups in the molecular structure, which have the properties of undergoing phase II conjugation reactions. The lowercase letters in alphabetical order were used to represent the elution orders of isomers of corresponding metabolites. Furthermore, the structures of metabolites were elucidated based on the targeted MS/MS spectra (shown in Figure 6). However, their exact conjugation sites could not be identified in this work. Table 1 showed the retention time (RT), measured mass, their calculated formula by elemental compositions, the mass error between the calculated and measured values, MS/MS fragment ions, and metabolic pathway for each metabolite as well as relative peak ratio [17] which could be useful to estimate the main metabolites.

3.3.2. Identification and Structure Elucidation of In Vivo Metabolites. In the EIC of m/z 321 (M1), three chromatographic peaks of isomers (RT at 49.0, 51.8, and 53.9 min) were observed in urine. M1 showed 16 mass units higher than those of parent drug M0, indicating that they were the monohydroxylated BG. Their retention times and MS^2 fragments were the same as those of M1a, M1b, and M1c in RLM incubation solution in section of in vitro investigation.

M2 was eluted at 13.9 min with the $[M-H]^-$ ion at m/z 169.0145 (calculated formula = $C_7H_6O_5$). The MS/MS spectrum of m/z 169 gave abundant daughter ion at m/z 125, which were produced by the loss of CO_2 (−44 Da) from precursor ion. Moreover, either retention time or fragment ion of M2 was identical as that of gallic acid by comparing with an authentic standard. Thus, M2 was identified as gallic acid, the hydrolysis product of BG.

M3 and M4 were tentatively assigned as metabolites originating from gallic acid. M3 gave a deprotonated molecule $[M-H]^-$ at m/z 345.0469 (calculated formula = $C_{13}H_{14}O_{11}$). Its MS/MS fragmentation was predominated by the elimination of glucuronide moiety (176 Da) to give product ion

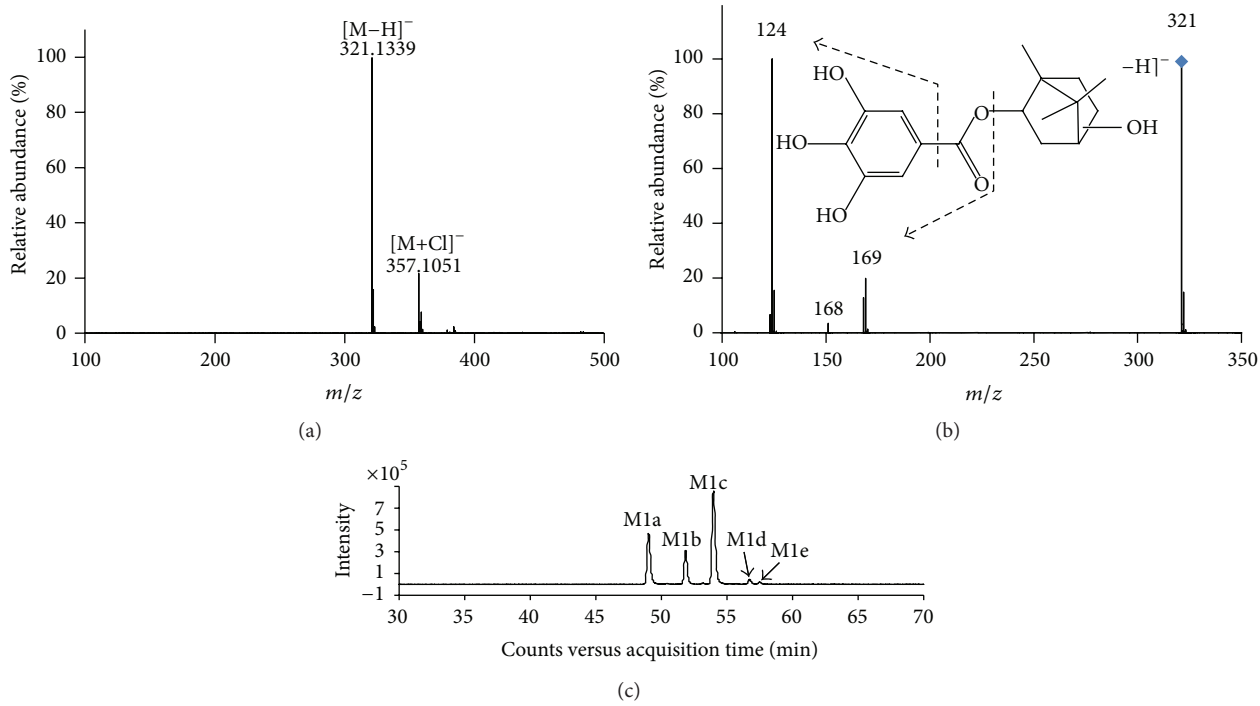

Figure 3: Representative MS, MS/MS spectrum, and extracted ion chromatogram (EIC) of in vitro metabolites of BG in rat liver microsomes (RLM). Incubations were performed at 37°C for 30 min in a system containing 3.06 mg/L BG and 0.5 mg/mL liver microsomal protein in 0.5 mL of 0.1 mol/L phosphate buffer (pH 7.4). (a) MS spectrum; (b) MS/MS spectrum and the predominant fragmentation pattern of M1a are shown as the representative spectra of five metabolites, which exhibited almost identical spectra; (c) EIC of m/z 321.1339 representing 5 isomers of in vitro metabolites with their RTs at 49.0, 51.8, 54.0, 56.8, and 57.5 min, respectively.

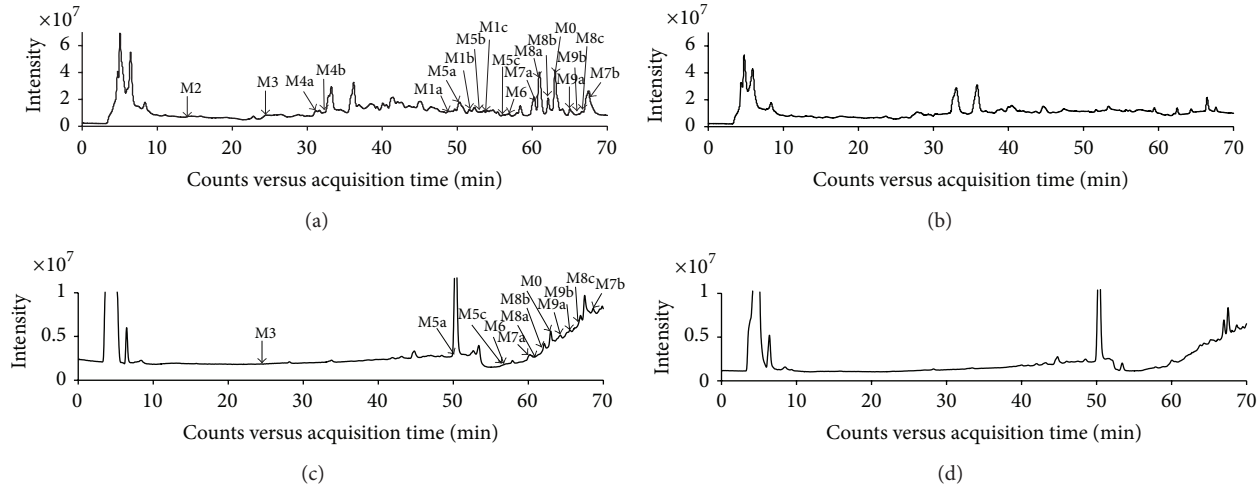

Figure 4: Total ion chromatograms (TICs) of rat urine and plasma samples by HPLC/Q-TOF/MS. (a) TIC of the urine sample after oral administration at a single dose of 50 mg/kg BG; (b) TIC of blank urine; (c) TIC of the plasma sample after oral administration at a single dose of 50 mg/kg BG; (d) TIC of blank plasma.

at m/z 169. M3 was identified as gallic acid-O-glucuronide. Although baseline separation was not achieved, two peaks were obviously observed in urine containing BG in the EIC of M4. The two peaks represented two isomers M4a and M4b, giving deprotonated molecular ions at m/z 183.0302 and 183.0304 (calculated formula = $C_8H_8O_5$) and daughter ions at m/z 168 $[M-H\text{-}CH_3]^-$ and m/z 124 $[M-H\text{-}CH_3\text{-}COO]^-$. The two isomers were considered to be O-methylation products of gallic acid, 4-O-methylgallic acid, or 3-O-methylgallic acid. Based on the previous studies on its metabolic fate, gallic acid will be metabolized through decarboxylation, O-methylation, sulfation, and glucuronidation reactions in rats

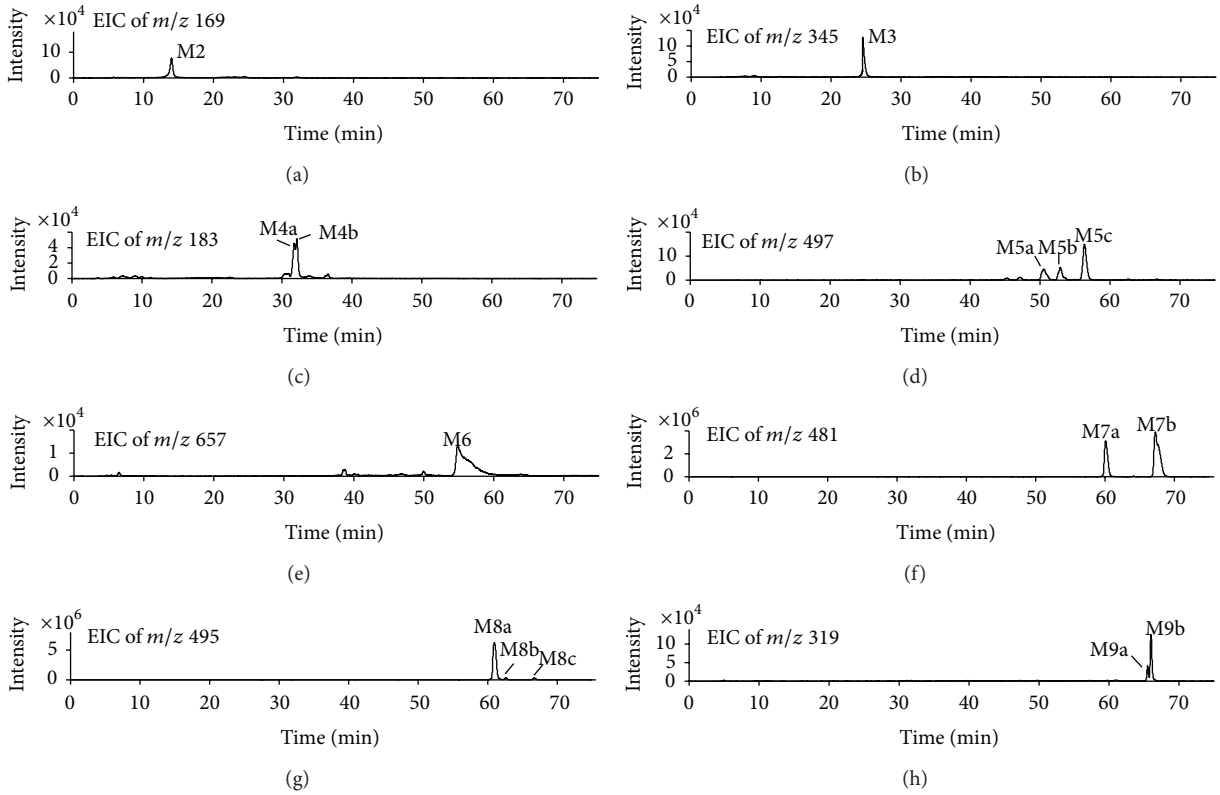

Figure 5: The extracted ion chromatograms (EICs) of in vivo metabolites M2 to M9 of BG in rat urine samples.

[18, 19]. In our work, the gallic acid, which was produced by the hydrolysis of BG, proved to undergo further metabolic reactions including O-methylation and glucuronidation. The decarboxylation and sulfation metabolites were not observed, probably because of their low concentration.

Two chromatographic peaks with their RTs at 65.5 (M9a) and 66.0 (M9b) min were detected in the EIC of m/z 319.1556. The MS/MS spectra of m/z 319 showed M9 produced fragment ion at m/z 304 $[M-H\text{-}CH_3]^-$, indicating that the metabolites M9a and M9b should be O-methyl BG, the O-methylation products of M0.

All the MS/MS fragmentation patterns of M5, M6, M7, and M8 presented neutral loss of 176 Da from precursor ions. Furthermore, the characteristic ions of glucuronide at m/z 175 and m/z 113 were observed in each of their MS/MS spectra, which confirmed the presence of glucuronide according to the reported literature [20, 21]. M5a, M5b, and M5c gave deprotonated ions $[M-H]^-$ at m/z 497.1674, 497.1681, and 497.1678, corresponding to a molecular formula of $C_{23}H_{30}O_{12}$. Their retention times were determined to be 50.5, 52.9 and 56.3 min, respectively. The targeted MS/MS spectra yielded a daughter ion at m/z 321. A loss of 176 Da to precursor ions is easily calculated for identifying M5a, M5b, and M5c as isomers of monohydroxylated BG-O-glucuronide, the glucuronidation products of M1. M6 presented a deprotonated ion $[M-H]^-$ at m/z 657.2043 and the daughter ions at m/z 481 and m/z 305. The two daughter ions denote the loss of 176 Da and 2 × 176 Da to the precursor ion at m/z 657, which paved the way to recognize M6 as BG-di-O-glucuronide. M7 had two isomers and showed the $[M-H]^-$ ions at m/z 481.1722 and 481.1728. In their MS/MS spectra, M7 further lose a glucuronic acid moiety (176 Da) to produce ions at m/z 305, indicating that M7a and M7b were BG-O-glucuronide, the glucuronide conjugates of M0. M8 had three isomers (M8a, M8b, and M8c), giving the deprotonated ions $[M-H]^-$ at m/z 495.1883, 495.1879, and 495.1877. The fragment ions of them were all investigated at m/z 319 and 304, indicating a neutral loss of 176 Da and the additional loss of CH_3 (−15 Da). M8a, M8b, and M8c thus were characterized as glucuronide conjugates of M9, O-methyl-BG-O-glucuronide.

3.4. Metabolic Pathway of BG. Based on the above discussion, the proposed metabolic pathways of BG in rats were presented in Figure 7. In the metabolic profile, BG (M0) was detected in plasma and excreted through urine. BG-O-glucuronide (M7) and O-methyl BG-O-glucuronide (M8) were the most abundant metabolites in vivo according to the relative peak ratio. The hydroxylation and hydrolysis metabolites in low concentration were observed only in the urine, while their further glucuronide conjugates were detectable in plasma. All of these results indicated that the major metabolites were present as conjugated forms in vivo and the main metabolic pathways of BG were glucuronidation and O-methylation.

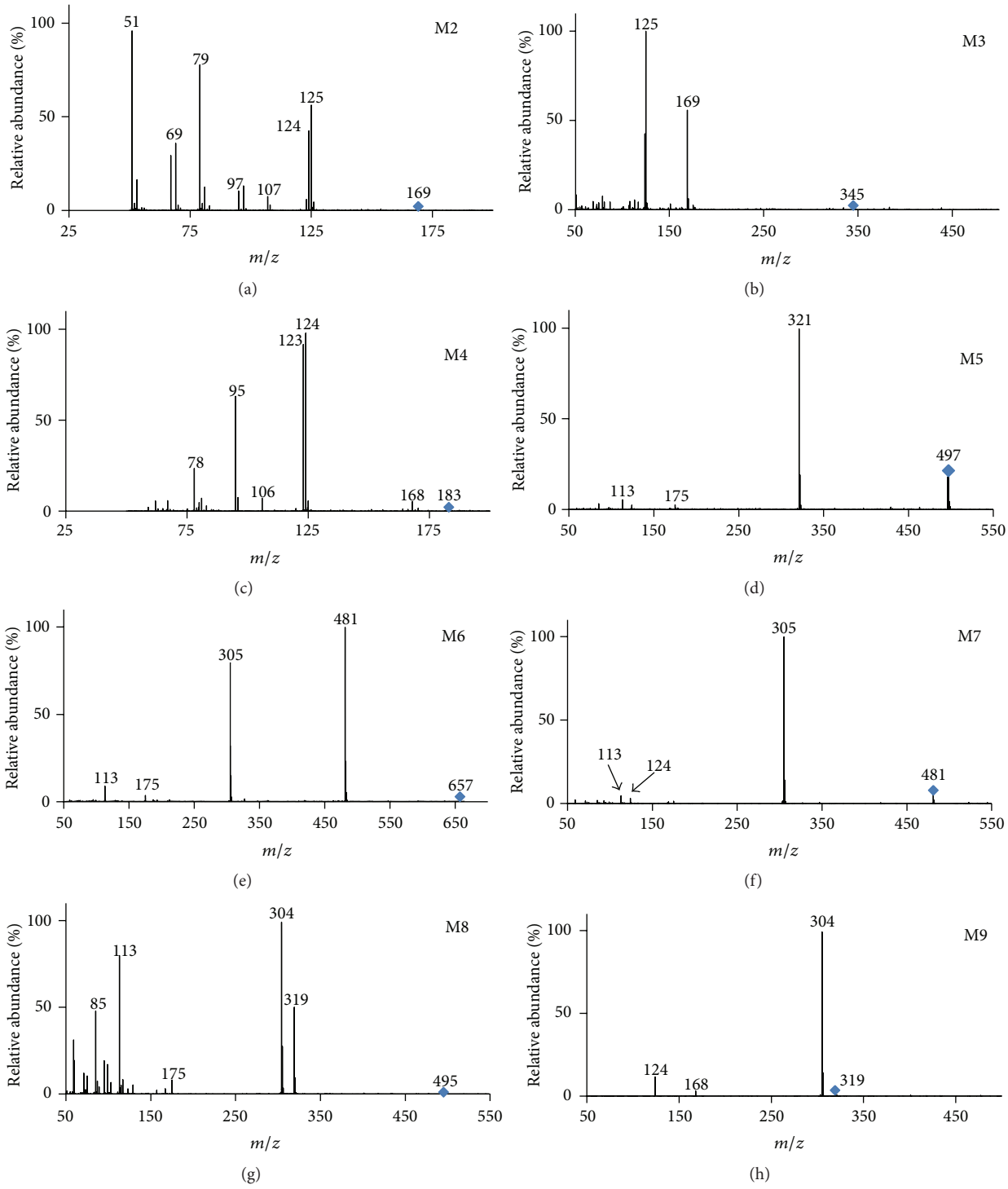

Figure 6: Representative MS/MS spectra of the in vivo metabolites M2 to M9 of BG in rats.

4. Conclusion

In this paper, a reliable and sensitive HPLC/Q-TOF/MS method was successfully applied to identify the metabolites of bornyl gallate in vitro and in vivo for the first time. In vitro, BG was metabolized to five isomers of monohydroxylated BG by CYP450 enzymes present in RLM. In vivo, 9 kinds of potential metabolites, altogether 18 compounds including all isomers, were detected and identified. BG is believed to undergo various phases I and II metabolic pathways including hydroxylation, hydrolysis, O-methylation, and glucuronidation, while the conjugation with sulfation or acetylation was not detected. We also proved that BG mainly became products of glucuronidation and O-methylation in

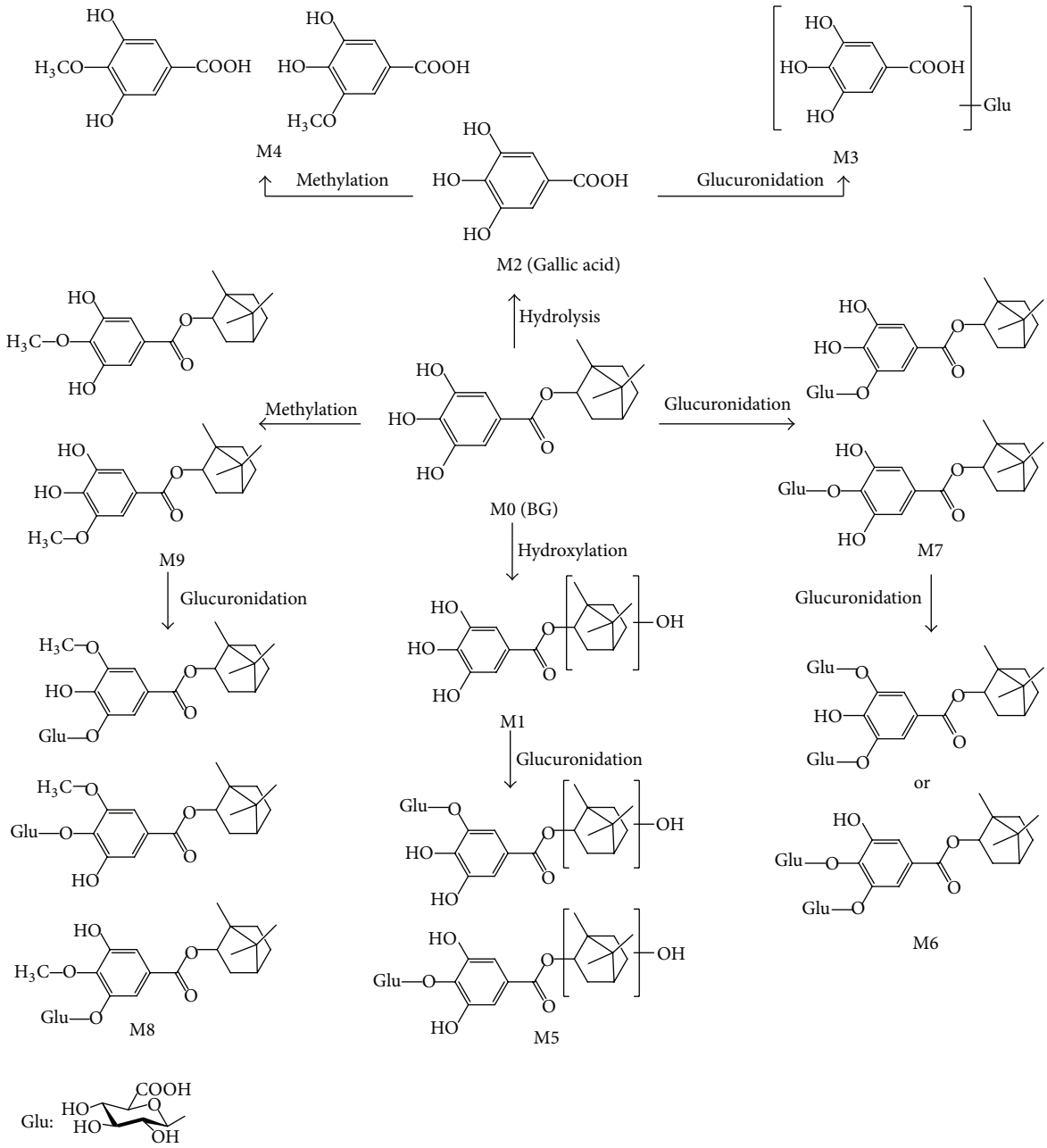

Figure 7: Proposed metabolic pathways of BG in rats.

vivo, which were identified as BG-O-glucuronide (M7) and O-methyl BG-O-glucuronide (M8).

Abbreviations

TCM:	Traditional Chinese medicine
BG:	Bornyl gallate
RLM:	Rat liver microsome
HPLC/Q-TOF/MS:	High performance liquid chromatography/quadrupole time-of-flight mass spectrometry
ESI:	Electrospray ionization
TIC:	Total ion chromatogram
EIC:	Extracted ion chromatograms
RT:	Retention time.

Conflict of Interests

There is no conflict of interests.

Acknowledgments

This work was financially supported by the National Major Scientific and Technological Special Project for "Significant New Drugs Development" (Grant no. 2009ZX09103-121),

Table 1: Retention time (RT), measured mass, calculated formula by elemental compositions, the mass error between the calculated and measured values, MS/MS fragment ions, and metabolic pathway as well as relative peak ratio for each metabolite of BG in rat plasma and urine after oral administration.

Compound	RT (min)	Measured mass (m/z)	Mass error (ppm)	Relative peak ratio[a] in urine	Relative peak ratio in plasma	Formula	MS/MS fragment ions	Metabolic pathway
M0	63.0	305.1400	−1.8	100	100	$C_{17}H_{22}O_5$	169, 168, 125, 124	Parent drug
M1a	49.0	321.1350	−2.0	0.68	\[b]			
M1b	51.8	321.1348	−1.4	0.53	\	$C_{17}H_{22}O_6$	169, 168, 125, 124	Hydroxylation
M1c	53.9	321.1349	−1.7	0.41	\			
M2	13.9	169.0145	−1.5	0.69	\	$C_7H_6O_5$	125, 124, 79, 51	Hydrolysis
M3	24.4	345.0469	−1.6	3.66	1.38	$C_{13}H_{14}O_{11}$	169, 125, 124	Hydrolysis + glucuronidation
M4a	31.8	183.0302	−1.7	0.38	\	$C_8H_8O_5$	168, 124, 123, 95, 78	Hydrolysis + O-methylation
M4b	32.1	183.0304	−2.8	0.32	\			
M5a	50.5	497.1674	−1.9	0.99	2.86	$C_{23}H_{30}O_{12}$	321, 175, 113	Hydroxylation + glucuronidation
M5b	52.9	497.1681	−3.3	0.90	\			
M5c	56.3	497.1678	−2.7	2.44	2.36			
M6	56.4	657.2043	−1.0	1.08	13.6	$C_{29}H_{38}O_{17}$	481, 305, 175, 113	Di-glucuronidation
M7a	60.1	481.1722	−1.4	24.64	105.24	$C_{23}H_{30}O_{11}$	305, 124, 113	glucuronidation
M7b	67.5	481.1728	−2.6	50.96	916.65			
M8a	60.9	495.1883	−2.3	95.36	31.7	$C_{24}H_{32}O_{11}$	319, 304, 175, 113	O-methylation + glucuronidation
M8b	62.6	495.1879	−1.4	3.66	16.95			
M8c	66.7	495.1877	−1.1	2.68	2.01			
M9a	65.5	319.1556	−1.6	0.39	3.09	$C_{18}H_{24}O_5$	304, 168, 124	O-methylation
M9b	66.0	319.1560	−2.8	1.31	0.86			

[a] Relative peak ratio was calculated on the basis of EIC as follows: (relative peak ratio) = (the peak area of metabolite)/(the peak area of parent, M0) × 100.
[b] \: undetected.

the National Natural Science Foundation of China (Grant no. 21005060), the Specialized Research Fund for the Doctoral Program of Higher Education on 2011 (Grant no. 20106101110001) and the National Key Technology R&D Program (Grant no. 2008BAI51B01).

References

[1] X. Xu, "New concepts and approaches for drug discovery based on traditional Chinese medicine," *Drug Discovery Today*, vol. 3, no. 3, pp. 247–253, 2006.

[2] Y. Z. Chen and S. Y. Chen, *Introduction of Chemical Methods in Study of Modernization of Traditional Chinese Medicines*, Science Publishing, Beijing, China, 2003.

[3] The State Commission of Chinese Pharmacopoeia, *Pharmacopoeia of People's Republic of China, Part I*, Chemical Industry Press, Beijing, China, 2010.

[4] X. Zhao, W. Zhang, S. Kong, X. Zheng, J. Zheng, and R. Shi, "A valid assay for the pharmacokinetic study of gallic acid from *Choerospondiatis fructus* in rabbit plasma by LC/MS/MS," *Journal of Liquid Chromatography and Related Technologies*, vol. 30, no. 2, pp. 235–244, 2007.

[5] B. H. Kroes, A. J. J. Van Den Berg, H. C. Quarles Van Ufford, H. Van Dijk, and R. P. Labadie, "Anti-inflammatory activity of gallic acid," *Planta Medica*, vol. 58, no. 6, pp. 499–504, 1992.

[6] D. Kalita, R. Kar, and J. G. Handique, "A theoretical study on the antioxidant property of gallic acid and its derivatives," *Journal of Theoretical and Computational Chemistry*, vol. 11, no. 2, pp. 391–402, 2012.

[7] D. H. Priscilla and P. S. M. Prince, "Cardioprotective effect of gallic acid on cardiac troponin-T, cardiac marker enzymes, lipid peroxidation products and antioxidants in experimentally induced myocardial infarction in Wistar rats," *Chemico-Biological Interactions*, vol. 179, no. 2-3, pp. 118–124, 2009.

[8] S. Umadevi, V. Gopi, S. P. Simna, A. Parthasarathy, S. M. J. Yousuf, and V. Elangovan, "Studies on the cardio protective role of gallic acid against age-induced cell proliferation and oxidative stress in H9C2 (2-1) cells," *Cardiovascular Toxicology*, vol. 12, no. 4, pp. 304–311, 2012.

[9] J. Gil-Longo and C. González-Vázquez, "Vascular pro-oxidant effects secondary to the autoxidation of gallic acid in rat aorta," *Journal of Nutritional Biochemistry*, vol. 21, no. 4, pp. 304–309, 2010.

[10] X. J. Lai, L. Zhang, J. S. Li et al., "Comparative pharmacokinetic and bioavailability studies of three salvianolic acids after the administration of *Salviae miltiorrhizae* alone or with synthetical borneol in rats," *Fitoterapia*, vol. 82, no. 6, pp. 883–888, 2011.

[11] H. Yang, Y. Xun, Z. Li, T. Hang, X. Zhang, and H. Cui, "Influence of borneol on in vitro corneal permeability and on in vivo and in vitro corneal toxicity," *Journal of International Medical Research*, vol. 37, no. 3, pp. 791–802, 2009.

[12] N. Masuoka, K. I. Nihei, and I. Kubo, "Xanthine oxidase inhibitory activity of alkyl gallates," *Molecular Nutrition and Food Research*, vol. 50, no. 8, pp. 725–731, 2006.

[13] X. Xie, S. Wang, L. Xiao et al., "DBZ blocks LPS-induced monocyte activation and foam cell formation via inhibiting nuclear factor-κB," *Cellular Physiology and Biochemistry*, vol. 28, no. 4, pp. 649–662, 2011.

[14] B. Prasad, A. Garg, H. Takwani, and S. Singh, "Metabolite identification by liquid chromatography-mass spectrometry," *Trends in Analytical Chemistry*, vol. 30, no. 2, pp. 360–387, 2011.

[15] A. E. F. Nassar and R. E. Talaat, "Strategies for dealing with metabolite elucidation in drug discovery and development," *Drug Discovery Today*, vol. 9, no. 7, pp. 317–327, 2004.

[16] J. Li and W. Chan, "Investigation of the biotransformation of osthole by liquid chromatography/tandem mass spectrometry," *Journal of Pharmaceutical and Biomedical Analysis*, vol. 74, pp. 156–161, 2013.

[17] S. H. Lee, H. O. Yang, H. C. Kwon, and B. H. Jung, "Identification of the urinary metabolites of Glionitrin A in rats using ultra-performance liquid chromatography combined with quadrupole time-of-flight mass spectrometry," *Journal of Chromatography B*, vol. 906, pp. 33–40, 2012.

[18] T. Yasuda, A. Inaba, M. Ohmori, T. Endo, S. Kubo, and K. Ohsawa, "Urinary metabolites of gallic acid in rats and their radical-scavenging effects on 1,1-diphenyl-2-picrylhydrazyl radical," *Journal of Natural Products*, vol. 63, no. 10, pp. 1444–1446, 2000.

[19] Z. Yan, Y. Chen, T. Li, J. Zhang, and X. Yang, "Identification of metabolites of Si-Ni-San, a traditional Chinese medicine formula, in rat plasma and urine using liquid chromatography/diode array detection/triple-quadrupole spectrometry," *Journal of Chromatography B*, vol. 885-886, pp. 73–82, 2012.

[20] F. Lu, Q. Sun, Y. Bai et al., "Characterization of eleutheroside B metabolites derived from an extract of Acanthopanax senticosus Harms by high-resolution liquid chromatography/quadrupole time-of-flight mass spectrometry and automated data analysis," *Biomedical Chromatography*, vol. 26, no. 10, pp. 1269–1275, 2012.

[21] D. G. Wang, T. J. Hang, C. Y. Wu, and W. Y. Liu, "Identification of the major metabolites of resveratrol in rat urine by HPLC-MS/MS," *Journal of Chromatography B*, vol. 829, no. 1-2, pp. 97–106, 2005.

Hindawi Publishing Corporation
Journal of Analytical Methods in Chemistry
Volume 2013, Article ID 602091, 5 pages
http://dx.doi.org/10.1155/2013/602091

Research Article

Alsterpaullone, a Cyclin-Dependent Kinase Inhibitor, Mediated Toxicity in HeLa Cells through Apoptosis-Inducing Effect

Chunying Cui,[1] Yuji Wang,[1] Yaonan Wang,[2] Ming Zhao,[1] and Shiqi Peng[1]

[1] *College of Pharmaceutical Sciences, Capital Medical University, Beijing 100069, China*
[2] *Medical Experiment and Test Center, Capital Medical University, Beijing 100069, China*

Correspondence should be addressed to Ming Zhao; mingzhao@bjmu.edu.cn and Shiqi Peng; sqpeng@bjmu.edu.cn

Received 30 December 2012; Accepted 13 February 2013

Academic Editor: Feng Sun

Alsterpaullone, a small molecule cyclin-dependent kinase (CDK) inhibitor, regulates the cell cycle progression. Beyond death-inducing properties, we identified the effect of alsterpaullone on cycle procedure and apoptosis of HeLa cell. It was found that alsterpaullone inhibited HeLa cells in a time-dependent (0–72 h) and dose-dependent (0–30 μM) manner. In the presence of alsterpaullone, HeLa cells were arrested in G_2/M prior to undergoing apoptosis via a mechanism that is involved in the regulation of various antiapoptotic genes, DNA-repair, transcription, and cell cycle progression. Compared to controls, alsterpaullone effectively prevented HeLa cells from entering S-phase. These potential therapeutic efficacies could be correlated with the activation of caspase-3.

1. Introduction

Cervical cancer is the third most common cancer among women in the world and has been associated with loss of cell cycle control that normally delays or even arrests proliferation [1, 2]. Cyclin-dependent kinase (Cdk) inhibitors have the potential to induce cell cycle arrest and apoptosis in cancer cells. As one of them, alsterpaullone was found to selectively inhibit Cdk enzymes, especially in Cdk1 [3, 4]. It has been reported that alsterpaullone not only causes cell cycle arrest but also induces the apoptosis of some cancer cells by activation of caspase-9 through perturbation of mitochondrial membrane potential [5–7]. Cdk inhibitors have been shown to possess a cytotoxic effect on tumor cells via cell cycle related proteins and caspase 3 activity. However, this pharmacologic aspect has yet to be studied in relation to alsterpaullone. In this study, we explored the roles of those proteins in the pharmacologic function of alsterpaullone in HeLa cells. In addition, we elucidated the mechanism of cell cycle arrest and apoptosis of HeLa cells treated with alsterpaullone. Our data showed alsterpaullone can inhibit the proliferation of HeLa cells in the dose- and time-dependent manner. Importantly, it induced cell cycle arrest at G_2/M phase and apoptosis via the regulation of anti-apoptotic proteins (caspase-3) and cell cycle proteins. This finding is significant, since it suggests that alsterpaullone provides a promising chemotherapeutic tool in anticervical cancer arsenal.

2. Materials and Methods

Alsterpaullone was purchased from Sigma-Aldrich (CAS: 237430-03-4). HeLa cell lines were purchased from the Institute of Basic Medical Sciences, Chinese Academy of Medical Sciences. Dulbecco's modified Eagle medium, fetal bovine serum, and trypsin were purchased from HyClone Laboratories Inc., USA. Penicillin and streptomycin were purchased from Sigma Chemical Company, USA. Dimethyl sulfoxide was purchased from AppliChem GmbH Company of Germany. 3-(4,5-Dimethylthiazol-2-yl)-2,5-diphenyl-tetrazolium bromide and acridine orange were purchased from Amresco Company, USA. Protease inhibitor cocktail (1%, Cat No: 539134) was purchased from Merck, USA. All reagents were chemical grade unless otherwise specified.

2.1. Cell Culture and Reagents. HeLa cell line was maintained in RPMI-1640 media (GIBCO, Invitrogen Corporation, USA) containing 10% fetal bovine serum (HYCLON, USA), 2 mmol/L L-glutamine (GIBCO, Invitrogen Corporation, USA), 100 U/mL penicillin (GIBCO, Invitrogen Corporation, USA), and 100 μg/mL streptomycin (GIBCO, Invitrogen Corporation, USA). Cells were cultured in an incubator at 37°C under 5% CO_2 in air. A stock solution of alsterpaullone in DMSO (10 mM) was prepared and diluted to the concentration. The final concentration of DMSO in culture medium was ≤0.3%.

2.2. Assessment of Cell Viability (Dose- and Time-Relationship of Alsterpaullone). HeLa cells (5×10^4/well) were grown in 24-well plates and treated with alsterpaullone (0–30 μM) or DMSO (0.3%, final concentration) to control wells in medium for 72 h. Attached cells were released by a trypsinization and combined with nonadherent cells. After centrifugation, cells were resuspended in PBS and treated with 0.2% trypan blue. Trypan blue excluding cells were counted using a haemocytometer. Experiments were performed in triplicates independently.

For cell growth inhibition, HeLa cells were seeded in 24-well culture plates at a density of 5×10^4/well. At 0, 2, 4, 6, 12, 24, 48 and 72 h 500 μL of alsterpaullone (final concentration: 10 μM and 20 μM) were added into the wells. Cell number and cell viability were determined using haemocytometer and the trypan blue dye exclusion test. Experiments were performed in triplicates independently.

2.3. MTT Cytotoxicity Assay. HeLa cells (5×10^3/well) were seeded into 96-well plates and incubated overnight at 37°C. Alsterpaullone was added to cells (in 6 replicates) and incubated for 72 h at 37°C. Stock solution (2 mg/mL) of 3-[4, 5-dimethylthiazol-2-yl]-2,5-diphenyltetrazolium bromide (MTT) was prepared in cell media and sterilized via filtration. Media were removed from cells, and 50 μL of MTT solution was then added into each well and incubated in the dark at 37°C for 4 h. MTT solution was removed, and MTT dye of each well was dissolved in 50 μL of DMSO with agitation. The absorbance was measured at 562 nm to determine the IC_{50} (concentration of alsterpaullone which inhibits cell growth by 50%). HeLa cells (5×10^3/well) were seeded in 96-well plates and incubated overnight, pretreated with 50 μL of Z-VAD-FMK (final concentration was 25 μM) for 2 h to block caspase activity, and treated with alsterpaullone for 72 h.

HeLa cells (5×10^3/well) were seeded in 96-well plates and incubated overnight and pretreated with 50 μL Z-VAD-FMK (final concentration was 25 μM) for 2 h to block caspase activity, followed by alsterpaullone treatment for 72 h. Cells were evaluated by MTT assay.

2.4. Cell Cycle Analysis and Detection of Apoptosis. Cells were treated with control (0.3% DMSO) and 20 μM alsterpaullone. Both detached and adherent cells were harvested at 0, 12 h, 24 h, 48 h, and 72 h and washed twice with ice-cold phosphate buffered saline (PBS) and then fixed in ice-cold 70% v/v ethanol for more than 2 h. Cells were washed twice in PBS to remove fixative and stained with 1 mL PI (propidium iodide)/Triton X-100 PBS solution with RNase A. After incubation at room temperature for 30 min, cells were filtered through 95 μm pore size nylon mesh. The analyses of cell cycle and apoptosis were analyzed using Flow cytometry. For each sample 10000 events were stored. The fractions of the cells in G_0/G_1, S, G_2/M phases were analyzed using cell cycle analysis software, winMDI v2.8 (Windows Multiple Document Interface for Flow Cytometry) (The Scrips Research Institute, La Jalla, CA, USA).

2.5. Protein Extraction and Western Immunoblotting. HeLa cells were cultured with 20 μM alsterpaullone for 0, 2, 4, 6, 12, and 24 h. After incubation, the nonadherent and adherent cells were harvested. The cells were lysed in RIPA lysis buffer (150 mmol/L NaCl, 1% NP-40, 0.5% Deoxycholate, 0.1% SDS, 50 mM pH 7.5 Tris-HCl, 1% protease inhibitor cocktail (Cat no: 539134, Merck)). The protein concentrations in the different samples were determined using the BCA protein assay kit (Pierce, Rockford, USA). Lysates (50 μg) were fractionated by SDS-PAGE using 8%–15% polyacrylamide gels, based upon the expected molecular weight. The resolved proteins were blotted to a nitrocellulose membrane by semi-dry electric transfer, and the membranes were blocked for 1 h in TBST buffer containing 5% blotting-grade non-fat milk. Membranes were incubated with primary antibodies diluted in 0.1% TBST overnight. Primary antibodies against caspase-3 (Cat no: 552785), PARP [Poly(ADP-ribose) Polymerase] (Cat no: 556494), and Mcl-1 (Cat no: 559027) were purchased from BD Pharmingen (BD Biosciences, San Jose, CA, USA). Survivin (Cat no: sc-17779), Bcl-2 (Cat no: sc-7382), p-Rb (Cat no: sc-12901), and p21 (Cat no: sc-817) were purchased from Santa Cruz (Santa Cruz Biotechnology, Inc. CA, USA). Membranes were washed three times in TBST for 10 min each time and then incubated in TBST containing the appropriate horseradish peroxidase conjugated anti-mouse or anti-rabbit secondary antibodies (Amersham Life Science, USA) for 1 h. The membranes were washed three times for 10 min each in TBST. The bound antibody complex was detected using an ECL chemiluminescence reagent and XAR film (Kodak, Japan) according to the manufacturer's instructions (Amersham Life Science, USA). Equal loading of samples was confirmed by probing for α-tubulin.

2.6. Statistics. All experiments were performed at least in triplicate. Data were represented as mean ± SD. Student's t-test was used for statistical analysis. A P value of <0.05 strongly statistically significant, and $P < 0.01$ was considered very statistically significant.

3. Results

3.1. Alsterpaullone Inhibited the Growth of HeLa Cells in Dose- and Time-Dependent Manner. The growth of HeLa cells was inhibited in a dose-dependent manner after exposures to alsterpaullone for 48 h and 72 h ranging from 0 to 30 μM

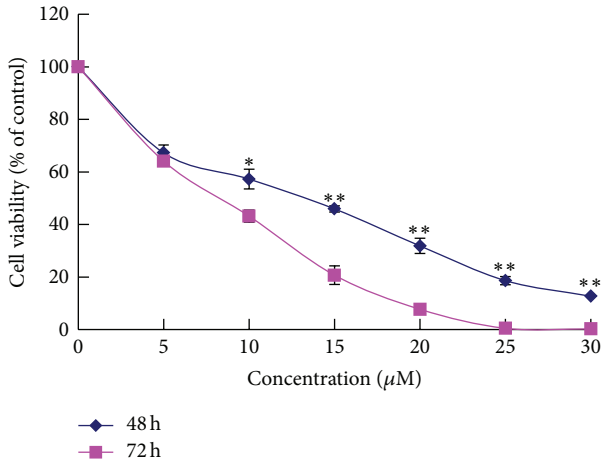

Figure 1: Effects of different concentration of alsterpaullone on the viability in treated HeLa cells. Results are expressed as mean ± SD of three independent experiments. $^{*}P < 0.05$ for statistical significance; $^{**}P < 0.01$ for very statistical significance.

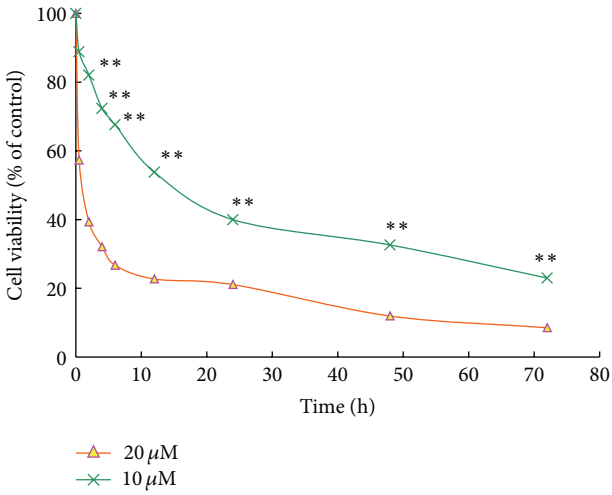

Figure 2: Effects of different time of alsterpaullone on the viability in treated HeLa cells. Results are expressed as mean ± SD of three independent experiments. $^{*}P < 0.05$ for statistical significance, and $^{**}P < 0.01$ for very statistical significance.

(Figure 1). The antiproliferation effect was evaluated by measuring the growth rates of HeLa cells seeded at 5×10^4/well in 24-well plates and treated with 10 μM and 20 μM alsterpaullone (Figure 2). Treatment with alsterpaullone caused a time-dependent inhibition of cell growth too. Cytotoxicity was determined by MTT assay following 72 h incubation with alsterpaullone. The IC_{50} value of HeLa cells was 13.80 ± 3.30 μM. Alsterpaullone showed a significant inhibition on HeLa cell proliferation from 10 μM (dose dependent) while from 2 h onwards (time dependent). The results indicate alsterpaullone is a cytotoxic agent in HeLa cells.

3.2. Alsterpaullone-Induced Apoptosis on HeLa is Caspase Dependent. To explore if the alsterpaullone-induced apoptotic levels are dependent on caspase activation, we

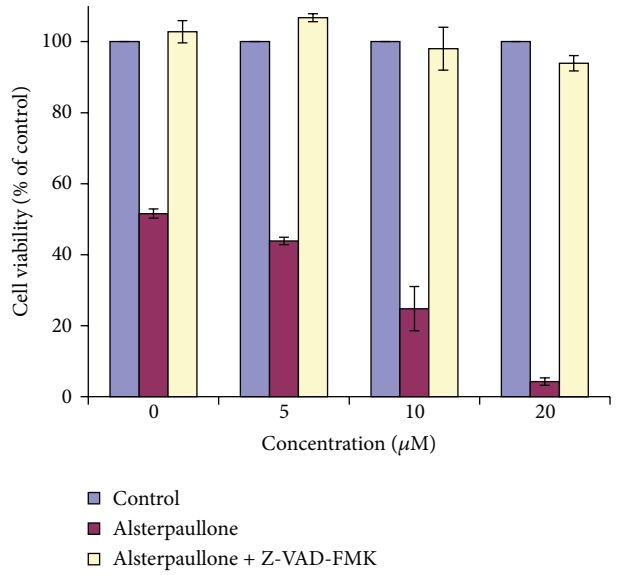

Figure 3: Effects of caspase inhibitor Z-VAD-FMK on apoptotic action induced by 0, 5, 10, and 20 μM alsterpaullone in HeLa cells. Results are given as percentage of viable cells 72 h after the indicated treatment and correspond to mean ± SD.

cultured cells for 72 h with or without alsterpaullone (0 μM, 5 μM, 10 μM, and 20 μM) in the presence or absence of the general caspase inhibitor VI, Z-VAD-FMK. Viable cells were measured by MTT assay. The apoptotic cells decreased after pretreatment with Z-VAD-FMK, suggesting that Z-VAD-FMK blocks the alsterpaullone-induced apoptosis. The results indicated that alsterpaullone induced apoptosis via caspase-dependent process (Figure 3).

3.3. Alsterpaullone Induced G_2/M Arrest of HeLa Cells. We analyzed the cell cycle profiles of growing HeLa cells exposed to 20 μM alsterpaullone using flow cytometry of propidium iodide stained nuclei. We found the cell cycle arrest occurred at G_2/M and then apoptosis was induced. Figure 4 showed a marked increase in the cells with G_2 contents at 12 h and then the occurrence of significant cell death. The cell cycle G_2/M arrest persisted and was followed by a sub-G_1 content increase at 48 h as indicated with cell death. The results indicated the mechanism of antiproliferative effects of alsterpaullone blocked cell cycle progression.

3.4. Apoptotic Proteins in Alsterpaullone-Treated HeLa cells. To understand the role of alsterpaullone in cervical cancer apoptosis, we performed a time-course study on the apoptotic proteins in 20 μM alsterpaullone treated HeLa cells. As indicated in Figure 5, the cleavage of PARP started at 4 h, while the activation of caspase-3 occurred at 2 h. PARP, a prominent substrate for several caspases, was cleaved in time-dependent fashion indicating the occurrence of apoptosis in alsterpaullone treated cells. Furthermore, direct caspase-3 activation was found in HeLa cells by the cleavage of procaspase-3. Inhibition of caspase activity by the caspase

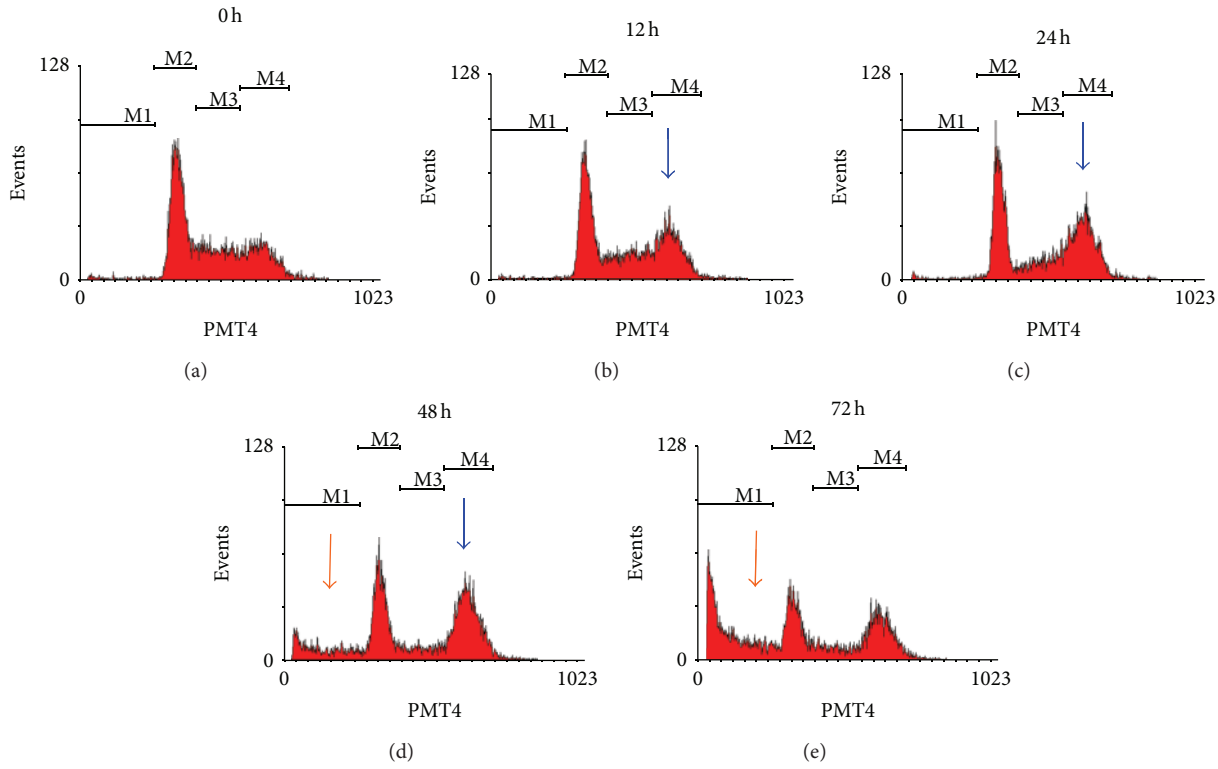

FIGURE 4: Effects of alsterpaullone on the cell cycle in HeLa cells. Blue arrow: G_2/M cell cycle arrest; red arrow: sub-G_1 increase indicating apoptosis occurred. HeLa cells were sensitive to alsterpaullone and arrested in G_2/M prior to undergoing apoptosis.

inhibitor Z-VAD-FMK suggests that alsterpaullone induces cell death depending on caspase activity.

Bcl-2 family proteins play a central role in controlling the mitochondrial pathway, including proteins that suppress apoptosis process (Bcl-2, Mcl-1). In this study a dramatic decline was seen in expression of Mcl-1 which was undetectable at 2 h onwards. The same trend was also observed in survivin but hardly detectable until 24 h. By contrast, the expression of anti-apoptotic protein Bcl-2 was unchanged all the time. These results suggest that the apoptosis induced by alsterpaullone was associated with loss in anti-apoptotic proteins such as Mcl-1 and survivin but not Bcl-2. In alsterpaullone-treated HeLa cells, the levels of pRB kept downregulated overtime whereas p21 upregulated (Figure 5).

4. Discussion

Alsterpaullone, as a Cdk inhibitor, competes with ATP for its binding site on Cdks [7, 8]. Alsterpaullone treatment induced not only cell cycle arrest but also apoptosis in various cell lines [5, 9, 10]. In this study, we showed for the first time that the novel CDK inhibitor, alsterpaullone, inhibited HeLa cell proliferation in a dose- and time-dependent manner. Alsterpaullone induced apoptosis rapidly in HeLa cells by a mechanism that regulates various proteins including anti-apoptotic proteins and cell cycle related proteins.

We found that alsterpaullone exhibited significant cytotoxicity towards HeLa cells, using Flow cytometry and Western blotting: HeLa cells were treated with alsterpaullone arrested in G_2/M phase prior to apoptosis. This inhibition also led to a drop in S-phase population in HeLa cells and thus disturbed cells' DNA replication [9, 10].

Apoptosis is an important approach through which chemotherapeutic compounds inhibit the growth of tumour cells. Cell death initiated by chemotherapeutic agents usually involves the mitochondrial pathway and releases proapoptotic factors to activate effector caspases, which cause DNA fragmentation and apoptosis [11, 12]. In this study, the results demonstrated the roles of apoptotic proteins in inhibition of alsterpaullone on HeLa cells. Mcl-1 is a short-lived protein because the PEST sequences present with the Bcl-2 family member, and it is an important anti-apoptotic protein [13, 14]. In the current study, we found that Mcl-1 protein was rapidly down-regulated and even undetectable as early as 2 h in HeLa cells. In studies by Lahusen et al., alsterpaullone did not regulate the expression of IAP, a member of XIAP family, in Jurkat cells and MCF10A cells [5, 15]. On the contrary, our results showed alsterpaullone continuously diminished the expression of survivin within 24 h, which is a member of the inhibitors of caspase (IAP) family. Therefore, in order to determine whether p21 protein plays a role in inhibiting cell proliferation, it was measured in alsterpaullone treated HeLa cells using Western blotting. The results showed that p21 protein was up-regulated during 2–24 h. Considering the essential role of p21 in G_0/G_1 cell cycle arrest and cleaved caspase-3 for apoptosis induction, we explored the PARP and caspase 3 proteins expression. The results showed the regulation of p21 was significantly earlier than that of caspase

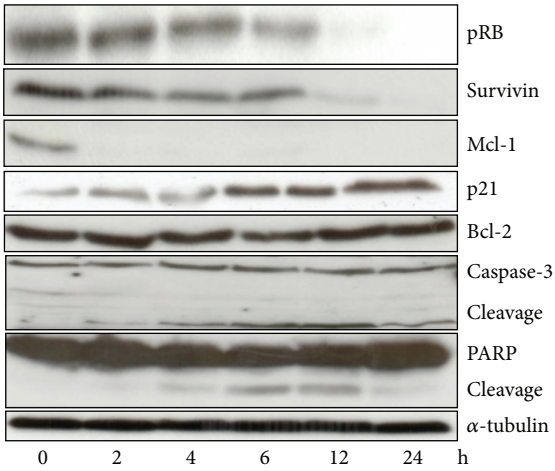

Figure 5: Western blot analysis of apoptotic related proteins in HeLa cells treated with alsterpaullone. HeLa cells were cultured with 20 μM alsterpaullone. Cells were then lysed and protein extracted. The proteins (50 μg) were then subjected to SDS-PAGE immunoblot analysis with the use of antibodies specific for α-tubulin, survivin, Mcl-1, PARP, pRB, Bcl-2, and Caspase-3. Cells were also exposed to 0.3% DMSO and showed stable basal levels of the various proteins at the different time points.

3 and PARP. As such, we speculated p21 was involved in cell cycle arrest, apoptosis, and growth inhibition via activation of caspase-3.

In summary, alsterpaullone can inhibit tumour cell proliferation in a dose-dependent and time-dependent manner and exhibit significant cytotoxicity in HeLa cells. It can induce rapid apoptosis and block cell cycle via regulation of various apoptotic proteins and activation of caspase. The significance behind this in vitro finding is that it suggests the possibility of using alsterpaullone as a new chemotherapeutic agent in the fight against cervical cancer.

Conflict of Interests

The authors report no conflict of interests in this work.

Acknowledgment

This work was finished in Beijing Area Major Laboratory of Peptide & Small Molecular Drugs and supported by the Importation and Development of High-Caliber Talents Project of Beijing Municipal Institutions and Basic-Clinical Key Research Grant (11JL02) from Capital Medical University.

References

[1] F. Zagouri, T. N. Sergentanis, D. Chrysikos, M. Filipits, and R. Bartsch, "Molecularly targeted therapies in cervical cancer. A systematic review," *Gynecologic Oncology*, vol. 26, no. 2, pp. 291–303, 2012.

[2] U. Saxena, C. Sauvaget, and R. Sankaranarayanan, "Evidence-based screening, early diagnosis and treatment strategy of cervical cancer for national policy in low-resource countries: example of India," *Asian Pacific Journal of Cancer Prevention*, vol. 13, no. 4, pp. 1699–1703, 2012.

[3] C. M. Martin and J. J. O'Leary, "Histology of cervical intraepithelial neoplasia and the role of biomarkers," *Best Practice & Research Clinical Obstetrics & Gynaecology*, vol. 25, no. 5, pp. 605–615, 2011.

[4] N. Takai, N. Kira, T. Ishii, M. Nishida, K. Nasu, and H. Narahara, "Novel chemotherapy using histone deacetylase inhibitors in cervical cancer," *Asian Pacific Journal of Cancer Prevention*, vol. 12, no. 3, pp. 575–580, 2011.

[5] T. Lahusen, A. de Siervi, C. Kunick, and A. M. Senderowicz, "Alsterpaullone, a novel cyclin-dependent kinase inhibitor, induces apoptosis by activation of caspase-9 due to perturbation in mitochondrial membrane potential," *Molecular Carcinogenesis*, vol. 36, no. 4, pp. 183–194, 2003.

[6] V. B. Arion, A. Dobrov, S. Göschl, M. A. Jakupec, B. K. Keppler, and P. Rapta, "Ruthenium- and osmium-arene-based paullones bearing a TEMPO free-radical unit as potential anticancer drugs," *Chemical Communications*, vol. 48, no. 68, pp. 8559–8561, 2011.

[7] P. Rivest, M. Renaud, and J. T. Sanderson, "Proliferative and androgenic effects of indirubin derivatives in LNCaP human prostate cancer cells at sub-apoptotic concentrations," *Chemico-Biological Interactions*, vol. 189, no. 3, pp. 177–185, 2011.

[8] D. V. Soni and J. W. Jacobberger, "Inhibition of cdk1 by alsterpaullone and thioflavopiridol correlates with increased transit time from mid G2 through prophase," *Cell Cycle*, vol. 3, no. 3, pp. 349–357, 2004.

[9] E. A. Sausville, J. Johnson, M. Alley, D. Zaharevitz, and A. M. Senderowicz, "Inhibition of CDKs as a therapeutic modality," *Annals of the New York Academy of Sciences*, vol. 910, pp. 207–222, 2000.

[10] M. Trevino, D. J. Stefanik, R. Rodriguez, S. Harmon, and P. M. Burton, "Induction of canonical Wnt signaling by alsterpaullone is sufficient for oral tissue fate during regeneration and embryogenesis in *Nematostella vectensis*," *Developmental Dynamics*, vol. 240, pp. 2673–2679, 2011.

[11] A. Fabres, C. P. de Andrade, M. Guizzo et al., "Effect of GSK-3 activity, enzymatic inhibition and gene silencing by RNAi on tick oviposition and egg hatching," *Parasitology*, vol. 137, no. 10, pp. 1537–1546, 2010.

[12] S. Soto, E. Vaz, C. Dell'Aversana, R. Álvarez, L. Altucci, and A. R. de Lera, "New synthetic approach to paullones and characterization of their SIRT1 inhibitory activity," *Organic and Biomolecular Chemistry*, vol. 14, no. 10, pp. 2101–2112, 2012.

[13] B. R. Seo, K. J. Min, S. Kim et al., "Anisomycin treatment enhances TRAIL-mediated apoptosis in renal carcinoma cells through the down-regulation of Bcl-2, c-FLIP(L) and Mcl-1," *Biochimie*, vol. 12, no. 20, pp. 1–8, 2012.

[14] J. Selent, A. A. Kaczor, R. Guixà-González, P. Carrió, M. Pastor, and C. Obiol-Pardo, "Rational design of the survivin/CDK4 complex by combining protein-protein docking and molecular dynamics simulations ," *Journal of Molecular Modeling*. In press.

[15] D. W. Zaharevitz, R. Gussio, M. Leost et al., "Discovery and initial characterization of the paullones, a novel class of smallmolecule inhibitors of cyclin-dependent kinases," *Cancer Research*, vol. 59, no. 11, pp. 2566–2569, 1999.

Hindawi Publishing Corporation
Journal of Analytical Methods in Chemistry
Volume 2012, Article ID 364013, 6 pages
doi:10.1155/2012/364013

Research Article

HPLC Method Determination of Isoliquiritin Apioside and Isoliquiritin in Rat Plasma for Application in Pharmacokinetic Study after an Oral Administration of Zhigancao Extract

Yan-yun Yang,[1] Liang Xu,[2] Song-yao Hao,[1] Yan Li,[1] and Zhen-Qiu Zhang[1]

[1] *School of Medicine, Liaoning University of Traditional Chinese Medicine, Dalian 116600, China*
[2] *Department of Medicinal Plant, Liaoning University of Traditional Chinese Medicine, Dalian 116600, China*

Correspondence should be addressed to Zhen-Qiu Zhang, 99yyy@163.com

Received 27 September 2012; Revised 27 November 2012; Accepted 29 November 2012

Academic Editor: Shuang-Qing Zhang

A sensitive HPLC method was developed for the quantitative determination of isoliquiritin apioside (ILA) and isoliquiritin (IL) in rat plasma. After protein precipitation with acetonitrile, chloroform was used to separate lipid-soluble impurities from the plasma samples and remove acetonitrile. A chromatography was carried out on Diamonsil C18 (150×4.6 mm; 5 μm) analytical column, using a mobile phase consisting of water (containing phosphoric acid 0.1%, v/v); acetonitrile (72 : 28, v/v) at a flow rate of 1.0 mL/min. The wavelength-switching technology was performed to determine ILA and IL at 360 nm and wogonoside (internal standard, IS) at 276 nm. The calibration curves of ILA and IL were fairly linear over the concentration ranges of 0.060–3.84 μg/mL ($r = 0.9954$) and 0.075–4.80 μg/mL ($r = 0.9968$), respectively. The average extract recoveries of ILA, IL, and IS were all over 80%. The precision and accuracy for all concentrations of quality controls and standards were within 15%. The lower limit of quantification (LLOQ) was 0.060 μg/mL for ILA and 0.075 μg/mL for IL. The method was used in pharmacokinetic study after an oral administration of Zhigancao extract to rats.

1. Introduction

Zhigancao, Glycyrrhizae Radix et Rhizoma Praeparata cum Melle, originates from the processed dried roots or rhizomes of *Glycyrrhriza uralensis* Fisch., *G. inflata* Bat., or *G. glabra* L. (family Fabaceae). It is most frequently used in traditional Chinese medical formulary to harmonize all drugs and detoxify the adverse effects of herbs. Clinically, it treats disorders such as shortness of breath, fatigue, epigastria and abdominal pain, musculoskeletal and smooth muscle cramp and pain, and diarrhea [1]. Due to the numerous bioactive compounds in it such as terpenoids, saponins, polysaccharides, and flavonoids, Zhigancao has been reported to possess anti-inflammatory activities [2], antioxidative [3, 4], neuroprotective [5], antiallergic [6], anticonvulsant activities [7], and so forth. Two chalcone derivatives in Figure 1, isoliquiritin apioside (ILA) and isoliquiritin (IL), which are important ingredients in Zhigancao, are selected to research their pharmacokinetics. ILA has shown the pharmacological activity to reduce oxidative stress-induced genotoxicity [8]. And IL has been reported to have shown various pharmacological activities such as antiangiogenic effect dependent upon antitube formation [9], antidepressant-like effects in mice induced by forced swimming and tail suspension [10], and inhibitory effects on tyrosinase [11].

The bioavailability of drugs is the cornerstone for extending their in vitro biological functions to humans in vivo. The flavonoid glycosides show low oral bioavailability possibly because of the extensive conjugation of the free hydroxyl groups [12–14] or/and glycosides hydrolysis to the aglycones in the intestinal lumen [14–16]. The pharmacokinetic study of ILA and IL is essential for us to comprehend the bioavailability of two analytes after an oral administration of Zhigancao extrat.

To my knowledge, ILA and IL quantification method (LC-MS/MS) has been performed to study pharmacokinetics of multiple licorice flavonoids after an oral dose of Xiaochaihu-tang to rats [17], but LC-MS/MS method

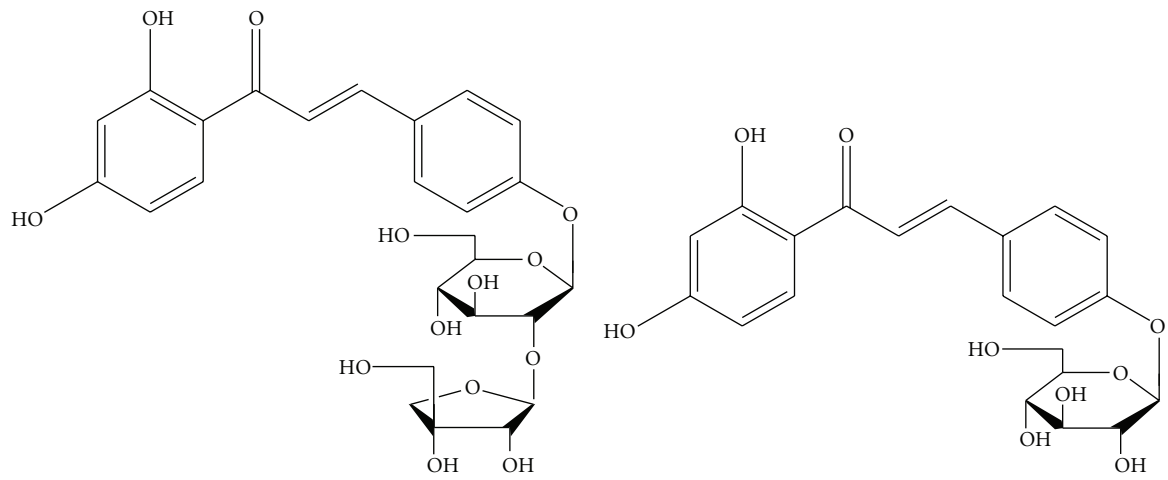

Figure 1: Isoliquiritin apioside (a) and isoliquiritin (b).

is simply not available in most laboratories. In this study, we established the HPLC method which was highly selective and sensitive for simultaneous quantification of ILA and IL in rat plasma. The method was used to explore the possible pharmacokinetics of ILA and IL after an oral administration of Zhigancao extract.

2. Experimental

2.1. Reagents and Chemicals. Isoliquiritin apioside (ILA) and isoliquiritin (IL) were purchased from Xi'an Xiaocao Botanical Development Co., Ltd. (purity > 98%, Shanxi, China). Wogonoside (internal standard, IS) was obtained from National Institute for Food and Drug Control (Beijing, China). Zhigancao which was produced under the guidance of the theory of traditional Chinese medicine science was provided by Chifeng Xinzhou Traditional Chinese Medicine Co., Ltd. (Inner Mongolia, China). The material was authenticated as the dried roots of *G. uralensis* by professor Ting-guo Kang from Liaoning University of Traditional Chinese Medicine. HPLC grade acetonitrile and analytical grade chloroform were purchased from Shandong Yuwang Chemical Industry Co., Ltd. (Shandong, China). The water in the study was purified with a Milli-Q water purification system from Millipore (Bedford, USA).

2.2. Preparation of the Zhigancao Extract. Powdered herb materials were extracted twice under reflux condition with 70% ethanol (1 : 10, w/v) for 1 h under 100°C. The extract was filtered and evaporated. Finally, the residue was dried in vacuum drying oven at 60°C to obtain a powder state of Zhigancao extract. The contents of ILA and IL in the extract were detected by HPLC, 33.72 and 28.17 mg/g, respectively. The dried powder was stored in vacuum dryer before use.

2.3. Liquid Chromatographic Condition. The liquid chromatography system employed was Agilent 1100 with a variable wave length UV detector (G1314A VWD). Data was analyzed by MassHunter software (Agilent, USA). The analytical column employed was Diamonsil C18 (150 × 4.6 mm I.D., 5 μm, Dikma Technologies, China) analytical column with a endcapped C18 ODS guard column. The mobile phase composed of water (containing phosphoric acid 0.1%, v/v) and acetonitrile (72 : 28, v/v) was filtered through 0.22 μm Millipore membrane filter. The flow rate was 1.0 mL/min. The detection wavelength was set at 360 nm (0–9 min) and 276 nm (9–12 min). An injection volume of 20 μL was optimized for final method.

2.4. Preparation of Standard Solution and Quality Control Samples. Stock solutions of IS, ILA and IL with concentrations of 440, 384, and 480 μg/mL, respectively, were prepared in methanol, and stored at 4°C. The working solution for IS was diluted with methanol to get a final concentration of 8.80 μg/mL. Stock solutions were diluted with methanol to serial standard working solutions at concentrations of 0.60, 1.20, 2.40, 4.80, 9.60, 19.2, and 38.4 μg/mL for ILA, 0.75, 1.50, 3.00, 6.00, 12.0, 24.0, 36.0, and 48.0 μg/mL for IL. These solutions were then added to blank plasma (1 : 10) to make standards of 0.060–3.84 μg/mL for ILA and 0.075–4.80 μg/mL for IL. The quality control (QC) samples which were used for the intra- and inter-day accuracy, and precision, extraction recovery and stability study, were prepared in the same way at 0.12, 0.48 and 3.07 μg/mL for ILA, and 0.15, 0.60 and 3.84 μg/mL for IL.

2.5. Sample Preparations. The 200 μL of rat plasma was mixed with 20 μL IS working solution. After protein was precipitated with 500 μL of acetonitrile in a 1.5 mL polypropylene tube by vortexing for 3 min, the sample was centrifuged at 6,677 g for 5 min. The supernatant was transferred into a 2.0 mL tube and was added with 1,000 μL of chloroform. After vortexing and centrifugation, 20 μL of water phase was injected for analysis.

2.6. Method Validation. The analysis method was completely validated using spiked rat plasma samples, including selectivity, linearity, intra- and inter-day precision, accuracy and stability, according to the FDA guideline for method validation of bioanalytical assays [18].

The selectivity of the method was demonstrated by comparing chromatograms of blank plasma samples (without IS) obtained from rats, plasma samples spiked with the analytes and IS, and plasma samples after an oral dose. All blank plasma samples were prepared and analyzed to ensure the absence of interfering peaks.

The linearity of the method was assessed by plotting calibration curves in plasma at seven concentration levels in triplicate on three consecutive days. The lower limit of quantification (LLOQ) was defined as the lowest concentration of the calibration curve, that was measured with accuracy and precision by analyzing samples in six replicates at the concentration of 0.060 μg/mL for ILA and 0.075 μg/mL for IL.

Precision and accuracy were evaluated by determining QC samples at three concentrations in six replicates on the same day (intra-day accuracy and precision) and three consecutive days (inter-day accuracy and precision). Accuracy was measured by relative error (RE) and precision was evaluated by intra- and inter-day relative standard deviation (RSD).

The extraction recovery was evaluated by comparing the peak areas of the extracted QC samples at three concentrations in six replicates with those of unextracted standards that represented 100% recovery. Similarly, the recovery of IS was evaluated at a single concentration of 0.88 μg/mL in the same way.

The stability of ILA and IL in rat plasma was evaluated by comparing the mean of back-calculated concentration of the stored QC samples at three concentrations in triplicate with the spiked concentration of analytes. The QC samples treated as sample preparation were kept at room temperature for 12 h and then the stability was determined. The freeze-thaw stability was determined afterthree freeze (–20°C, 24 h) and thaw (room temperature) cycles. Long-term stability was assessed by keeping QC samples at –20°C for 15 days.

2.7. Applications in Pharmacokinetic Study

2.7.1. Sample Collection. Female Sprague-Dawley rats (200 ± 20 g) were kept in environmental controlled breeding room for 7 days until the experiment. The rats were fasted for 12 h but allowed water ad libitum before the Zhigancao extract was orally administered at a dose of 1.21 g/kg. Orbital venous blood samples (0.5 mL) were collected before dosing, and at 0.5, 1.0, 1.5, 2, 3, 4, 6, 8, 12, 24, 36, and 48 h after an administration. After centrifuging at 6,677 g for 5 min, the plasma samples were obtained and frozen at –20°C until analysis.

2.7.2. Pharmacokinetic Analysis. HPLC analysis procedure was applied to analyze plasma concentration-time profiles of ILA and IL. Data was processed by noncompartmental method using Drug and Statistics (DAS) 2.0 software package (Chinese Pharmacological Society, Shanghai, China).

3. Results

3.1. Method Validation. The selectivity was evaluated by analyzing blank samples, spiked samples at LLOQ, and middle QC levels, and actual samples obtained from rats after an oral administration of Zhigancao extract. The typical HPLC chromatograms were shown in Figure 2. For all blank samples, ILA, IL, and IS retention windows were free from endogenous interfering peaks. No plasma matrix effect was observed under the condition described above.

The calibration curves were linear over the concentration range of 0.060–3.84 μg/mL for ILA and 0.075–4.80 μg/mL for IL by weighted ($1/x^2$) linear least-squares regression method. The correlation coefficient values of the calibration curves were over 0.995. The REs of the back-calculated values of the standards from their nominal values were constantly within 15% for all values, including the LLOQ. The LLOQ measurement showed the respective averages 0.060 μg/mL with RSD 14.5% for ILA and 0.077 μg/mL with RSD 12.3% for IL. The typical chromatogram at the LLOQ was shown in Figure 2(b). Typical regression equations were calculated as follows: ILA, $y = 1.024x - 0.004$ ($r = 0.9954$); IL, $y = 1.004x + 0.007$ ($r = 0.9968$).

The precision and accuracy data was shown in Table 1. The intra- and inter-day RSD values were lower than 10%, and the RE values were within ±5%. The results revealed satisfactory precision and accuracy of this present method.

The extraction recoveries of ILA and IL from rat plasma were 79.5 ± 4.2%, 82.5 ± 4.4%, 84.7 ± 4.0% at 1.2, 4.8, and 3.07 μg/mL and 81.3 ± 4.9%, 82.3 ± 6.6%, 86.4 ± 3.4% at 1.5, 6.0, and 3.84 μg/mL, respectively. The extraction recovery of IS was 81.8 ± 3.2%. These results indicated that the extraction method was suitable to extract ILA, IL, and IS from plasma.

All stability tests showed sufficient stability of ILA and IL under various test conditions. As shown in Table 2, stability of analytes showed no significant sample loss over 12 h at room temperature, three freeze-thaw cycles, and 15 days storage condition.

3.2. Pharmacokinetic Study. The developed method was applied in pharmacokinetic study of ILA and IL in rat plasma after an oral administration of Zhigancao extract (at a dose containing 40.8 mg/kg ILA and 34.1 mg/kg IL, resp.). The mean plasma concentration-time profiles ($n = 6$) were shown in Figure 3. The pharmacokinetic parameters were shown in Table 3. The assay was sensitive enough for the determination of ILA and IL in rat plasma after an oral administration of Zhigancao extract.

4. Discussion

In this study, we established an HPLC method to simultaneously quantify ILA and IL in rat plasma. Due to the stronger polarity of ILA and IL, protein precipitation was

Table 1: Intraday and interday precision and accuracy for QC samples.

Analyte	Spiked concentration (μg/mL)	Measured concentration (μg/mL)	Intraday ($n = 6$) RSD (%)	RE (%)	Measured concentration (μg/mL)	Interday ($n = 3$) RSD (%)	RE (%)
ILA	0.12	0.12 ± 0.01	6.2	−3.6	0.12 ± 0.01	9.0	0.4
	0.48	0.46 ± 0.02	5.6	−3.4	0.48 ± 0.03	7.0	−0.8
	3.07	3.08 ± 0.16	5.4	0.2	3.02 ± 0.16	4.8	0.7
IL	0.15	0.15 ± 0.01	5.9	1.4	0.15 ± 0.01	9.7	−2.3
	0.6	0.62 ± 0.03	6.8	3.1	0.61 ± 0.04	6.8	1.0
	3.84	3.78 ± 0.24	5.0	−1.7	3.73 ± 0.18	3.5	−2.7

(Inter-day) RSD = $(\sqrt{(\sum_{i=1}^{I}\sum_{j=1}^{n}(X_{ij}-\overline{X}_{..})^2 - n\sum_{i=1}^{I}(\overline{X}_{i.}-\overline{X}_{..})^2)/(N-I)}/\overline{X}_{..}) \times 100\%$, (Inter-day) RSD = $(\sqrt{n\sum_{i=1}^{I}(\overline{X}_{i.}-\overline{X}_{..})^2/(I-1)}/\overline{X}_{..}) \times 100\%$.

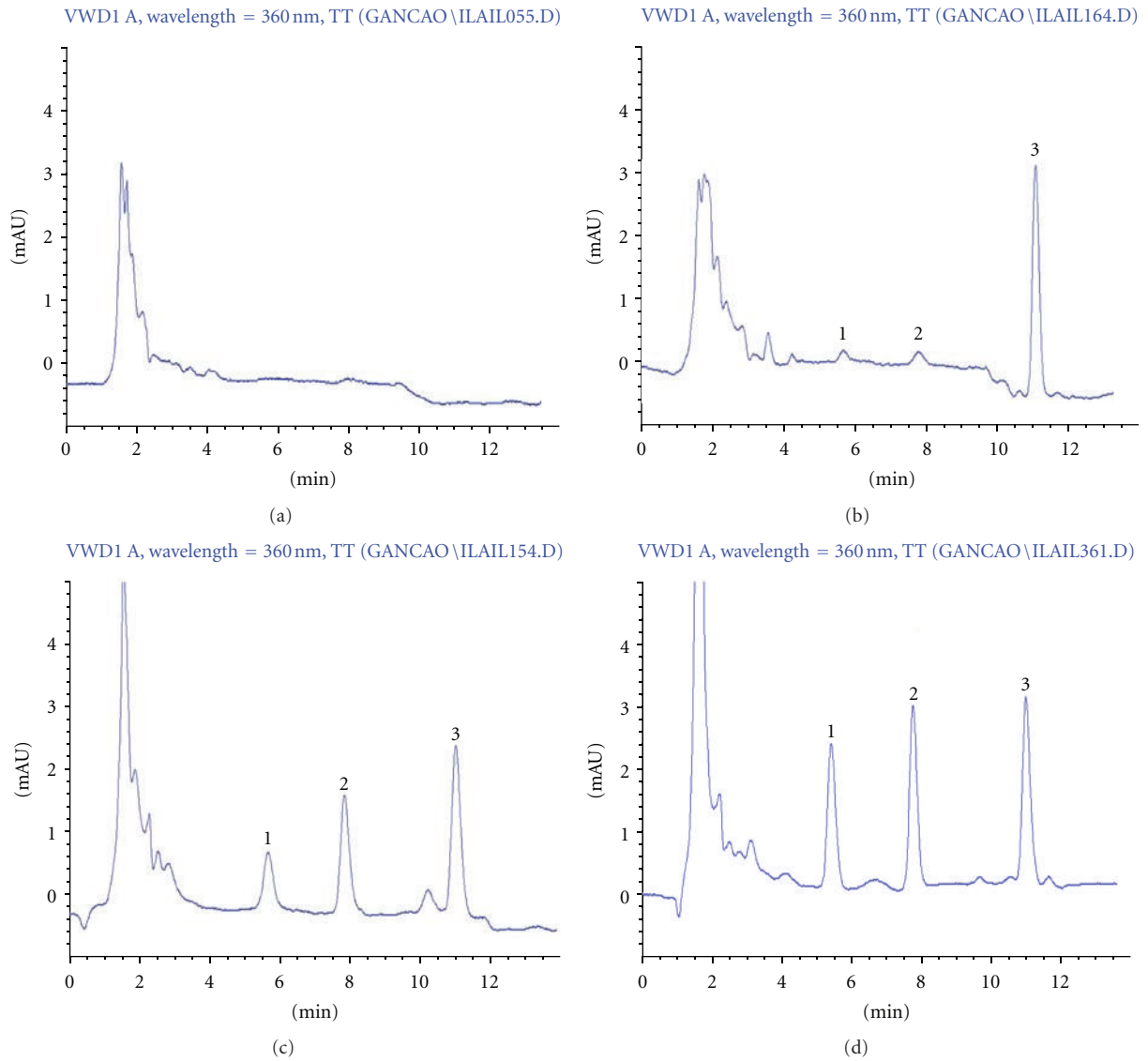

Figure 2: Typical HPLC chromatograms of the analytes in rat plasma (1, ILA; 2, IL; 3, IS). (a) Chromatogram of blank plasma; (b) chromatogram of plasma sample at LLOQ level (ILA 0.060 μg/mL and IL 0.075 μg/mL); (c) chromatogram of plasma sample at middle QC level (ILA 0.48 μg/mL and IL 0.60 μg/mL); (d) chromatogram of plasma sample obtained from rat (No. 2) at 1 h after an oral administration of Zhigancao extract (ILA 0.78 μg/mL and IL 1.04 μg/mL by calculation).

Table 2: Stability of ILA and IL under various conditions in plasma ($n = 3$).

Analyte	Spiked concentration (μg/mL)	Stored at room temperature for 12 h Measured concentration (μg/mL)	RE (%)	Three freeze-thaw stability Measured concentration (μg/mL)	RE (%)	Stored at -20°C for 15 days Measured concentration (μg/mL)	RE (%)
ILA	0.12	0.12 ± 0.001	2.7	0.12 ± 0.003	−0.5	0.12 ± 0.002	−0.5
	0.48	0.48 ± 0.008	−3.6	0.45 ± 0.018	−5.6	0.48 ± 0.002	0.07
	3.07	3.07 ± 0.028	0.03	2.91 ± 0.029	−5.2	2.97 ± 0.006	−3.2
IL	0.15	0.16 ± 0.005	4.3	0.16 ± 0.006	3.9	0.15 ± 0.004	−2.6
	0.6	0.59 ± 0.015	−1.1	0.62 ± 0.019	2.7	0.57 ± 0.010	−4.4
	3.84	3.82 ± 0.065	−0.4	3.85 ± 0.077	0.19	3.72 ± 0.157	−3.2

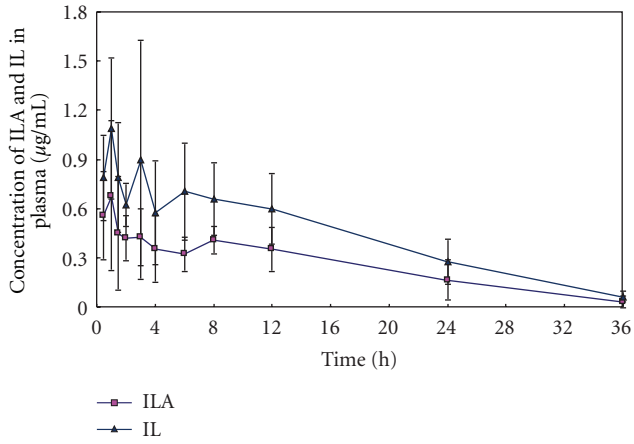

Figure 3: Mean plasma concentration-time profiles ($n = 6$) after an oral administration of Zhigancao extract.

Table 3: Pharmacokinetic parameters of ILA and IL in following an oral administration of Zhigancao extract. The C_{max} was the measured maximal concentration of ILA and IL, and the t_{max} was the time to reach maximal concentration of ILA and IL, obtained directly from the observed value. Plasma concentrations in the terminal phase for each subject were fit to a log-linear regression by the method of least squares to obtain the elimination rate constant (k_e). The $t_{1/2z}$ value was calculated with the following formula: $t_{1/2} = \ln(2)/k_e$. The AUC_{0-t} value was the area under the concentration-time curve from 0 to 36 h (calculated using the linear trapezoidal rule), and $AUC_{0-\infty}$ value was calculated using the formula: $AUC_{0-\infty} = AUC_{0-t} + C_{last}/k_e$, where C_{last} was the last measurable concentration. The mean residence time (MRT) was obtained from the formula AUMC/AUC (AUMC-area under the concentration × time curve), and $MRT_{0-\infty}$ was calculated using the formula: $MRT_{0-\infty} = AUMC_{0-\infty}/AUC_{0-\infty}$.

Parameter	ILA	IL
C_{max} (μg/mL)	0.88 ± 0.34	1.45 ± 0.47
T_{max} (h)	2.08 ± 2.11	1.92 ± 2.06
$t_{1/2z}$ (h)	8.12 ± 1.72	8.56 ± 1.17
AUC_{0-t} (μg/mL ∗ h)	8.93 ± 3.06	15.39 ± 3.91
$AUC_{0-\infty}$ (μg/mL ∗ h)	9.49 ± 3.35	16.20 ± 4.23
MRT_{0-T} (h)	11.17 ± 2.72	11.53 ± 1.66
$MRT_{0-\infty}$ (h)	12.27 ± 4.35	13.20 ± 2.34

employed for the extraction of analytes from biological matrix [19]. Acetonitrile and methanol were tested as protein precipitating agent. The recovery with methanol was comparable to acetonitrile, during both processes the analyte concentration in the plasma was diluted when 2.5-fold organic solvent volume was added, so that ILA and IL couldnot be detected at a low concentration. Yet evaporating supernatant to dryness and then dissolving it in a small amount of solvent to increase the concentration would be time-consuming and would cause the loss of analyte. So removing the organic solvent from the supernatant was employed. When the supernatant was added with chloroform, a clear water phase could be obtained by precipitating the protein with acetonitrile, but no stratification could be observed when methanol was used instead of acetonitrile Therefore, plasma samples were processed by precipitating protein with acetonitrile which was then removed with chloroform.

Wogonoside was selected as the IS because of its appropriate retention and extraction recovery. Some other compounds such as rutin, baicalin and hesperidin were also tested with the selected condition above, but without ideal results. Due to its satisfactory separation from the analytes, wogonoside was selected as the IS. Because wogonoside couldnot be detected at 360 nm at the concentration 0.88 μg/mL, the wavelength was switched to 276 nm at 9 min.

The extrapolated fraction of the $AUC_{0-\infty}$ accounted for only 5-6%, which indicated a suitability of the analytical method for ILA and IL pharmacokinetic study. These two analytes exhibited consistent tendencies in plasma concentration-time profiles and similar T_{max}, $t_{1/2z}$ and MRT values after an oral administration of Zhigancao extract. The fact that these two compounds had the similar pharmacokinetic behavior could be tentatively attributed to their having similar structures.

Comparing the pharmacokinetic data of ILA with that of IL, C_{max} and AUC of ILA were lower than that of IL although there was more content of the former in Zhigancao extract. It was possible that ILA could be hydrolysis to the IL in the intestinal tract or transformed into IL after being absorbed.

5. Conclusion

We have developed and validated a selective and sensitive HPLC method for simultaneous quantification of ILA and IL in rat plasma. The method was successfully applied to the pharmacokinetic study of ILA and IL in rat plasma after an oral administration of Zhigancao extract.

Conflict of Interests

The authors declare that they have no conflict of interests.

Acknowledgments

The authors thank Liaoning University of Traditional Chinese Medicine (no. YXRC0920) and Liaoning Department of Science and Technology (no. 20111133) for supporting this study.

References

[1] Chinese Pharmacopeia Committee, *Pharmacopeia of People's Republic of China*, Chinese Medicine Science and Technology Publishing House, Beijing, China, 2010.

[2] J. K. Kim, S. M. Oh, H. S. Kwon, Y. S. Oh, S. S. Lim, and H. K. Shin, "Anti-inflammatory effect of roasted licorice extracts on lipopolysaccharide-induced inflammatory responses in murine macrophages," *Biochemical and Biophysical Research Communications*, vol. 345, no. 3, pp. 1215–1223, 2006.

[3] K. Wojcikowski, L. Stevenson, D. Leach, H. Wohlmuth, and G. Gobe, "Antioxidant capacity of 55 medicinal herbs traditionally used to treat the urinary system: a comparison using a sequential three-solvent extraction process," *Journal of Alternative and Complementary Medicine*, vol. 13, no. 1, pp. 103–109, 2007.

[4] Y. J. Choi, S. S. Lim, J. Y. Jung et al., "Blockade of nitroxidative stress by roasted licorice extracts in high glucose-exposed endothelial cells," *Journal of Cardiovascular Pharmacology*, vol. 52, no. 4, pp. 344–354, 2008.

[5] I. K. Hwang, S. S. Lim, K. H. Choi et al., "Neuroprotective effects of roasted licorice, not raw form, on neuronal injury in gerbil hippocampus after transient forebrain ischemia," *Acta Pharmacologica Sinica*, vol. 27, no. 8, pp. 959–965, 2006.

[6] T. Majima, T. Yamada, E. Tega, H. Sakurai, I. Saiki, and T. Tani, "Pharmaceutical evaluation of liquorice before and after roasting in mice," *Journal of Pharmacy and Pharmacology*, vol. 56, no. 5, pp. 589–595, 2004.

[7] A. Yazdi, S. Sardari, M. Sayyah, and M. H. Ezzati, "Evaluation of the anticonvulsant activity of the leaves of *Glycyrrhiza glabra* var. glandulifera grown in Iran, as a possible renewable source for anticonvulsant compounds," *Iranian Journal of Pharmaceutical Research*, vol. 10, no. 1, pp. 75–82, 2011.

[8] P. Kaur, S. Kaur, N. Kumar, B. Singh, and S. Kumar, "Evaluation of antigenotoxic activity of isoliquiritin apioside from *Glycyrrhiza glabra* L.," *Toxicology In Vitro*, vol. 23, no. 4, pp. 680–686, 2009.

[9] S. Kobayashi, T. Miyamoto, I. Kimura, and M. Kimura, "Inhibitory effect of isoliquiritin, a compound in licorice root, on angiogenesis in vivo and tube formation in vitro," *Biological and Pharmaceutical Bulletin*, vol. 18, no. 10, pp. 1382–1386, 1995.

[10] W. Wang, X. Hu, Z. Zhao et al., "Antidepressant-like effects of liquiritin and isoliquiritin from *Glycyrrhiza uralensis* in the forced swimming test and tail suspension test in mice," *Progress in Neuro-Psychopharmacology and Biological Psychiatry*, vol. 32, no. 5, pp. 1179–1184, 2008.

[11] B. Fu, H. Li, X. Wang, F. S. C. Lee, and S. Cui, "Isolation and identification of flavonoids in licorice and a study of their inhibitory effects on tyrosinase," *Journal of Agricultural and Food Chemistry*, vol. 53, no. 19, pp. 7408–7414, 2005.

[12] C. Manach and J. L. Donovan, "Pharmacokinetics and metabolism of dietary flavonoids in humans," *Free Radical Research*, vol. 38, no. 8, pp. 771–785, 2004.

[13] G. Williamson and C. Manach, "Bioavailability and bioefficacy of polyphenols in humans. II. Review of 93 intervention studies," *The American journal of clinical nutrition*, vol. 81, no. 1, pp. 243S–255S, 2005.

[14] T. Walle, "Absorption and metabolism of flavonoids," *Free Radical Biology and Medicine*, vol. 36, no. 7, pp. 829–837, 2004.

[15] A. J. Day, F. J. Cañada, J. C. Díaz et al., "Dietary flavonoid and isoflavone glycosides are hydrolysed by the lactase site of lactase phlorizin hydrolase," *FEBS Letters*, vol. 468, no. 2-3, pp. 166–170, 2000.

[16] E. U. Graefe, J. Wittig, S. Mueller et al., "Pharmacokinetics and bioavailability of quercetin glycosides in humans," *Journal of Clinical Pharmacology*, vol. 41, no. 5, pp. 492–499, 2001.

[17] L. Li, S. Liang, F. Du, and C. Li, "Simultaneous quantification of multiple licorice flavonoids in rat plasma," *Journal of the American Society for Mass Spectrometry*, vol. 18, no. 4, pp. 778–782, 2007.

[18] U.S. Department of Health and Human Services, Food and Drug Administration, Center for Drug Evaluation and Research (CDER), and Center for Veterinary Medicine (CVM), *Guidance for Industry-Bioanalytical Method Validation*, Center for Drug Evaluation and Research (CDER), Rockville, Md, USA, 2001.

[19] S. Bankey, G. Tapadiya, J. Lamale, D. Jain, S. Saboo, and S. S. Khadabadi, "RP-HPLC method development and its validation for quantitative determination of rimonabant in human plasma," *Journal of Analytical Methods in Chemistry*, vol. 2012, Article ID 625979, 4 pages, 2012.

Hindawi Publishing Corporation
Journal of Analytical Methods in Chemistry
Volume 2012, Article ID 254391, 3 pages
doi:10.1155/2012/254391

Research Article

^{1}H and ^{13}C NMR Assignments of Cytotoxic 3*S*-1,2,3,4-Tetrahydro-*β*-carboline-3-carboxylic Acid from the Leaves of *Cichorium endivia*

Fu-Xin Wang, An-Jun Deng, Jin-Feng Wei, Hai-Lin Qin, and Ai-Ping Wang

Institute of Materia Medica, Chinese Academy of Medical Sciences and Peking Union Medical College, Beijing 100050, China

Correspondence should be addressed to Hai-Lin Qin, qinhailin@imm.ac.cn and Ai-Ping Wang, wangaiping@imm.ac.cn

Received 17 September 2012; Accepted 26 November 2012

Academic Editor: Feng Wei

An amino acid, 3*S*-1,2,3,4-tetrahydro-*β*-carboline-3-carboxylic acid, was isolated for the first time from the leaves of *Cichorium endivia*. The complete assignment of its ^{1}H and ^{13}C NMR spectroscopic data was carried out also for the first time based on extensive 1D and 2D NMR experiments. Cytotoxicity of this isolated compound against HCT-8 and HepG2 human cancer cell lines was evaluated for the first time, with moderate activities being found.

1. Introduction

Cichorium endivia L. is a popular vegetable from the family of Compositae and is widely cultivated and consumed all over the world. Its popularity is also attributed to the healthy properties mainly due to supply of antioxidant activity [1, 2]. However, phytochemical investigation on this plant is very rare up to now, to the best of our knowledge, only a few papers had reported a few compounds, including five ones by our group [3]. The ongoing research aims at confirming the bioactive compounds from this popular vegetable, and a prevailing and known amino acid, 3*S*-1,2,3,4-tetrahydro-*β*-carboline-3-carboxylic acid (**1**), was isolated for the first time. By way of the literature survey, it can be learned that the complete assignment of the NMR data of **1** was very deficient up to now, with no practical conducting being obtained due to the poor solubility of **1** in most prevalent solvents and causing the citation of literatures an obvious state of chaos [4, 5]. In this paper, we describe the complete assignment of the ^{1}H and ^{13}C NMR spectroscopic data of **1** based on the determining of optimized solvent and extensive 1D and 2D NMR experiments. An investigation focusing on the cytotoxicity of compound **1** against HCT-8 and HepG2 human cancer cell lines showed that **1** inhibits the cells growth by a moderate reduction in viability of subjects.

2. Results and Discussion

Compound **1** was isolated as an amorphous pale-yellow powder (MeOH/H_2O). Its positive-ion ESI-MS spectrum showed the quasimolecular ion peaks at m/z 217.1 $[M+H]^+$and 239.1 $[M+Na]^+$, and its molecular formula was established to be $C_{12}H_{12}N_2O_2$ by the quasimolecular ion peak in the positive mode HRESI-MS experiment at m/z 217.0967 $[M+H]^+$. The IR spectrum showed strong absorptions at υ_{max} 3284, 3019, 1642, 1598, 1452, 1409, and 740 cm^{-1}, indicating the presence of 1,2-disubstitued benzene moiety and labile hydrogen. It was preliminarily identified as 3*S*-1,2,3,4-tetrahydro-*β*-carboline-3-carboxylic acid by comparison of the ^{1}H NMR spectroscopic data obtained in DMSO-d_6 with the literature values [4, 5], but some obvious errors or inconsistency were evident, including the coupling constants and data ownership (Table 1). Whereas the obtainment of ^{13}C NMR spectrum in the NMR solvent of DMSO-d_6 was very difficult due to the above-mentioned poor solubility, compound **1** was then recorded the 1D and 2D NMR spectra within D_2O + drops of F_3CCOOD, which proved to be a good solvent for **1**. The ^{1}H NMR spectroscopic data also clearly revealed the existence of 1,2-disubstitued benzene moiety, with four diagnostic signals from an aromatic ABCD spin system resonating at δ_H 7.13 (1H, t, J = 7.6 Hz, H-6),

Table 1: ^{1}H and ^{13}C NMR spectroscopic data for compound **1**.

Number	δ_H[ab]	δ_C[ac]	δ_H[de]	δ_H[d] [4]	δ_H[d] [5]	δ_C[d] [5]
1a	4.38 d (15.6)	40.5 t	4.15 d (15.3)	—	—	40.3
1b	4.54 d (15.6)		4.23 d (15.9)	4.22 d (4.8)	—	
3	4.27 dd (10.4, 5.6)	55.0 d	3.60 m	3.14	—	55.3
4a	3.13 dd (10.8, 16.4)	21.7 t	2.81 dd-like	2.83 ddd (10.5, 5.0, 2.4)	—	18.0
4b	3.38 dd (5.6, 16.4)		3.13 br d-like	3.69 dd (10.5, 5.0)	—	
4a′		104.9 s				104.3
4b′		125.6[f] s				128.5
5	7.53 d (8.0)	118.2 d	7.32 d (7.5)	7.33 d (8.0)	7.38 d (8.2)	118.5
6	7.13 t (7.6)	120.0 d	7.06 t (7.5)	7.08 t (8.0)	7.06 t (8.2)	117.5
7	7.22 t (8.0)	122.9 d	6.97 t (7.8)	6.99 t (7.5)	6.96 t (8.2)	121.1
8	7.43 d (8.0)	111.9 d	7.43 d (7.5)	7.44 d (7.5)	7.44 d (8.2)	111.8
8a		136.7 s				136.1
9a		125.4[f] s				—
COOH		171.3 s	10.91 s	10.93 s	—	165.6
9-NH				—	10.66 s	

[a] D_2O + drops of F_3CCOOD; [b]400 MHz. [c]100 MHz. [d]in DMSO-d_6; [e]300 MHz. [f]Assignments may be interchanged.

7.22 (1H, t, J = 8.0 Hz, H-7), 7.43 (1H, d, J = 8.0 Hz, H-8), and 7.53 (1H, d, J = 8.0 Hz, H-5), which correlated to the aromatic carbon signals at δ_C 120.0 (C-6), 122.9 (C-7), 111.9 (C-8), and 118.2 (C-5), respectively, in the HSQC spectrum. In addition, five well-resolved and characteristic signals at δ_H 4.38 (1H, d, J = 15.6 Hz, H-1$_a$), 4.54 (1H, d, J = 15.6 Hz, H-1$_b$), 4.27 (1H, dd, J = 10.4, 5.6 Hz, H-3), 3.13 (1H, dd, J = 10.8, 16.4 Hz, H-4$_a$), and 3.38 (1H, dd, J = 5.6, 16.4 Hz, H-4$_b$) were also examined in the ^{1}H NMR spectrum, which were, conveniently according to their coupling constants and with the aid of ^{1}H, ^{1}H-COSY spectrum, assigned to one AB spin system from an isolated methylene group and one ABX system from one methylene and one methine correlated together by sp^3 hybridized bond. These three functional groups were obviously deshielded and were correlated to their corresponding carbon signals at δ_C 40.5 (C-1), 55.0 (C-3), and 21.7 (C-4), respectively, in the HSQC spectrum. Simply, these three groups were arranged to either sp^2 hybridized carbons or nitrogen atoms when considering the ^{1}H and ^{13}C NMR chemical shifts and examining the ^{13}C and DEPT NMR data which exhibited twelve carbon signals with two aliphatic methylenes, one aliphatic methine, four sp^2 hybridized methines, and five sp^2 hybridized quaternary carbons being categorized (Table 1). The above NMR data were compatible with a benzene moiety, a tetrasubstituted ethylene, and a carbonyl except for the above-mentioned three aliphatic carbons. The long range ^{1}H,^{13}C-correlations from δ_H 7.53 to δ_C 104.9, 125.6, 136.7, and 122.9, from δ_H 7.43 to δ_C 122.9, 120.0, and 125.6, from δ_H 7.22 to δ_C 111.9, 136.7, and 118.2, from δ_H 7.13 to δ_C 118.2, 125.6, 122.9, and 111.9, from δ_H 4.38 and 4.54 to δ_C 125.4, 104.9, and 55.0, from δ_H 3.13 and 3.20 to δ_C 104.9, 55.0, 171.3, and 125.6/125.4, and from δ_H 4.27 to δ_C 171.3, 40.5, 21.7, and 104.9 established the constitutional formula of **1** as indicated by Figure 1. The complete assignment of the NMR data is listed in Table 1.

On evaluation of compound **1** for its cytotoxic effects on two human cancer cell lines, cell growth was measured using a sulforhodamine B (SRB) assay. Results of means of three replicates are expressed as the percentage of viability compared to negative control. Compound **1** exhibited moderate cytotoxicities against HCT-8 and HepG2 cell-lines in the evaluation, with viability of HepG2 and HCT-8 cells being 80.42% and 80.22% after treatment for 48 hours, and 76.14% and 71.48% after 72 hours, respectively, when using a concentration of 140 μg/mL. The viabilities at other time points were relatively lower.

3. Experimental

3.1. General Experimental Procedures. IR spectra were obtained on a Nicolet 5700 spectrometer. 1D and 2D NMR spectra were recorded on a Mercury-400 or a MERCURY-300 NMR spectrometer. Chemical shifts (δ) were given in ppm using tetramethylsilane (TMS) as internal standard (δ 0.00). ESI-MS and HRESI-MS were measured on an Agilent 1100 series LC-MSD-Trap-SL spectrometer. RP-18 (YMC-GEL, ODS-A, 12 nm, S-50 mm; YMC Co., Kyoto, Japan) were used for column chromatography. Solvents were of analytical grade and were purchased from Beijing Chemical Company (Beijing, China).

3.2. Plant Material. *Cichorium endivia* was purchased from Beijing Xinfadi agricultural products wholesale market on July 2009 and authenticated by Associate Professor Ma Lin

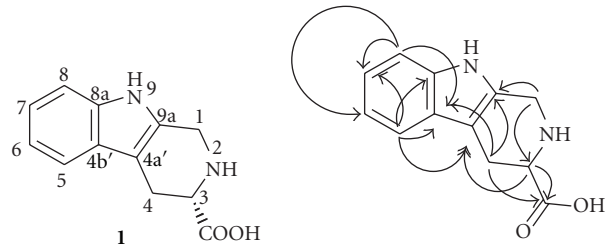

Figure 1: The structure of compound **1** and the key HMBC (→ : H → C) correlations.

(Institute of Material Medica, Chinese Academy of Medical Sciences and Peking Union Medical College). A voucher specimen was deposited in New Drug Safety Evaluation Center, Institute of Materia Medica, Peking Union Medical College & Chinese Academy of Medical Sciences, China.

3.3. Extraction and Isolation. The air-dried and pulverized *C. endivia* (5.8 kg) was extracted three times under reflux conditions with 95% EtOH (80 L, 2 h; 70 L, 1 h; 68 L, 1 h). The combined EtOH extracts were evaporated in vacuum to yield a dark-green residue (1233 g, crude EtOH extract), which was suspended in 80% aq. EtOH. The resulting suspension was extracted with petroleum ether (60–90°C, 2 L, 1.5 L, 1.5 L, and 1.5 L). Evaporation of the aq. layers in vacuum yielded also a dark-green residue (940 g, 80% EtOH extract). The residue was redissolved in water and subsequently partitioned with EtOAc in separatory funnel exhaustively. The rest of water soluble fraction was loaded on a column filled with Daion HP-20 and eluted with H_2O, 60% EtOH, and 95% EtOH, respectively. The eluates of 60% EtOH were evaporated in vacuum which yielded a black residue (40 g).

The 60% EtOH fraction was redissolved in solvent of *n*-BuOH and washed with aq. 5% $NaHCO_3$ then H_2O, respectively. Evaporation of *n*-BuOH under reduced pressure gave 5.5 g of brown-green residue, which was submitted to an ODS-A column eluted with MeOH-H_2O of decreasing polarity (40%–100%) to yield compound **1** (108 mg) as pale-yellow powder.

*3.3.1. 3S-1,2,3,4-Tetrahydro-β-carboline-3-carboxylic Acid(**1**).* Pale-yellow powder. IR (KBr) υ_{max} (cm^{-1}): 3284, 3019, 2849, 1642, 1598, 1452, 1409, 1271, 1221, and 740; ^1H and ^{13}C NMR spectroscopic data are listed in Table 1. ESI-MS (positive mode) m/z: 217.1 $[M+H]^+$and 239.1 $[M+Na]^+$; HRESI-MS (positive mode) m/z: 217.0967 $[M+H]^+$(calcd for $C_{12}H_{12}N_2O_2$, 217.0972).

3.4. Cytotoxicity Assay. HCT-8 and HepG2 cells were cultivated in RPMI1640 medium containing 0.22% sodium bicarbonate, 10% fetal bovine serum (FBS), 100 U/mL penicillin, and 100 μg/mL streptomycin. The cells were incubated in 5% CO_2-air at 37°C. Compound **1** was dissolved in phosphate-buffered saline (PBS) at a concentration of 1.4 mg/mL and was diluted to the required concentration with RPMI1640 medium immediately before use.

The cell viability was measured by using sulforhodamine B (SRB) assay. Briefly, the cells were seeded in 96-well plates (1×10^4 cells/well) and routinely cultured for 24 h. Compound **1** was added to in-serial concentrations (from 14 μg/mL to 140 μg/mL), while PBS was added alone to control wells as a negative control, and incubation was continued for an additional 48 h. SRB (1 mg/mL) was added to each well after the plates were fixed using TCA (0.4% m/v). After 20 minutes of incubation, each well was washed by acid (1% v/v) three times. Then wells were added into Tris (100 mmol/L), respectively. The absorbance of each well was recorded on a microplate spectrophotometer at 515 nm.

Acknowledgments

The authors thank Associate Professor L. Ma for the sample authentication. The authors are also thankful to the State Key Laboratory of Bioactive Substance and Function of Natural Medicine and Drug Safety Evaluation Center, Institute of Materia Medica, for providing cells and equipment for research.

References

[1] M. S. DuPont, Z. Mondin, G. Williamson, and K. R. Price, "Effect of variety, processing, and storage on the flavonoid glycoside content and composition of lettuce endive," *Journal of Agricultural and Food Chemistry*, vol. 48, no. 9, pp. 3957–3964, 2000.

[2] R. Llorach, A. Martínez-Sánchez, F. A. Tomás-Barberán, M. I. Gil, and F. Ferreres, "Characterisation of polyphenols and antioxidant properties of five lettuce varieties and escarole," *Food Chemistry*, vol. 108, pp. 1028–1038, 2008.

[3] C. J. Chen, A. J. Deng, C. Liu, R. Shi, H. L. Qin, and A. P. Wang, "Hepatoprotective activity of *Cichorium endivia* L. extract and its chemical constituents," *Molecules*, vol. 16, pp. 9049–9066, 2011.

[4] J. P. Peng, Y. Q. Qiao, and X. S. Yao, "Nitrogen-containing compounds from Allium macrostmon Bunge. and Allium chinese G. Don," *Chinese Journal of Medicinal Chemistry*, vol. 5, p. 134, 1995.

[5] S. Yahara, N. Uda, E. Yoshio, and E. Yae, "Steroidal alkaloid glycosides from tomato (*Lycopersicon esculentum*)," *Journal of Natural Products*, vol. 67, no. 3, pp. 500–502, 2004.